UNIVERSITY OF CALIFORNIA
RIVERSIDE

The Application of Carborane Anions in Ligand Design and Materials Development

A Dissertation submitted in partial satisfaction
of the requirements for the degree of

Doctor of Philosophy

in

Chemistry

by

Sarah Elizabeth Lee

June 2018

Dissertation Committee:

Dr. Vincent Lavallo, Chairperson
Dr. Francisco Zaera
Dr. Catharine Larsen

The Dissertation of Sarah Elizabeth Lee is approved:

Committee Chairperson

University of California, Riverside

Acknowledgements

I would like to thank Dr. Vincent Lavallo for the opportunity to join his research group. I am extremely grateful for his guidance and support throughout my graduate career. I would also like to thank the faculty at UCR for the mentorship and knowledge they have provided. The staff at UCR has also played a huge role in my success, and I would like to thank Dr. Dan Borchardt, Dr. Fook Tham, Prisciliano Saavedra, and Christina Youhas.

I am grateful for the many members of the Lavallo research group that I've had the pleasure of working with and learning from here at UCR. I would like to thank Matt Asay and Ahmad El-Hellani for their time and guidance during my first year of graduate school. I owe a lot of my success and laboratory skills to Matt. I was very fortunate to work with several remarkable chemists over the last few years: Gregorio Guisado-Barrios, Jess Estrada, Scott McArthur, and Steven Fisher. I would also like to thank Jack Kleinsasser and Anton Tomich for not only reading and editing chapters of this thesis, but also helping with and continuing the BCIL electrolytes project.

At SJSU, I would like to thank Dr. Monika Kress for her invaluable help and guidance, and for giving me the opportunity to participate in hands-down the coolest undergraduate research ever at NASA Ames through the URSA program. I would like to thank Dr. Dan Straus for instilling in me an appreciation of organic chemistry, and for encouraging me to go to graduate school.

Finally, I would like to thank my parents, my brother John, and my best friend Esther for their encouragement and support.

The text, figures, and schemes for the following chapters have been reproduced, in part, from the following published manuscripts.

Chapter 5:
Asay MJ, Fisher SP, Lee SE, Borchardt D, Tham FS, Lavallo V. Synthesis of Unsymmetrical N-Carboranyl NHCs: Directing Effect of the Carborane Anion. *Chemical Communications* 2015, **51**: 5359-5362.

Chapter 6:
Dziedzic R, Waddington M, Lee SE, Kleinsasser J, Plumley J, Ewing W, Bosley B, Lavallo V, Peng T, Spokoyny A. Reversible Silver Electrodeposition from Boron Cluster Ionic Liquid (BCIL) Electrolytes. *ACS Applied Materials and Interfaces* 2018*,* **10**: 6825-6830.

ABSTRACT OF THE DISSERTATION

The Application of Carborane Anions in Ligand Design and Materials Development

by

Sarah Elizabeth Lee

Doctor of Philosophy, Graduate Program in Chemistry
University of California Riverside, June 2018
Dr. Vince Lavallo, Chairperson

Since the discovery of polyhedral boranes, these molecules have expanded from items of molecular curiosity to having a wide scope of applications in contemporary chemistry. Borane clusters range in size and shape and can possess various heteroatoms. The term 'carborane' denotes a class of borane clusters containing one or more carbon atom in the polyhedral boron framework. Carboranes are structurally and electronically unique; while the carbon and boron atoms appear to exceed normal bonding configurations, these atoms are actually participating in delocalized bonding throughout the cluster. During the Cold War, the American government invested in rocket propulsion fuels featuring clusters primarily composed of boron, but the fuels were ultimately determined to be impractical. As the rush for boron fuel came to an end, research performed on borane clusters was published in the early 1960's, revealing the first carboranes. The work presented here utilizes two different anionic carboranes: the 12-vertex cluster, carba-closo-dodecaborate anion ($HCB_{11}H_{11}^-$), and the smaller 10-vertex cluster, carba-closo-decaborate anion ($HCB_9H_9^-$). Each anionic cluster possesses an overall charge of -1 delocalized throughout the 3-dimensional cluster, contributing to the tremendous stability of these

structures. Substitution of the clusters' hydride substituents with halides renders the carboranes even more weakly coordinating and much less susceptible toward chemical decomposition.

A large component of this work addresses the incorporation of both the 10 and 12-vertex carborane anions into ligand motifs. Carborane clusters are not typically included in catalyst design, and since the 1960's there have been only a few investigations exploring the applications of carboranes in ligand development. Carboranes are excellent synthons for constructing covalently bonded, architecturally novel molecules whose electronic and steric properties can be tailored to specific purposes. Beyond their use in ligand design, this thesis also contains work developing carborane-functionalized materials. Due to the charged nature of the carboranes, they are ideal building blocks for ionic liquids. Carboranes possess an array of favorable properties and the goal of the work presented in this thesis is to contribute to a more comprehensive understanding of these unique molecules.

Table of Contents

List of Figures

List of Schemes

List of Tables

Chapter 1: Introduction

1.1 Background

The focus of this dissertation is the synthetic development and characterization of novel ligands featuring covalently tethered carborane clusters. The term 'carborane' refers to a class of polyhedral clusters composed of boron and carbon, bearing a substituent at each vertex.[1] During the Cold War, the American government rushed to develop a new class of rocket propulsion fuels featuring clusters primarily composed of boron.[2] Compared to hydrocarbon fuels available at the time, boron hydride combustion resulted in much higher energy outputs. The U.S. Army, Navy, and Air Force all invested in boron-based fuel research and production plants, but the fuels were ultimately determined to be impractical. The combustion of these boron clusters produced boron oxide as a side product, fouling the jet engine turbines and reducing thrust. In the early 1960's, the rush for boron fuel came to an end. The research performed on these clusters was declassified, revealing new compound, 1,2-*closo*-dicarbadodecaborane **1** $H_2C_2B_{10}H_{10}$ (Figure 1-1), also known as *ortho*-carborane or simply *o*-carborane.[3-7] This compound had been prepared by both Reaction Motors and Olin Mathieson Corporation in attempts to develop boron-based fuels. Previously known boron clusters were considered unstable and reactive with air and water, hence their application

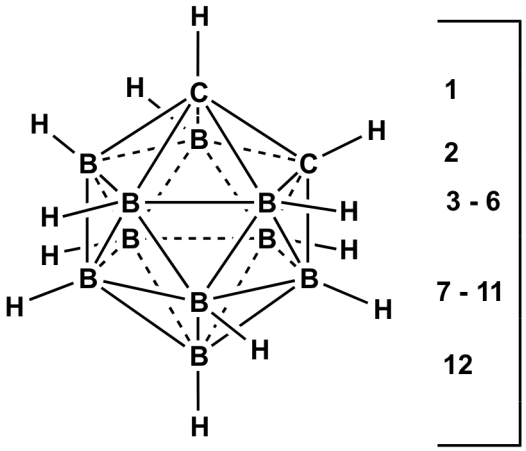

Figure 1-1. 1,2-*closo*-dicarbaborane **1**. The two carbon vertices occupy positions 1 and 2. The remaining 10 boron atoms construct the icosahedral *closo* structure.

in rocket fuels. However, **1** demonstrated unexpected stability to thermal, oxidative, and chemical conditions, which can be attributed to the closed icosahedral shape. While the carbon and boron atoms of **1** appear to exceed normal bonding configurations, these atoms are actually participating in delocalized bonding throughout the cluster.[1,8] This delocalized bonding has earned closed carborane clusters classification as three dimensionally aromatic, attributing to the notable stability of these clusters.[3] Following the discovery of **1**, fundamental curiosity and chemical developments have led to the development of numerous carborane clusters.[1,9-17] The work described in this dissertation specifically focuses on two carborane anion clusters, carba-*closo*-dodecaborate **2** and carba-*closo*-decaborate **3**.

The anionic analog of *o*-carborane **1**, known as the carba-*closo*-dodecaborate anion **2** $HCB_{11}H_{11}^-$ (Figure 1-2), was synthesized by Knoth in 1967.[18] The name carba-*closo*-dodecaborate, describes the icosahedral cluster: carba for one carbon, *closo* for the closed shell cluster, and dodeca indicates the twelve vertices of the polyhedron. Instead of a skeletal structure composed of two carbon and ten boron atoms like **1**, the anionic carborane **2** is composed of one carbon atom with eleven boron atoms. The twelve vertex carborane anion **2** is structurally similar and isoelectronic to the neutral *o*-carborane **1**, composed of twelve vertices each with a delocalized electron sigma

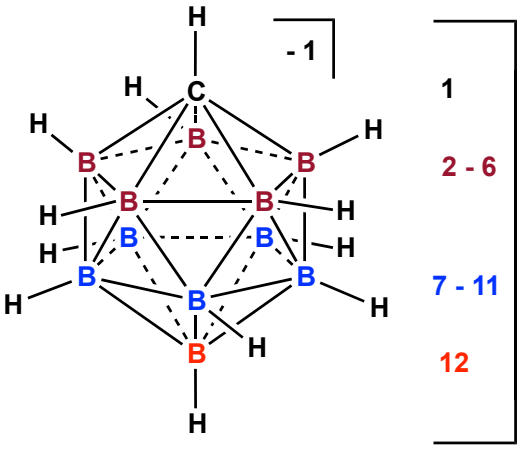

Figure 1-2. The 12-vertex carborane anion, carba-*closo*-dodecaborate, **2**.

bonding framework that consists of 6 bonds hyper-coordinated to each skeletal atom, for a total of twenty-six electrons delocalized throughout the skeletal structure.[12]

The exceptional stability of carborane clusters is attributed to their unique bonding framework. The unusual bonding exhibited by carborane clusters can be described using an electron counting technique known as Wade's rules, based on polyhedral skeleton electron pair theory.[19] This description of bonding within the polyhedron provides a rational explanation of how each atom of the cluster does not exceed their octet. This theory provides a formula to determine the number of skeletal electron pairs in relation to geometry and the number of vertices, which is n+1. This equation is equal to the number of electron pairs, where n is the number of vertices. In the case of an icosahedral structure, there are twelve vertices, so there are thirteen electron pairs, resulting in a total of twenty-six skeletal electrons are required. Each boron atom contributes two of its three valence electrons, while carbon contributes three of its four valence electrons. For *o*-carborane **1**, the ten boron atoms of the cluster skeleton contribute twenty electrons, while the two carbon atoms provide the remaining 6 electrons necessary. However, for the twelve vertex carborane anion **2**, one carbon atom of the cluster is replaced with a boron atom, and an additional electron is required to fulfill the twenty-six necessary electrons for bonding, rendering the cluster anionic. The assignment of three-dimensional aromaticity to this molecule is supported by a large negative value of -34.36 ppm for the nucleus independent shift (NICS), in comparison to -9.7 ppm for benzene.[12, 20]

Possessing an overall charge of -1 delocalized throughout the three-dimensional icosahedron of **2** contributes to the tremendous stability of the cluster in addition to

rendering this species chemically inert and very weakly coordinating. In contrast to *o*-carborane **1**, the carborane anion **2** is significantly more stable and not susceptible to nucleophilic attack and the ensuing boron vertex extrusion.[12] This carborane **2** and its derivatives have been most notably used as noncoordinating spectator anions[15, 21-37] to stabilize highly reactive cationic intermediates, such as protonated fullerene,[38] protonated benzene, and aryl cations for the activation of a wide variety of hydrocarbons.[39] In addition, the anionic nature of the carborane anion **2** presents interesting properties that our research group is currently exploring for applications in various fields of chemistry, including catalysis,[40, 41] battery applications,[42, 43] and the development of novel materials.[44]

In 1971, Knoth reported the synthesis of the carba-*closo*-decaborate anion **3** $HCB_9H_9^-$, the ten-vertex analog of **2**.[45] The gyroelongated antiprism structure contains nine boron and one pentacoordinate carbon center, following the same skeletal bonding patterns of **1** and **2**. The atoms participating in the skeletal structure contribute 21 electrons, while a total of 22 electrons are necessary for bonding, requiring one additional electron which renders the cluster anionic. Akin to the larger icosahedral clusters, the delocalized sigma skeletal bonding in **3** provides exceptional stability and is also considered three-dimensionally aromatic with a NICS value of -29.91.[46] Compared to the larger icosahedral parent carborane anion **2**, fewer investigations have been made utilizing the smaller carborane

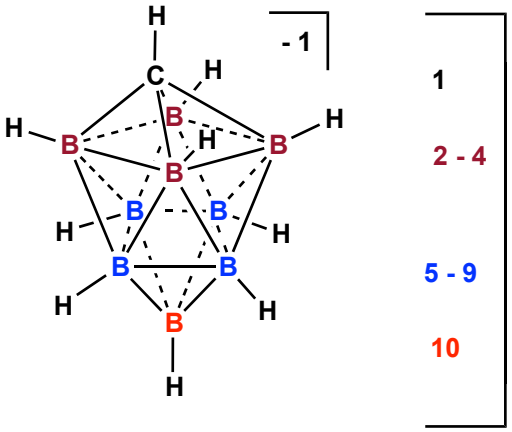

Figure 1-3. The 10-vertex carborane anion, carba-*closo*-decaborate.

anion **3**. However, the ten-vertex carborane anion **3** has found application in multiple chemical industries including nonlinear optics, liquid crystals, and cancer treatment drugs by delivery of radioactive halogens, and similar to the parent carborane anion **2**, it has been utilized as a weakly coordinating anion.[1, 8, 47-58]

1.2 Synthesis and Functionalization of $HCB_{11}H_{11}^-$

The twelve-vertex carborane anion **2** was first synthesized by Knoth in 1967 from decaborane.[18] In 2010, further improvements on the chemical synthesis were made by Reed,[15] resulting in the synthesis depicted in Scheme 1-1, and is currently used in our laboratory. Although we perform this reaction on multi-gram scales, the synthesis is difficult to scale for commercial use as it is costly with several dangerous steps. Starting

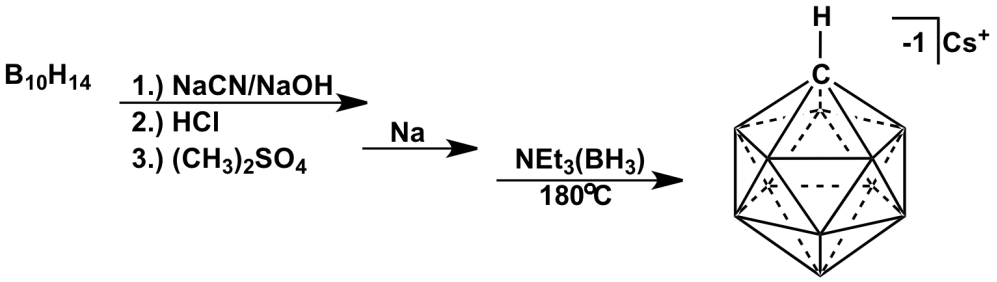

Scheme 1-1. The carba-*closo*-dodecaborate **2** synthesis from decaborane. Note the unlabeled vertices of the cluster each represent B-H.

from decaborane ($B_{10}H_{14}$), the carbon vertex is installed using sodium cyanide. Hydrochloric acid is used to protonate the cyanide group, followed by methylation to produce the zwitterionic open *nido* cluster bearing a trimethyl amine. In the next step, the open cluster is refluxed in tetrahydrofuran with elemental sodium to remove trimethyl amine, producing an open *nido* cluster with no functional group attached to the carbon vertex. The cluster is closed by refluxing in borane triethylamine at 190 °C for forty-eight hours under an inert atmosphere. Several alternative approaches to this reaction have been

developed in attempts to reduce cost and mitigate risky synthetic steps, but these methods are not yet practical for laboratory scale synthesis.[59]

When functionalizing these clusters at the boron vertices, the aromatic nature and stability of the cluster dictates its reactivity, which is similar to electrophilic aromatic substitution. The overall negative charge of -1 is distributed throughout the cluster, and the presence of carbon, a more electronegative atom, creates a polarized distribution of charge. The majority of the negative charge resides on the antipodal boron vertex, the furthest position from carbon (boron 12), and hence it is the most susceptible to electrophilic substitution.[1, 12] Following the antipodal boron, stepwise substitution progresses through the lower pentagonal belt (boron 7-11), and lastly the upper pentagonal belt (boron 2-6).[60] The upper pentagonal belt is adjacent to carbon, the most electronegative atom in the cluster, which depletes the charge of adjoining boron atoms therefore reducing reactivity. Substitution of the cluster's hydride substituents with halides (Cl-, Br-, I-) renders the carborane even more weakly coordinating and much less susceptible toward chemical decomposition. This results in enhanced thermal, oxidative, and chemical stability that further exceeds the abilities of standard alkyl and aryl R-groups, thus eliminating the risk of structural decomposition during catalysis.[1, 12]

In practice, not all reagents follow the stepwise substitution as precisely as others. Some reactions are less selective for functionalization and require precise reaction conditions, often followed by separation techniques to purify the target compound from mixtures. Substitution of only the lower pentagonal belt and antipodal boron is described as poly-substituted, where the upper five boron atoms directly bound to carbon still bear a

hydrogen atom. Full substitution of the entire cluster is described as per-substitution. When attempting to poly-substitute the cluster, there can be a mixture of over- and under-substitution, requiring several purification steps to separate the desired compound. Going from partial poly-substitution to fully per-substitution requires more extreme conditions to functionalize the upper pentagonal belt. The elevated pressures, high temperatures, acidic conditions, and harsh reagents required to fully functionalized these clusters demonstrates the superior stability of these molecules (Scheme 1-2).

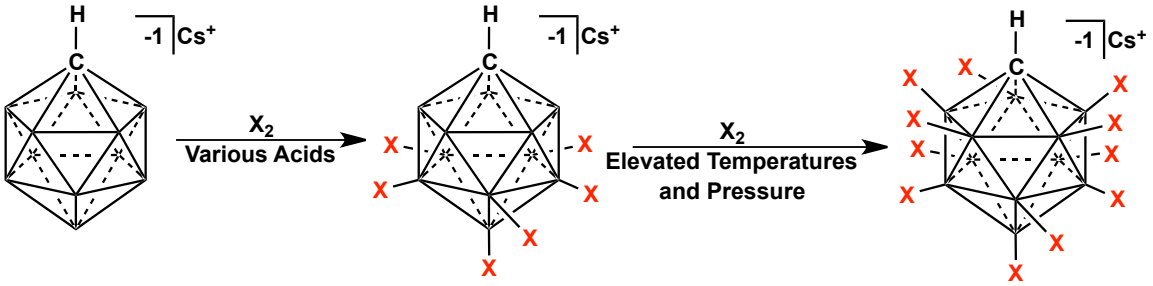

Scheme 1-2. Functionalization pathway of the 12-vertex carborane anion **2**.

In addition to the boron vertices, the carbon vertex can also be functionalized. There are two approaches to functionalizing the carbon vertex, either as part of the cluster synthesis or after fully forming the cluster. The carbon vertex of the hydridic species of **2** has a pKA of 21.8 and can be deprotonated with a strong base such as *n*-butyllithium. Deprotonating **2** forms the dianionic species, which can be reacted with a strong electrophile to functionalize the carbon vertex. Our lab has used this synthetic method to form carboranyl phosphines and azides.[40, 41, 61-64] The other approach to functionalizing the carbon vertex is through the cluster synthesis. The amine functionalized carba-*closo*-dodecaborate anion compound **4** is commonly utilized in our lab to prepare ligands through synthetic routes utilizing condensation chemistry.[65,66] The amine functionalized carborane

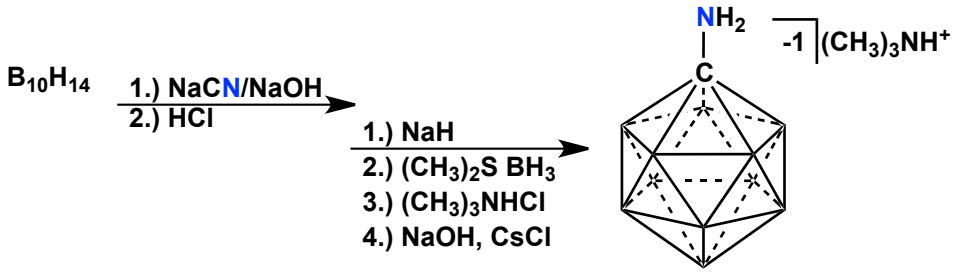

Scheme 1-3. Synthesis of the amine functionalized carborane anion, **4.**

anion **4** is prepared from decaborane by using sodium cyanide to install the carbon vertex bearing the amine functional group in the intermediate *nido* structure. Prolonged heating at 200 °C in a neat solution of borane triethylamine installs the final boron vertex, producing the *closo* structure bearing an amine through the carbon vertex (Scheme 1-3).

1.3 Synthesis and Functionalization of $HCB_9H_9^-$

Since the initial discovery of the 10-vertex carborane anion **3** by Knoth in 1971,[45] the synthesis has been greatly improved. The modern synthesis of this cluster also begins with decaborane, as does the 12-vertex cluster **2**, but instead the first step requires the

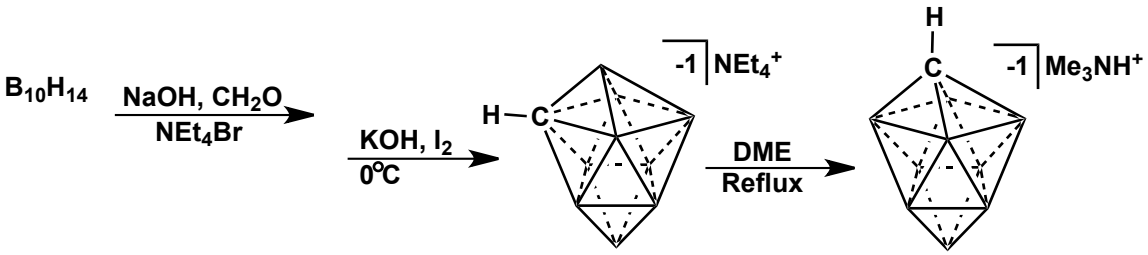

Scheme 1-4. Synthesis of the carba-*closo*-decaborate anion **3**.

substitution of a boron vertex with a carbon atom. This is known as a Brellochs[67] reaction, where a boron vertex is removed in basic conditions and a carbon is installed in the cluster framework. In the synthesis of the fully hydridic species of **3**, the Brelloch's reaction is performed with formaldehyde. Once the carbon vertex is install, the cluster is closed by

oxidation with elemental iodine. The resulting *closo* species is initially the 2-isomer, with the carbon vertex in the quaternary belt. Refluxing in DME isomerizes the carbon atoms to the apex position, forming the 1-isomer **3**.[68] As the 2-isomer, the carbon atom is hypercoordinated to 5 boron atoms in the cluster skeletal structure. As the 1-isomer, the carbon atom is only hypercoordinated to 4 boron atoms, which is a more stable bonding arrangement for the single carbon atom of the cluster.

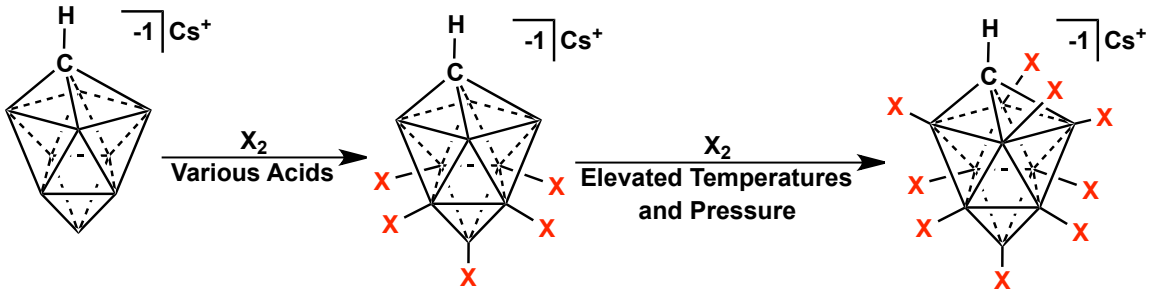

Scheme 1-5. Functionalization pathway of the 10-vertex carba-*closo*-decaborate anion **3**.

This cluster can be functionalized at both the carbon and boron vertices, as described for the 12-vertex mono-anion **2**. The overall negative charge distributed throughout the cluster is polarized as a result of the carbon at the apex position. The antipodal position B9 is the furthest from carbon and hence the most susceptible to electrophilic substitution. Substitution then proceeds to the lower quaternary belt, and finally the upper pentagonal belt (Scheme 1-5).[69] For functionalizing at the carbon vertex, this can be accomplished as part of the cluster synthesis or after constructing the closed cluster. After forming the cluster, Strong bases such as *n*-butyllithium can deprotonate the carbon vertex and the now nucleophilic cluster can be functionalized at the carbon. When synthesizing **3**, a functionalized carbon source can be used in the initial Brellochs reaction instead of formaldehyde, prior to closing the cluster via elemental iodine oxidation.[70]

Derivatives of **3** have been synthesized with variety of other functional groups tethered to the carbon vertex.[1,71,72] In Chapter 4, there is a more detailed discussion regarding the formation of the carboxylic acid functionalized derivative of **3** and attempts to form the amine functionalized derivative of **3**.

1.4 References

1. Grimes, R. N. In *Carboranes (Second Edition)*; Academic Press: Oxford, **2011**, p 1.

2. Dequasie, *The Green Flame: Surviving Government Secrecy*. American Chemical Society, Washington, DC, **1991**, p 1.

3. Heying, T. L.; Ager, J. W.; Clark, S. L.; Mangold, D. J.; Goldstein, H. L.; Hillman, M.; Polak, R. J.; Szymanski, J. W. *Inorganic Chemistry* **1963,** *2*, 1089.

4. Fein, M. M.; Bobinski, J.; Mayes, N.; Schwartz, N.; Cohen, M. S. *Inorganic Chemistry* **1963**, *2*, 1111.

5. Fein, M. M.; Grafstein, D.; Paustian, J. E.; Bobinski, J.; Lichstein, B. M.; Mayes, N.; Schwartz, N. N.; Cohen, M. S. *Inorganic Chemistry* **1963**, *2*, 1115.

6. Grafstein, D.; Bobinski, J.; Dvorak, J.; Paustian, J. E.; Smith, H. F.; Karlan, S.; Vogel, C.; Fein, M. M. *Inorganic Chemistry* **1963**, *2*, 1125.

7. Grafstein, D.; Bobinski, J.; Dvorak, J.; Smith, H.; Schwartz, N.; Cohen, M. S.; Fein, M. M. *Inorganic Chemistry* **1963**, *2*, 1120.

8. Kaszynski, P. *Collection of Czechoslovak Chemical Communications* **1999,** *64*, 895.

9. Popescu, A. R.; Teixidor, F.; Vinas, C. *Coordination Chemistry Reviews* **2014,** *269*, 54.

10. Spokoyny, A. M. *Pure Applied Chemistry*, **2013**, *85*, 903.

11. Olid, D.; Nunez, R.; Vinas, C. Teixidor, F. *Chemical Society Reviews* **2013***, 42,* 3318.

12. Douvris, C.; Michl, J. *Chemical Reviews* **2013***, 113,* PR179.

13. Farras, P.; Juarez-Perez, E. J.; Lepsik, M.; Luque, R.; Nunez, R.; Teixidor, F. *Chemical Society Reviews* **2012***, 41*, 3445.

14. Scholz, M.; Hey-Hawkins, E. *Chemical Reviews,* **2011***, 111*, 7035.

15. Reed, C. A. *Accounts of Chemical Research* **2010**, *43*, 121.

16. Li, Y.; Carroll, P. J.; Sneddon, L. G. *Inorganic Chemistry* **2008***, 47*, 9193.

17. Plesek, J. *Chemical Reviews* **1992**, *92*, 269.

18. Knoth, W. H. *Journal of the American Chemical Society* **1967**, *89*, 1274.

19. Wade, K. *Journal of the Chemical Society D: Chemical Communications* **1971**, 792.

20. Schleyer, P. V. R.; Maerker, C.; Dransfield, A.; Jiao, H.; Hommes, N. J. R. v. E. *Journal of the American Chemical Society* **1996***, 118*, 6317.

21. Finze, M. *Angewandte Chemie International Edition* **2007,** *46*, 8880.

22. Molinos, E.; Brayshaw, S. K.; Kociok-Kohn, G.; Weller, A. S. *Dalton Transactions* **2007,** *42*, 4829.

23. Douvris, C.; Ozerov, O. V. *Science* **2008,** *321,* 1188.

24. Geis, V.; Guttsche, K.; Knapp, C.; Scherer, H.; Uzun, R., *Dalton Transactions* **2009,** 15, 2687.

25. Gu, W.; Haneline, M. R.; Douvris, C.; Ozerov, O. V. *Journal of the American Chemical Society* **2009,** *131*, 11203.

26. Knapp, C.; Schulz, C. *Chemical Communications* **2009,** *33*, 4991.

27. Bolli, C.; Derendorf, J.; Keßler, M.; Knapp, C.; Scherer, H.; Schulz, C.; Warneke, J., *Angewandte Chemie International Edition* **2010,** *49*, 3536.

28. Derendorf, J.; Ke; Knapp, C.; Ruhle, M.; Schulz, C. *Dalton Transactions* **2010,** *39*, 8671.

29. Douvris, C.; Nagaraja, C. M.; Chen, C.-H.; Foxman, B. M.; Ozerov, O. V. *Journal of the American Chemical Society* **2010,** *132*, 4946.

30. Duttwyler, S.; Douvris, C.; Fackler, N. L. P.; Tham, F. S.; Reed, C. A.; Baldridge, K. *Angewandte Chemie International Edition* **2010,** *49*, 7519.

31. Finze, M.; Sprenger, J. A. P.; Schaack, B. B. *Dalton Transactions* **2010,** *39*, 2708.

32. Kessler, M.; Knapp, C.; Sagawe, V.; Scherer, H.; Uzun, R. *Inorganic Chemistry* **2010,** *49,* 5223.

33. Nava, M. J.; Reed, C. A. *Inorganic Chemistry* **2010,** *49*, 4726.

34. Valášek, M.; Štursa, J.; Pohl, R.; Michl, J. *Inorganic Chemistry* **2010,** *49*, 10255.

35. Kessler, M.; Knapp, C.; Zogaj, A. *Organometallics* **2011,** *30*, 3786.

36. Bolli, C.; Köchner, T.; Knapp, C. *Zeitschrift für anorganische und allgemeine Chemie* **2012,** *638,* 559.

37. Ibad, M. F.; Langer, P.; Reid, F.; Schulz, A.; Villinger, A. *Journal of the American Chemical Society* **2012,** *134*, 17757.

38. Ramirez-Contreras, R.; Ozerov, O. V. *Dalton Transactions* **2012,** *41,* 7842.

39. Shao, B.; Bagdasarian, A. L.; Popov, S.; Nelson, H. M. *Science* **2017**, *355,* 1403.

40. Lavallo, V.; Wright, J. H.; Tham, F. S.; Quinlivan, S. *Angewandte Chemie International Edition* **2013**, *52*, 3172.

41. Estrada, J.; Woen, D. H.; Tham, F. S.; Miyake, G. M.; Lavallo, V. *Inorganic Chemistry* **2015***, 54,* 5142.

42. McArthur, S. G.; Geng, L.; Guo, J.; Lavallo, V. *Inorganic Chemical Frontiers* **2015***, 2,* 1101.

43. McArthur, S. G.; Jay, R.; Geng, L.; Guo, J.; Lavallo, V. *Chemical Communications* **2017**, *53*, 4453.

44. Dziedzic, R.; Waddington, M.; Lee, S. E.; Kleinsasser, J.; Plumley, J.; Ewing, W.; Bosley, B.; Lavallo, V.; Peng, T.; Spokoyny, A. *American Chemical Society Applied Materials & Interfaces* **2018,** *10*, 6825.

45. Knoth, W. H. *Inorganic Chemistry* **1971**, *10*, 598.

46. Schleyer, P. v. R.; Najafian, K.; Mebel, A. M. *Inorganic Chemistry* **1998**, *37*, 6765.

47. Kaszynski, P.; Pakhomov, S.; Young, V. G. *Collection of Czechoslovak Chemical Communications* **2002***, 67,* 1061.

48. Hawthorne, M. F.; Olsen, F. P. *Journal of the American Chemical Society* **1965***, 87,* 2366.

49. Zakharkin, L. I.; Pisareva, I. V.; Sulaimankulova, D. D.; Antonovich, V. A. *Journal of General Chemistry USSR* **1990***, 60,* 2453.

50. Knoth, W. H. *Journal of the American Chemical Society,* **1966,** *88*, 935.

51. Hertler, W. R.; Knoth, W. H.; Muetterties, E. L. *Inorganic Chemistry,* **1964***, 4,* 288.

52. Pakhomov, S.; Kaszynski, P.; Young, V. G. *Inorganic Chemistry* **2000***, 39*, 2243.

53. Kaszynski, P.; Douglass, A. G. *Journal of Organometallic Chemistry* **1999***, 581*, 28.

54. Kaszynski, P.;Huang, J.; Jenkins, G. S.; Bairamov, K. A.; Lipiak, D. *Molecular Crystals and Liquid Crystals* **1995**, *260*, 315.

55. Ringstrand, B.; Monobe, H.; Kaszynski, P. *Journal of Material Chemistry* **2009***, 19,* 4805.

56. Ringstrand, B.; Kaszynski, P.; Young, V. G. Janousek, Z. *Inorganic Chemistry* **2010***, 49*, 1166.

57. Ringstrand, B.; Kaszynski, P.; Janousek, Z.; Young, V. G. *Journal of Material Chemistry* **2009***, 19,* 9204.

58. Batsanov, A. S.; Fox, M. A.; Goeta, A. E.; Howard, J. A. K.; Hughes, A. K.; Malget, J. M. *Journal of the Chemical Society, Dalton Transactions* **2002**, 2624.

59. Zharov, I.; Weng, T.-C.; Orendt, A. M.; Barich, D. H.; Penner-Hahn, J.; Grant, D. M.; Havlas, Z.; Michl, J. *Journal of the American Chemical Society* **2004**, *126*, 12033.

60. Valliant, J. F.; Guenther, K. J.; King, A. S.; Morel, P.; Schaffer, P.; Sogbein, O. O.; Stephenson, K. A. *Coordination Chemistry Reviews* **2002**, *232*, 173.

61. Asay, M.; Kefalidis, C. E.; Estrada, J.; Weinberger, D. S.; Wright, J.; Moore, C. E.; Rheingold, A. L.; Maron, L.; Lavallo, V. *Angewandte Chemie International Edition* **2013**, *52*, 11560.

62. Chan, A. L.; Fajardo, J.; Wright, J. H.; Asay, M.; Lavallo, V. *Inorganic Chemistry* **2013**, *52*, 12308.

63. Wright, J. H.; Kefalidis, C. E.; Tham, F. S.; Maron, L.; Lavallo, V. *Inorganic Chemistry* **2013**, *52*, 6223.

64. Fajardo, J.; Chan, A. L.; Tham, F. S.; Lavallo, V. *Inorganica Chimica Acta* **2014**, *422*, 206.

65. El-Hellani, A.; Lavallo, V. *Angewandte Chemie International Edition* **2014***, 53*, 4489.

66. Asay, M. J.; Fisher, S. P.; Lee, S. E.; Borchardt, D.; Tham, F. S.; Lavallo, V. *Chemical Communications* **2015***, 51*, 5359.

67. Brellochs, B.; Backovsky, J.; Stibr, B.; Jelinek, T.; Holub, J.; Bakardjiev, M.; Hnyk, D.; Hofmann, M.; Cisarova, I.; Wrackmeyer, B. *European Journal of Inorganic Chemistry* **2004**, *18*, 3605.

68. Ringstrand B.; Bateman, D.; Schoemaker, R. K.; Janousek, Z. *Collection of Czechoslovak Chemical Communications* **2009**, *74*, 419.

69. Tsang, C.-W.; Yang, Q.; Sze, E. T.-P.; Mak, T. C. W.; Chan, D. T. W.; Xie, Z. *Inorganic Chemistry* **2000**, *39*, 3582.

70. Jelinek, T.; Stibr, B.; Plesek, J.; Thornton-Pett, M.; D. Kennedy, J. *Journal of the Chemical Society, Dalton Transactions* **1997**, 4231.

71. Franken, A.; Carr, M. J.; Clegg, W.; Kilner, C. A.; Kennedy, J. D. *Dalton Transactions* **2004**, *21*, 3552.

72. Ringstrand, B.; Kaszynski, P.; Franken, A. *Inorganic Chemistry* **2009***, 48*, 7313.

Chapter 2: Dianionic 12-Vertex Carboranyl Diimines

2.1 Introduction

In 2013, the Lavallo group reported the synthesis of N-heterocyclic carbenes (NHCs) from an imidazolium bearing two carborane anions **2** bound through the nitrogen atoms (Scheme 2-1).[1] The synthesis of the imidazolium precursor to the NHC is analogous to that of classical dialkyl or aryl substituted versions with the exception of using the anionic carboranyl amine **4** in place of aryl and alkyl amines. This synthesis is the first demonstration of the carboranyl amine **4** to undergo condensation reactions with an aldehyde, resulting in the dianionic carboranyl diimine precursor **5** to the imidazolium salt **6**. Based on this discovery, my initial work in the Lavallo group involved synthetic methods utilizing the twelve-vertex anionic carboranyl amine's reactivity with aldehydes and

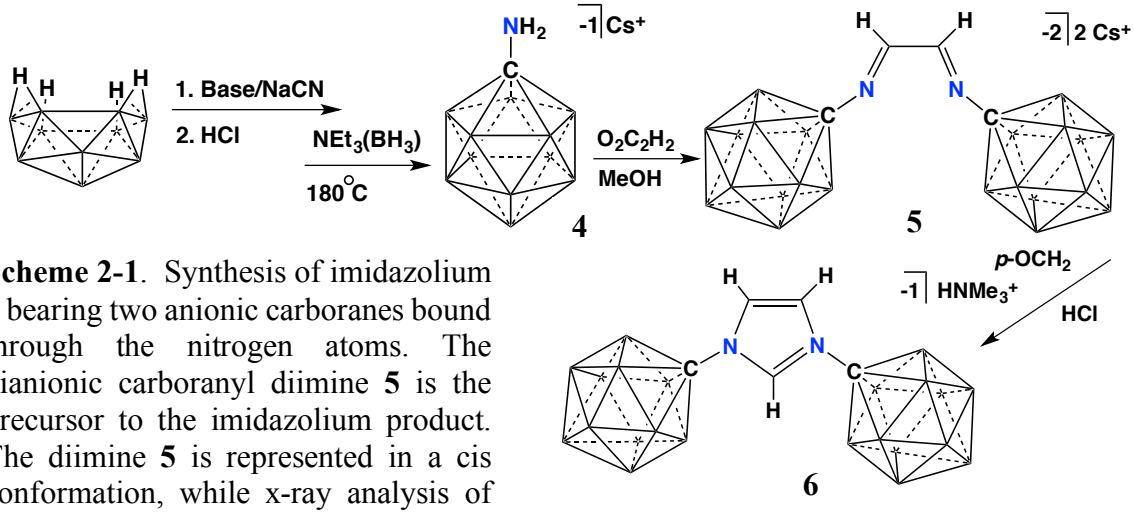

Scheme 2-1. Synthesis of imidazolium **6** bearing two anionic carboranes bound through the nitrogen atoms. The dianionic carboranyl diimine **5** is the precursor to the imidazolium product. The diimine **5** is represented in a cis conformation, while x-ray analysis of the crystal structure (Figure 2-3) indicates trans.

ketones. My intention was to determine if a diimine ligand structure bearing the anionic carba-*closo*-dodecaborate cluster could be complexed with a metal center, forming a metal

catalyst comparable to known late transition metal catalysts[2,3] featuring bulky alkyl and aryl α-diimine ligands.

The dianionic carboranyl diimine **5** precursor to the imidazolium **6** is analogous to alkyl and aryl diimine ligands (Figure 2-1) commonly used in catalysis, especially copolymerization applications.[2,3] Traditional diimine ligands utilize bulky aryl R-groups to sterically direct polymerization at the metal center. In the mid 1990's, Brookhart and coworkers first demonstrated that late transition metal catalysts (palladium and nickel)

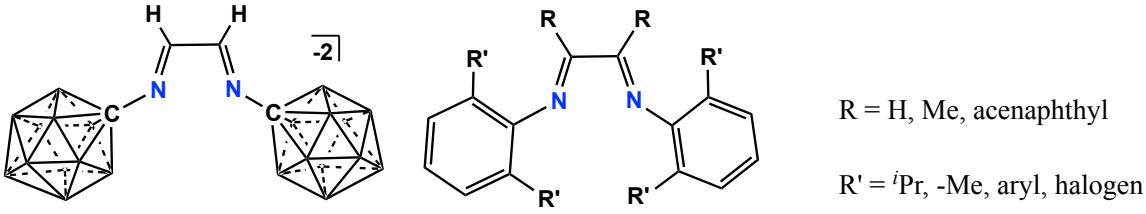

Dianionic Carboranyl Diimine, 5 Brookhart-type Diimine Ligand

Figure 2-1. The dianionic 12-vertex carboranyl diimine **5** (left) and the diimine ligand structure used by Brookhart and coworkers for the synthesis of polymerization catalysts.

featuring sterically hindered α-diimine ligands acted as highly successful olefin polymerization catalysts.[3-7] These catalysts featured several distinct characteristics favoring olefin polymerization that included highly electrophilic and cationic metal centers paired with non-coordinating counter ions, and neutral bulky α-diimine ligand substituents. Several problems are still faced by late transition metal catalysts for copolymerization.[8,9] First, the presence of polar group directly attached to olefin bond changes the electronic environment, reducing the rate of coordination and incorporation of polar monomer in the polymer chain. After insertion of the polar monomer, the functional group can coordinate to the metal center, forming a stable chelate and slowing down the insertion rate. Least

favorable of all outcomes, β-hydride elimination of the functional group will terminate the polymer chain. Traditional polymerization catalysts also require the presence of an activator.[3] This generates ion pairs with the precatalyst, creating a cationic metal center for olefin coordination. Ion association, even ions considered non-coordinating, can compete with olefins as the counter anion and will weakly coordinate to the active site of the metal center, lowering catalytic activity.

Since Brookhart's discovery, numerous efforts have been made to improve upon this design for the creation of a more robust and effective catalyst capable of polymerizing polar monomers.[2-14] A new class of zwitterionic and anionic metal complexes offers the same and expanded abilities as traditional catalysts without the need for the presence of an activator to generate ions pairs. Brookhart's catalysts relied on the addition of a co-catalyst to abstract a halide from the complex, generating a vacant coordination site at the metal center and rendering the metal catalyst cationic, balanced by the co-catalyst counter anion. By incorporating the anionic counterpart(s) into the ligand structure, the anion cannot associate with the active site of the metal complex.[10]

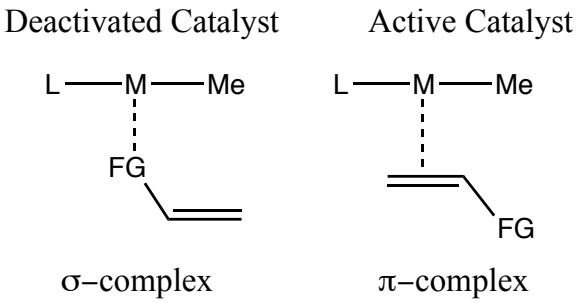

Figure 2-2. σ bond and π-bond of a substrate to a metal center; FG = functional group

Additionally, the metal center is less electrophilic in zwitterionic complexes, allowing for a monomer bearing a functional group to coordinate to the metal center through the π bond rather than forming a σ bond with the functional group. Coordination to the π-bond is necessary for polymerization to occur whereas coordination to the functional group inhibits

polymer growth[8,9] (pictured in Figure 2-2). Ziegler and coworkers have reported zwitterionic and anionic versions of Brookhart type α-diimine catalysts, which have reduced rates of σ bonding to the functional group, promoting π coordination in the copolymerization of ethylene and acrylonitrile, but these complexes used simple anions such as SO_3^- and BH_4^- .[10] Other modifications to this design have increased steric bulk of the ligand so that the structure fully shields the axial sites of the complex.[12] The presence of a large sterically bulky ligand, such as Guan's cyclophane inspired diimine, has also shown increased rates of polar olefin coordination to the metal center, leading to a higher rate of incorporated polar monomer.[13,14] By strategically using the influence of steric bulk to limit olefin access to only the cis-coordination site, the growing polymer chain is inhibited from β-hydride elimination, producing highly linear chains.

A unique alternative to the more traditional ligand R-groups is the anionic carba-*closo*-dodecaborate cluster. While ancillary ligands such as Brookhart's are typically constructed of classical alkyl and aryl R-groups, icosahedral carboranes are a unique alternative not typically included in catalyst design. In 2012, the Lavallo Group published the first successful late transition metal catalyst containing a ligand bearing an icosahedral carborane anion **2** R-group.[15] This first reported catalyst, a gold metal center bearing a perhalogenated carba-closo-dodecaborate phosphine substituent, is nearly two orders of magnitude more active as an alkyne hydroamination catalyst than all known comparable systems containing classic alkyl and aryl groups. Previous investigations with carborane-functionalized ligands have focused on the use of neutral dicarbaborane clusters **1**, which have not yielded catalysts that go beyond the state-of-the-art.[16-19] By functionalizing α-

diimine ligands with carborane clusters, the corresponding metal complexes would be anionic and zwitterionic catalysts. Anionic carboranes are distinctly large ligand substituents, which have the capability to influence the active site for catalysis and manipulate stereo-selectivity.[15,20] The van der Waals volume (VvwV) of the non-halogenated carborane cluster **2** is ~144 Å^3, comparable to an adamantyl group (136 Å^3).[21] When I first joined the Lavallo group, investigations of the carboranyl functionalized NHCs were already underway but the stability and reactivity of the dianionic carboranyl diimine **5** was unexplored.

2.2 Results and Discussion

After learning to prepare the anionic carboranyl amine **4**,[20,21] my first project consisted of the isolation and purification of the dianionic carboranyl diimine **5**. I synthesized the diimine **5[Me$_3$NH$^+$]** according to literature[1] and performed a simple salt exchange (Cs^+ to Me_3NH^+) to purify the ligand by forming the Me_3NH^+ salt, which crystallized in methanol by slow evaporation (Figure 2-31, Experimental Section). The crystal was twinned and bond lengths could not accurately be resolved, but we were able to obtain confirmation of the structure. Next, I prepared **5[Me$_3$NH$^+$]** as the lithium salt, **5[Li$^+$]** in anticipation of performing halide abstraction upon complexation to a metal center. Inspired by Brookhart and coworkers' catalysts, I attempted the synthesis of late transition metal complexes, focusing on palladium and nickel metal centers. There was no observed reactivity with a variety of substrates and reaction conditions. Only one precursor, methyl(1,5-cyclooctadiene)palladium(II) chloride, formed a light brown precipitation in solution with the lithium salt of the dianionic carboranyl diamine, and free cyclooctadiene

is observed in solution. This reaction results in the formation of a precipitate that has proven to be insoluble in all available solvents. Due to this compound's insolubility, I was unable to further confirm the structure or test for homogenous catalytic activity.

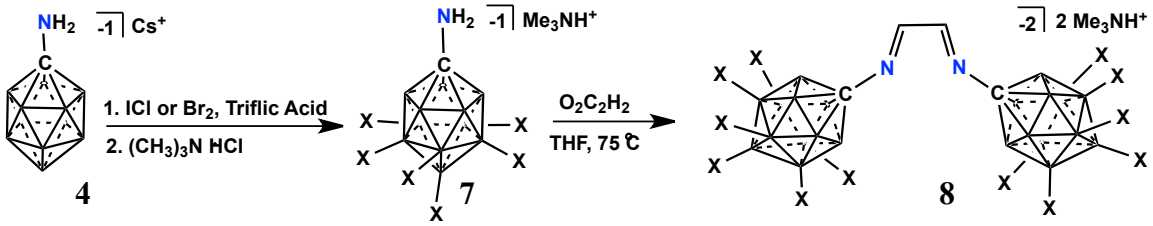

Scheme 2-2. Synthesis of polyhalogenated dianionic carboranyl diimine **8**, where the boron atoms of the lower pentagonal belt and the antipodal position all bear a halogen (I or Br). The upper pentagonal belt boron atoms maintain hydride substituents.

Due to the lack of reactivity I encountered with the fully hydridic carboranyl diimine, I started exploring modifications of this ligand structure. I first investigated modifications of the carborane cluster. The carboranyl amine **4** compound undergoes stepwise substitution of the B-H vertices in the same manner as anionic carba-*closo*-dodecaborate **1** and our lab is capable of preparing the fully (per-) and polyhalogenated carboranyl amine. Replacement of the B-H hydrides with halides provides an array of substitution patterns that dictate tunable electronic and steric properties. Hexa-substitution of carboranyl amine readily occurs in triflic acid (CF_3SO_3H) with iodine monochloride (ICl) or glacial acetic acid (CH_3COOH) with liquid bromine (Br_2), resulting in the hexa-iodinated $\mathbf{7_I}$ and hexa-brominated $\mathbf{7_{Br}}$ clusters, respectively.[23-26] Both polyhalogenated carborane amine clusters undergo condensation with glyoxal in a similar manner as the non-halogenated amine, however both polyhalogenated amines required heat (60 °C) for the condensation reactions to reach completion. The diimine ligands constructed from hexa-halogenated carboranyl amine species as cesium salts are also more sensitive to acidic

conditions and hydrolyzed during the $(CH_3)_3NH^+$ salt exchange from Cs^+, reducing the diimine back to the carboranyl amine species. I proceeded to try the condensation reaction again using the $(CH_3)_3NH^+$ salt instead, and successfully produced both α-diimine ligands, $\mathbf{8_I}$ and $\mathbf{8_{Br}}$ for the hexa-brominated and hexa-iodinated species (Scheme 2-2). I again prepared these ligands as Li^+ species ($\mathbf{8_I[Li^+]}$ and $\mathbf{8_{Br}[Li^+]}$) and attempted to coordinate these ligands to a variety of metal substrates, particularly methyl(1,5-cyclooctadiene)palladium(II) chloride. Neither ligand appears to bind to the metal center, regardless of reaction conditions. Based on ^{1}H NMR analysis, no shift is seen for either the diimine backbone or the methyl group adjacent to the metal center, indicating that the ligand is unable to coordinate to the metal center.

Based on these results, I concluded that the additional steric bulk of the hexahalogenated carborane clusters possibly hinders the coordination of the $\mathbf{8_I[Li^+]}$ and $\mathbf{8_{Br}[Li^+]}$ diimine ligands. Also, the presence of halogens on the carborane cluster may impose an electron withdrawing effect on the nitrogen atoms, reducing their electron donating behavior. I next sought to modify the backbone of the ligand. Based on the crystal structure of the 12-vertex anionic carborane diimine ligand $\mathbf{5[Me_3NH^+]}$ (Figure 2-31, experimental section), I hypothesized that additional steric bulk in the backbone of the amine would improve coordination of the diimine to a metal center.

Based on the successful condensation of carboranyl amine (halogenated and nonhalogenated) with glyoxal, I sought out to form a diimine ligand from another aldehyde. *O*-phthalaldehyde not only possesses two aldehydes adjacent to one another on a benzene ring, but also has a planar nature that would provide steric hindrance to direct the potential

coordination of a diimine ligand with a metal center. However, the condensation of *o*-phthalaldehyde and carboranyl amine **4[Cs$^+$]** does not proceed to full completion as seen before with glyoxal. In addition to the disubstituted product **9**, a percentage (7-30%) of the mono-substituted product **10** appears in the crude reaction mixture and a portion of this

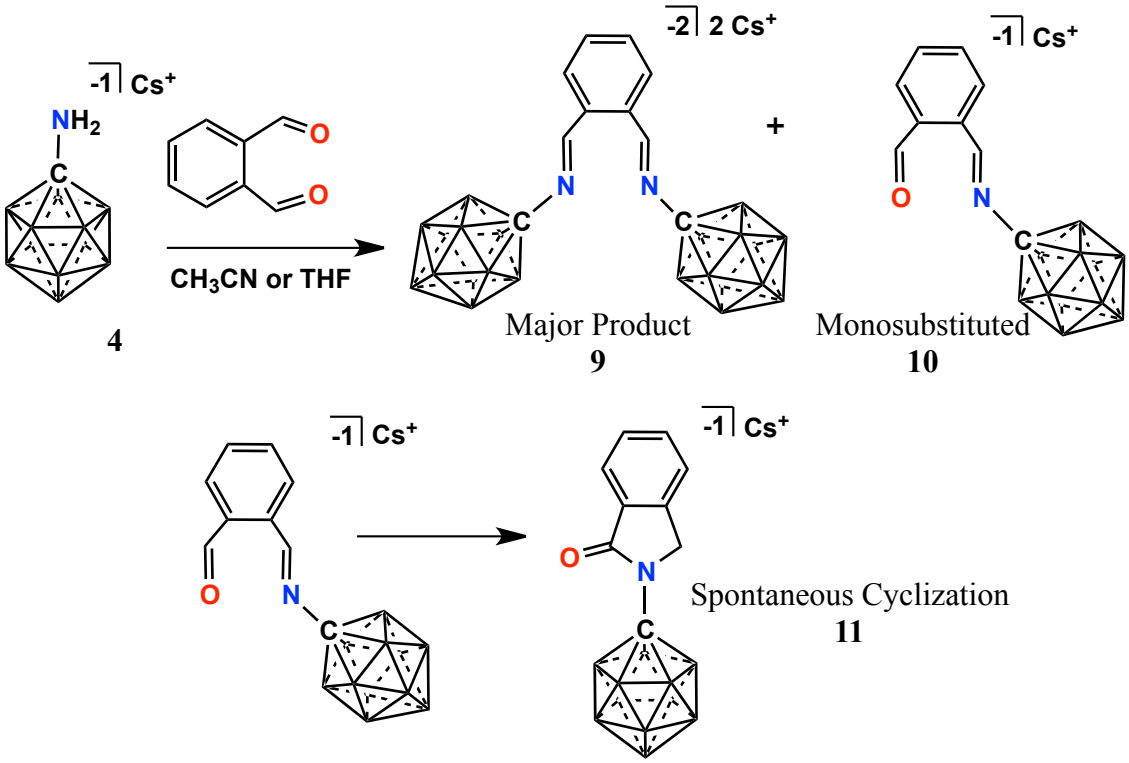

Scheme 2-3. Condensation reaction of carboranyl amine **4[Cs$^+$]** and *o*-phthalaldehyde.

monosubstituted product consistently undergoes spontaneous isomerization to a bicyclic structure **11** (Scheme 2-3). Regardless of the various tested conditions, the mono-substituted product is formed in the reaction solution. As the Me_3NH^+ salt, the mono-substituted bicyclic product **11** exhibits slight solubility in methylene chloride and some of this side product can be extracted from the reaction mixture. Separation from the reaction

mixture of the monosubstituted product **10** prior to cyclization in order to purify the benzene backbone dianionic carboranyl diimine **9** was not resolved.

Using the methylene chloride extractions, I was able to obtain a crystal structure of the monosubstituted bicyclic product **11[Me_3NH^+]** and confirm the suggested structure based on NMR analysis (Figure 2-32, Experimental Section). The C2-C7 bond length remains within the range for a substituted aromatic ring (C2 – C7 = 1.379(2) Å), and the adjacent C-C bond lengths of the new five membered ring are within the standard range for single bonds (C1-C2 = 1.492(2) Å, C7-C8 = 1.474(2) Å).[27] The carborane cluster adjacent to the nitrogen atom appears to have no significant effect on the nature of the amide, as the bond length between the carbon and nitrogen atom (N1-C8 = 1.369(2) Å) is only minimally longer than the standard length for tertiary amides (N-C = 1.346 Å).[27] Hydrogen bonding is observed between the nitrogen proton of $(CH_3)_3NH^+$ and the oxygen atom of the bicyclic ring (N2-H(N2) …O1 = 1.866 Å). The sum of the C-N-C angles equals 360°, indicating that the nitrogen atom is planar with sp^2 hybridization.

While testing the various reaction conditions for the double condensation of *o*-phthaldehyde and carboranyl amine, I came across a method for the formation of only the monosubstituted product **10[Cs^+]**. When performing the condensation reaction in cold H_2O, the monosubstituted *o*-phthaldehyde bearing one carborane readily precipitates from solution prior to the spontaneous cyclization, confirmed by ^1H NMR. Once formed, the mono-substituted product **10[Cs^+]** does not undergo a clean second condensation with carboranyl amine, but again forms a mixture of monosubstituted, disubstituted, and the isomerized bicyclic product. However, this mono-substituted product is an advantageous

precursor and could be used for constructing an asymmetrically substituted anionic diimine ligand.

2.3 Conclusion

Based on the lack of reactivity with several late transition metals and the tendency to hydrolyze, I have concluded that the dianionic carboranyl diimine **5** is not a favorable ligand for constructing a well-defined metal complex. Modifiying the clusters with halogens (**7$_{I}$** and **7$_{Br}$**) did not improve reactivity of the corresponding diimines **8$_{I}$** and **8$_{Br}$**, as the additional steric bulk from the presence of halogens on the carborane clusters also appears to hinder coordination and may impose an electron withdrawing effect on the nitrogen atoms, reducing their electron donating behavior. Condensation with *o*-phthaldehyde to form a dianionic carboranyl diimine **9** with a benzene backbone produced a mixture of single and double condensation products, **10** and **11**.

2.4 Experimental

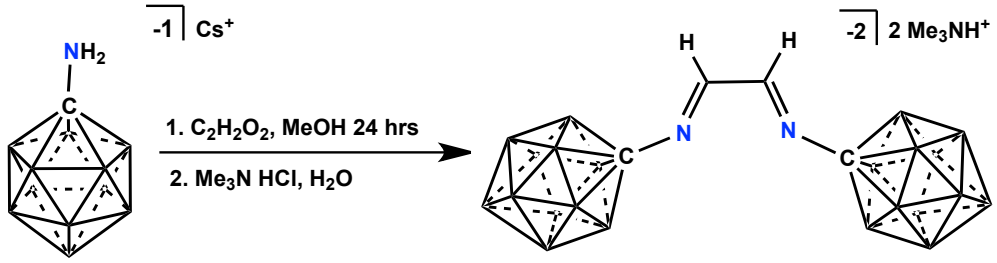

Scheme 2-4. Synthesis of Dianionic Carboranyl Diimine, **5[Me_3NH^+]**

In 30 mL of methanol, $NH_2CB_{11}H_{11}^-Cs^+$ **4** (1.83 grams, 6.29 mmol) was dissolved and an aqueous solution of glyoxal ($O_2C_2H_2$) (40% w/w, 0.39 mL, 3.4 mmol) was added. The reaction mixture was stirred for 24 hours. Volatiles were removed under reduced pressure to afford the crude product dianionic 12-vertex carboranyl diimine **5** [$N_2C_2H_2C_2B_{22}H_{22}^{2-}$][$2Cs^+$]. **2** was purified by salt exchange to Me_3NH^+ by dissolving it in H_2O (100 mL) followed by the addition of 4 eq. (13.6 mmol, 1.3 grams) of trimethylammonium hydrochloride, NMe_3HCl. A white precipitate formed of **5[Me_3NH^+]** and was collected by filtration and dried under vacuum to afford the product in 92% yield (1.66 grams, 3.13 mmol). ^1H NMR (300 MHz, acetonitrile-d_3, 25 °C): δ = 7.64 (s, 2H), 3.50- 0.20 (bm, 22H, B-H); ^1H (^{11}B-dec) NMR (300 MHz, acetonitrile-d_3, 25 °C): δ = 7.64 (s, 2H), 1.83 (s, 10H, B-H), 1.49 (s, 10H, B-H), 1.40 (s, 2H, B-H); ^{11}B (^1H-dec) NMR (96 MHz, acetonitrile-d_3, 25 °C): δ = -5.6, -9.7 ppm. HRMS (negative mode ESI/APCI) $[M + H]^-$ m/z calc'd for $N_2C_2C_2B_{22}H_{25}^-$: 339.4215; found 339.4203.

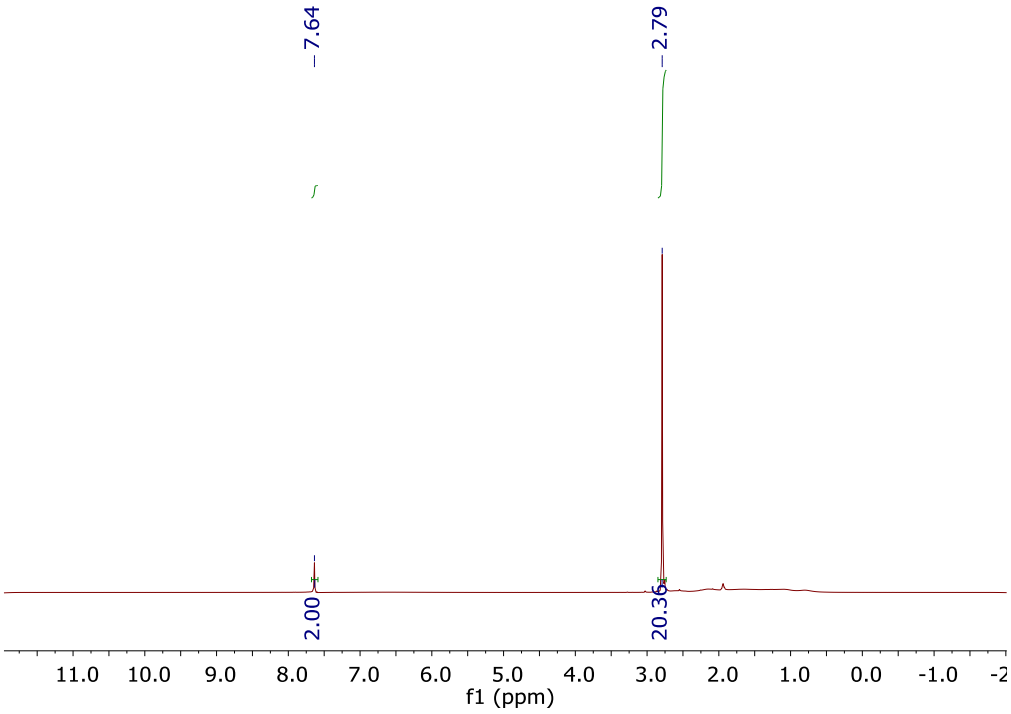

Figure 2-3. ^{1}H NMR of **5[Me$_3$NH$^+$]** in acetonitrile-d$_3$. The Me$_3$NH$^+$ countercations appears at 2.79 ppm and integrates to 2 equivalents.

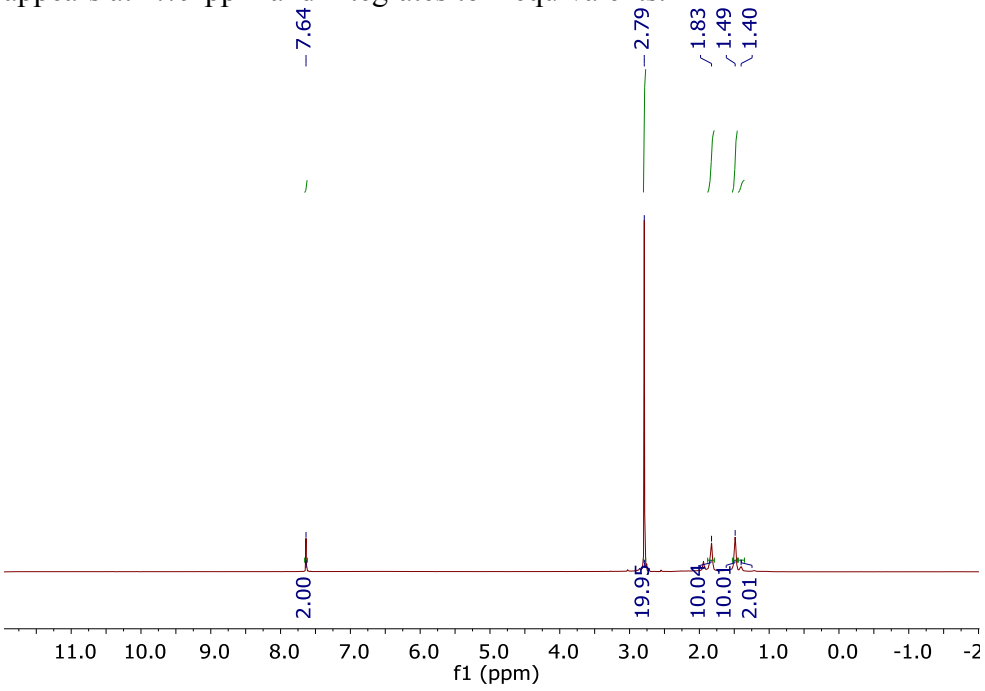

Figure 2-4. ^{1}H (^{11}B-dec) NMR of **5[Me$_3$NH$^+$]** in acetonitrile-d$_3$. The Me$_3$NH$^+$ countercations appears at 2.79 ppm and integrates to 2 equivalents.

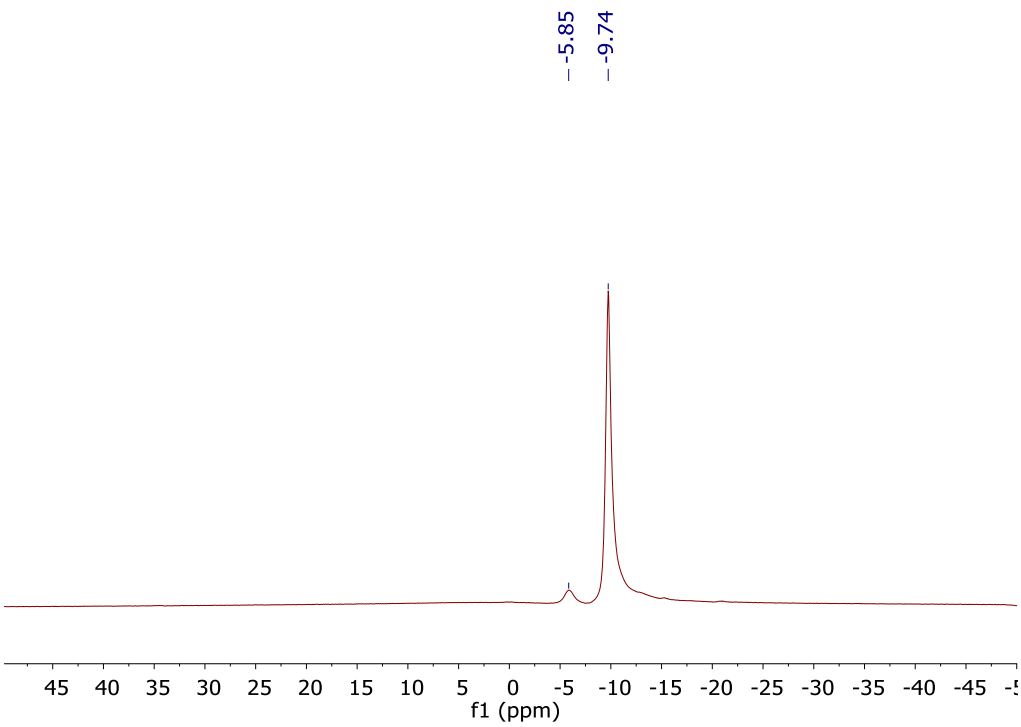

Figure 2-5. ^{11}B (^{1}H-dec) NMR of **5[Me_3NH^+]** in acetonitrile-d_3.

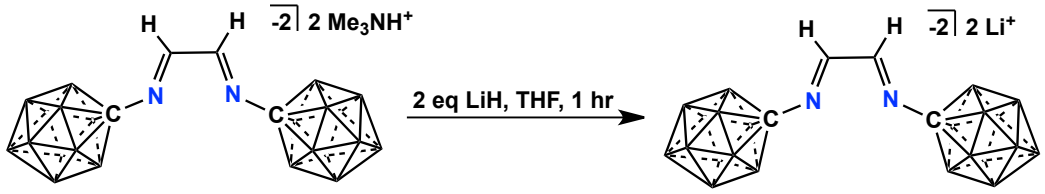

Scheme 2-5. Synthesis of Dianionic Carboranyl Diimine, **5[Li$^+$]**

5[Me$_3$NH$^+$] was dried under high vacuumn and brought into the glove box. Under inert atmosphere, 0.45 grams (0.85 mmol) of **5[Me$_3$NH$^+$]** was weighed out and added to a 20 mL scintillation vial equipped with a stir bar. To the vial, ~ 8 mL of tetrahydrofuran was added. On a weigh paper, 16 mg (2.0 mmol) of lithium hydride was weighed out. While stirring, the LiH was added in small portions to the vial of **5[Me$_3$NH$^+$]**. The reaction began to vigorously bubble at the addition of each portion, and when it subsided the next portion was added. After all of the LiH was added to the vial, it was capped and stirred for an additional 30 minutes. The crude solution of **5[Li$^+$]** was concentrated to ~ 3 mL, and added dropwise to a second scintillation vial containing 15 mL of hexanes, while stirring. The vial was capped and stirred for 2 hours. The hexanes were decanted and the product was dried under vacuumn, affording **5[Li$^+$]** in 98% yield (0.771 grams, 0.83 mmol). Note: there are 4 equivalents of tetraydrofuran coordinated to each Li$^+$. ^{1}H NMR (300 MHz, tetrahydrofuran-d$_8$, 25 °C): δ =7.68 (s, 2H), 2.70-0.20 (bm, 22H, B-H); ^{1}H (^{11}B-dec) NMR (300 MHz, tetrahydrofuran-d$_8$, 25 °C): δ = 7.68 (s, 2H), 1.50 (s, 12H, B-H), 1.39 (s, 8H, B-H); ^{11}B (^{1}H-dec) NMR (96 MHz, tetrahydrofuran-d$_8$, 25 °C): δ = 3.0, 0.9 ppm.

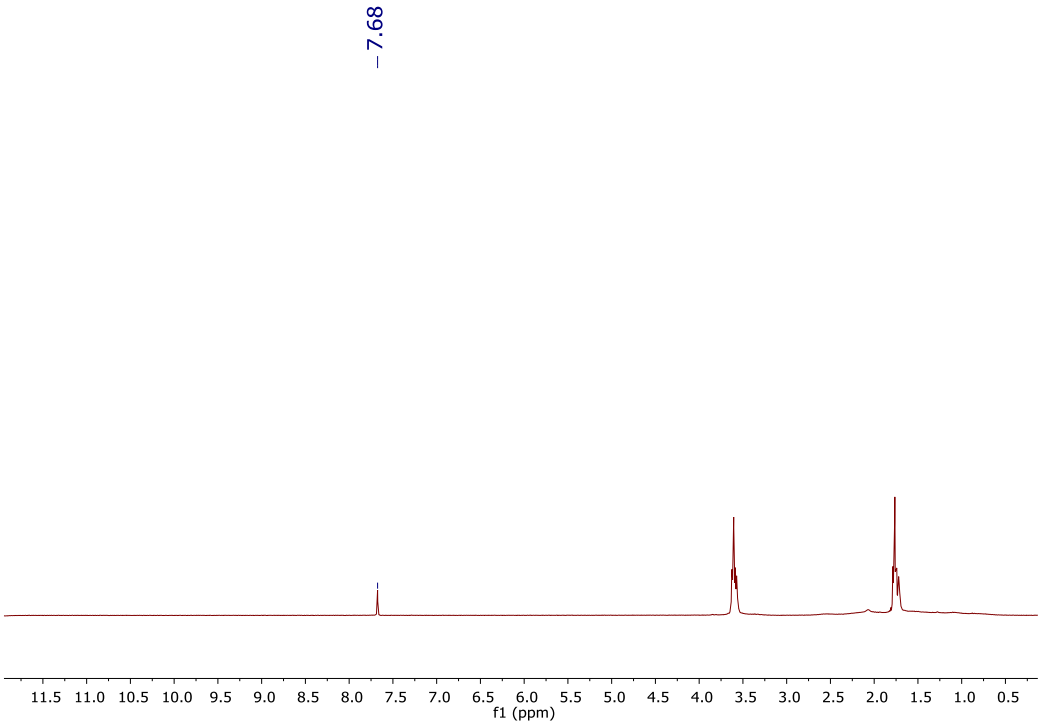

Figure 2-6. ^{1}H NMR of **5[Li^{+}]** in tetrahydrofuran-d_8.

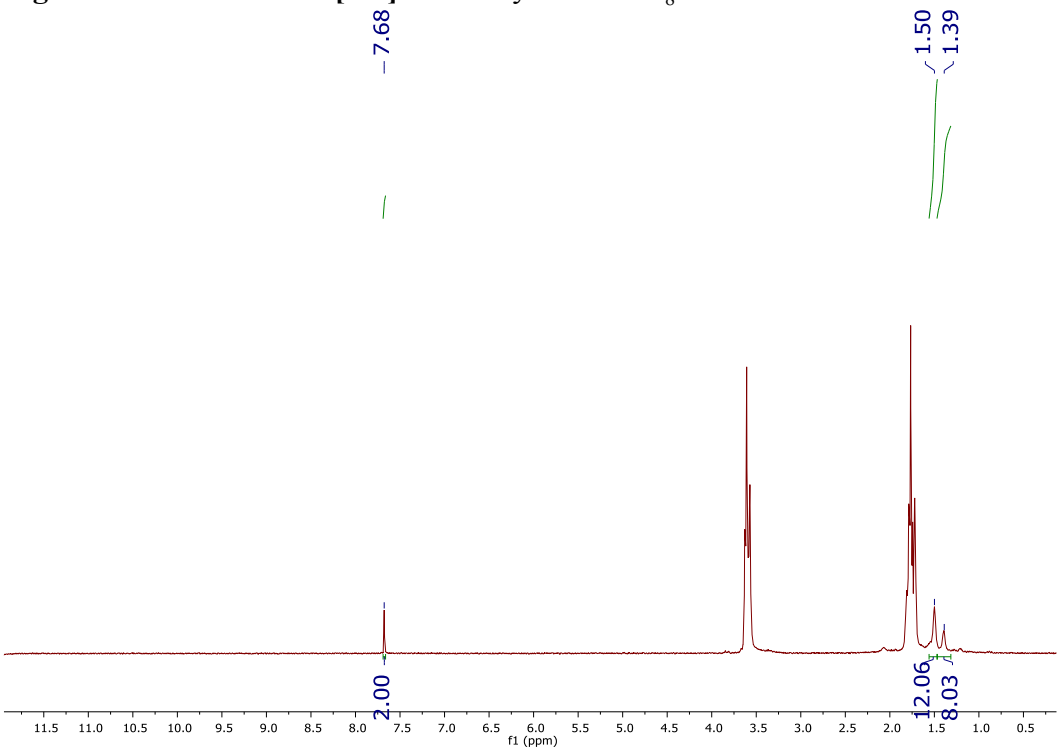

Figure 2-7. ^{1}H (^{11}B-dec) NMR of **5[Li^{+}]** in tetrahydrofuran-d_8.

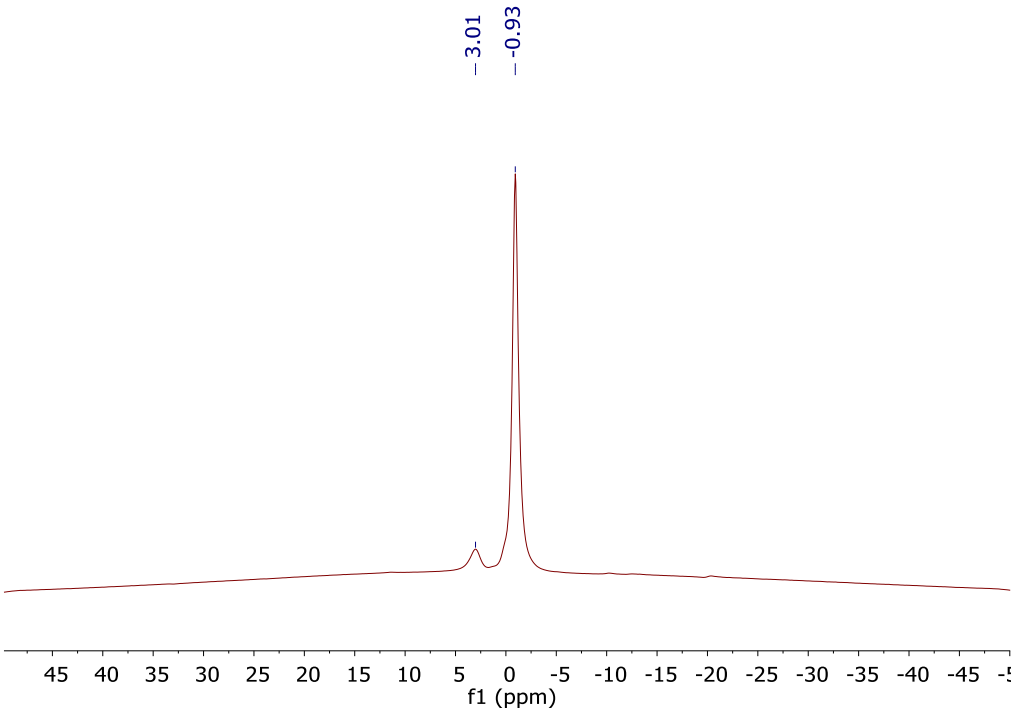

Figure 2-8. ^{1}B (^{1}H-dec) NMR of **5[Li^{+}]** in tetrahydrofuran-d_8.

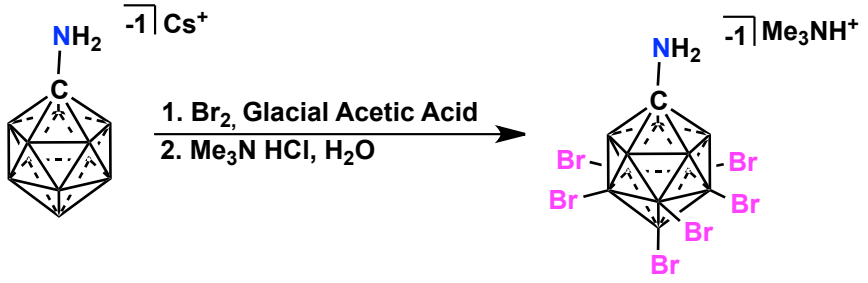

Scheme 2-6 Synthesis of Hexabrominated Carboranyl Amine, $\mathbf{7_{Br}[Me_3NH^+]}$

4[Cs$^+$] (1.0 g, 2.06 mmol) was placed in a 100 mL round bottom flask, and 10 mL of bromine and 5 mL of triflic acid were added. The reaction was heated to 50 °C and stirred open to atmosphere for 5 days, monitored by mass spectroscopy. The reaction was filtered on a medium porosity fritted funnel and washed with 10 mL of dichloromethane. The solid on the fritted funnel was then dissolved in ethyl acetate. 150 mL of water was added to the ethyl acetate solution and was titrated with a 10% aq. sodium sulfite solution. The organic layer was then separated, and the aqueous solution was extracted with another 100 mL of ethyl acetate. The organic layers were combined and then pumped down to dryness. In 100 mL of H_2O, **7_{Br}[Cs$^+$]** was stirred with an excess of trimethylammonium hydrochloride, NMe_3HCl. A white precipitate formed of **$7_{Br}[Me_3NH^+]$** and was collected by filtration and dried under vacuum to afford the product in 68% yield (1.41 grams, 1.40 mmol). ^{1}H NMR (300 MHz, acetonitrile-d$_3$, 25°C): δ = 2.49 (s, 2H, N-H), 3.50-0.80 (bm, 5H, B-H); ^{1}H (^{11}B-dec) NMR (124 MHz, acetonitrile-d$_3$, 25°C): δ = 2.58, (s, 5H, B-H), 2.49 (s, 2H, N-H); ^{11}B (^{1}H-dec) NMR (96 MHz, acetonitrile-d$_3$, 25 °C): δ = 0.1, -7.3, -15.6 ppm.

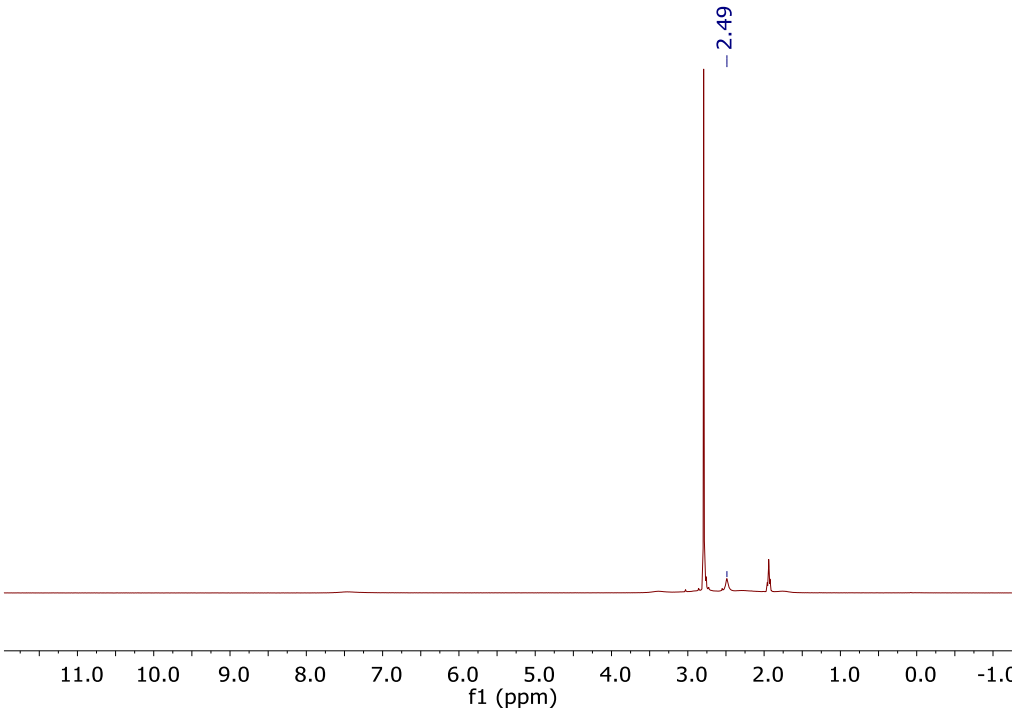

Figure 2-9. ^{1}H NMR of **7_{Br}[Me_3NH^+]** in acetonitrile-d_3. The Me_3NH^+ countercation appears at 2.73 ppm.

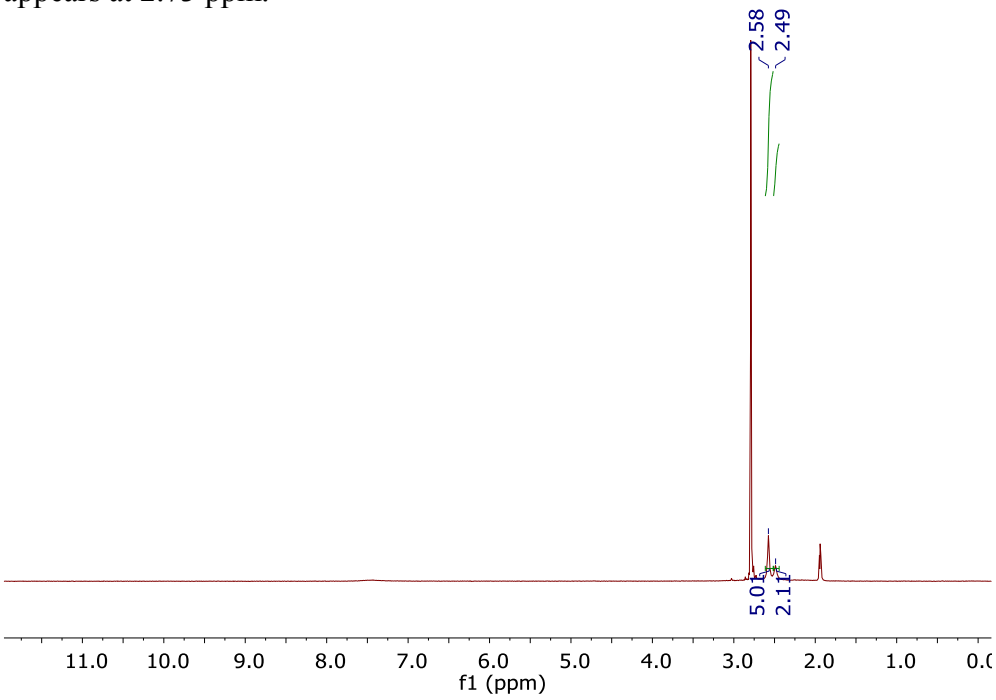

Figure 2-10. ^{1}H (^{11}B-dec) NMR of **7_{Br}[Me_3NH^+]** in acetonitrile-d_3. The Me_3NH^+ countercation appears at 2.73 ppm.

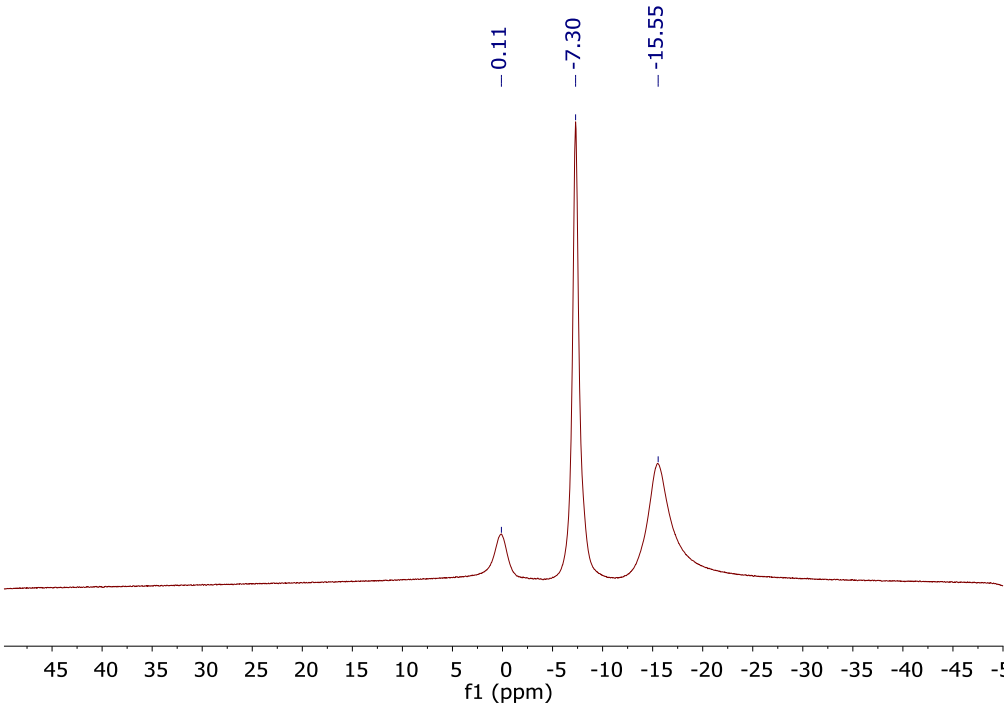

Figure 2-11. ^{11}B (^{1}H-dec) NMR of $\mathbf{7_{Br}[Me_3NH^+]}$ in acetonitrile-d_3.

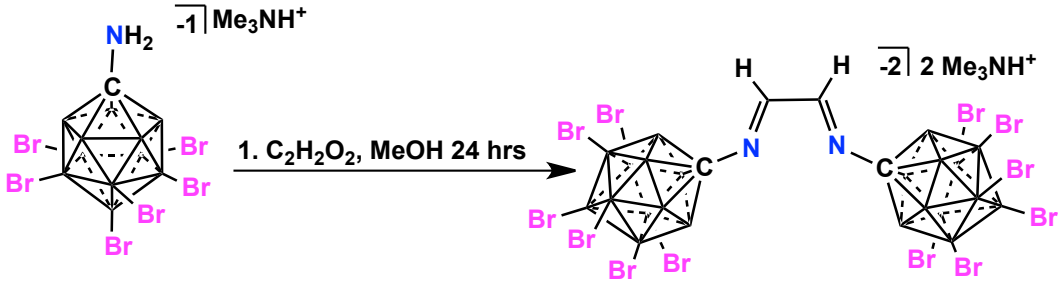

Scheme 2-7. Synthesis of Dianionic Carboranyl Diimine, $\mathbf{8_{Br}[Me_3NH^+]}$

In 50 mL of tetrahydrofuran, $\mathbf{7_{Br}[Me_3NH^+]}$ (0.51 grams, 0.74 mmol) was dissolved and an aqueous solution of glyoxal ($O_2C_2H_2$) (40% w/w, 0.50 mL, 0.40 mmol) was added. The reaction mixture was stirred for 24 hours, heating at 60 °C. Volatiles were removed under high vacuum to afford the product $\mathbf{8_{Br}[Me_3NH^+]}$: $[N_2C_4B_{22}H_{12}Br_{12}{}^{2-}]2[(CH_3)_3NH^+]$. 98% yield (0.50 grams, 0.72 mmol). ^{1}H NMR (300 MHz, acetonitrile-d_3, 25 °C): δ = 7.75 (s, 2H), 3.50- 1.0 (bm,10H, B-H); ^{1}H (^{11}B-dec) NMR (300 MHz, acetonitrile-d_3, 25 °C): δ = 7.75 (s, 2H), 2.61 (s, 10H, B-H); ^{11}B (^{1}H-dec) NMR (96 MHz, acetonitrile-d_3, 25 °C): δ = 0.9, -6.6, -14.7 ppm.

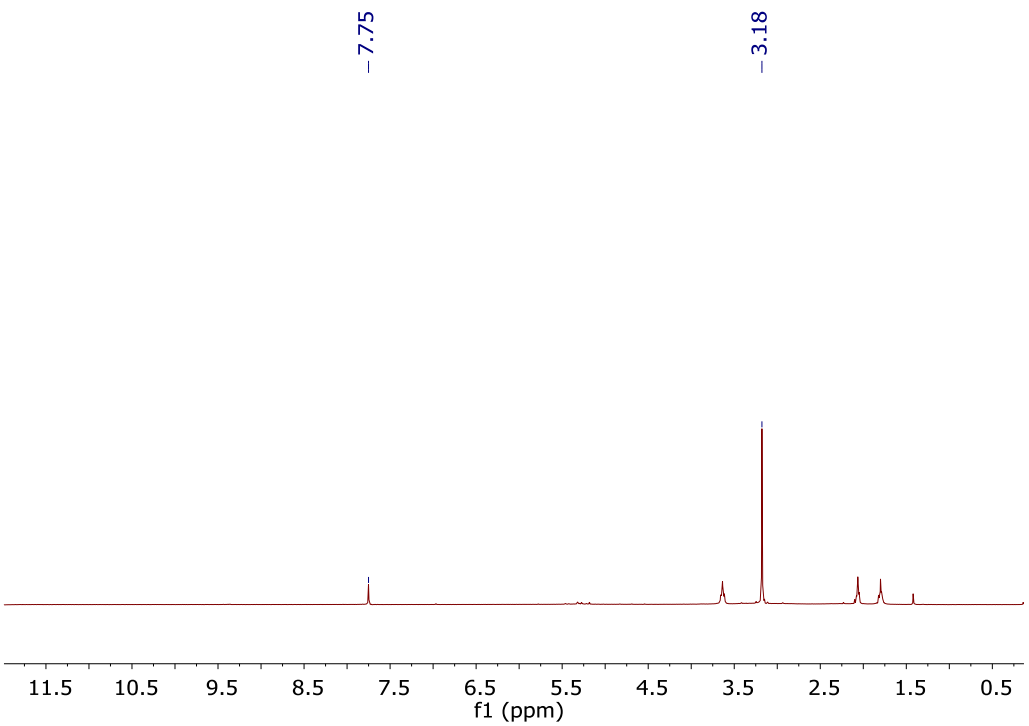

Figure 2-12. ^{1}H NMR of **8_{Br}[Me_3NH^+]** in acetonitrile-d_3. The Me_3NH^+ countercation appears at 3.18 ppm. Note: trace tetrahydrofuran at 1.77 and 3.65 ppm.

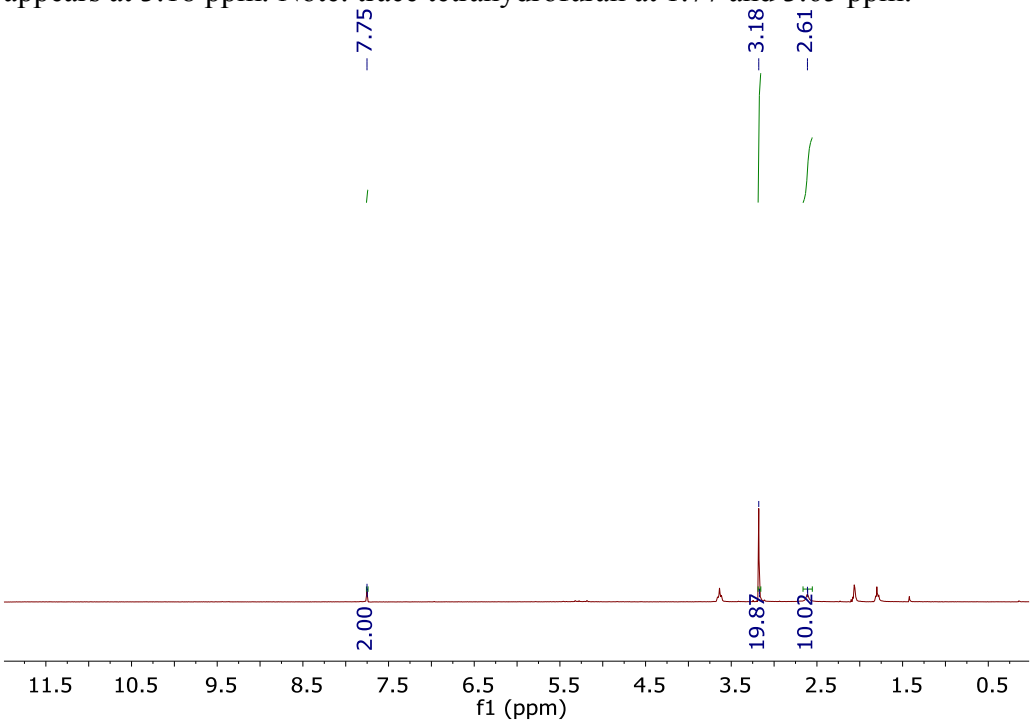

Figure 2-13. ^{1}H (^{11}B-dec) NMR of **8_{Br}[Me_3NH^+]** in acetonitrile-d_3. Me_3NH^+ appears at 3.18 ppm and integrates to 2 equivalents. Note: trace tetrahydrofuran at 1.77 and 3.65 ppm.

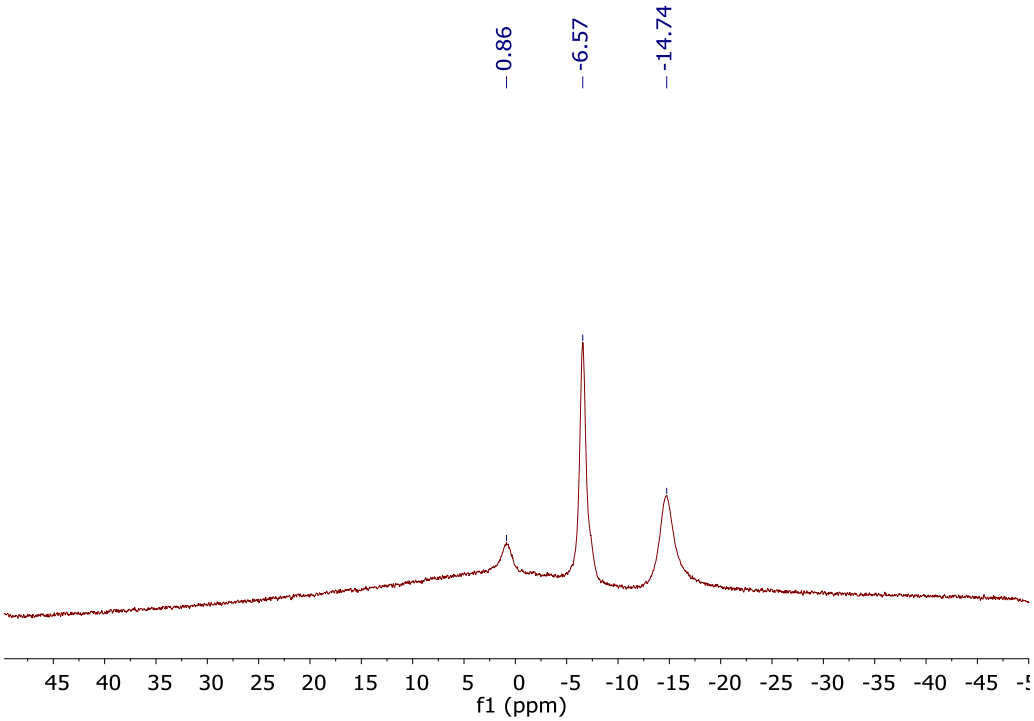

Figure 2-14. ^{11}B (^{1}H-dec) NMR of **8_{Br}[Me_3NH^+]** in acetonitrile-d_3.

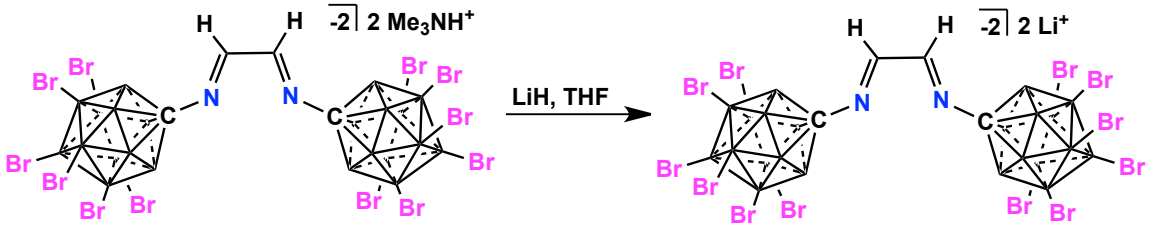

Scheme 2-8. Synthesis of Hexabrominated Dianionic Carboranyl Diimine, $\mathbf{8_{Br}[Li^+]}$

$\mathbf{8_{Br}[Me_3NH^+]}$ was dried under high vacuumn and brought into the glove box. Under inert atmosphere, 0.20 grams (0.14 mmol) of $\mathbf{8_{Br}[Me_3NH^+]}$ was weighed out and added to a 20 mL scintillation vial equipped with a stir bar. To the vial, ~ 10 mL of tetrahydrofuran was added. On a weigh paper, 5 mg (0.63 mmol) of lithium hydride was weighed out. While stirring, the LiH was added to the vial of $\mathbf{8_{Br}[Me_3NH^+]}$. The reaction began to bubble at the addition of each portion, and when it subsided the next portion was added. After all of the LiH was added to the vial, it was capped and stirred for an additional hour. The crude solution of $\mathbf{8_{Br}[Li^+]}$ was filtered and then concentrated to ~ 3 mL, and added dropwise to a second scintillation vial containing 15 mL of diethyl ether, while stirring. The vial was capped and stirred for 2 hours. The diethyl ether was decanted and the product was dried under vacuumn, affording $\mathbf{8_{Br}[Li^+]}$ in 89% yield (225 mg, 0.12 mmol). Note: There are 4 THF coordinated to each Li^+ countercation. ^{1}H NMR (300 MHz, acetonitrile-d_3, 25 °C): δ =7.64 (s, 2H), 3.50-0.70 (bm, 10H, B-H); ^{1}H (^{11}B-dec) NMR (300 MHz, acetonitrile-d_3, 25 °C): δ = 7.64 (s, 2H), 2.54 (s, 10H, B-H); ^{11}B (^{1}H-dec) NMR (96 MHz, acetonitrile-d_3, 25 °C): δ = 0.6, -6.6, -14.6 ppm.

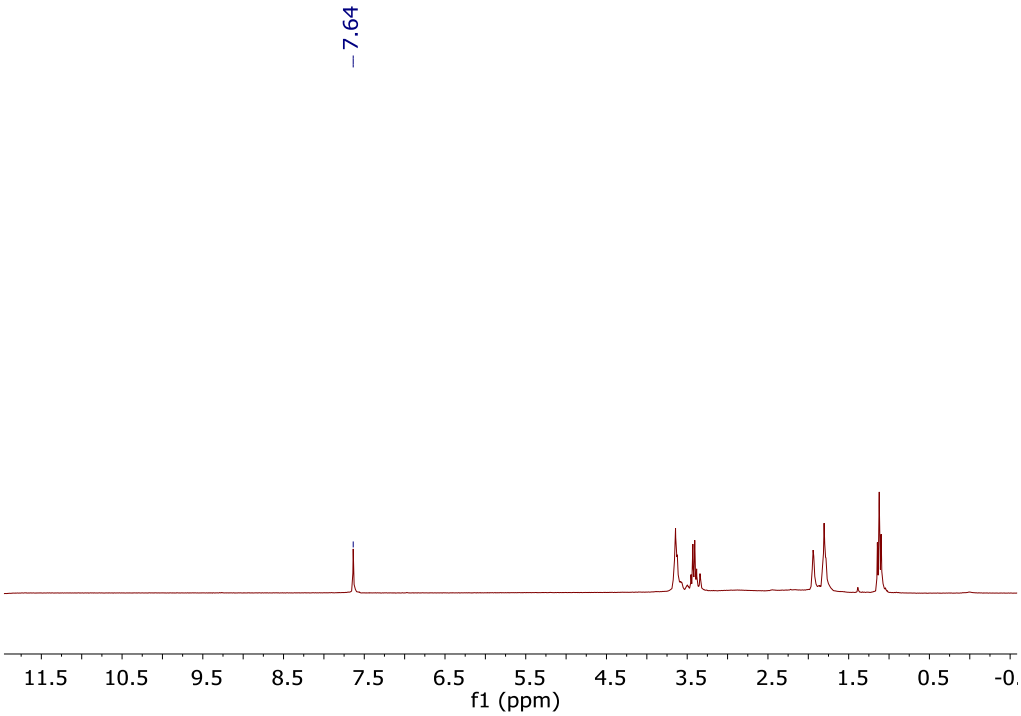

Figure 2-15. ^{1}H NMR of $\mathbf{8_{Br}[Li^{+}]}$ in acetonitrile-d_3. Note: tetrahydrofuran at 1.77 and 3.65 ppm, and diethyl ether at 1.12 and 3.40 ppm.

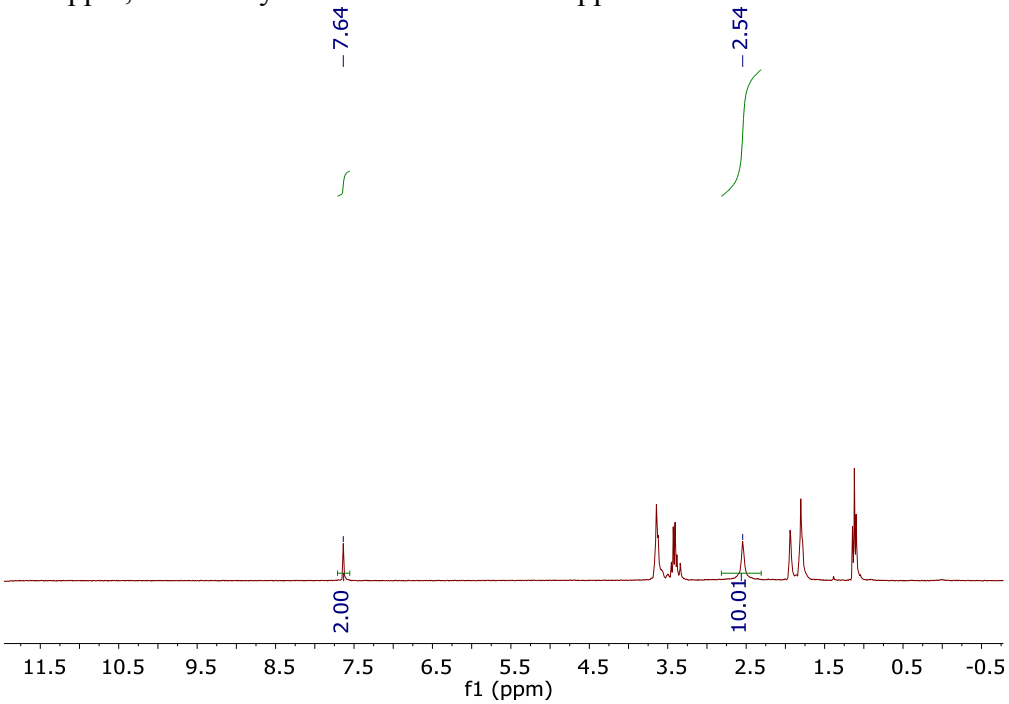

Figure 2-16. ^{1}H (^{11}B-dec) NMR of $\mathbf{8_{Br}[Li^{+}]}$ in acetonitrile-d_3. Note: tetrahydrofuran at 1.77 and 3.65 ppm, and diethyl ether at 1.12 and 3.40 ppm.

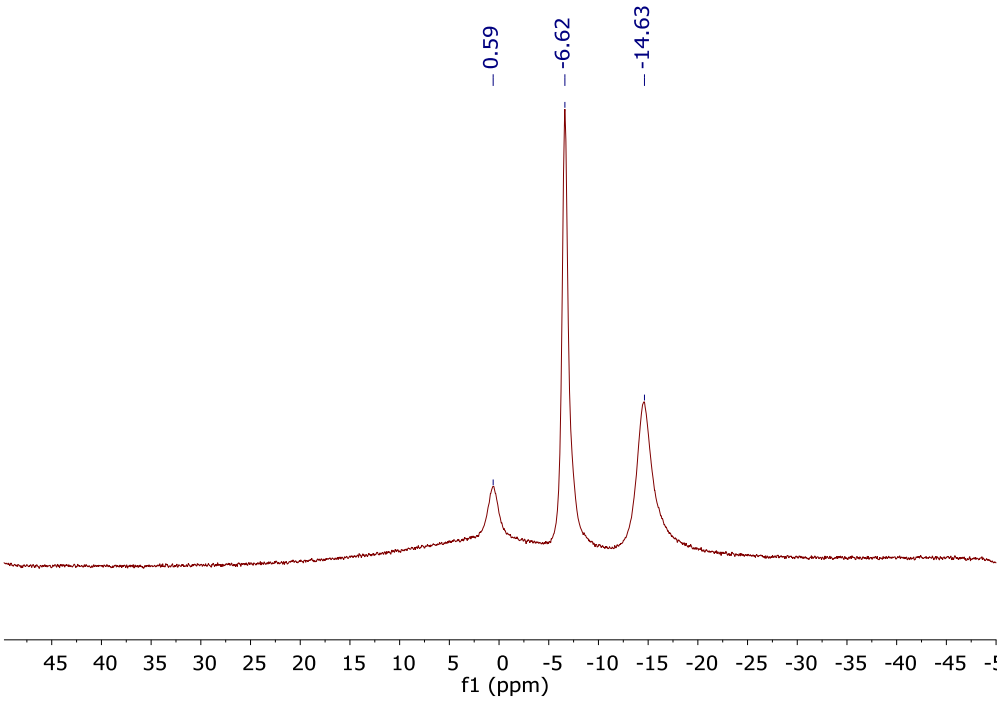

Figure 2-17. ^{11}B (^{1}H-dec) NMR of $\mathbf{8_{Br}[Li^{+}]}$ in acetonitrile-d_3.

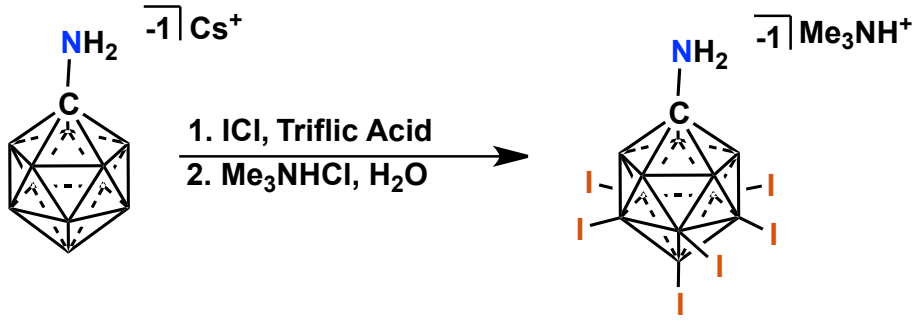

Scheme 2-9. Synthesis of Hexaiodinated Carboranyl Amine, **7_I[Me_3NH^+]**

4[Cs^+] (1.0 g, 2.06 mmol) was placed in a 100 mL round bottom flask, and 20 mL of triflic acid and 20 mL of iodine monochloride were added. The reaction was heated to 50 °C and stirred open to atmosphere for 5 days, monitored by mass spectroscopy. The reaction was filtered on a medium porosity fritted funnel and washed with 100 mL of dichloromethane. The solid on the fritted funnel was then dissolved in ethyl acetate. 150 mL of water was added to the ethyl acetate solution and was titrated with a 10% aq. sodium sulfite solution. The organic layer was then separated, and the aqueous solution was extracted with another 100 mL of ethyl acetate. The organic layers were combined and then pumped down to dryness. In 100 mL of H_2O, **7_I[Cs^+]** was stirred with an excess of trimethylammonium hydrochloride, NMe_3HCl. A white precipitate formed of **7_I[Me_3NH^+]** and was collected by filtration and dried under vacuum to afford the product in 72% yield (1.42 grams, 1.48 mmol). ^{1}H NMR (300 MHz, acetonitrile-d_3, 25°C): δ = 4.20-0.10 (bm, 5H, B-H); ^{1}H (^{11}B-dec) NMR (124 MHz, acetonitrile-d_3, 25°C): δ = 3.25 (s, 5H, B-H); ^{11}B (^{1}H-dec) NMR (96 MHz, acetonitrile-d_3, 25 °C): δ = -6.2, -8.8, -16.9 ppm.

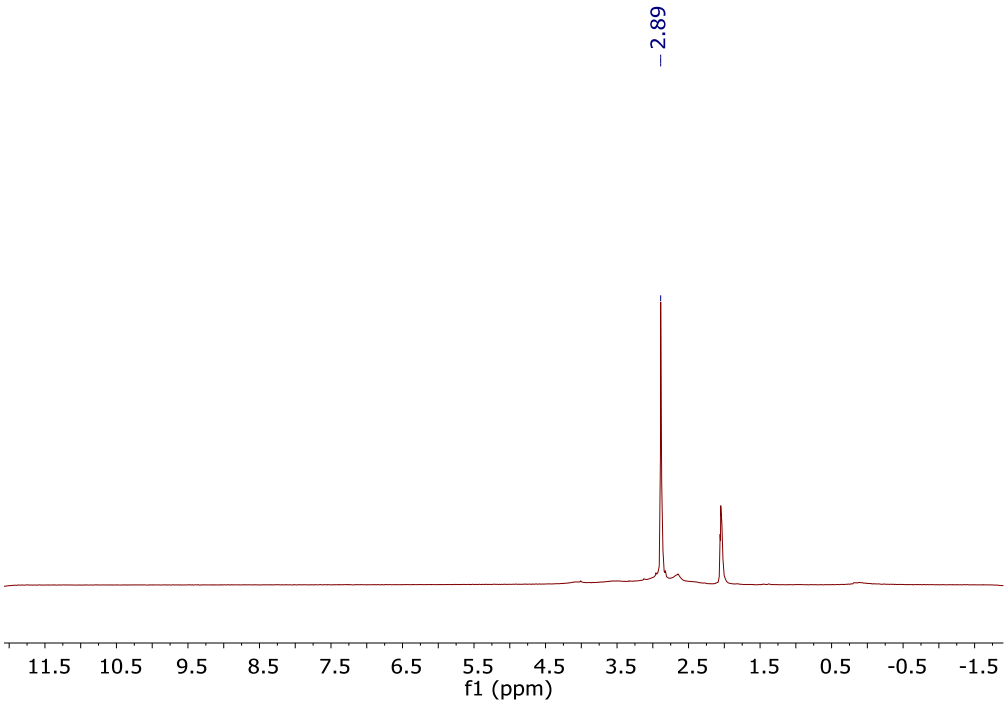

Figure 2-18. ^{1}H NMR of **7_I[Me_3NH^+]** in acetonitrile-d_3. The Me_3NH^+ countercation appears at 2.89 ppm.

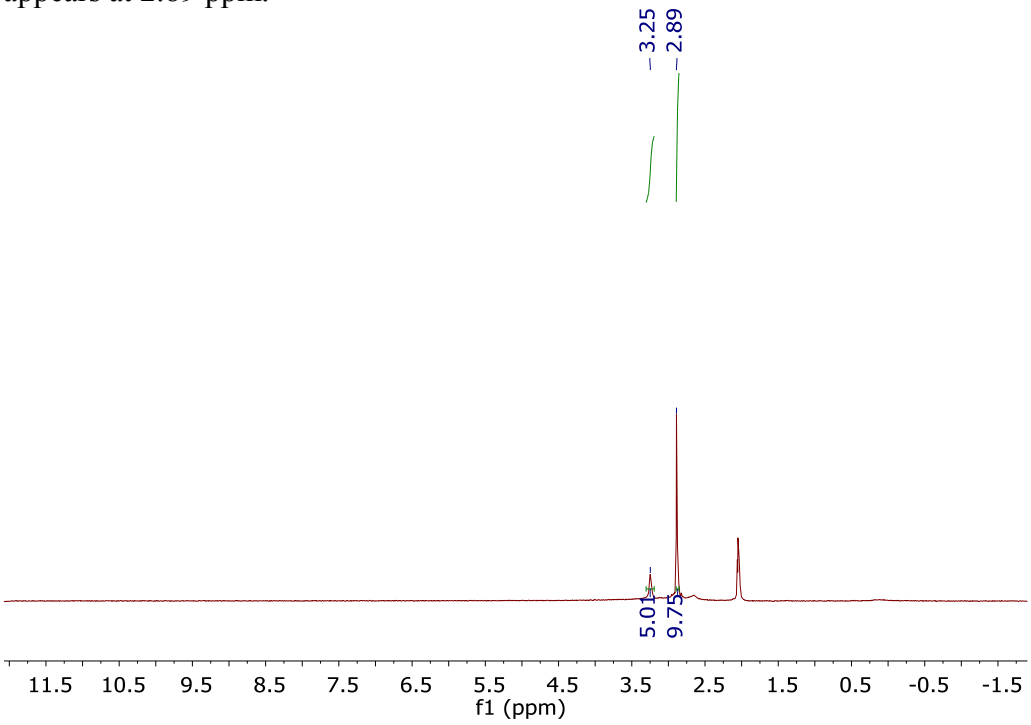

Figure 2-19. ^{1}H (^{11}B-dec) NMR of **7_I[Me_3NH^+]** in acetonitrile-d_3. The Me_3NH^+ countercation appears at 2.83 ppm and integrates to 1 equivalent.

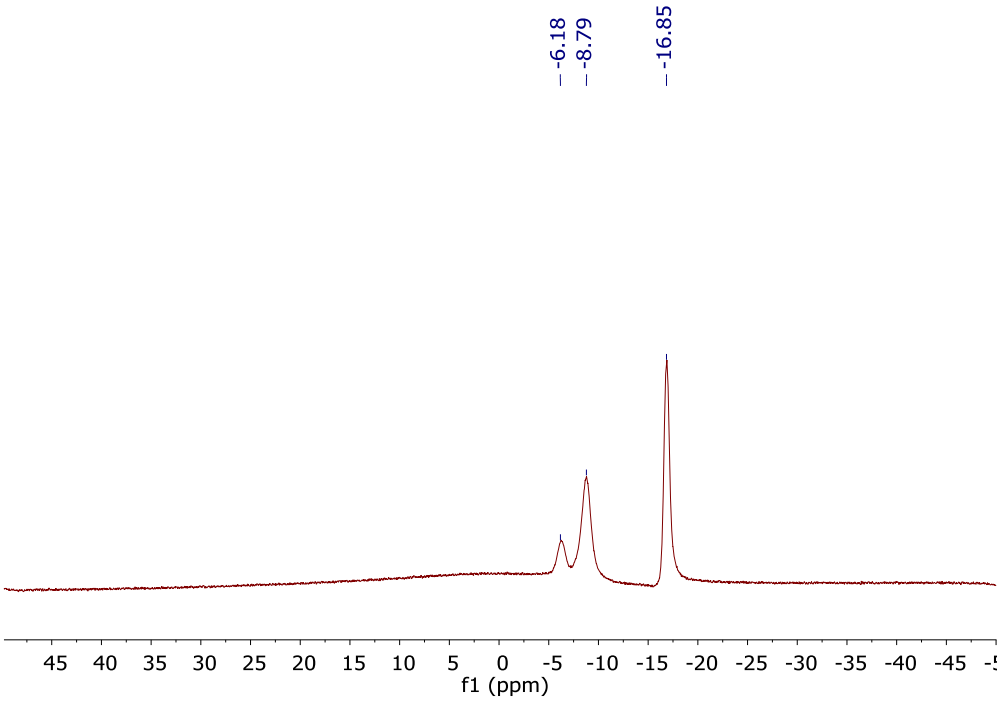

Figure 2-20. ^{11}B (^{1}H-dec) NMR of **7_I[Me_3NH^+]** in acetonitrile-d_3.

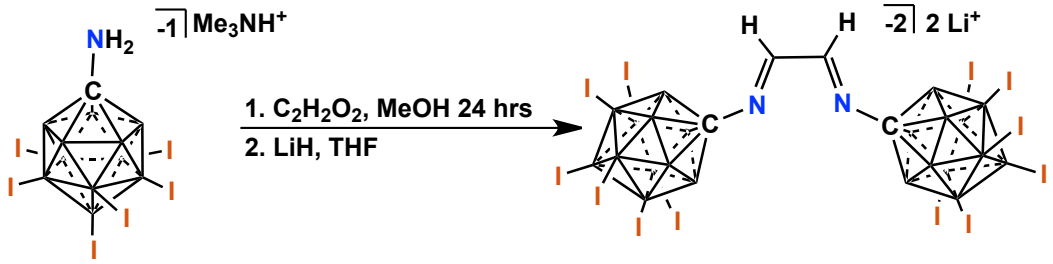

Scheme 2-10. Synthesis of Hexaiodinated Dianionic Carboranyl Diimine, $\mathbf{8_I[Li^+]}$:

In 50 mL of tetrahydrofuran, $\mathbf{7_I[Me_3NH^+]}$ (0.50 grams, 0.52 mmol) was dissolved and an aqueous solution of glyoxal ($O_2C_2H_2$) (40% w/w, 0.03 mL, 0.28 mmol) was added. The reaction mixture was stirred for 24 hours, heating at 60 °C. Volatiles were removed under high vacuum to afford the product $\mathbf{8_I[Me_3NH^+]}$: $[N_2C_4B_{22}H_{12}I_{12}{}^{2-}]2[(CH_3)_3NH^+]$. $\mathbf{8_I[Me_3NH^+]}$ was dried under high vacuumn and brought into the glove box. Under inert atmosphere, 0.30 grams (0.15 mmol) of $\mathbf{8_I[Me_3NH^+]}$ was weighed out and added to a 20 mL scintillation vial equipped with a stir bar. To the vial, ~ 10 mL of tetrahydrofuran was added. On a weigh paper, 10 mg of lithium hydride was weighed out. While stirring, the LiH was added in small portions to the vial of $\mathbf{8_I[Me_3NH^+]}$. The reaction began to bubble at the addition of each portion, and when it subsided the next portion was added. After all of the LiH was added to the vial, it was capped and stirred for an additional hour. The crude solution of $\mathbf{8_I[Li^+]}$ was filtered and then concentrated to ~ 3 mL, and added dropwise to a second scintillation vial containing 15 mL of hexanes, while stirring. The vial was capped and stirred for 2 hours. The hexanes were decanted and the product was dried under vacuumn, affording $\mathbf{8_I[Li^+]}$ in 62% yield (0.219 grams, 0.09 mmol). ^{1}H NMR (300 MHz, tetrahydrofuran-d_8, 25 °C): δ = 7.75 (s, 2H), 4.50-0.70 (bm, 10H, B-H); ^{1}H (^{11}B-dec) NMR

(300 MHz, tetrahydrofuran-d_8, 25 °C): δ = 7.75 (s, 2H), 3.11 (s, 10H, B-H); ^{11}B (^{1}H-dec) NMR (96 MHz, tetrahydrofuran-d_8, 25 °C): δ = -7.6, -12.6, -19.6 ppm.

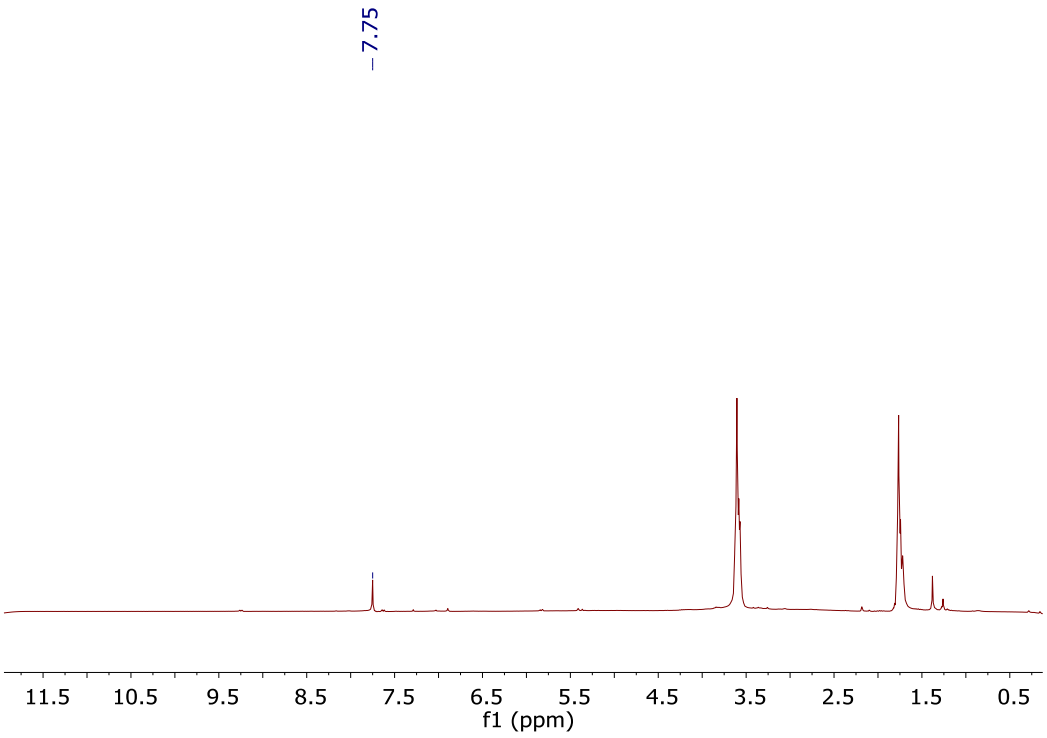

Figure 2-21. ^{1}H NMR of **8_I[Li^+]** in tetrahydrofuran-d_8.

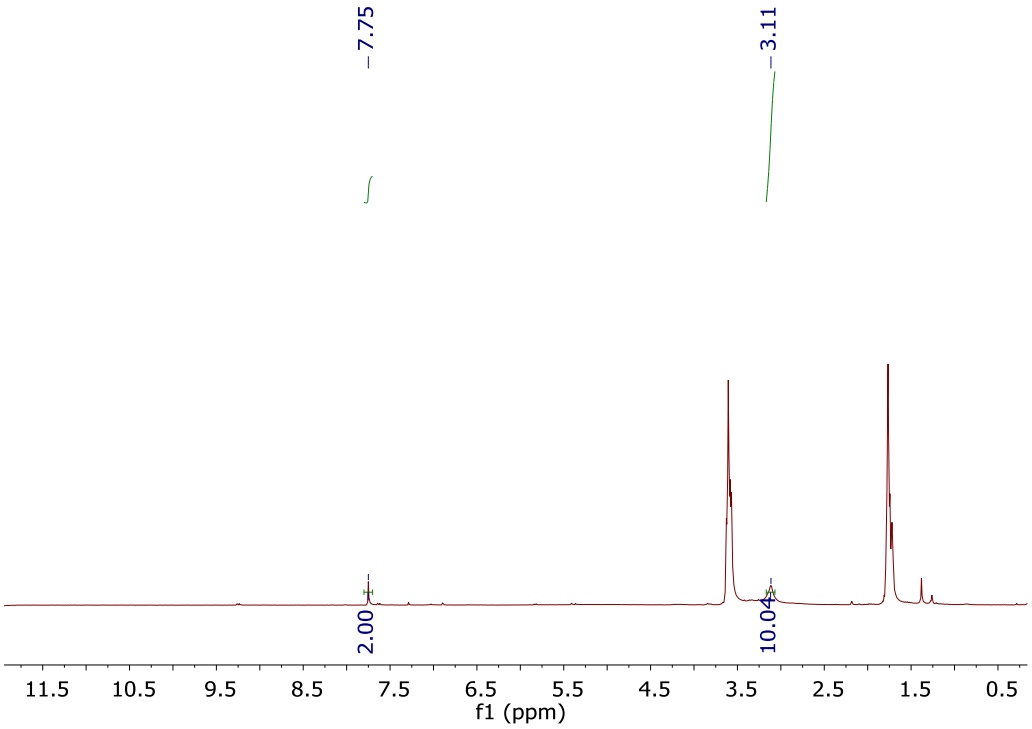

Figure 2-22. ^{1}H (^{11}B-dec) NMR of **8_I[Li^+]** in tetrahydrofuran-d_8.

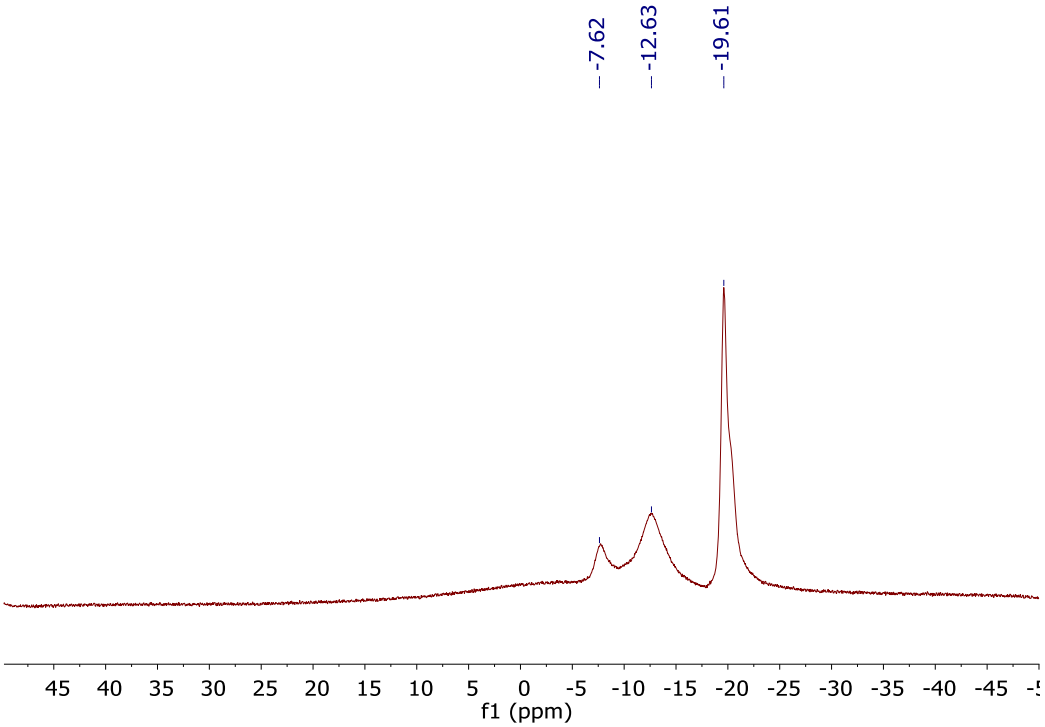

Figure 2-23. ^{11}B (^{1}H-dec) NMR of **8_I[Li^+]** in tetrahydrofuran-d_8.

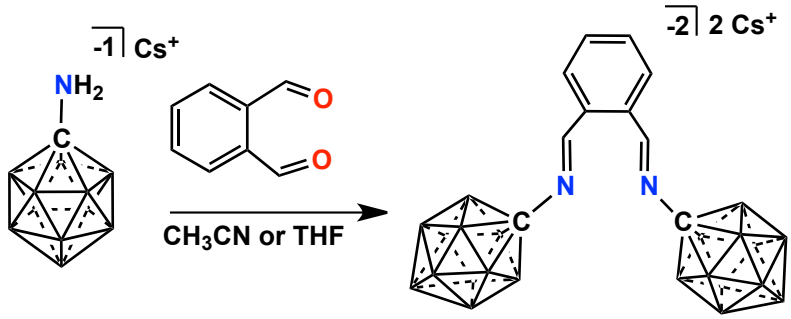

Scheme 2-11. Synthesis of Dianionic Carboranyl Phenyl Diimine, **9[Cs$^+$]**:

In 30 mL of tetrahydrofuran, $NH_2CB_{11}H_{11}^-Cs^+$ **4** (1.30 grams, 4.47 mmol) was dissolved and *o*-phthaldehyde ($O_2C_8H_6$) (0.30 g, 2.24 mmol) was added. The solution was stirred for 24 hours. Volatiles were removed under reduced pressure to afford the crude mixture of **9[Cs$^+$]**, **10[Cs$^+$]**, **11[Cs$^+$]**. The mixure was converted to the trimethyl ammonium cation by dissolving it in H_2O (100 mL) followed by the addition of 4 eq. (13.6 mmol, 1.3 grams) of trimethylammonium hydrochloride, NMe_3HCl. A white precipitate formed and was collected by filtration and dried under vacuum. The product was washed 5 x 70 mL with methylene chloride, extracting **11[Me$_3$NH$^+$]**. The remaining insoluble precipitate was dried, redissolved in a solution of H_2O and excess CsCl, forming **9[Cs$^+$]** with traces of **10[Cs$^+$]**, **11[Cs$^+$]**.The precipitate was collected and washed with diethyl ether. ^{1}H NMR (300 MHz, acetonitrile-d_3, 25 °C): δ = 8.95 (s, 2H), 7.80 (m, 2H), 7.40 (m, 2H) 2.75-0.50 (bm, 22H, B-H) ppm.

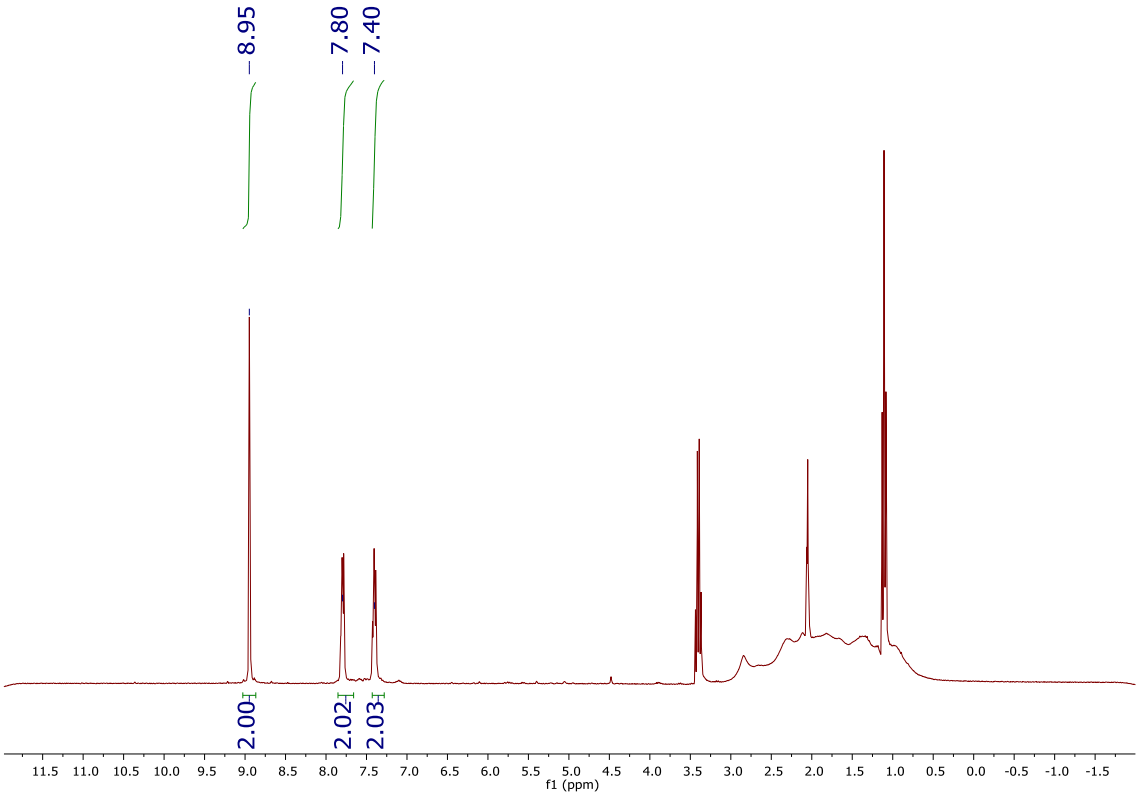

Figure 2-24. ^{1}H NMR of **9[Cs^{+}]** in acetonitrile-d_3. Trace amount of **11[Cs^{+}]** appears at 4.5 ppm and in the aromatic reigon. Diethyl ether appears at 1.13 and 3.48 ppm.

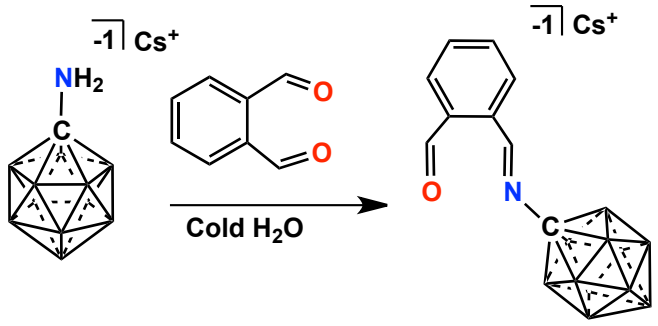

Scheme 2-12. Synthesis of Benzene-1-Carboxaldehyde-2-Carboranyl Imine, **10[Cs$^+$]**:

In an ice bath, a 100 mL round bottom flask containing a solution of $NH_2CB_{11}H_{11}^-Cs^+$ **1** (0.50 grams, 1.72 mmol) dissolved in 30 mL H_2O was cooled to 0 °C. *O*-phthaldehyde ($O_2C_8H_6$) (0.115 g, 0.86 mmol) was added. A yellow precipitate formed within 10 minutes. The reaction mixture was filtered and the precipitate was washed with 2 x 5 mL with ice cold water. The product was dried under vacuumn, affording the product **10[Cs$^+$]**. 43% yield (0.146 grams, 0.37 mmol) ^{1}H NMR (300 MHz, acetonitrile-d_3, 25 °C): δ = 10.22 (s, 1H), 8.87 (s, 1H), 7.80 (m, 2H), 7.63 (m, 2H) 2.75-0.0 (bm, 22H, B-H); ^{1}H (^{11}B-dec) NMR (300 MHz, acetonitrile-d_3, 25 °C): δ =10.22 (s, 1H), 8.87 (s, 1H), 7.79 (m, 2H), 7.62 (m, 2H) 1.96 (s, 6H, B-H) 1.51 (s, 5H, B-H); ^{11}B (^{1}H-dec) NMR (96 MHz, acetonitrile-d_3, 25 °C): δ = -5.4, -8.7 ppm.

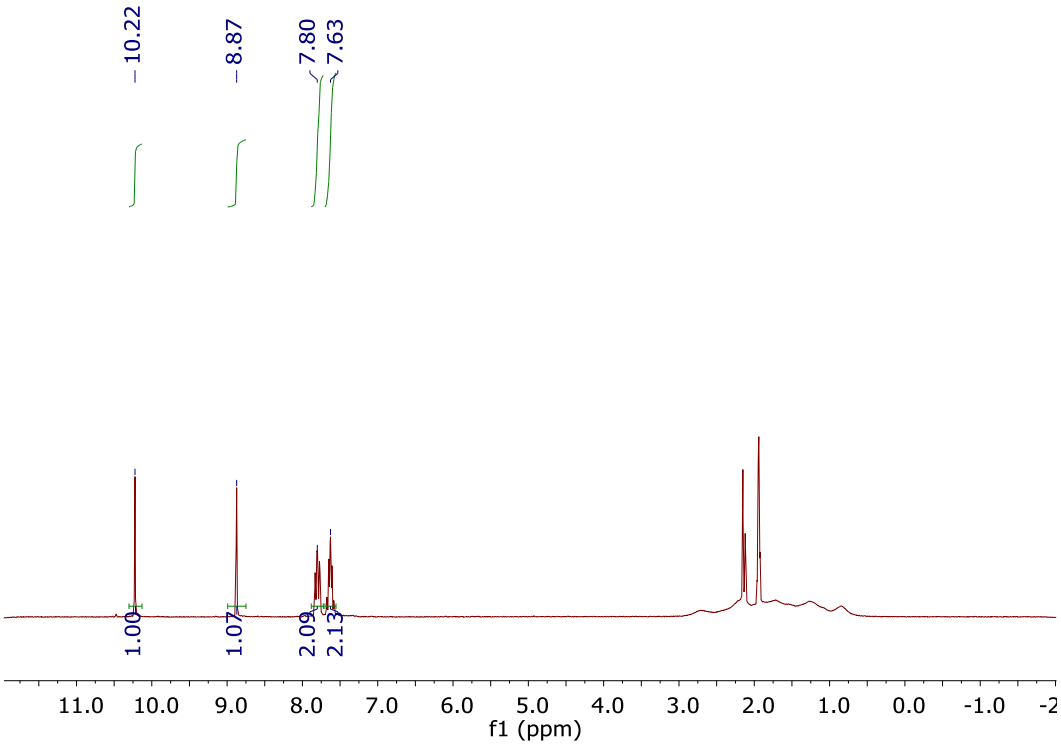

Figure 2-25. ^{1}H NMR of **10[Cs^{+}]** in acetonitrile-d$_3$, H$_2$O is present at 2.23 ppm.

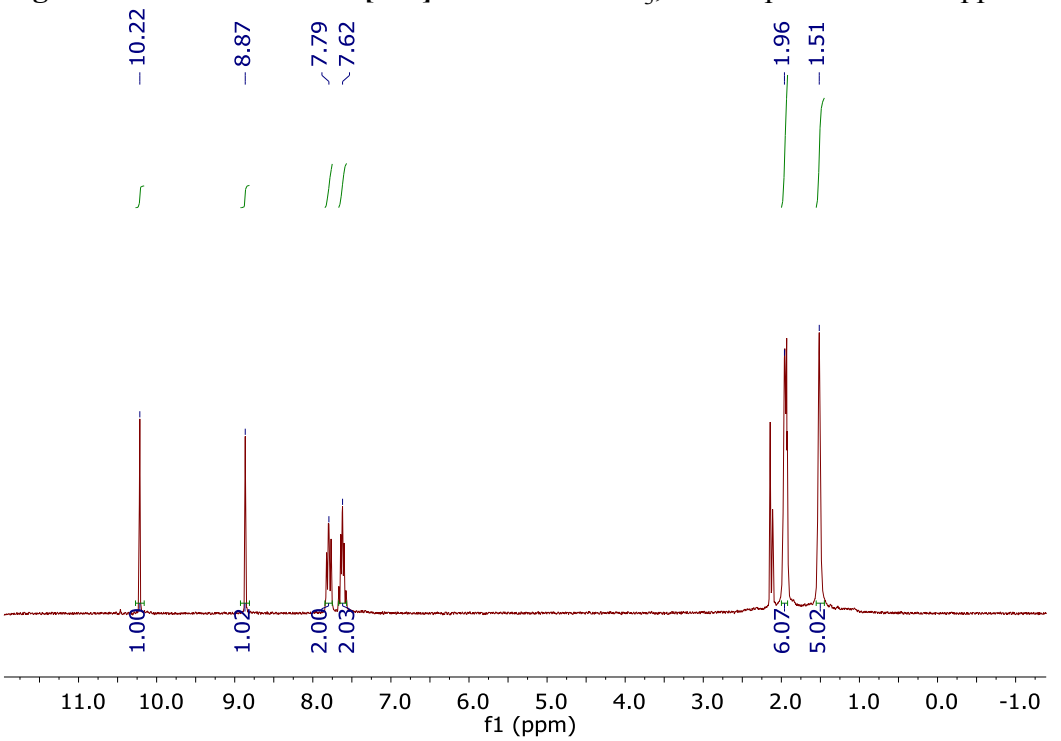

Figure 2-26. ^{1}H (^{11}B-dec) NMR of **10[Cs^{+}]** in acetonitrile-d$_3$, H$_2$O is present at 2.23 ppm.

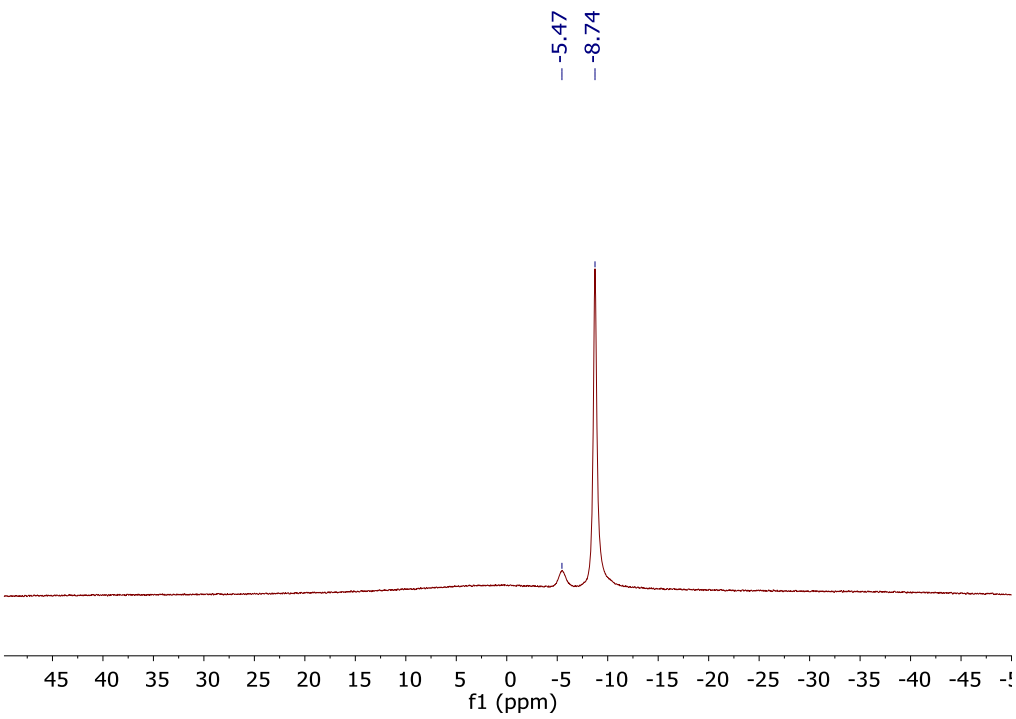

Figure 2-27. ^{11}B (^{1}H-dec) NMR of **10[Cs^+]** in acetonitrile-d_3.

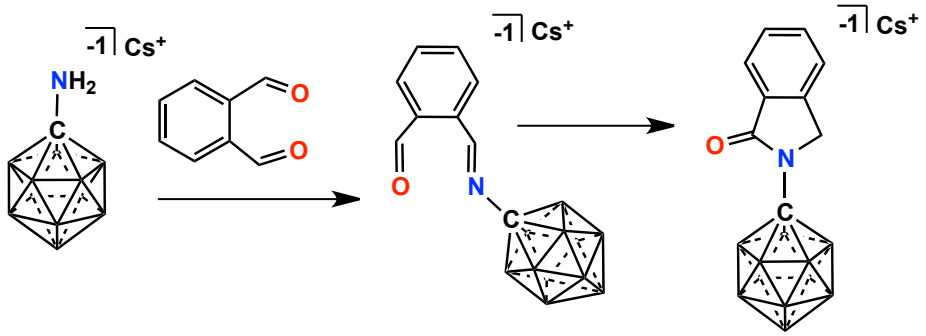

Scheme 2-13. Synthesis of Bicyclic Functionalized Carborane, **11[Me_3NH^+]:**

A crude mixture of **9[Me_3NH^+], 10[Me_3NH^+], 11[Me_3NH^+]** was washed 5 x 70 mL with methylene chloride. The washes were combined and the solution was concentrated down to ~ 10 mL. Crystals suitable for X-ray diffraction formed via slow evaporation. ^1H NMR (300 MHz, acetonitrile-d_3, 25 °C): δ = 7.57 (m, 2H), 7.43 (m, 2H), 4.48 (s, 2H) 3.75-0.50 (bm, 11H, B-H) ppm. ^1H (^{11}B-dec) NMR (300 MHz, acetonitrile-d_3, 25 °C): δ == 7.57 (m, 2H), 7.43 (m, 2H), 4.48 (s, 2H), 2.21 (s, 5H, B-H), 1.58 (s, 1H, B-H) 1.48 (s, 5H, B-H); ^{11}B (^1H-dec) NMR (96 MHz, acetonitrile-d_3, 25 °C): δ = -5.9, -10.9 ppm.

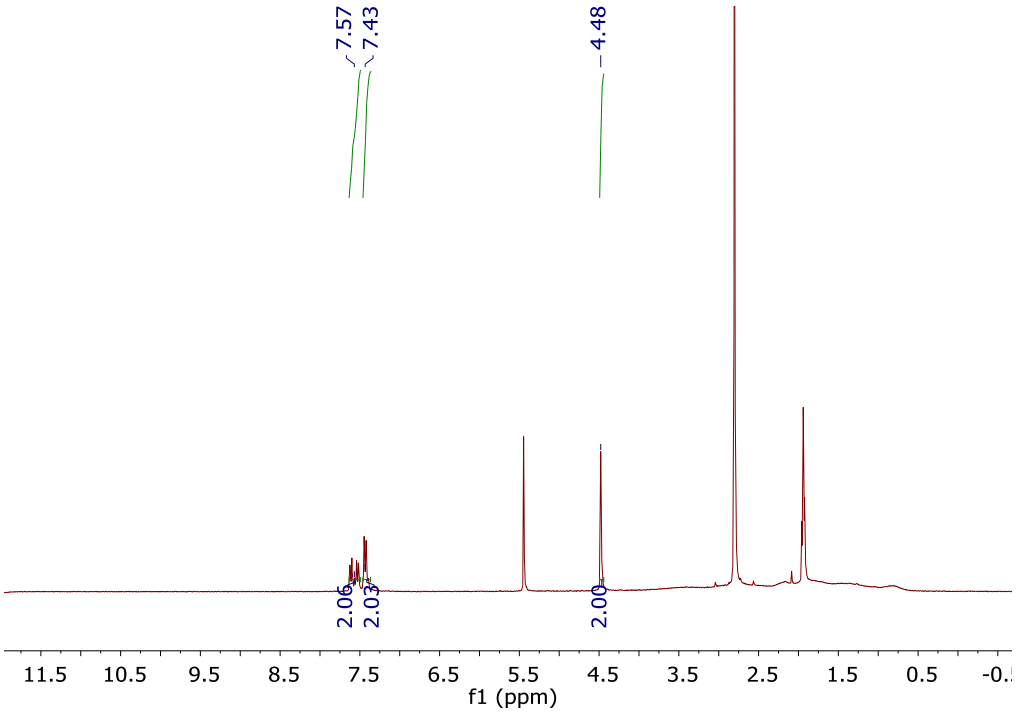

Figure 2-28. ^{1}H NMR of **11[Me$_3$NH$^+$]** in acetonitrile-d$_3$, trimethylammonium cation is present at 2.85 ppm. Dichloromethane is present at 5.44 ppm.

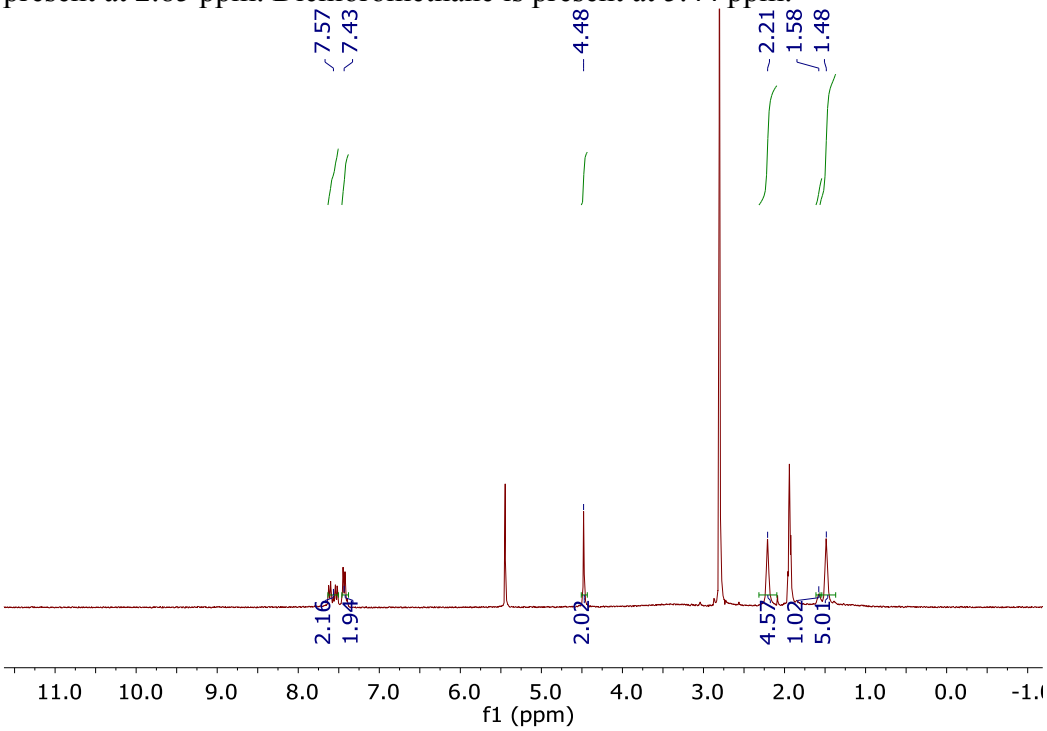

Figure 2-29. ^{1}H (^{11}B-dec) NMR of **11[Me$_3$NH$^+$]** in acetonitrile-d$_3$, trimethylammonium cation is present at 2.85 ppm. Dichloromethane is present at 5.44 ppm.

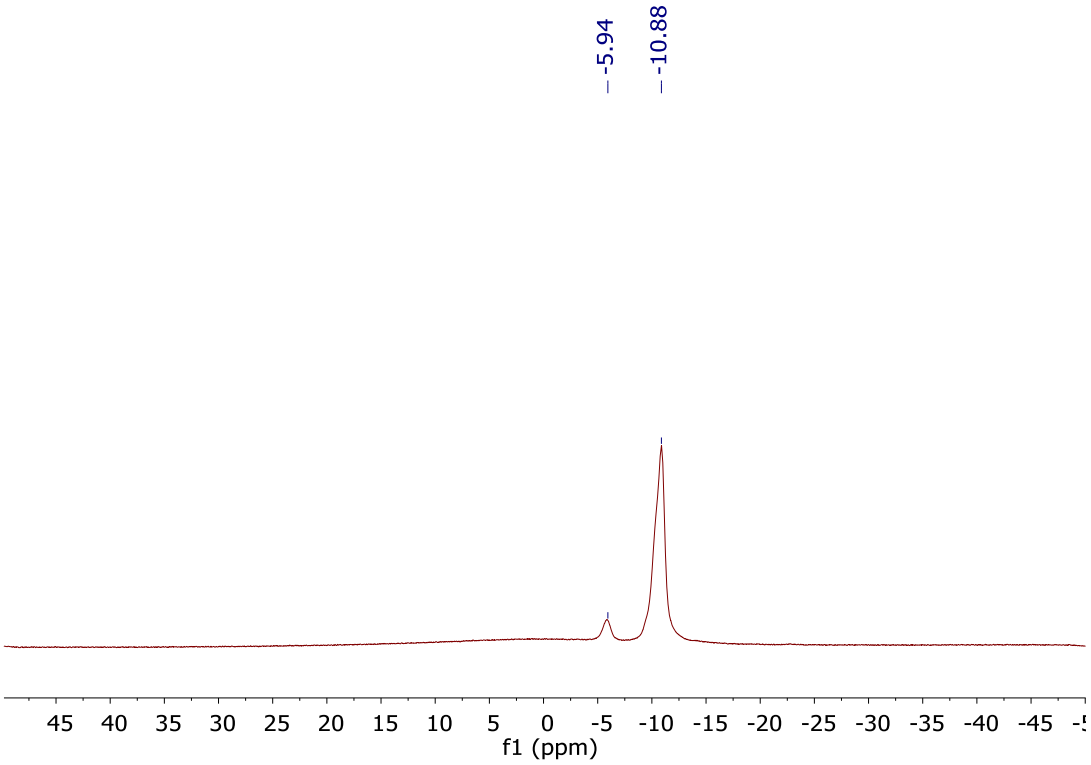

Figure 2-30. ^{11}B (^{1}H-dec) NMR of **11[Me_3NH^+]** in acetonitrile-d_3.

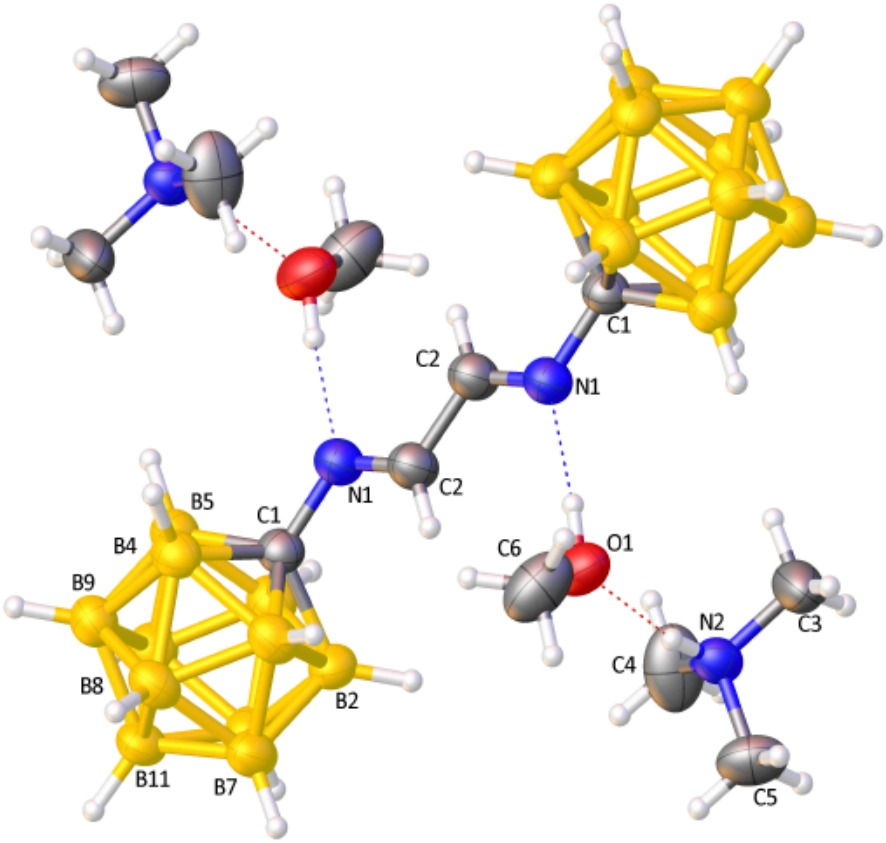

Figure 2-31. X-ray crystal structure of **5[Me_3NH^+]**. Ortep diagram of **5** showing ellipsoids at 50% probability Notes: (a) The crystals were twinned. (b) The $(CH_3)_3NH^+$ was modeled as being disordered over two positions (major shown).

Table 2-1. Crystal data and structure refinement for **5[Me_3NH^+]**.

Identification code	Lavallo08	
Empirical formula	C12 H52 B22 N4 O2	
Molecular formula	C4 H24 B22 N2, 2(C3 H10 N), 2(C H4 O)	
Formula weight	522.39	
Temperature	100.0 K	
Wavelength	1.54178 Å	
Crystal system	Monoclinic	
Space group	P 1 21/c 1	
Unit cell dimensions	a = 7.3464(5) Å	α= 90°.
	b = 9.8692(7) Å	β= 96.234(5)°.
	c = 22.9986(17) Å	γ = 90°.
Volume	1657.6(2) $Å^3$	
Z	2	
Density (calculated)	1.047 Mg/m^3	
Absorption coefficient	0.401 mm^{-1}	
F(000)	556	
Crystal size	0.25 x 0.05 x 0.02 mm^3	
Crystal color, habit	Colorless plate	
Theta range for data collection	3.867 to 68.361°.	
Index ranges	-8<=h<=8, 0<=k<=11, 0<=l<=27	
Reflections collected	2990 (after detwin)	
Independent reflections	2990 [R(int) = 0.1028] (after detwin)	
Completeness to theta = 68.000°	99.4 %	
Absorption correction	Semi-empirical from equivalents	
Max. and min. transmission	0.753056 and 0.526423	
Refinement method	Full-matrix least-squares on F^2	
Data / restraints / parameters	2990 / 38 / 224	
Goodness-of-fit on F^2	1.066	
Final R indices [I>2sigma(I)]	R1 = 0.0953, wR2 = 0.2790	
R indices (all data)	R1 = 0.1061, wR2 = 0.2926	
Extinction coefficient	n/a	
Largest diff. peak and hole	0.330 and -0.294 $e.Å^{-3}$	

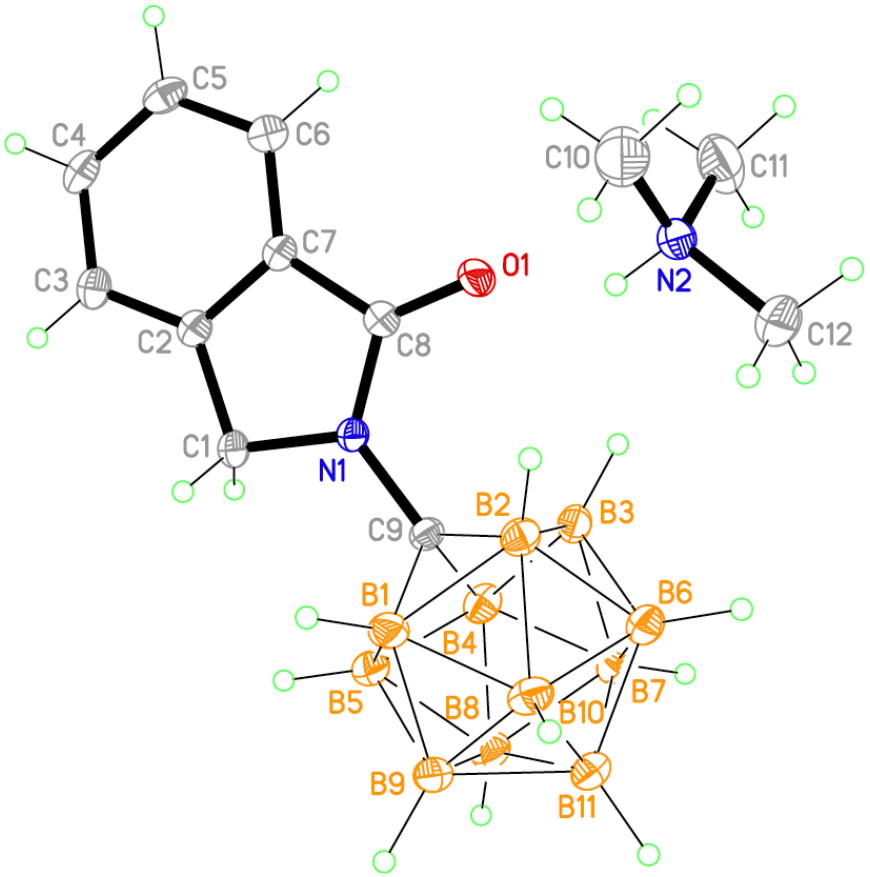

Figure 2-32. X-ray crystal structure of the bicyclic side product, **11[Me_3NH^+]**, resulting from the condensation reaction of *o*-phthaldehyde and **4**.

Table 2-2. Crystal data and structure refinement for **11[Me_3NH^+]**.

Identification code	lavallo12 (SEL-1-94A)	
Empirical formula	C12 H27 B11 N2 O	
Molecular formula	C9 H17 B11 N O, C3 H10 N	
Formula weight	334.27	
Temperature	100(2) K	
Wavelength	0.71073 Å	
Crystal system	Monoclinic	
Space group	P2(1)/n	
Unit cell dimensions	a = 6.9795(6) Å	α= 90°.
	b = 15.4462(14) Å	β = 100.594(3)°.
	c = 18.1602(16) Å	γ = 90°.
Volume	1924.4(3) $Å^3$	
Z	4	
Density (calculated)	1.154 Mg/m^3	
Absorption coefficient	0.062 mm^{-1}	
F(000)	704	
Crystal size	0.25 x 0.15 x 0.12 mm^3	
Crystal color, habit	colourless / BLOCK	
Theta range for data collection	1.74 to 27.01°.	
Index ranges	-8<=h<=8, -19<=k<=19, -22<=l<=23	
Reflections collected	27811	
Independent reflections	4185 [R(int) = 0.0623]	
Completeness to theta = 25.00°	99.9 %	
Absorption correction	multi-scan / sadabs	
Max. and min. transmission	0.9926 and 0.9846	
Refinement method	Full-matrix least-squares on F^2	
Data / restraints / parameters	4185 / 1 / 241	
Goodness-of-fit on F^2	1.037	
Final R indices [I>2sigma(I)]	R1 = 0.0506, wR2 = 0.1330	
R indices (all data)	R1 = 0.0700, wR2 = 0.1465	
Largest diff. peak and hole	0.419 and -0.249 $e.Å^{-3}$	

2.5 *References*

1. Ahmad, E. H.; Vincent, L. *Angewandte Chemie International Edition* **2014**, *53*, 4489.

2. Boffa, L. S.; Novak, B. M. *Chemical Reviews* **2000**, *100*, 1479.

3. Ittel, S. D.; Johnson, L. K.; Brookhart, M. *Chemical Reviews* **2000**, *100*, 1169.

4. Johnson, L. K.; Killian, C. M.; Brookhart, M. *Journal of the American Chemical Society* **1995**, *117*, 6414.

5. Johnson, L. K.; Mecking, S.; Brookhart, M. *Journal of the American Chemical Society* **1996**, *118*, 267.

6. Mecking, S.; Johnson, L. K.; Wang, L.; Brookhart, M. *Journal of the American Chemical Society* **1998**, *120*, 888.

7. Gottfried, A. C.; Brookhart, M. *Macromolecules* **2003**, *36*, 3085.

8. Foley, S. R.; Stockland, R. A.; Shen, H.; Jordan, R. F. *Journal of the American Chemical Society* **2003**, *125*, 4350.

9. Shen, H.; Jordan, R. F. *Organometallics* **2003**, *22*, 1878.

10. Szabo, M. J.; Galea, N. M.; Michalak, A.; Yang, S.-Y.; Groux, L. F.; Piers, W. E.; Ziegler, T. *Journal of the American Chemical Society* **2005**, *127*, 14692.

11. Rosario, N.; Pau, F.; Francesc, T.; Clara, V.; Reijo, S.; Raikko, K. *Angewandte Chemie International Edition* **2006**, *45*, 1270.

12. Chen, Y.; Boardman, B. M.; Wu, G.; Bazan, G. C. *Journal of Organometallic Chemistry* **2007**, *692*, 4745.

13. Popeney, C. S.; Camacho, D. H.; Guan, Z. *Journal of the American Chemical Society* **2007**, *129*, 10062.

14. Popeney, C. S.; Guan, Z. *Journal of the American Chemical Society* **2009**, *131*, 12384.

15. Vincent, L.; H., W. J.; S., T. F.; Sean, Q. *Angewandte Chemie International Edition* **2013**, *52*, 3172.

16. Röhrscheid, F.; Holm, R. H. *Journal of Organometallic Chemistry* **1965**, *4*, 335.

17. Hoel, E. L.; Hawthorne, M. F. *Journal of the American Chemical Society* **1975**, *97*, 6388.

18. Francesc, T.; Rosario, N.; Clara, V.; Reijo, S.; Raikko, K. *Angewandte Chemie International Edition* **2000**, *39*, 4290.

19. Spokoyny, A. M.; Lewis, C. D.; Teverovskiy, G.; Buchwald, S. L. *Organometallics* **2012**, *31*, 8478.

20. Douvris, C.; Michl, J. *Chemical Reviews* **2013**, *113*, PR179.

21. Scholz, M.; Hey-Hawkins, E. *Chemical Reviews* **2011**, *111*, 7035.

22. Knoth, W. H. *Journal of the American Chemical Society* **1967**, *89*, 1274.

23. Jelinek, T.; Plešek, B.; Heřmánek, S. *Journal of Organometallic Chemistry* **1986**, *307*, C13.

24. Srivastava, R. R.; Hamlin, D. K.; Wilbur, D. S. *The Journal of Organic Chemistry* **1996**, *61*, 9041.

25. Reed, C. A. *Accounts of Chemical Research* **1998**, *31*, 133.

26. Reed, C. A. *Accounts of Chemical Research* **2010**, *43*, 121.

27. Allen, F.H.; Kennard, O.; Watson, D. G.; Brammer, L.; Orpen, A. G.; and R. Taylor, R. *Journal of the Chemical Society, Perkin Transactions II* **1987**, S1.

Chapter 3: Carborane Ligands for Application in C-H Functionalization

3.1 Introduction

One of the challenges of contemporary transition metal catalysis is the development of selective, efficient, and practical alkane C-H functionalization systems.[1] Another challenge is to accomplish this task while utilizing inexpensive and abundant base metals.[2] Systems based on oxidative addition/reductive elimination sequences have received the most attention, but most of these catalysts utilize precious metals and often require harsh reaction conditions. One promising strategy for mild, base metal catalyzed alkane functionalization systems is to utilize the reactivity of highly electrophilic metal carbenes for selective C-H insertion reactions (Figure 3-1).[1-4]

The generally accepted catalytic cycle begins with the contact of a diazo reagent with a transition metal fragment to form complex **A** (Figure 3-1).[3] Diazo reagents that feature at least one electron withdrawing (EWG) substituent are often employed because the EWG increases the stability of the diazo compound and also enhances the electrophilicity of the ensuing metal carbene.[1] Subsequent metal promoted N_2 elimination from **A** generates the metal carbene **B**. Although all groups 8-11 transition metals have shown some propensity to catalyze diazo decomposition to afford metal carbenes, catalytic alkane insertion reactions are primarily limited to Rh(II) dimers and the coinage metals.[1-4] Single examples of catalytic metal carbene alkane insertion reactions exist for both Fe and Ru.[5,6] The reason that Rh(II) dimers and coinage metals are efficient for catalyzing alkane insertion reactions is because they have little propensity to π-backbond to the ensuing carbene center. As shown by resonance structure **B'** (Figure 3-1, bottom right), such

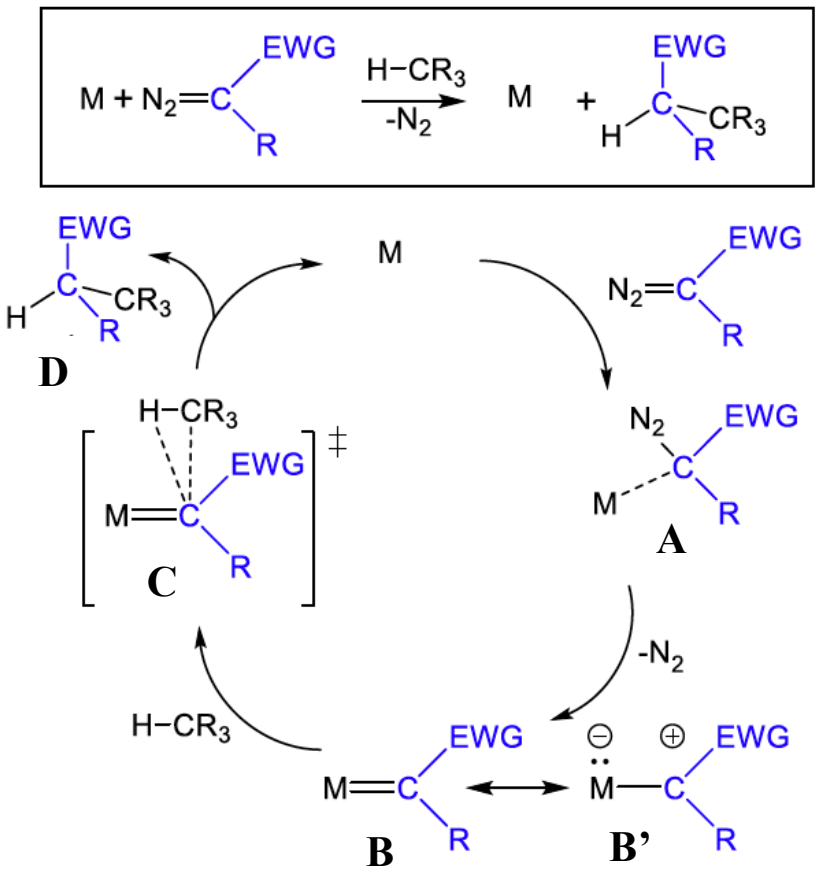

Figure 3-1. Generic representation of a metal catalyzed carbene insertion reaction (top). Generally accepted catalytic cycle of carbene insertion (bottom).

electrophilic carbenes can also be described as carbocation-like, since the M-carbon bond is essentially a pure σ-bond with little or no π-character.[7] The electrophilic metal carbene insertion into alkanes involves the outer sphere attack of the hydrocarbon at the carbene center **C** (Figure 3-1) with subsequent release of the product **D**.

While steric effects can influence the reactivity of alkane substrates toward C-H insertion, in general tertiary C–H bonds are more reactive than secondary C-H sites, and primary C-H bonds are the least reactive. This trend correlates with the insertion preferentially occurring at C-H sites with the lowest bond dissociation energies.[1-4] The primary problem associated with metal carbene alkane insertion catalysts is that the metal

carbenes are so reactive that it is difficult to control their behavior. Catalytic metal carbene alkane insertion reactions are typically run in neat hydrocarbons[1], since the transient and highly reactive metal carbenes will insert into nearly all chemical bonds. The most common side reactions that reduce the efficiency of this methodology are carbene dimerization and catalyst deactivation by insertion of the metal carbene into the ligand framework.[1,3] Carbene dimerization is thought to occur by bimolecular coupling of two metal carbenes or via the nucleophilic attack of diazo substrates at the metal carbene center.

Although the first reported metal carbene alkane insertion catalysts were discovered utilizing the base metal Cu[8], there has been a shift toward the implementation of noble metals, such as Rh and Ag. It is commonly accepted that Ag and Rh generate metal carbenes that are stable and potent enough electrophiles to undergo alkane insertion reactions.[4] State-of-the-art systems (Figure 3-2) have been developed by Perez,[9-11] who introduced super critical CO_2 ($scCO_2$) as a reaction medium to allow for the functionalization of gaseous alkanes and utilized perfluorinated tris(indazolyl)borate species to retard decomposition by ligand C-H insertion. Interestingly, the lone B-H bond of the ligand backbone has not been reported to undergo metal carbene insertion, perhaps because of the steric protection offered by surrounding perfluoroindazole rings. The Perez-type catalysts are one of the only systems capable of functionalizing the most challenging substrate, methane.[10] This system still displays diazo dimerization problems, low turnover frequency/numbers, and

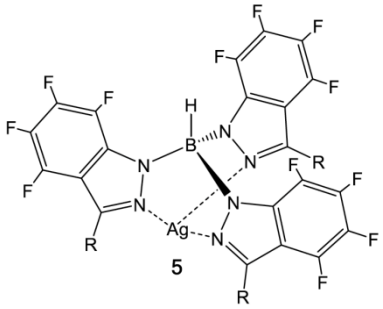

Figure 3-2. Perez's Ag catalyst supported by a perfluorinated tris(indazolyl)borate ligand.

relies on a precious metal. Novel strategies are needed to control the reactivity of electrophilic carbenes in order to develop catalytic carbene insertion reactions with alkanes that are selective, efficient, and practical. Moreover, in order for these systems to be sustainable, future catalyst design should focus on the development of earth abundant base metal catalysts.

3.2 C-H Functionalization Metal Catalyst Design with Carborane Ligands

Ancillary ligands for metal catalysts are typically constructed with alkyl and aryl substituents. An interesting alternative to classical ligand substituents are icosahedral carboranes.[12-14] The most commonly used carboranes are neutral icosahedral dicarbaborane clusters (C_2B_{10}).[13] The *ortho*-carborane (*o*-carborane) isomer **1** (Figure 3-3) has historically been the most utilized due to its ready availability.[12] While this cluster offers many interesting characteristics, such as a distinct steric profile and the ability to form H-H hydrogen bonds, it exhibits reactivity that is undesirable for catalysis, such as B-H cyclometalation and B-vertex extrusion to afford anionic nido-carboranes.[15] In contrast to icosahedral dicarbaboranes, the isoelectronic monocarbaborane anion **2** is far less reactive (Figure 3-3), and essentially inert when partially or fully halogenated at the B-H vertices.[14] In addition, halogenated derivatives of carborane anions are one of the weakest coordinating anions that exist. The implementation of the polyhalogenated

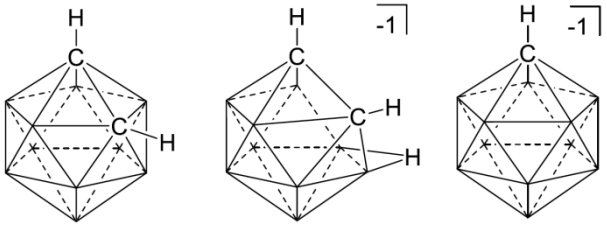

Figure 3-3. *o*-carborane **1** (left), *nido*-carborane anion (middle) and *closo*-carborane anion **2** (right) Unlabeled vertices = B-H.

carborane anions as weakly coordinating counteranions for super electrophiles has led to the isolation of extraordinarily reactive species, such as H^+ and CH_3^+.[16] The solid-state structures of these materials show that the electrophile rests on the substituents bound to the carborane cage. Halogenated carboranes are the counter anions of choice for hydrodefluorination reactions via silylium catalysis since they are inert toward decomposition by the carbocation intermediates.[17]

In 2013, the Lavallo research group demonstrated the first example of a condensation reaction between carboranyl amine **4** and a carbonyl compound.[18] This reaction resulted in the dianionic diimine **5** with pendant N-carboranyl groups. This diimine can be cyclized to form the monoanionic imidazolium salt **6**. Deprotonation with alkali metal hexamethyldisilazide bases produces the corresponding dianionic N-heterocyclic carbene (NHC) salts.[19-23] Both the diimine **5** and the NHC **12** have the potential to form

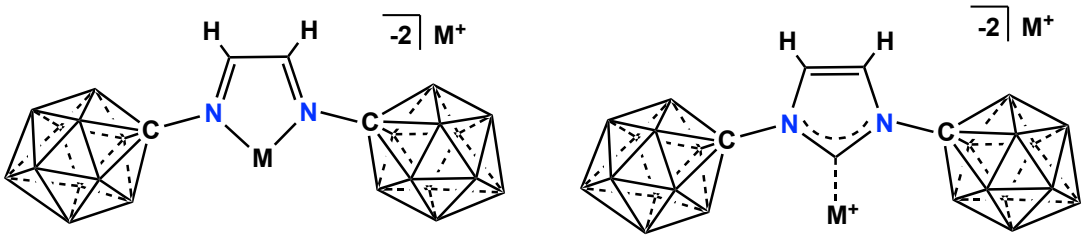

Figure 3-4. Dianionic carboranyl diimine **5** (left) and N-heterocyclic carbene **12** (right) depicted as ligands for transition metal complexes.

complexes with transition metals where the metal center is flanked by two sterically demanding and highly stable caborane anions (Figure 3-4).

Considering the highly electrophilic nature of late transition metal carbenes, implementing ligands that contain two weakly coordinating carboranyl anion R-groups

would potentially shield the electron deficient metal carbene and protect the site of catalysis. This could result in more stable and controllable systems for alkane insertion reactions. The rationale for this hypothesis is that the inert properties of the cluster substituents and enormous steric profile would prevent the catalyst from decomposing via insertions of the metal carbene into the ligand or bimolecular carbene dimerization pathways. In addition, the weakly coordinating and electronically tunable nature of the cluster substituents will produce more electrophilic base metals and thus enhanced reactivity of the metal carbenes towards alkanes.

3.3 C-H Functionalization Screening with Ethyl Diazoacetate (EDA)

Mentioned previously in Chapter 2, the carboranyl diimine dianion **5** showed no propensity towards several transition metals. However, **5** did exhibit reactivity towards copper(I)chloride (Figure 3-5, experimental section) and formed a new singular product according to ^{1}H NMR, as the single resonance corresponding to the two protons on the backbone of **5[Li^{+}]** shifted downfield from 7.55 ppm to 8.05 ppm. Following this result, I began to investigate potential catalytic activity of copper complexes of the hydridic carboranyl diimine **5** and its halogenated derivatives $\mathbf{8_{Br}}$ and $\mathbf{8_{I}}$. Copper is among the few metals known to perform catalytic C-H functionalization of alkanes via carbene insertion.[1-3,8] New C-C bonds are traditionally formed by the displacement of a suitable leaving group, whereas C-H functionalization requires breaking a C-H bond to form a new C-C bond. The activation of a C-H bond faces several challenges, such as the unreactive nature of alkanes and the selectivity of product formation. In C-H functionalization, the carbene unit is bound to the metal following insertion into the C-H bond without direct interaction of the metal

center with the alkane substrate. A ligand framework bearing carboranes for a metal catalyst would be favorable for C-H functionalization since the cluster is inert towards the metal-carbene insertion reaction. Also, the cluster would stabilize and protect the electron deficient metal center and the metal-carbene intermediate.

Initially I screened the ability of crude reaction mixtures containing $CuCl_2$ and

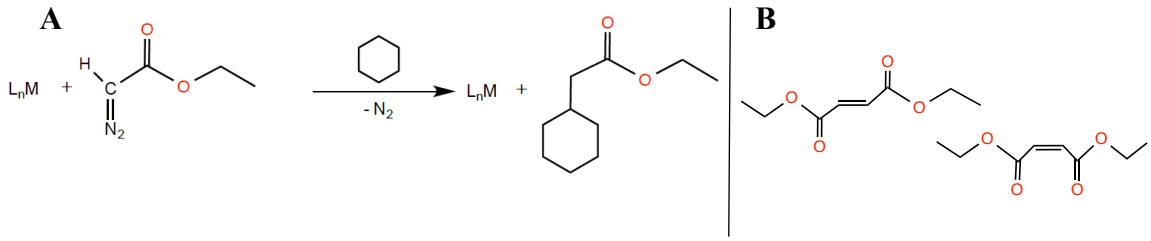

Scheme 3-1. A: Catalyzed insertion of ethyl diazoacetate into cyclohexane to form ethyl-2-cyclohexylacetate. B: Undesired dimerization products, diethyl maleate and diethyl fumarate.

carborane functionalized diimines (**5**, $\mathbf{8_{Br}}$, $\mathbf{8_I}$) to catalyze the insertion of ethyl diazoacetate (EDA) into cyclohexane using standard conditions from literature[1] (4.6% catalyst loading). A solution of EDA in cyclohexane was added via liquid addition funnel over a period of 3 hours. Copper(II) was used instead of copper(I) because the higher oxidation state would render the metal more electrophilic and more reactive. Li^+ salts of **5**, $\mathbf{8_{Br}}$, and $\mathbf{8_I}$ were used in excess with $CuCl_2$ to prevent free copper ions in solution, which are known to promote the dimerization of EDA over the of C-H functionalization of the alkane substrate. A control experiment of $CuCl_2$ was conducted, demonstrating that for this experimental setup the metal halide produced a turnover number (TON) of 5.8 (Table 3-1, Entry 1). Only 50% of the EDA was converted to either the desired product, ethyl-2-cyclohexylacetate, or dimerization side products (diethyl maleate and diethyl fumarate). The prepared Cu^{2+} salts of $\mathbf{8_I}$ and $\mathbf{8_{Br}}$ fully converted EDA at 4.6% catalyst loading and exhibited higher catalytic

activity than $CuCl_2$ alone, with the TONs of 10.0 and 14.3, respectively (Table 3-1, entries 2 and 3). The unfunctionalized carborane diimine **5** was also screened as a Cu^{2+} salt, but I was unable to calculate the accurate percent conversion of EDA or turnover number since unreacted EDA was lost under vacuumn during the experimental work up. Of the EDA products formed by **5[Cu^{2+}]**, the majority was dimerization side products.

Table 3-1. Insertion of ethyl diazoacetate (EDA) with cyclohexane, EDA added in increments via liquid addition funnel; *For Entry 4 (Cu^{2+} **5**), accurate values could not be calculated as unreacted EDA was lost via evaporation (heating under vacuum).

Entry	Catalyst	Cat. Loading	t [hr]	T [°C]	% conversion	% product	% dimer	TON	TOF
1	$CuCl_2$	4.6%	3	90	50	26.6	73.4	5.8	1.9
2	Cu^{2+} $\mathbf{8_{Br}}$	4.6%	3	90	100	65.8	34.2	14.3	4.7
3	Cu^{2+} $\mathbf{8_{I}}$	4.6%	3	90	100	46.5	53.5	10.1	3.4
4	Cu^{2+} **5**	4.6%	3	90	N/A*	38.5	61.5	N/A*	N/A*
5	Cu^{2+} **12**	4.6%	3	90	84	48.4	51.6	8.5	2.8
6	Cu^{2+} **14**	4.6%	3	90	96	91.5	11.8	19.9	6.6

Based on the success of $\mathbf{8_I}$ and $\mathbf{8_{Br}}$, I expanded my screening reactions to the dianionic carboranyl N-heterocyclic carbene **12**, and the poly-iodinated N-carboranyl NHC, **14**. A fellow lab member, Scott McArthur, had previously explored functionalization pathways for **6**, and found that the imidazolium salt undergoes late stage halogenation in the same substitution pattern as **4**. To prepare the functionalized imidazolium salt precursor **13**, I followed a procedure developed by Scott using iodine monochloride and triflic acid. The crude catalyst solutions of $CuCl_2$ with the fully hydridic N-carboranyl NHC **12** resulted

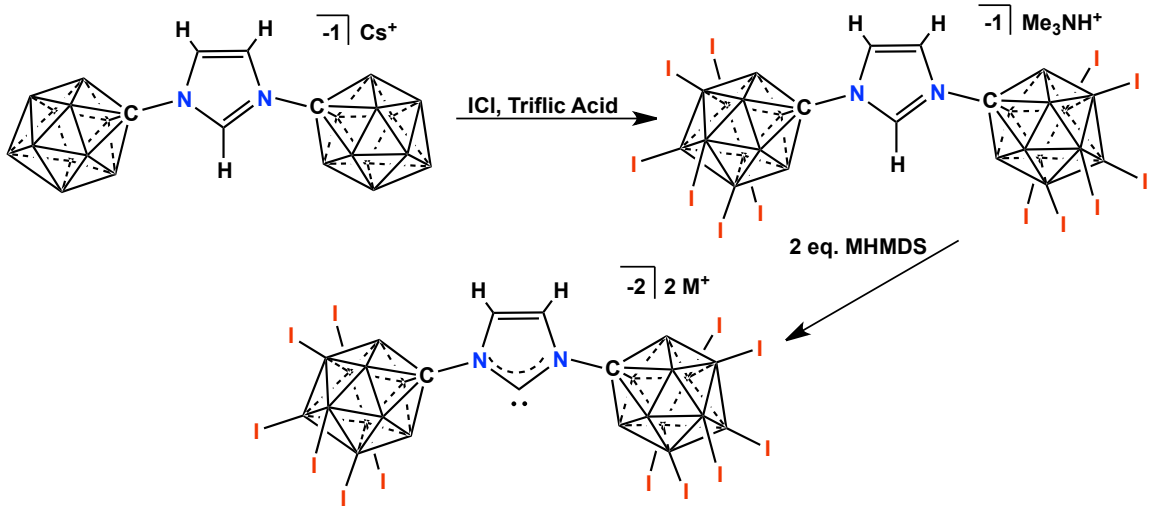

Scheme 3-2. Functionalization pathway from the fully hydridic 12-vertex carborane imidazolium salt **6** to the hexa-iodinated derivative **13**. The iodinated imidazolium **13** can be deprotonated in the same fashion as **6** to form the N-heterocyclic carbene **14**.

in a modest TON of 10.1, whereas the hexaiodinated NHC **14** had the highest catalytic activity observed, with a TON of 19.9 (Table 3-1, entries 5 and 6).

The crude reaction mixtures containing $CuCl_2$ and either carboranyl diimines (**5**, $\mathbf{8_{Br}}$, $\mathbf{8_I}$) or NHCs (**12**, **14**) all produced turnover numbers and percent conversion values of EDA higher than $CuCl_2$ alone. Encouraged by these results, I sought to optimize my reaction conditions by utilizing a syringe pump for the addition of EDA in a more controlled fashion. At 4.6% catalyst loading, the Cu^{2+} $\mathbf{8_I}$ and $\mathbf{8_{Br}}$ crude catalysts converted 100% of EDA, both with over 85% of the desired insertion product (Table 3-2, entries 1 and 2). With $\mathbf{8_I}$, I also prepared a crude metal complex with $CoCl_2$, inspired by recent work utilizing cobalt for C-H activation. Although $\mathbf{8_I[Co^{2+}]}$ was catalytically active, the majority of product was the undesired dimerization products. (Table 3-2, entry 3) The NHC copper complex $\mathbf{14[Cu^{2+}]}$ was again the best performing catalyst, with ethyl-2-cyclohexylacetate accounting for 90% of the conversion product, and a TON of 19.6. Lowering the catalyst

loading drastically increased the production of dimers for **8_{Br}**, **8_{I}**, and **14**. For all three catalysts, dimerization products accounted for approximately 50% of the total yield. At 0.1% catalyst loading, both **8_{Br}[Cu^{2+}]** and **8_{I}[Cu^{2+}]** did not go to completion after 3 hours, with only 68 and 54% conversion of EDA, respectively.

Table 3-2. Insertion of ethyl diazoacetate (EDA) with cyclohexane, EDA added in increments via syringe pump.

Entry	Catalyst	Cat. Loading	t [hr]	T [°C]	% conversion	% product	% dimer	TON	TOF
1	Cu^{2+} **8_{Br}**	4.6%	3	90	100	86.4	13.6	18.8	6.2
2	Cu^{2+} **8_{I}**	4.6%	3	90	100	87.8	12.2	19.1	6.3
3	Co^{2+} **8_{I}**	4.6%	3	90	85	35.2	64.8	9.0	3.0
4	Cu^{2+} **14**	4.6%	3	90	94	90.2	9.8	19.6	6.5
5	Cu^{2+} **14**	1.0%	3	90	100	52.3	47.7	52	17
6	Cu^{2+} **8_{Br}**	0.1%	3	90	68	58.5	41.5	398	133
7	Cu^{2+} **8_{Br}**	0.1%	6	90	100	56.2	43.8	563	94
8	Cu^{2+} **8_{I}**	0.1%	3	90	54	46.3	53.7	250	83
9	Cu^{2+} **8_{I}**	0.1%	6	90	100	45.5	55.5	456	76

3.4 Characterization of Cu^{2+} Catalyst

Having found a catalytically active complex, I began to work towards characterizing the Cu^{2+} complexes. Although ^{1}H NMR data collected for the Cu^{+} complexes of **5**, **8_{Br}**, and **8_{I}** all showed a downfield shift indication coordination to a metal center, I was unable to obtain any crystal structures. I also began to work towards characterizing a well-defined complex of the Cu^{2+} hexaiodinated NHC **14**. Attempts to prepare the metal complex with stoichiometric amounts of the hexaiodinated NHC **14** and

$CuCl_2$ gave a mixture of products, mostly composed of the protonated imidazolium **13**. I then tried a metal base complex using Cu(*t*BuO)$_2$, prepared from potassium tertbutoxide and $CuCl_2$.[24] Reaction with **13** again gave an intractable mixture of products. However, by first preparing the K^+ salt of **14** and adding it in a 1:1 equivalence to Cu(*t*BuO)$_2$, a clean product is obtained. The ^{1}H NMR resonance of the NHC backbone shifts from 7.09 ppm (K^+) to 7.52 ppm (Cu^{2+}) and the ^{11}B NMR maintains symmetry, indicating no cyclometallation of the carborane cluster. There is a resonance in the ^{13}C NMR at 179.2 ppm for the carbene-metal bond, and at 123.1 ppm for the two carbons of the backbone. Unfortunately, a single crystal was not obtained of the metal complex **15**.

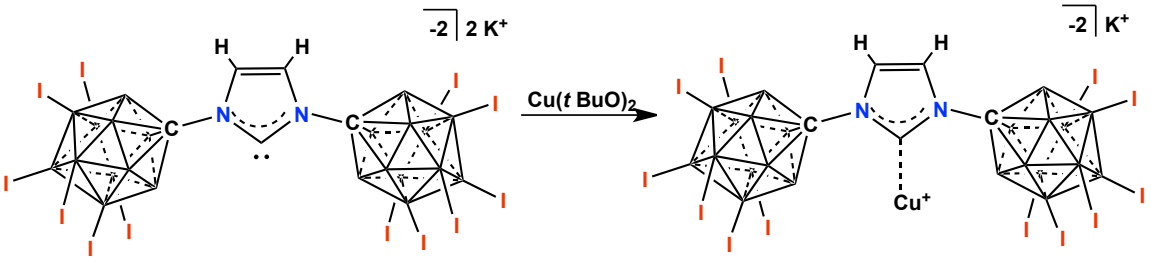

Scheme 3-3. Reaction of **14[K$^+$]** with Cu(*t*BuO)$_2$ formed a singular product according to NMR. On the right is a proposed structure.

3.5 Conclusion

Several N-carboranyl diimine and NHC ligands were screened as crude reaction mixtures with $CuCl_2$ for activity as C-H functionalization catalysts. The fully hydridic species **5** as well as the polyhalogenated cluster species **8$_I$** and **8$_{Br}$** of the dianionic carboranyl diimine were tested for catalytic activity. The fully hydridic carboranyl NHC **12** and the hexa-iodinated species **14** were screened as well. Initially, screening reactions were performed with a liquid addition funnel, and second with a syringe pump. For both

experimental setups, the crude complex **14[Cu^{2+}]** at 4.6% catalyst loading produced the highest TONs and selectivity for the desired products. Attempts to characterize and isolate a well-defined Cu^{2+} complex of **14** produced NMR data indicative of a singular product, however a crystal structure was not obtained for further investigations.

3.6 Experimental

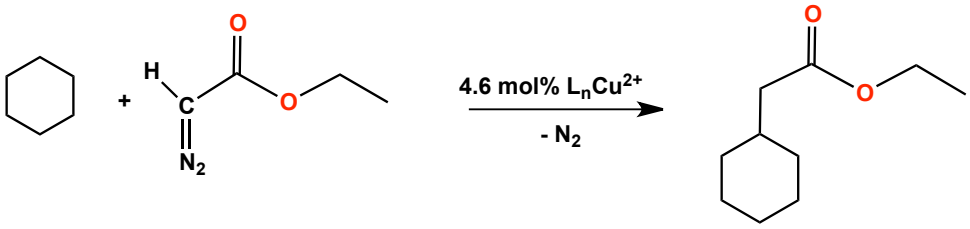

Scheme 3-4. C-H Functionalization Reaction Conditions – Liquid Addition Funnel

Each catalyst (see Table 3-1) was prepared from 1 equivalent $CuCl_2$ and 3 equivalents of the corresponding carborane functionalized ligand as the Li^+ salt in dichloromethane or tetrahydrofuran. The solution was stirred for 6 hours, and the solvent was removed under reduced pressure. A calculated amount of crude catalyst (4.6% catalyst loading) was directly added to 20 mL of cyclohexane and heated to 90 °C under argon. Once the reaction reached reflux, 20 mL of cyclohexane containing a calculated amount of ethyl diazoacetate (EDA) was added dropwise via liquid addition funnel over 3 hours. Excess cyclohexane was removed under vacuum for ^{1}H NMR analysis. Integration of the ^{1}H NMR spectra from the reaction solutions revealed total rates of conversion of EDA (% conversion column, Table 3-1) and the ratio of expected insertion product, ethyl 2-cyclohexylacetate to dimer formation of diethyl maleate and diethyl fumarate (% product, % dimer, Table 3-1). Turnover numbers and frequencies were calculated accordingly based on ^{1}H NMR integration.

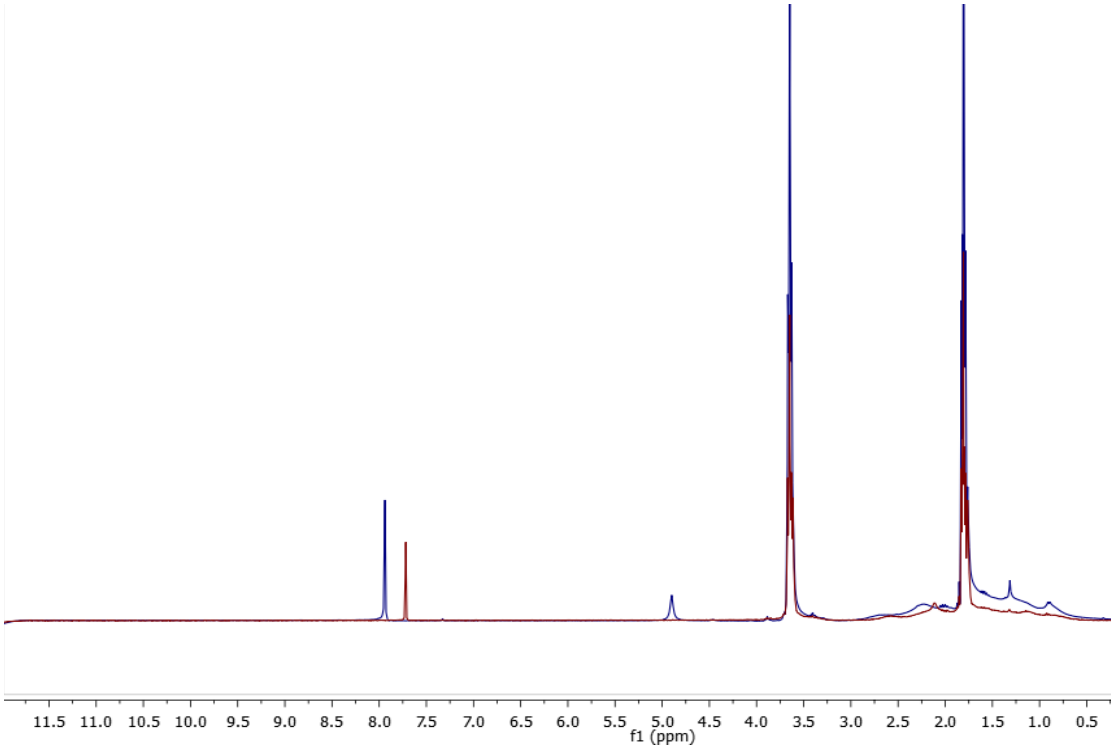

Figure 3-5. Overlapping ^{1}H NMR spectra; red corresponds to **5[Li^{+}]**, and blue is after the addition of $CuCl_2$. Note: the peak at 4.90 corresponds to trace dichloromethane.

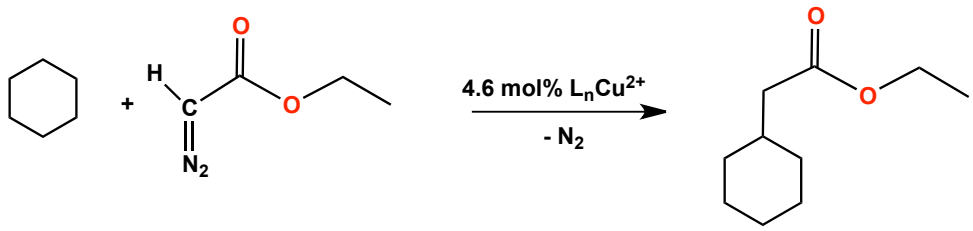

Scheme 3-5. C-H Functionalization Reaction Conditions – Syringe Pump

Each catalyst (see Table 3-2) was prepared from 1 equivalent $CuCl_2$ or $CoCl_2$ and 3 equivalents of the corresponding carborane functionalized ligand as the Li^+ salt in dichloromethane or tetrahydrofuran. The solution was stirred for 6 hours, and the solvent was removed under reduced pressure. A calculated amount of crude catalyst (4.6% catalyst loading) was directly added to 20 mL of cyclohexane and heated to 90 °C under argon. Once the reaction reached reflux, 20 mL of cyclohexane containing a calculated amount of ethyl diazoacetate (EDA) was added in increments via syringe pump over 3 hours. Excess cyclohexane was removed under vacuum for ^1H NMR analysis. Integration of the ^1H NMR spectra from the reaction solutions revealed total rates of conversion of EDA (% conversion column, Table 3-2) and the ratio of expected insertion product, ethyl 2-cyclohexylacetate to dimer formation of diethyl maleate and diethyl fumarate (% product, % dimer, Table 3-2). Turnover numbers and frequencies were calculated accordingly based on ^1H NMR integration.

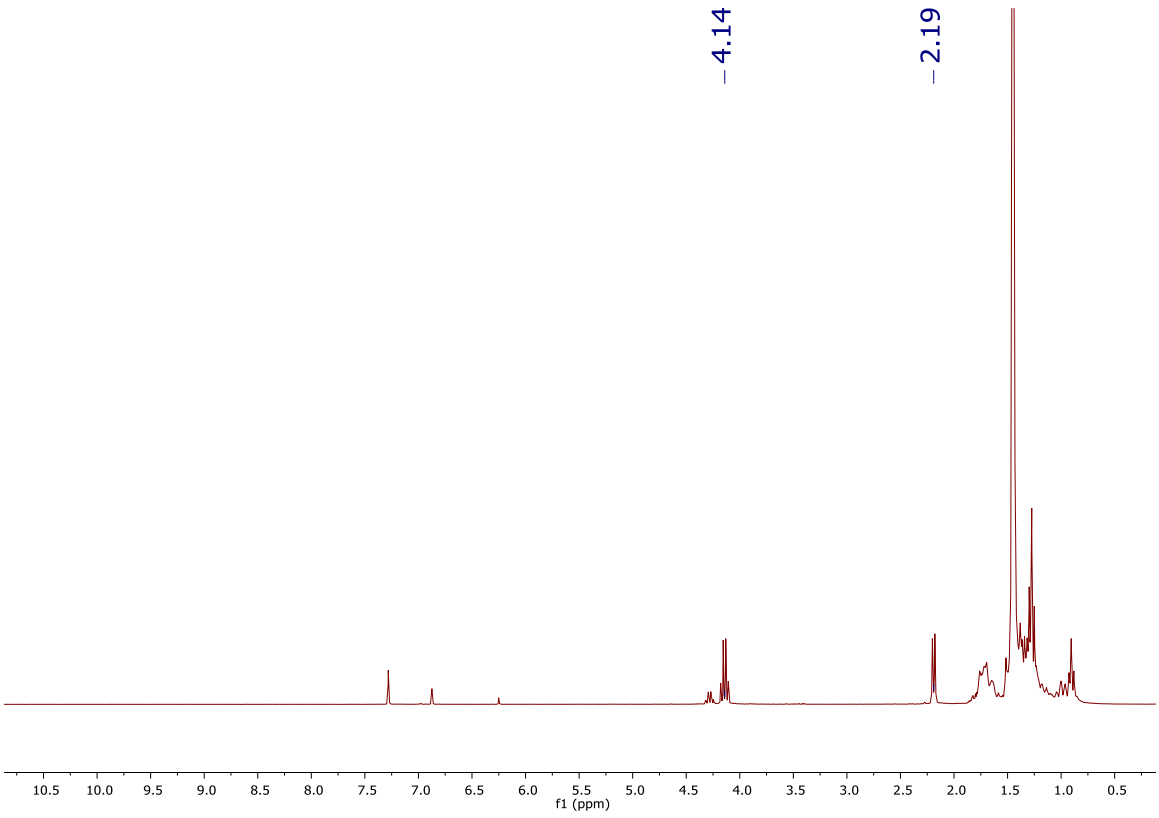

Figure 3-6. ^{1}H NMR of **14[Cu^{2+}]** in chloroform-d$_3$, 4.6% cat. loading (Table 3-2, entry 4). Signals labeled at 2.19 and 4.14 ppm correspond to ethyl diazoacetate insertion product, ethyl 2 cyclohexylacetate. Signals at 6.87 and 6.25 are from dimerization products, diethyl maleate and diethyl fumarate. The signal at 2.19, and each of the dimerization products signals corresponds to two protons and are used via integration to determine the percent amount of each product present.

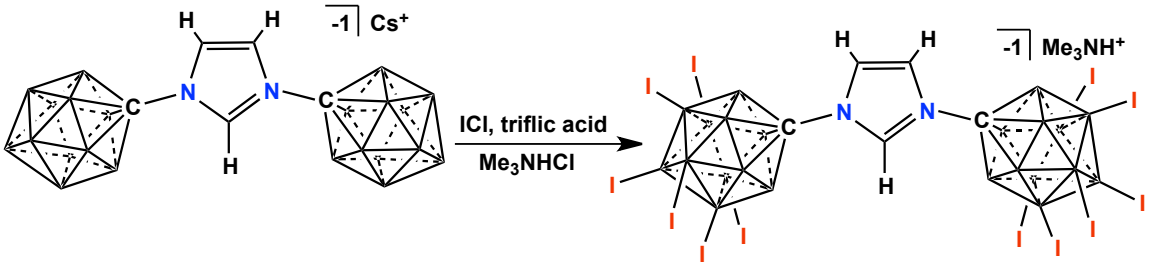

Scheme 3-6. Iodination N-Carboranyl Imidazolium **6[Cs$^+$]** to form **13**

The 12-vertex carboranyl imidazolium **6[Cs$^+$]** (1.0 g, 2.07 mmol) was placed in a 100 mL round bottom flask, and 20 mL each of triflic acid and iodine monochloride were added. The reaction was heated to 50 °C and stirred open to atmosphere. After 24 hours, the reaction was filtered on a medium porosity fritted funnel and washed with 100 mL of dichloromethane. The collected solid was then dissolved in ethyl acetate. 150 mL of water was added to the ethyl acetate solution and was subsequently titrated with 10% aq. sodium sulfite solution. The organic layer was removed, and the aqueous solution was extracted with another 100 mL of ethyl acetate. The organic layers were combined and then pumped down to dryness. The solid was transferred to an aqueous solution, and an excess of trimethylammonium hydrochloride was added, precipitating **13[Me$_3$NH$^+$]** Yield 88% (3.63g, 1.82 mmol). ^{1}H NMR (300 MHz, acetonitrile-d$_3$, 25 °C): δ = 8.64 (t, $^4J(H,H)$ = 1.8 Hz, 1H), 7.49 (d, $^4J(H,H)$ = 1.8 Hz, 2H); ^{1}H (^{11}B-dec) NMR (300 MHz, acetonitrile-d$_3$, 25 °C): δ = 8.64 (t, $^4J(H,H)$ = 1.8 Hz, 1H), 7.49 (d, $^4J(H,H)$ = 1.8 Hz, 2H), 3.37 (s, 10H, B-H); ^{13}C (^{1}H-dec) NMR (124 MHz, acetone-d$_6$, 25 °C): δ = 137.1, 123.6, 81.6; ^{11}B (^{1}H-dec) NMR (96 MHz, acetone-d$_6$, 25 °C): δ = -2.9, -9.2, -16.8 ppm.

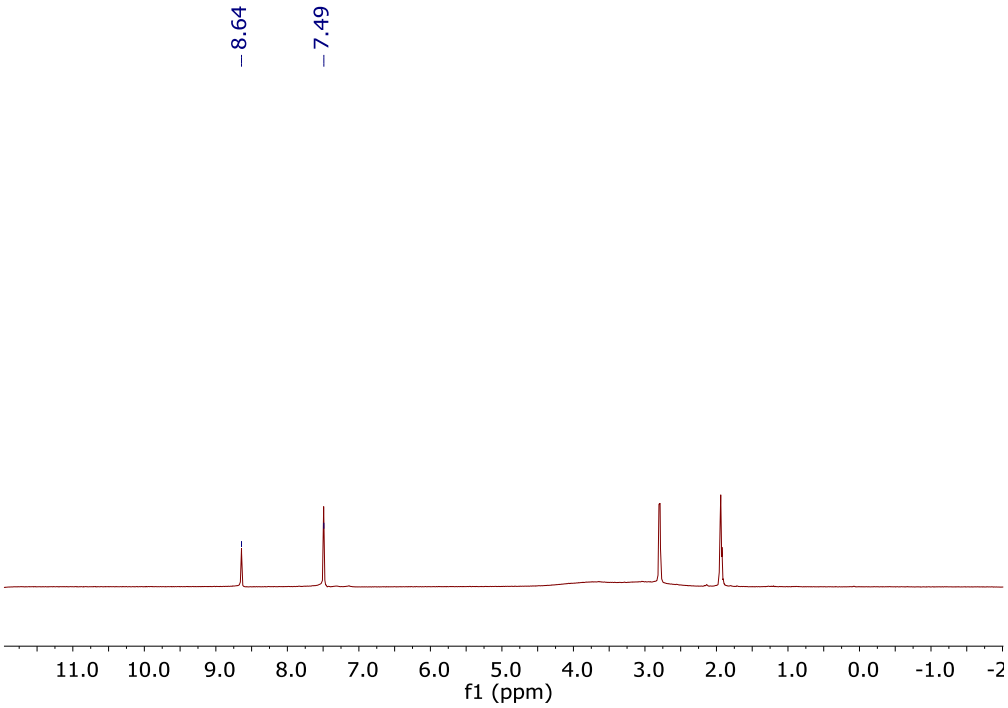

Figure 3-7. ^{1}H NMR of **13** in acetonitrile-d_3. Note the presence of water at 2.80 ppm.

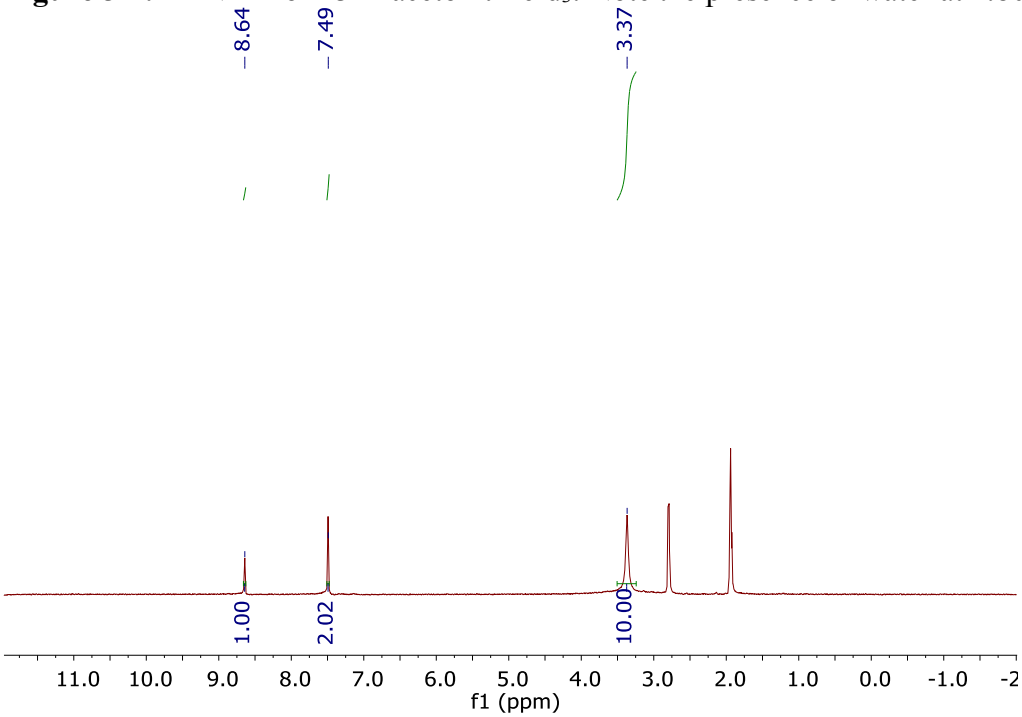

Figure 3-8. ^{1}H (^{11}B-dec) NMR of **13** in acetonitrile-d_3. Note the presence of water at 2.80 ppm.

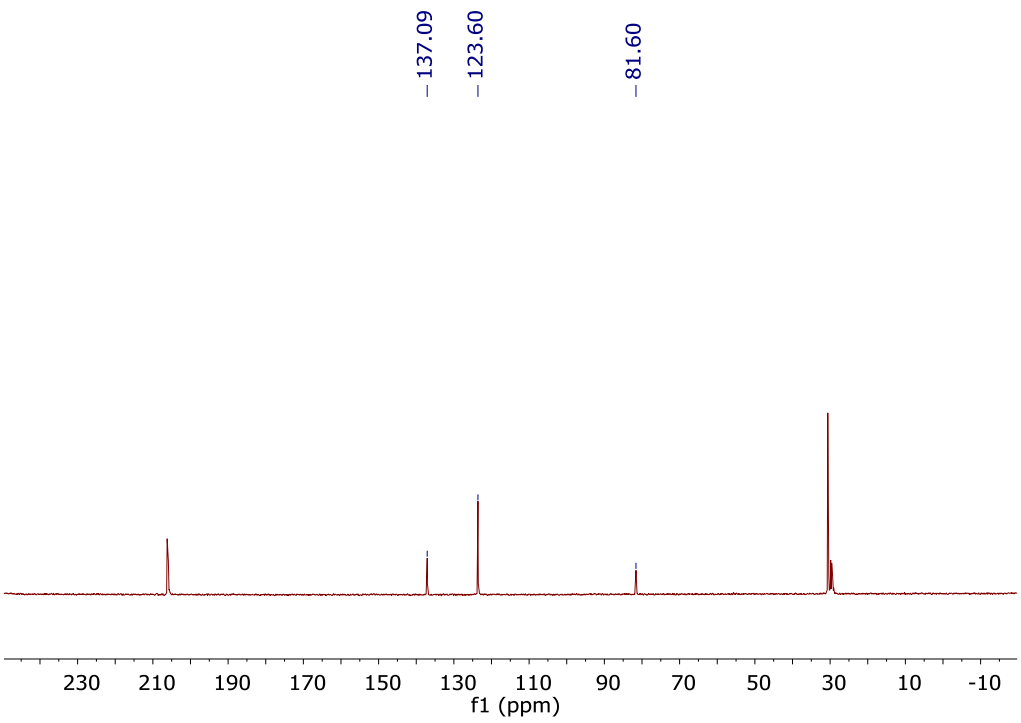

Figure 3-9. ^{13}C (^{1}H-dec) NMR of **13** in acetone-d_6.

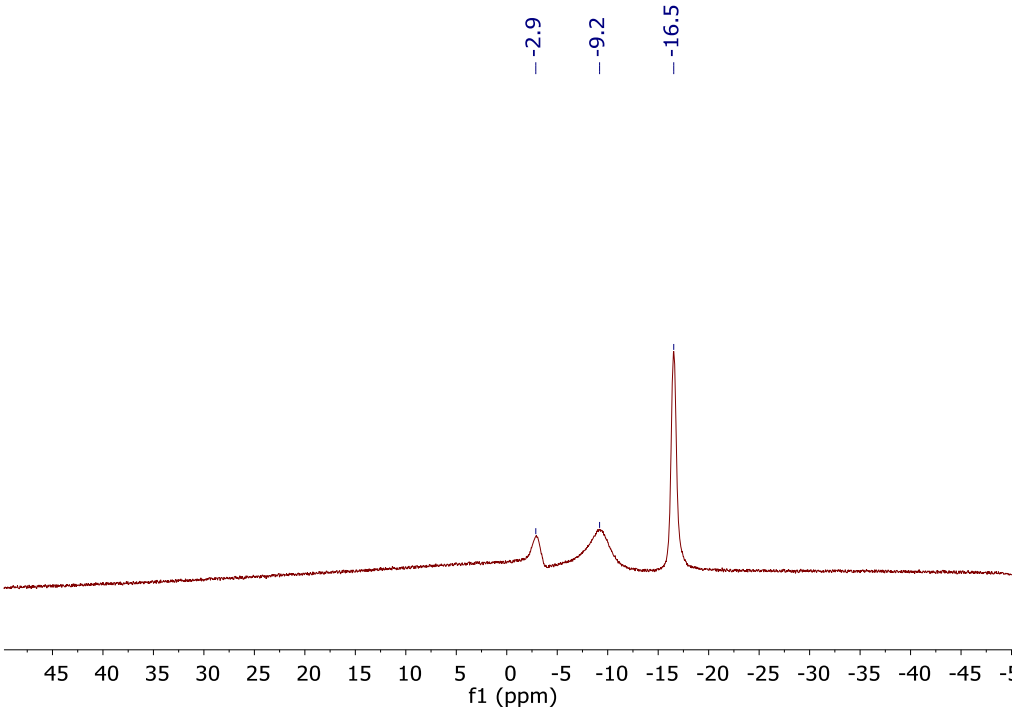

Figure 3-10. ^{11}B (^{1}H-dec) NMR of **13** in acetone-d_6.

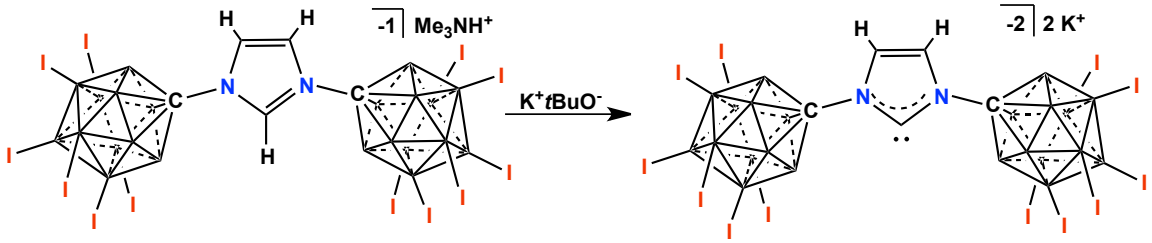

Scheme 3-7. Synthesis of Poly-iodinated N-Carboranyl NHC **14[K$^+$]**

13[Me$_3$NH$^+$] imidazolium (0.200 grams, 0.10 mmol) was dissolved in 10 mL of tetrahydrofuran. A 20 mL scintillation vial with a stir bar was loaded with 2 equivalents of potassium tert-butoxide (22 mg, 0.20 mmol) and the 10 mL THF solution was added. The solution was stirred for 30 minutes and then concentrated under vacuum to 3 ml. The reaction solution was added drop-wise to a second scintillation vial containing a stirring solution of diethyl ether, forming a white precipitate. The mixture was stirred for two hours, after which the white precipitate was allowed to settle. The diethyl ether wash was decanted from the vial, and the compound was dried under vacuum. 83% yield (0.184 grams, 0.083 mmol) ^{1}H NMR (300 MHz, tetrahydrofuran-d$_8$, 25 °C): δ = 7.07 (s, 2H); ^{13}C (^{1}H-dec) NMR (124 MHz, tetrahydrofuran-d$_8$, 25°C) δ = 221.2, 120.7; ^{11}B (^{1}H-dec) NMR (96 MHz, tetrahydrofuran-d$_8$, 25 °C): δ = -5.3, -9.6, -17.5 ppm.

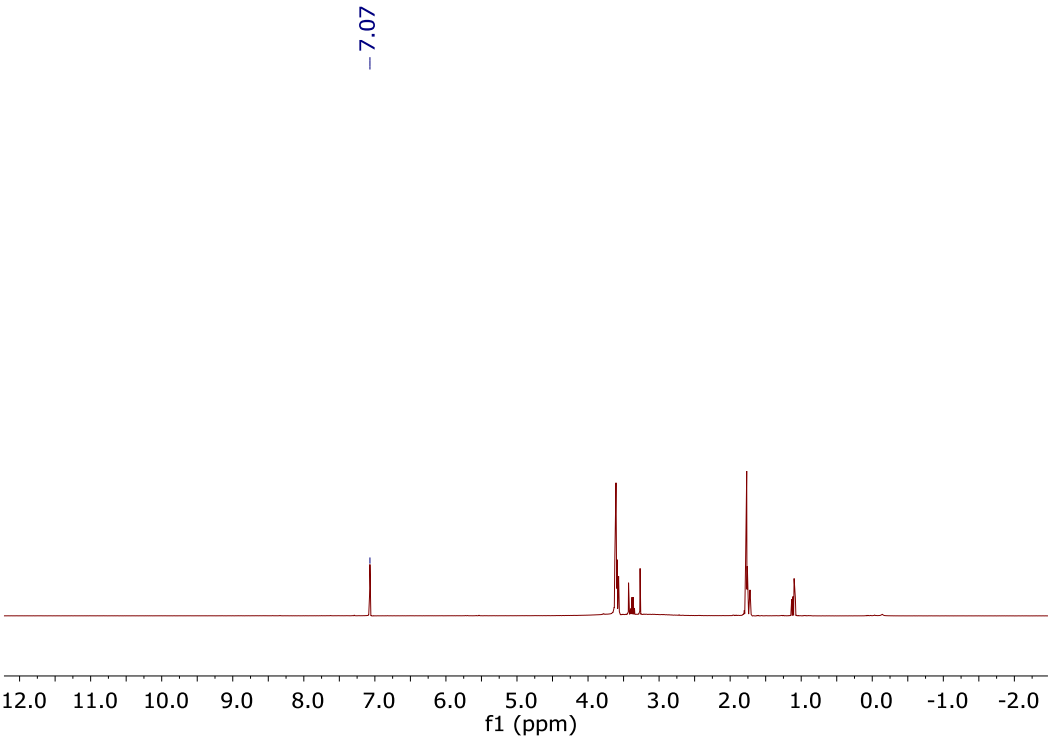

Figure 3-11. ^{1}H NMR of **14[K^{+}]** in tetrahydrofuran-d$_8$. Note the presence of dimethoxyethane (DME) at 3.28 and 3.56 ppm and diethyl ether at 1.12 and 3.58 ppm.

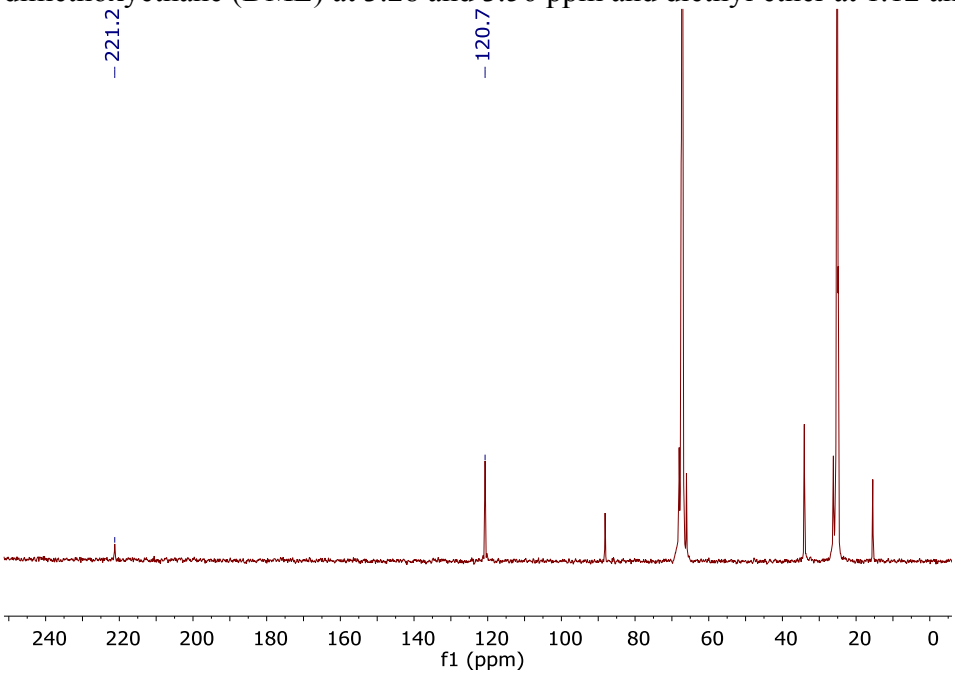

Figure 3-12. ^{13}C (^{1}H-dec) NMR of **14[K^{+}]** in tetrahydrofuran-d$_8$.

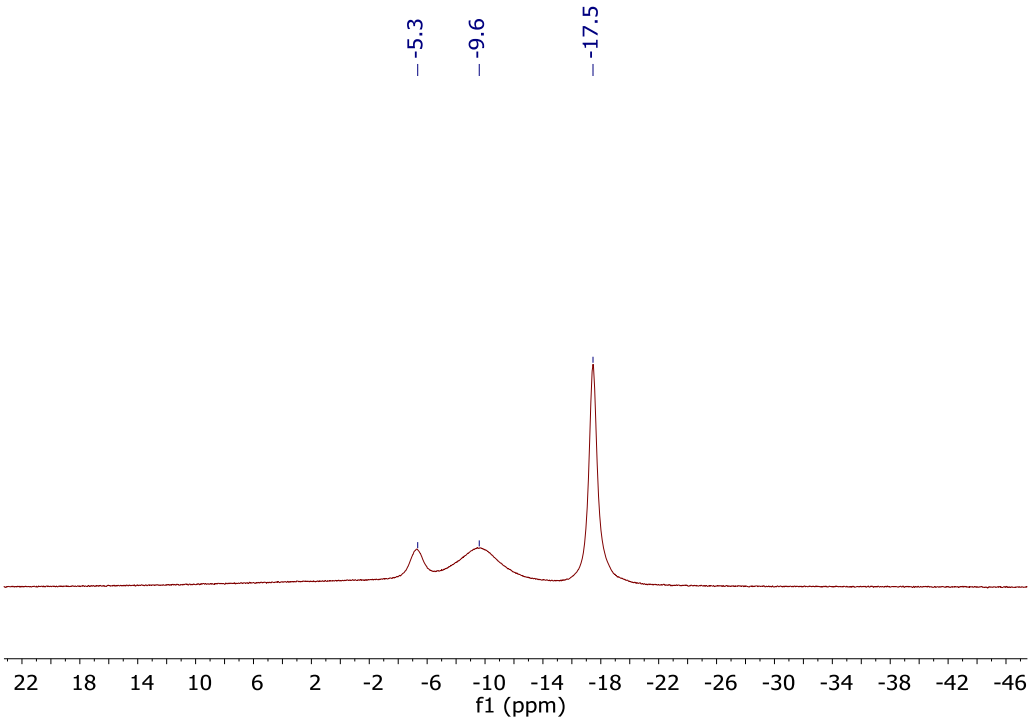

Figure 3-13. ^{11}B (^{1}H-dec) NMR of **14[K^+]** in tetrahydrofuran-d_8.

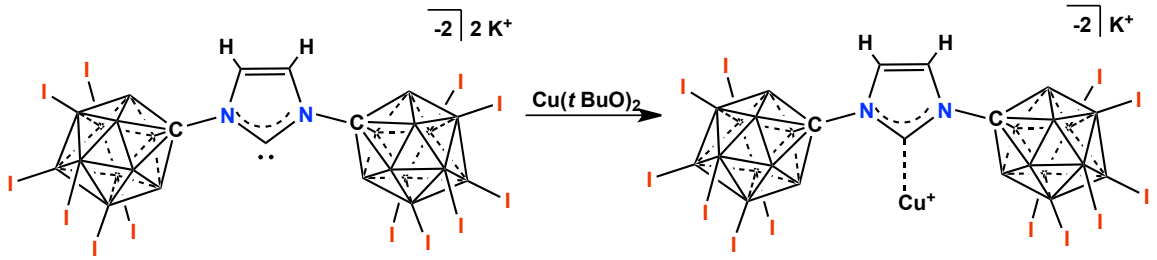

Scheme 3-8. Synthesis of Cu(II) Polyiodinated NHC, **14[Cu$^+$]**

In a 20 mL scintillation vial equipped with a stirbar, 70 mg (0.003 mmol) of **14[K$^+$]** was added and dissolved in approximately 5 mL of tetrahydrofuran. Cu(*t*BuO)$_2$ was prepared according to literature[24] from potassium tertbutoxide and $CuCl_2$. One equivalent of Cu(*t*BuO)$_2$ dissolved in minimal THF was added dropwise to **14[K$^+$]** solution while stirring, forming a dark russet colored solution. The vial was capped and stirred for 24 hours. The solution was concentrated under vacuum to 2 mL of THF, and added dropwise to stirring solution of diethyl ether, forming a suspension. The suspension was stirred for 2 hours, after which the precipitate was allowed to settle at the bottom of the vial, and the solvent was decanted. The solid was dried under vacuum, affording **14[Cu$^+$]**. ^{1}H NMR (300 MHz, tetrahydrofuran-d$_8$, 25 °C): δ = 7.53 (s, 2H); ^{13}C (^{1}H-dec) NMR (124 MHz, tetrahydrofuran-d$_8$, 25°C) δ = 178.3, 122.2; ^{11}B (^{1}H-dec) NMR (96 MHz, tetrahydrofuran-d$_8$, 25 °C): δ = -2.5, -8.3, -15.9 ppm.

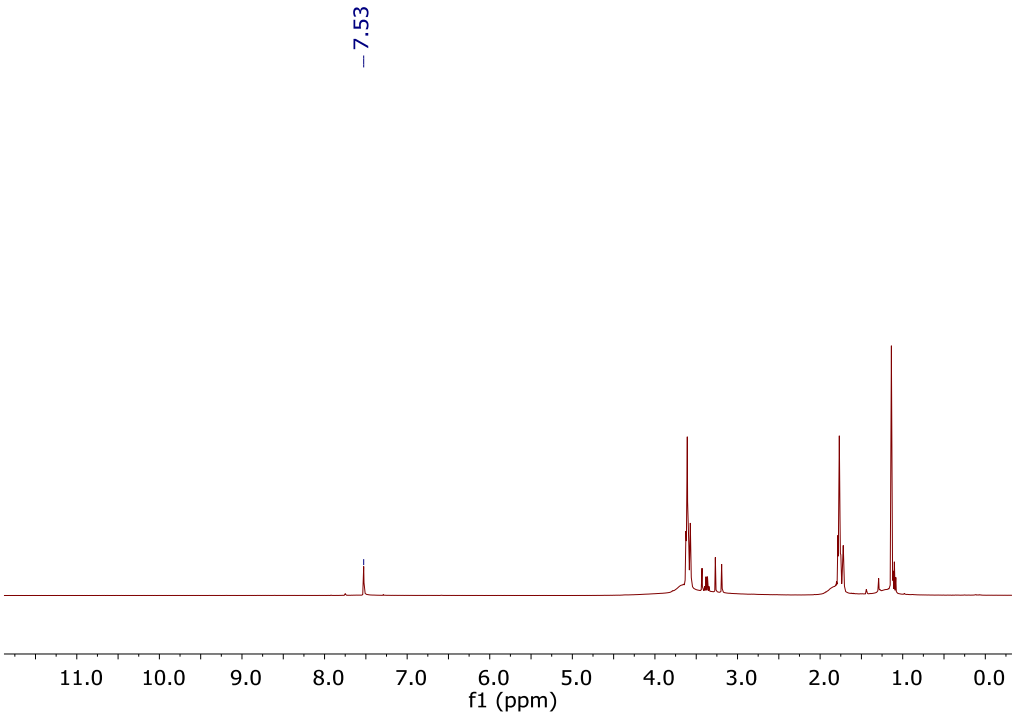

Figure 3-14. ^{1}H NMR of **14[Cu^{2+}]** in tetrahydrofuran-d$_8$. Note the presence of dimethoxyethane (DME) at 3.28 and 3.56 ppm and diethyl ether at 1.12 and 3.58 ppm.

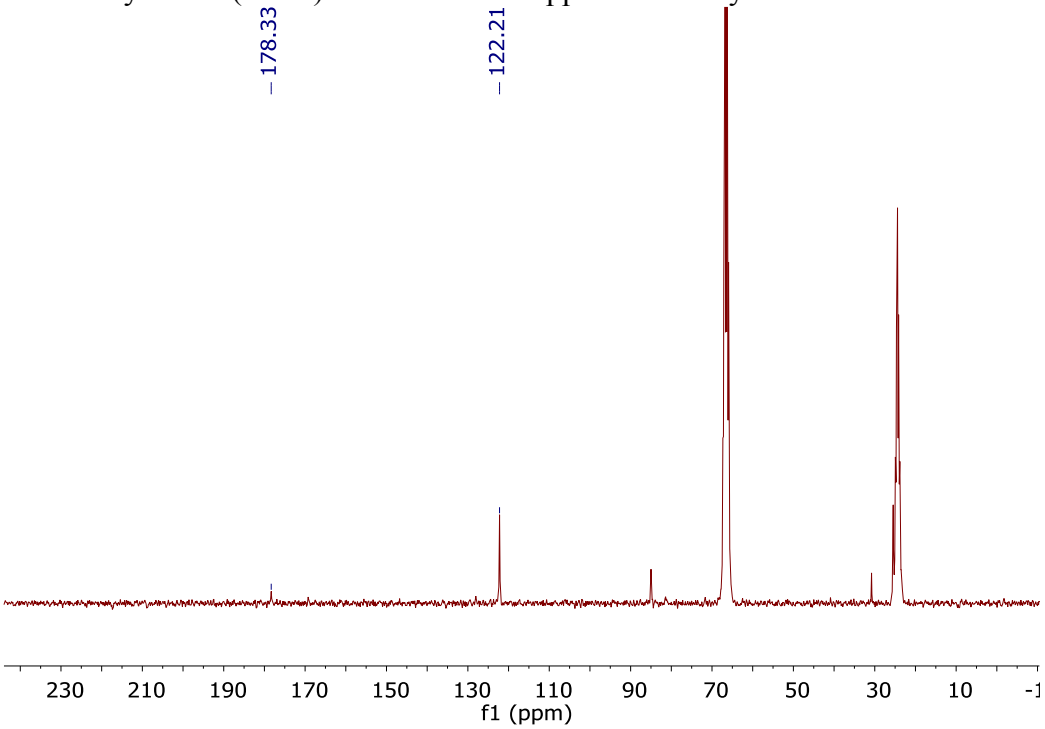

Figure 3-15. ^{13}C NMR of **14[Cu^{2+}]** in tetrahydrofuran-d$_8$.

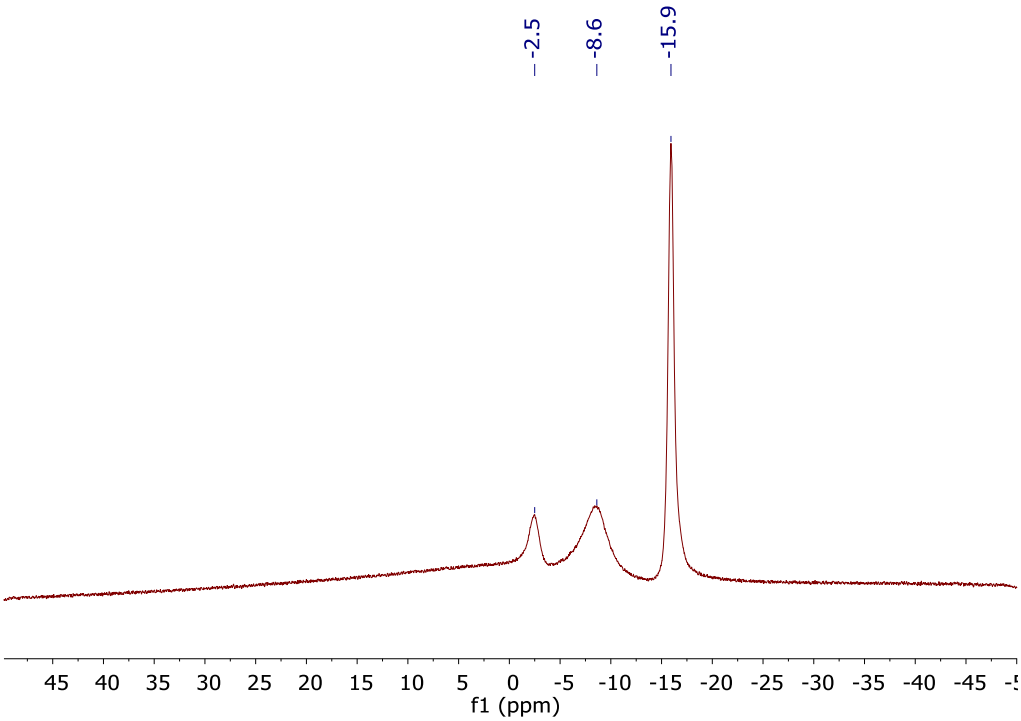

Figure 3-16. ^{11}B (^{1}H-dec) NMR. of **14[Cu^{2+}]** in tetrahydrofuran-d_8.

3.7 References

1. Pérez, P. J. (ed.), *Alkane C–H Activation by Single-Site Metal Catalysis, Catalysis by Metal Complexes*, **2012**, 1, 1-270.

2. Chirik, P. J.; Wieghardt, K. *Science* **2010**, *327*, 794.

3. Davies, H. M. L.; Dick, A. R. *Topics in Current Chemistry* **2010**, *292*, 303.

4. Doyle, M. P.; Duffy, R.; Ratnikov, M.; Zhou, L. *Chemical Reviews* **2009**, *110*, 704.

5. Mbuvi, H. M.; Woo, L. K. *Organometallics* **2008**, *27*, 637.

6. Choi, M. K.-W.; Yu, W.-Y.; So, M.-H.; Zhou, C.-Y.; Deng, Q.-H.; Che, C.-M., *Chemistry: An Asian Journal* **2008**, *3*, 1256.

7. Benitez, D.; Shapiro, N. D.; Tkatchouk, E.; Wang, Y.; Goddard, W. A.; Toste, F. D. *Nature Chemistry* **2009**, *1*, 482.

8. Scott, L. T.; DeCicco, G. J. *Journal of the American Chemical Society* **1974**, *96*, 322.

9. Fuentes, M. Á.; Olmos, A.; Muñoz, B. K.; Jacob, K.; González-Núñez, M. E.; Mello, R.; Asensio, G.; Caballero, A.; Etienne, M.; Pérez, P. J. *Chemistry: A European Journal* **2014**, *20*, 11013.

10. Caballero, A.; Despagnet-Ayoub, E.; Mar Díaz-Requejo, M.; Díaz-Rodríguez, A.; González-Núñez, M. E.; Mello, R.; Muñoz, B. K.; Ojo, W.-S.; Asensio, G.; Etienne, M.; Pérez, P. J. *Science* **2011**, *332*, 835.

11. Besora, M.; Braga, A. A. C.; Sameera, W. M. C.; Urbano, J.; Fructos, M. R.; Pérez, P. J.; Maseras, F. *Journal of Organometallic Chemistry* **2014**, *784*, 2.

12. Li, Y.; Carroll, P. J.; Sneddon, L. G. *Inorganic Chemistry* **2008**, *47*, 9193.

13. Scholz, M.; Hey-Hawkins, M.; *Chemical Reviews* **2011**, *111*, 7035.

14. Douvris, C.; Michl J. *Chemical Reviews* **2013**, *113*, PR179.

15. Popescu, A. R.; Teixidor, F.; Viñas, C. *Coordination Chemistry Reviews* **2014**, *269*, 54.

16. Reed, C. A. *Accounts of Chemical Research* **2009**, *43*, 121.

17. Douvris, C.; Ozerov, O. V. *Science* **2008**, *321*, 1188.

18. El-Hellani, A.; Lavallo, V. *Angewandte Chemie International Edition* **2014**, *53*, 4489.

19. Crabtree, R. H. *Coordination Chemistry Reviews* **2013**, *257*, 755.

20. Bode, J. W. *Nature Chemistry* **2013**, *5*, 813.

21. Moerdyk, J. P.; Bielawski, C. W. *Nature Chemistry* **2012**, *4*, 275.

22. Krüger, A.; Albrecht, M. *Australian Journal of Chemistry* **2011**, *64*, 1113.

23. Wang, Y.; Xie, Y.; Abraham, M. Y.; Wei, P.; Schaefer, H. F.; Schleyer, P. v. R.; Robinson, G. H. *Journal of the American Chemical Society* **2010**, *132*, 14370.

24. Singh, J.V.; Baranwal, B.P.; Mehrotra. R.C. *Zeitschrift Für Anorganische und Allgemeine Chemie* **1981**, *477*, 235.

25. Moselage, M.; Li, J.; Ackermann, L. *ACS Catalysis* **2016**, *6*, 498.

Chapter 4: Fusing 10-vertex *closo*-Carborane Anions with N-Heterocyclic Carbenes

4.1 Introduction

At the turn of the 20th century, both Buchner and Staudinger proposed a neutral divalent carbon atom that only possessed six valence electrons. These molecules are now known commonly as carbenes.[1,2] Carbenes have transformed in the last 100 years from a theoretical concept to molecules of synthetic utility in chemical industries.[3] In 1988, Bertrand reported the first isolable or "bottleable" carbene[4] (Figure 4-2, **A**), and since then there has been an explosion of research and developing applications of these molecules.[5-15] Carbenes are described by the electronic state of the nonbonding electrons residing on the carbon atom, which are either singlet or triplet states, as illustrated in Figure 4-1. For a singlet carbene, both electrons are paired in the nonbonding sp^2 hybridized orbital of the carbon atom, leaving the orthogonal p orbital vacant. The two electrons of a triplet carbene are not paired together, and instead one occupies the sp^2 hybridized orbital while the other occupies the p orbital. The electronic state of a carbene's nonbonding electrons is determined by whether the energy required to pair the electrons is greater or less than the energy difference between the two unpaired electrons.

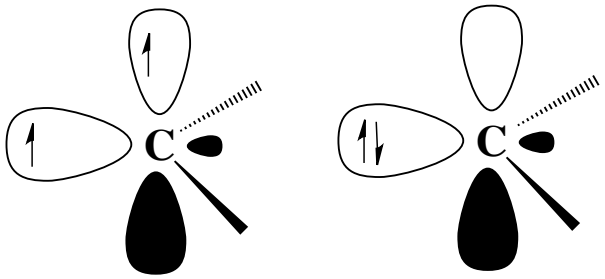

Figure 4-1. Triplet state (left) and singlet state (right) configuration of carbenes.

One class of carbene, N-heterocyclic carbenes (NHCs) has been extensively studied as both the free isolated species and as ligands for organometallic complexes.[6,10,16-18]

Exploration of NHCs began as early as the 1960's,[19,20] but the first isolated NHC, or imidazolylidene (Figure 4-2, **B**), was reported by Arduengo[11] in 1991. Since then, these molecules have proven to be tremendous ligands for catalyst design[16-18] and have been used alone as organocatalysts.[21-24] The nitrogen atoms on either side of the carbene carbon atom, referred to as the C-2 position, simultaneously act as π-donors and strong σ-withdrawing groups, stabilizing the carbene. The carbene carbon is a strong σ-donor and weak π-acceptor, leading to the formation of electron rich metal complexes that are favored for

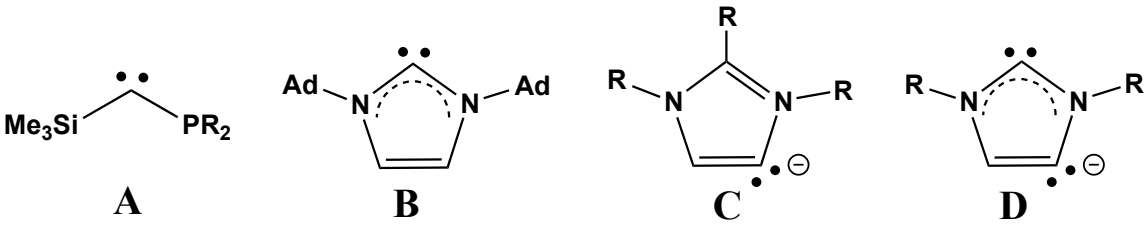

Figure 4-2. The first reported isolable stable carbene by Bertrand, phosphine-silyl carbene **A**; Arduengo's N-heterocyclic carbene **B**; Bertrand's abnormal NHC **C**; Robinson's doubly deprotonated anionic NHC **D**.

catalytic reactions. Bulky substituents are typically positioned on each nitrogen atom to prevent dimerization, although NHCs with smaller substituents have been synthesized as well despite being far less stable. A variety of alkyl and aryl substrates can be implemented at the nitrogen positions, allowing for tuning of the steric and electronic properties of NHCs.

Usually, NHCs are generated from imidazolium cations by deprotonation with a strong base at the most acidic position of the aromatic ring, C-2. Alternatively, Bertrand and coworkers[25] demonstrated that if the C-2 position is blocked, one of the backbone positions (C-4, C-5) can be removed with an equivalent of strong base (Figure 4-2, **C**). These "abnormal" NHCs or C-5 imidazolylidenes, offer an alternative in ligand design,

and in some instances have been known to exhibit superior catalytic properties.[26-32] Following Bertrand's discovery of the abnormal NHC, Robinson and coworkers simultaneously deprotonated the C-2 and C-5 positions of the imidazolium ring with two equivalents of base, forming an anionic molecule[33] (Figure 4-2, **D**).

4.2 Carboranyl Imidazoliums and N-Heterocyclic Carbenes

Not typically included in catalyst design, the icosahedral carborane anion [$HCB_{11}H_{11}^{1-}$] **2** and its derivatives are among an elite set of weakly coordinating anions that feature unmatched chemical robustness.[34-38] Polyhalogenation of the B-H vertices of this cluster amplifies its robustness and also enhances the weak coordinative ability of the cluster as a whole.[33,34,39] These properties have allowed for the isolation of a variety of super reactive cations[34,40-45] as well as the design of main group catalysts capable of C-F and C-H functionalization.[46] Recently, the Lavallo group has shown that clusters including the 12-vertex carborane anion **2** can be utilized as substituents for ligands in catalyst design, which in some cases has led to superior catalysts compared to systems containing ligands with pure hydrocarbon groups.[47] In addition, we have shown that it is possible to prepare stable monoanionic **6**, dianionic normal **12**, dianionic abnormal **15**, and trianionic **16** N-Heterocyclic Carbene (NHC) Li^+ adducts (Scheme 4-1).[48] Thus, these species are actually carbenoids and not carbenes since they are ligating their countercations. Another interesting feature in these systems is that the polyanionic carbenoids **12, 15,** and **16** can be selectively formed from the single anionic imidazolium precursor **6**, which is not possible with hydrocarbon N-substituents. There has been growing interest in anionic NHC ligands since they offer the possibility of preparing distinct coordination environments as

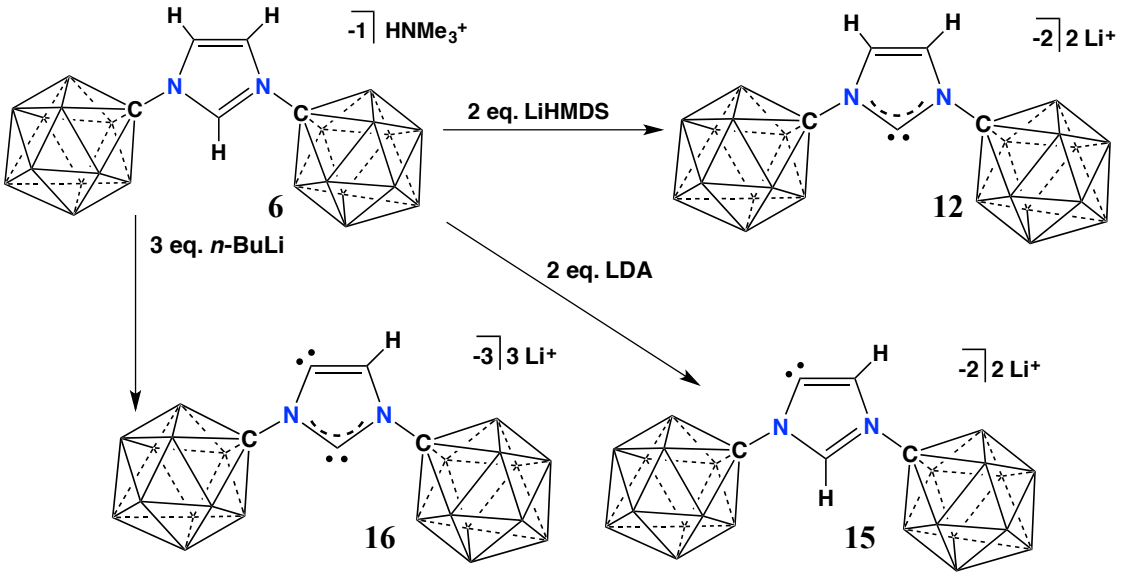

Scheme 4-1. From the N-carboranyl imidazolium anion **6**, either the normal carboranyl NHC dianion **12**, the abnormal carboranyl NHC dianion **15**, or the doubly deprotonated NHC trianion **16** can be selectively formed utilizing different bases.
Unlabeled vertices = B-H.

well as allowing for the formation of zwitterionic transition metal complexes with enhanced solubility in hydrocarbons compared to standard cationic catalysts. Tamm has elegantly demonstrated the advantages of such systems and recently reviewed the topic.[49,50] Nearly all of the known anionic NHCs are carbenoids that strongly bind their countercations.

Compared to the icosahedral carborane anion **2**, the smaller ten-vertex bicapped square antiprism [$HCB_9H_9^{1-}$] **3**, which was discovered by Knöth[51] in 1971, has been far less investigated (Figure 4-3). A survey of the literature indicates that this anion is compatible with strong acids/bases and studies from our lab have shown it is very stable towards redox chemistry.[52,53] Similar to **2**, the closed

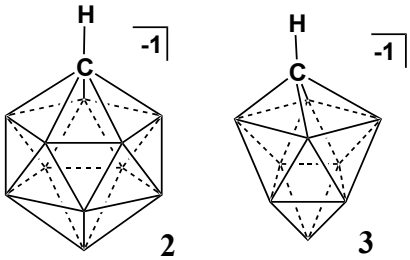

Figure 4-3. The Carba-*closo*-dodecaborate anion **2** (left) and carba-*closo*-decaborate anion **3** (right).

anionic cluster **3** can undergo selective B-H halogenation to form more weakly coordinating derivatives.[54] We therefore became interested in the use of **3** as a less sterically demanding surrogate of **2** in ligand design. Recently we reported the first phosphine ligands containing this smaller cluster and showed that the 10-vertex carborane cluster **3** is not only less sterically demanding than **2**, but also a significantly stronger σ-inductive donor.[55] Subsequently, we became curious if it were possible to prepare N-carboranyl NHCs featuring **3** as a ligand substituent. Here we report the isolation of the first 10-vertex N-carboranyl carbenoids. In addition, we show that the anionic imidazolium precursor can be directly perchlorinated, rendering the ensuing NHC more weakly coordinating, and allowing for the isolation of the first true dianionic carbene, which happens to be water stable.

4.3 Synthesis of the 10-Vertex closo-Carboranyl Amine

Previously we utilized simple condensation chemistry for the first step on the imidazolium synthesis with the known 12-vertex carboranyl amine **4**.[48] Surprisingly, this amine had been known for over 40 years but no one had attempted condensation chemistry with ketones or aldehydes until the Lavallo research group. The analogous 10-vertex *closo*-amine [$H_2NCB_9H_9^{1-}$] **17** was first reported by Kennedy and coworkers in 1997,[56] but similar condensation reactions with C=O multiple bonds have not been reported (Scheme 4-2). Given our experience with the 12-vertex amine **4**[48,57,58] we predicted an analogous approach could be utilized to build an appropriate NHC precursor. Although the 10-vertex carborane cluster **3** was discovered alongside the 12-vertex carborane **2**,[59] fewer studies have been done regarding the properties and stability of this molecule. As a result, there

was not yet a comparable synthetic route to 10-vertex carboranyl amine **17** as exists for **4**. Of the known synthetic routes, the most direct methods resulted in a mixture of inseparable products or extremely low yields. When Kennedy and coworkers[56] first reported of the 10-

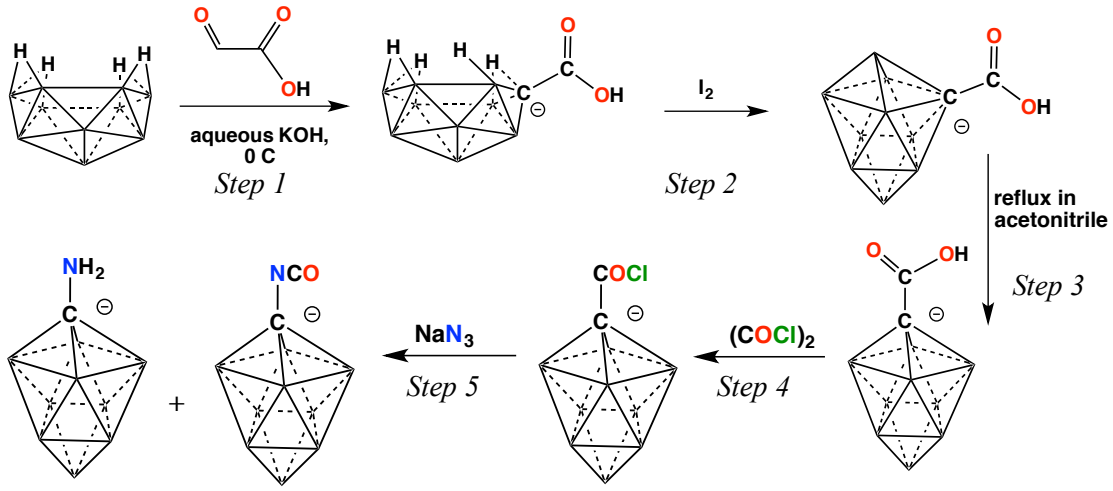

Scheme 4-2. Synthesis of 10-vertex carboranyl amine **17**, starting from decaborane and forming the *closo*-carboxylic acid cluster prior to the amine.

vertex *closo*-amine **17**, they initially formed a mixture of both the 10- and 12-vertex *closo*-amine clusters (**4** and **17**) and were able to separate these compounds over multiple crystallizations. These routes had been previously attempted in our lab with unsuccessful results, and so I sought out an alternative method, first preparing the carba-*closo*-decaborate anion bearing a carboxylic acid at the carbon vertex and then transforming this functional group into the amine.

In 2004, Kennedy and coworkers disclosed the carba-*closo*-decaborate cluster functionalized with a carboxylic acid (Scheme 4-2, steps 1-3).[60] This *closo*-cluster is synthesized using a Brellochs reaction[61] with decaborane and glyoxylic acid, abstracting a boron vertex in basic aqueous conditions and replacing it with a carbon atom bearing the carboxylic acid moiety. The functionalized *arachno* cluster undergoes oxidation with

elemental iodine to produce the 2-isomer of the 10-vertex *closo*-carborane. Refluxing in acetonitrile quickly converts the cluster to the 1-isomer. In my attempts to scale up this reaction, I found that the open *arachno*-cluster is susceptible to spontaneous combustion when drying the compound exposed to air. During the occurrences where ignition of the compound took place, I noted that it consistently occurred with batches of compound on scales larger than those reported in literature (>2 grams). To avoid losing the product via spontaneous combustion, the compound should be filtered under an inert atmosphere. Once the open cluster has been successfully obtained, oxidation with I_2 and the following isomerization step proceed according to literature. To transform the carboxylic acid to the amine, I implemented a procedure from Kaszynski and coworkers originally intended for disubstituted 10-vertex carborane derivatives, with iodide substitution of the antipodal position (Scheme 4-2, steps 4 and 5).[62] Treatment with oxalyl chloride promptly results in the formation of the acid chloride derivative, which upon reflux with NaN_3 produces a mixture of isocyanate and amine derivatives. Upon hydrolysis, the mixture should be converted to the 10-vertex *closo*-amine **17** cluster. Despite my efforts to maintain rigorously dry and consistent reaction conditions, the obtained product contained varying amounts of impurities that I have been unable to identify. Multiple crystallizations were needed to obtain a purified product.

Recently, my fellow labmate Scott McArthur reexamined the synthetic route for the anionic 10-vertex carborane amine **17** published by Kennedy and coworkers.[56] After his experience with the unfunctionalized 10-vertex carborane synthesis, he was convinced there must be a more accessible route to the 10-vertex carboranyl amine. The synthesis first

reported by Kennedy and coworkers results in a mixture of both the 10- and 12-vertex *closo*-amine clusters (**4** and **17)**. The previous step to the *closo*-carborane clusters in this

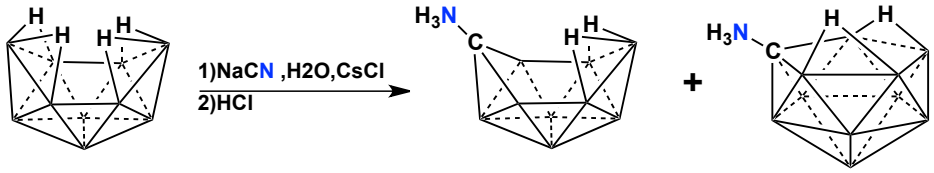

Scheme 4-3. Synthesis from Kennedy and coworkers, 10- and 11-vertex open zwitterionic amine clusters.

reaction was published in earlier work from 1981, reacting decaborane with NaCN to install a carbon vertex, which was subsequently protonated with HCl.[63] This initial reaction results in a mixture of 7-NH_3-7-$CB_{10}H_{12}$ and 6-NH_3-6-CB_9H_{11}. In a following publication, the separation of these two compounds is reported by adding acetone to the crude reaction mixture, forming the corresponding isopropylidene amine open clusters (Scheme 4-3).[64] In aqueous solution, the CB_9 isopropylidene amine cluster is less soluble, precipitating from solution. Kennedy's synthesis for the 10-vertex carboranyl amine **17** uses the CB_9 isopropylidene cluster, heating at 200 °C in the presence of borane triethylamine. My

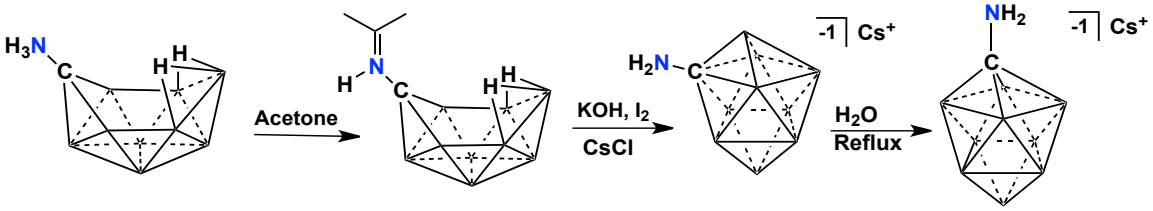

Scheme 4-4. Synthesis from Scott McArthur (unpublished) for 10-vertex carboranyl amine **17.**

labmate Scott recognized that borane triethylamine is an additional boron source, and results in the mixture of cluster sizes. The open *arachno* CB_9 isopropylidene amine cluster already contains all of the necessary boron atoms to form the 10-vertex *closo*-cluster, and

Scott hypothesized that similar reaction conditions to the unfunctionalized 10-vertex carborane **3** synthesis would result in the desired product (Scheme 4-4). He found that stirring the CB_9 isopropylidene amine with excess KOH and elemental iodine leads directly to the singular product of the *closo*-carboranyl amine 2-isomer. This is easily converted to the 1-isomer via reflux. Following Scott's discovery, this is the synthetic route now utilized to obtain the 10-vertex carboranyl amine **17** in our research group.

4.4 Synthesis of the N-Heterocyclic Carbenes Featuring 10-Vertex Carborane Anions

With the 10-vertex carboranyl amine **17** in hand, we reacted the two equivalents of the anionic amine **17** with glyoxal and observed the formation of the corresponding dianionic carboranyl diamine **18**, as indicated by ^{1}H NMR spectroscopy. Subsequent ring

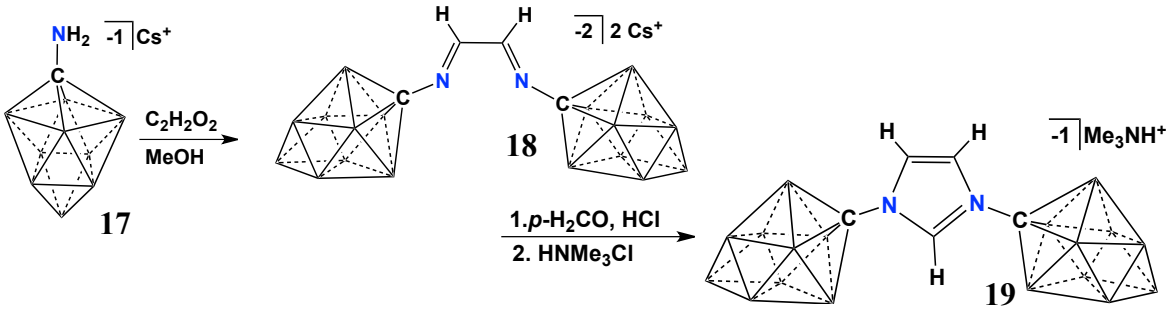

Scheme 4-5. Synthesis of 10-vertex carboranyl imidazolium anion **19**.

closure with *para*-formaldehyde and cation exchange with trimethylammonium chloride afforded the desired anionic imidazolium salt **19** in excellent yield (Scheme 4-5). Cation exchange for trimethylammonium is adventitious, *vide infra*, since in subsequent imidazolium anion deprotonations one can choose the countercation the ensuing NHCs will have depending on the nature of the base employed.

We next turned our attention to the possibility of preparing the corresponding normal C-2 deprotonated NHC Li Complex **20[Li$^+$]** (Scheme 4-6). Imidazolium anion **19**

was thus reacted with two equivalents of lithium hexamethyldisilazide (LiHMDS) and the reaction was monitored by multinuclear NMR spectroscopy. The ^{1}H NMR spectrum shows the disappearance of the characteristic triplet/doublet pattern at 10.26 and 8.45 ppm, respectively, of the imidazolium ring and the formation of a new upfield singlet resonance at 7.75 ppm, which is consistent with the formation of **20[Li^{+}]**. The ^{11}B NMR spectrum shows a set of three resonances (31.4; -12.8; -22.2 ppm) in 1:4:4 ratio, indicating that the new species retains the local C_{4v} symmetry of the cluster. Analysis of the ^{13}C NMR spectrum shows the appearance of a new resonance at 197.7 ppm, which is also consistent with the generation of the carbenoid **20[Li^{+}]**. All attempts to grow a single crystal of **20[Li^{+}]** for X-ray diffraction studies were unsuccessful. However, utilizing KHMDS in lieu of LiHMDS afforded **20[K^{+}]**, which readily crystallized (Figure 4-52, experimental section), but the structure is too disordered to have a meaningful discussion of bond lengths and angles.

We next sought to investigate if these small 10-vertex carborane anions would allow for the selective formation of the abnormal C-5 deprotonated NHC Li^{+} adduct **21**. Regardless of the conditions or bases employed we did not observe any evidence for the formation of **21**, which is in stark contrast to the exquisite selectivity previously reported for formation of **12** and **15** (Scheme 4-1).[48] Therefore, the selectivity induced by the bulkier anionic icosahedral carborane substituents is likely a steric effect and not related to the charge of such anions. While we were unable to prepare **21**, the trianionic doubly deprotonated species **22** was readily accessible by reacting **19** with three equivalents of *n*-butyllithium (Scheme 4-6). The formation of **22** was corroborated by ^{1}H NMR

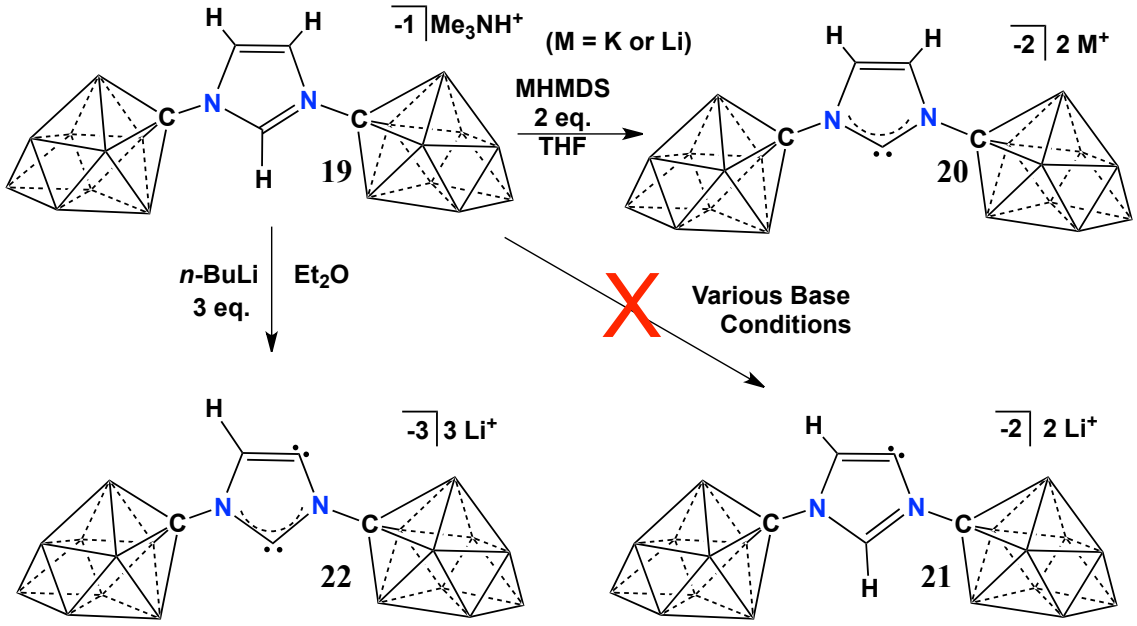

Scheme 4-6. 10-vertex N-carboranyl imidazolium anion **19** and its subsequent deprotonation to form the normal NHC dianion **20** or the doubly deprotonated NHC trianion **22**.

spectroscopy, which shows an upfield shift of the carbenoid backbone proton to 7.0 ppm. In addition, the ^{13}C spectrum shows two distinct downfield carbon resonances at 169.3 and 197.6 ppm, which is consistent with C-5 and C-2 imidazolium deprotonation, respectively. In the ^{11}B NMR spectrum the two sets of resonances for the inequivalent carborane clusters are superimposed by coincidence. The carbenoid structure of **22** was unambiguously determined by a single crystal X-ray diffraction study, but the data is not of sufficient quality to discuss structural parameters (Figure 4-53, experimental section).

4.5 Late-Stage Halogenation of 10-Vertex Carboranyl Imidazolium and Corresponding N-Heterocyclic Carbene

Given the fact that *closo*-carborane anions become more weakly coordinating when halogenated, we envisioned that it might be possible to render these 10-vertex N-carboranyl

NHCs more weakly coordinating by appending them with two perchlorinated N-carboranyl groups. We hypothesized that if this were achieved the dianionic NHC might be able to exist as a free carbene in the presence of Li^+ and not form a carbenoid complex. Initially we attempted to utilize the known perchlorinated version of amine **4** in condensation chemistry to access the prerequisite perchlorinated imidazolium anion, but this amine does not react with glyoxal. The reluctance of this amine to condense with glyoxal is likely due to the deactivating effect of the electronegative chlorine atoms as well as steric constraints of the four chlorines crowning the amine functionality.

We then attempted a direct late stage perchlorination of the imidazolium salt **19** utilizing ICl with triflic acid as a solvent. Although elevated temperatures (200 ^oC) were required, we gratifyingly observed the slow perhalogenation of **19** to ultimately afford the imidazolium anion **23**. The reaction is conveniently monitored by negative mode mass spectrometry, which shows the initial formation of numerous collections of hill-like peaks, corresponding to the different isotopic distributions of ^{11}B and ^{10}B as well as different halogen isotopes. Initially the clusters are iodinated and over time Cl- displaces the iodides in the presence of triflic acid. Ultimately, the mixture is cleanly converted to the thermodynamic product **23** (Scheme 4-7). We have attempted similar reactions with the precursor to the 12-vertex carboranyl carbenoids (**12, 15,** and **16**) but perchlorination of the entire molecule is not possible. With **23** in hand we next sought to generate the corresponding dianionic NHC **24**. Thus, **23** was reacted with two equivalents of LiHMDS in THF and monitored by multinuclear NMR spectroscopy. Analysis of the ^1H NMR spectrum of the mixture showed the disappearance of the sole characteristic low field

singlet proton of the imidazolium ring, which is consistent with the formation of **24**. Analysis of the ^{13}C spectrum shows the disappearance of the imidazolium CH carbon signal at 141.7 ppm and the appearance of a new lowfield resonance at 239.0 ppm, which is indicative of carbene formation.

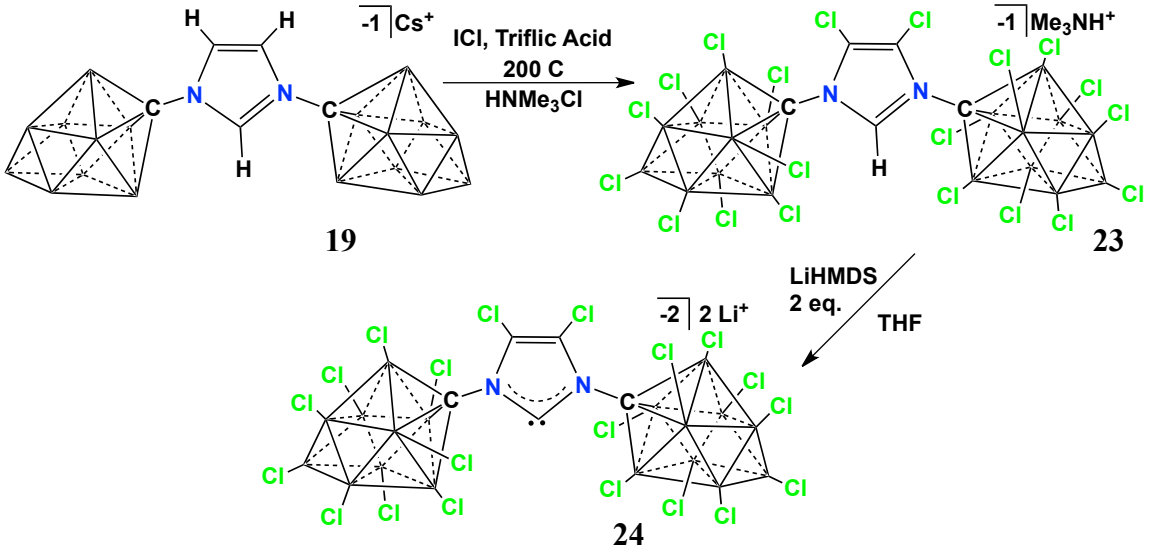

Scheme 4-7. Synthesis of perchlorinated 10-vertex carboranyl imidazolium **23**, and the subsequent deprotonation to form carboranyl NHC carbene **24.**

The structure of **24** was unambiguously determined by a single crystal X-ray diffraction study. The crystal structure reveals, that indeed, **24** is the first true dianionic carbene. The closest Li^+ ion to the carbene center is 7.293 angstroms away, which is well outside of the range for covalent bonding between C and Li^+. Furthermore, the Li^+ ions are tetrahedrally coordinated by four THF molecules, rendering them coordinatively saturated. The carbene ring parameters and exocyclic N-C cluster bonds are in the typic al range for NHCs and N-functionalized CB_9 clusters, respectively (Figure 4-54, experimental section)

Amazingly, we found that the dianionic NHC **24** is completely stable towards water. While the compound is not at all soluble in water itself, suspensions of **24** in distilled

water can be rendered a solution by the addition of THF. Analysis of these solutions by ^{13}C NMR show the pristine NHC, which persists indefinitely if sealed under an atmosphere of N_2. Opening the NMR tube to air slowly (over several days) leads to protonation to reform **23**, likely via the formation of carbonic acid via reaction of CO_2 with water. In contrast, the nonchlorinated carbenoid **20** reacts instantly with water to form **19**. The only other NHC that is reportedly persistent for short periods of time in air, but not liquid water, is Arduengo's classical N,N-dimesityl imidazolylidene with a chlorinated carbene ring backbone, analogous to **24**.

4.6 Conclusion

Here we have shown that it is possible to prepare both a 10-vertex *closo*-carborane anion [$HCB_9H_9^{1-}$] dianionic N-heterocyclic carbene (NHC) Li^+ adduct as well as a trianionic C-2, C-5 dilithio species featuring two 10-vertex carborane anion substituents. Furthermore, the anionic imidazolium salt precursor to these carbenoids can be perchlorinated utilizing ICl in triflic acid solvent. Deprotonation of the ensuing perchlorinated imidazolium anion has led to the first true dianionic carbene, which was fully characterized by multinuclear NMR spectroscopy as well as a single crystal X-ray diffraction study.

4.7 Experimental

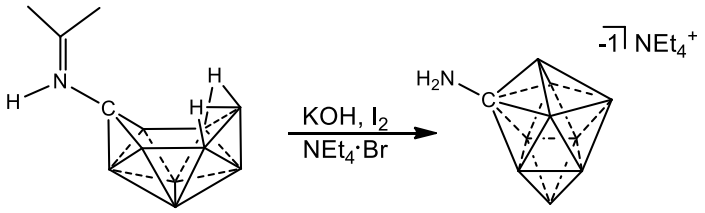

Scheme 4-8. Synthesis of 10-vertex Carborane Amine, 2 Isomer

In a 1 L beaker, 5 grams of 6-C_3H_6N-6-CB_9H_{11} (28.3 mmol) was added to 650 mL of a 1M solution of KOH, in an ice bath. To the stirring solution, 5 portions of 11g of I_2 are added 30 min apart. After the final addition of I_2 the reaction was stirred at room temperature for 12 hours. The reaction solution is then filtered and precipitated by the addition of tetraethyl ammonium bromide. The white precipitate is then collected via vacuum filtration and washed with water. 88% yield (6.59 g, 24.9 mmol). ^{1}H NMR (300 MHz, acetonitrile-d_3, 25 °C): δ = 1.87 (s, 2H, N-H), 4.45-0.0 (bm, 9H, B-H); ^{1}H (^{11}B-dec) NMR (300 MHz, acetonitrile-d_3, 25 °C): δ = 3.51 (s, 1H, B-H), 3.11 (s, 1H, B-H), 2.70 (s, 1H, B-H), 1.86 (s, 2H, N-H), 1.78 (s, 1H, B-H), 1.75 (s, 1H, B-H), 1.56 (s, 1H, B-H), 0.60 (s, 1H, B-H), 0.54 (s, 2H, B-H); ^{11}B (^{1}H-dec) NMR (96 MHz, acetonitrile-d_3, 25 °C): δ = -0.5, -6.7, -13.3, -22.7, -25.3; ^{11}B NMR (96 MHz, acetonitrile-d_{63}, 25 °C): δ = 1.1, -5.2, -11.8, -21.1, -23.7; ^{13}C-(^{1}H-dec) NMR (124 MHz, acetonitrile-d_6, 25°C): δ = 65.8 ppm.

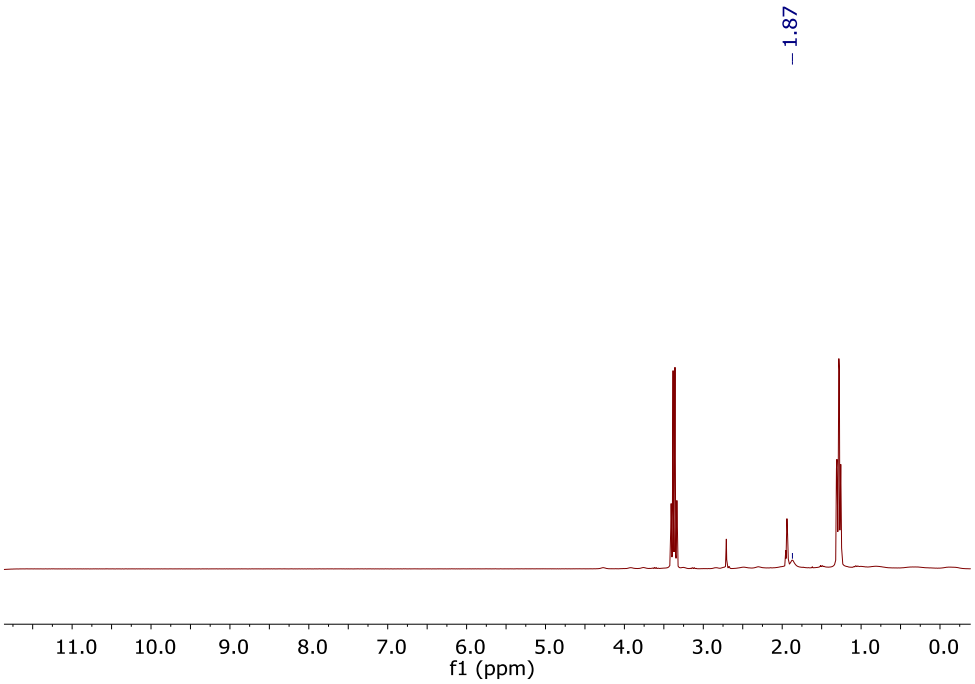

Figure 4-4. ^{1}H NMR of 2-isomer [NEt_4^+] in acetonitrile-d_3.

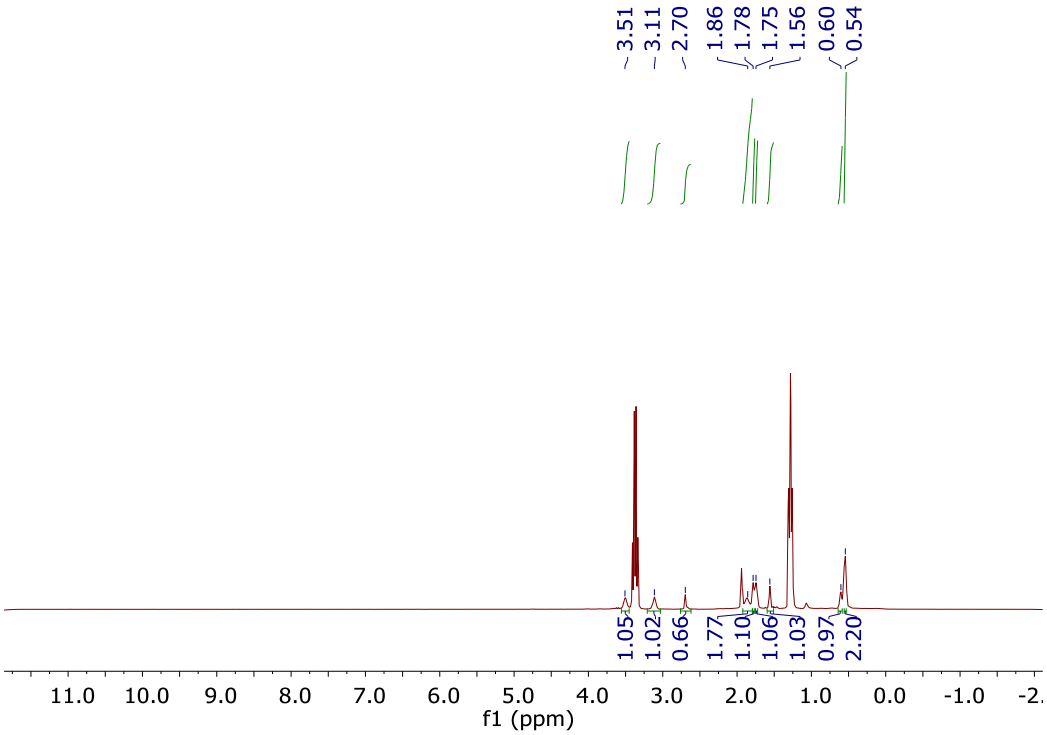

Figure 4-5. ^{1}H (^{11}B-dec) NMR of 2-isomer [NEt_4^+] in acetonitrile-d_3.

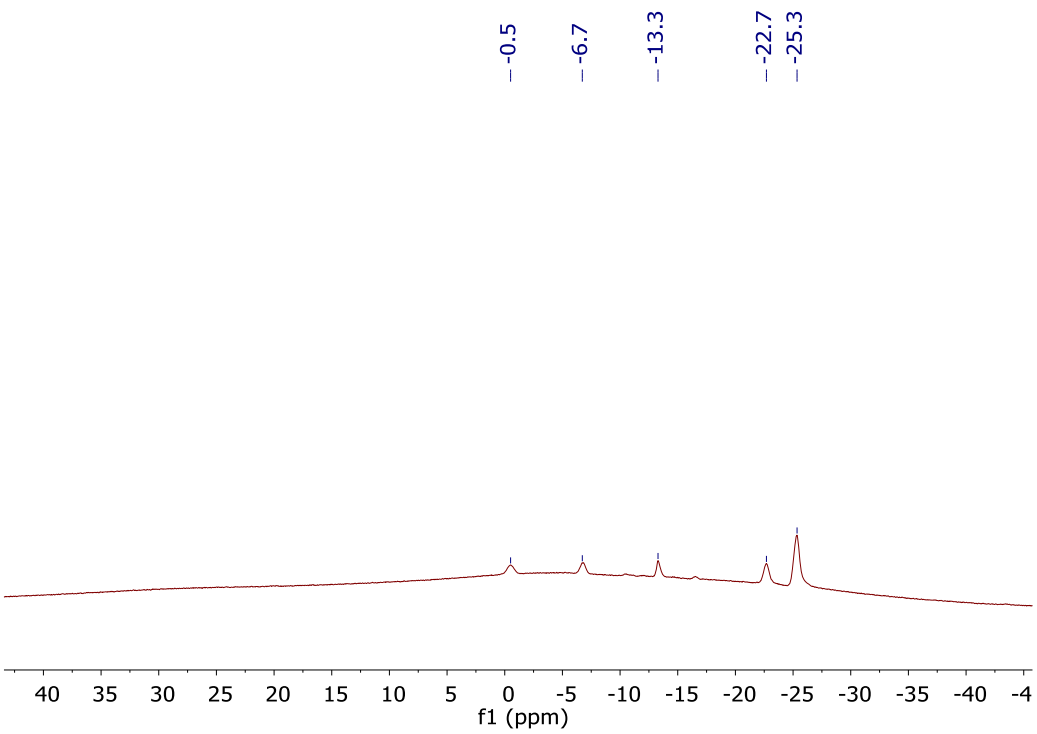

Figure 4-6. ^{11}B (^{1}H-dec) NMR of 2-isomer [NEt_4^+] in acetonitrile-d_3.

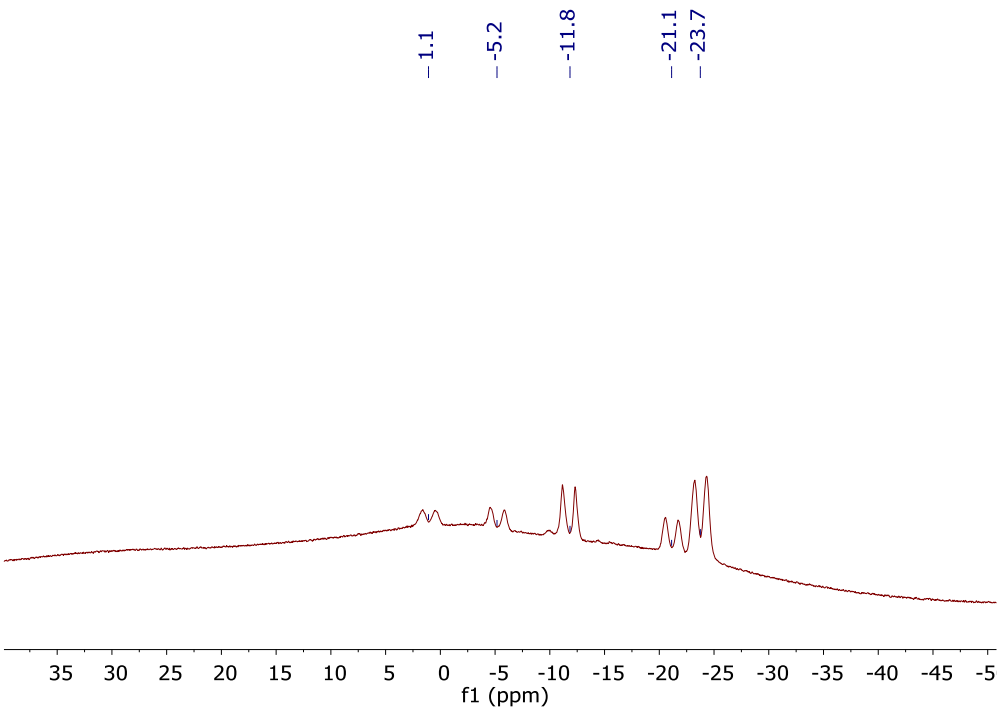

Figure 4-7. ^{11}B NMR of 2-isomer [NEt_4^+] in acetonitrile-d_3.

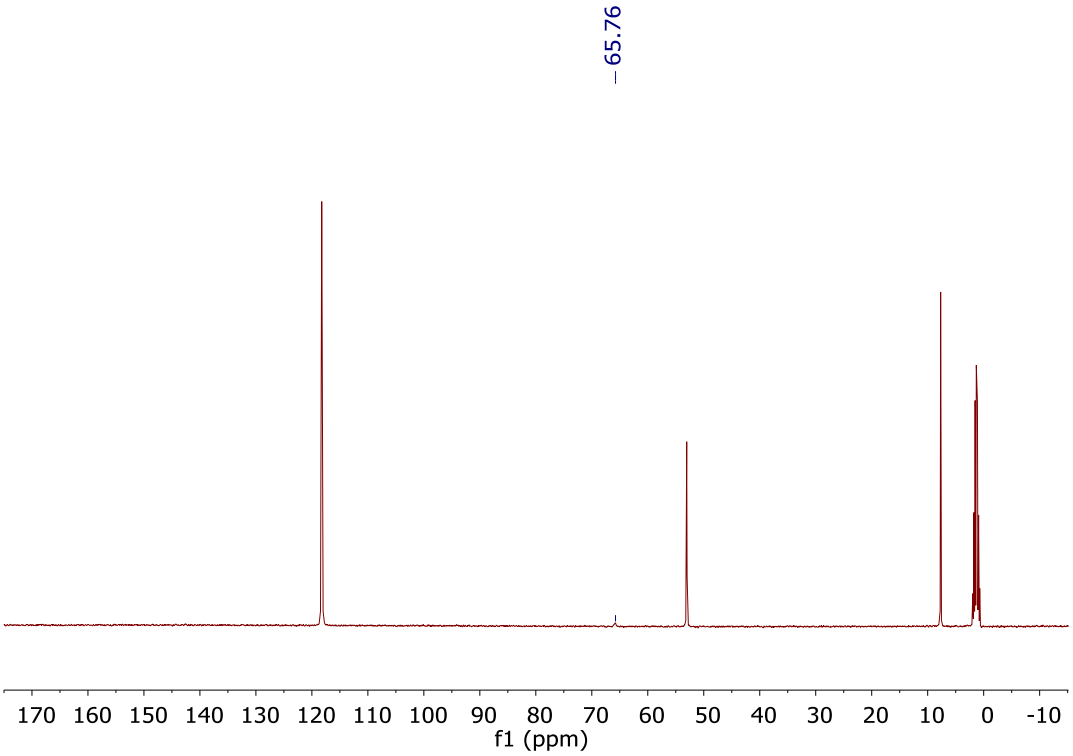

Figure 4-8. ^{13}C-(^{1}H-dec) NMR of 2-isomer [NEt_4^+] in acetonitrile-d_3.

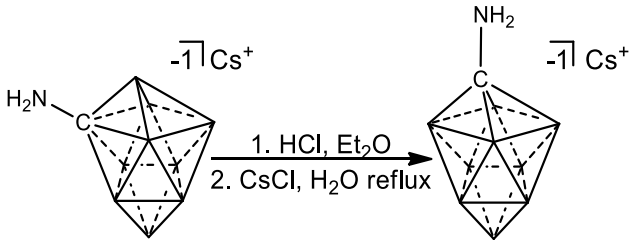

Scheme 4-9. Synthesis of 10-vertex Carborane Amine **17**, 1 Isomer

The NEt_4^+ salt of the 2-isomer (3g, 11.3 mmol) was added to 175 mL of 5% HCl, forming a suspension of white precipitate. The suspension was stirred in acidic water, and then extracted with diethyl ether. The ether is then removed by vacuum and a solution of 250 mL of H_2O containing 2 grams CsCl and 0.5 grams NaOH was added. This solution is then refluxed for 24 hours giving the Cs^+ salt of the 1-isomer **17**, 89% yield (2.70 g, 10.1 mmol). ^{1}H NMR (400 MHz, acetonitrile-d_3, 25 ℃): 3.21 (s, 2H, N-H), 5.5-0.0 (bm, 9H, B-H); ^{1}H (^{11}B-dec) NMR (300 MHz, acetonitrile-d_3, 25 °C): 3.20 (s, 2H, N-H), 1.50 (s, 5H, B-H), 0.47 (s, 4H, B-H); ^{11}B (^{1}H-dec) NMR (96 MHz, acetonitrile-d_3, 25 °C): δ = 19.8, -16.6, -25.9; ^{11}B NMR (96 MHz, acetonitrile-d_{63}, 25 °C): δ = 19.2, -17.2, -26.5; ^{13}C-(^{1}H-dec) NMR (124 MHz, acetonitrile-d_6, 25°C): δ = 85.1 ppm.

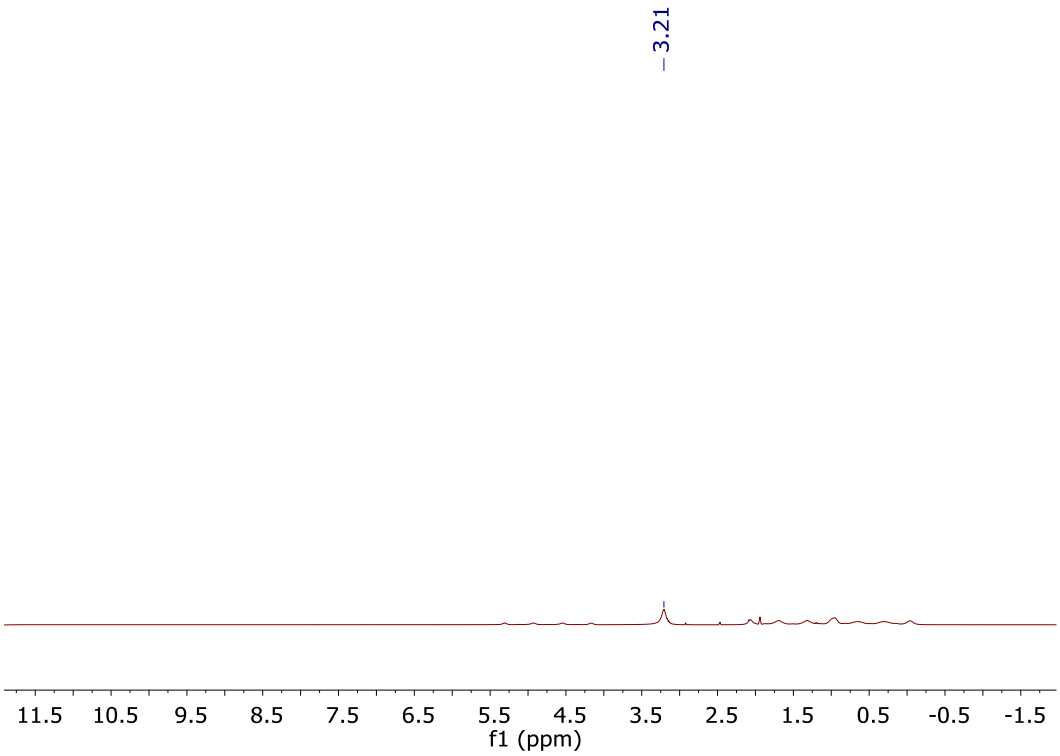

Figure 4-9. ^{1}H NMR of 1-isomer **17[Cs^{+}]** in acetonitrile-d$_3$.

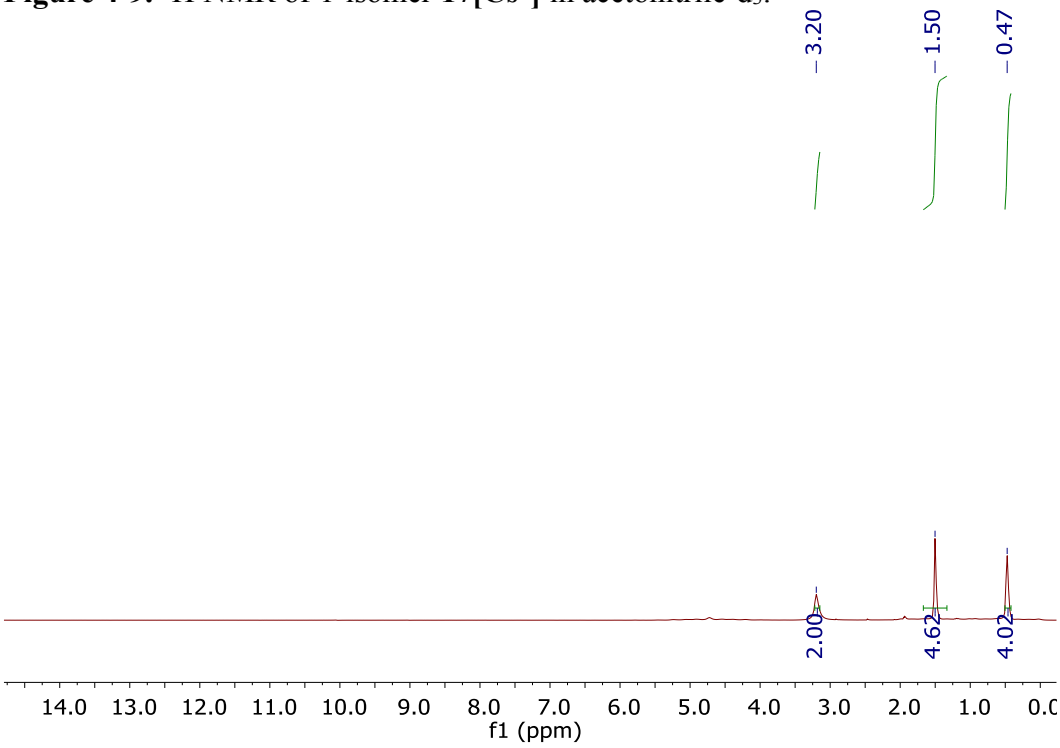

Figure 4-10. ^{1}H (^{11}B-dec) NMR of 1-isomer **17[Cs^{+}]** in acetonitrile-d$_3$.

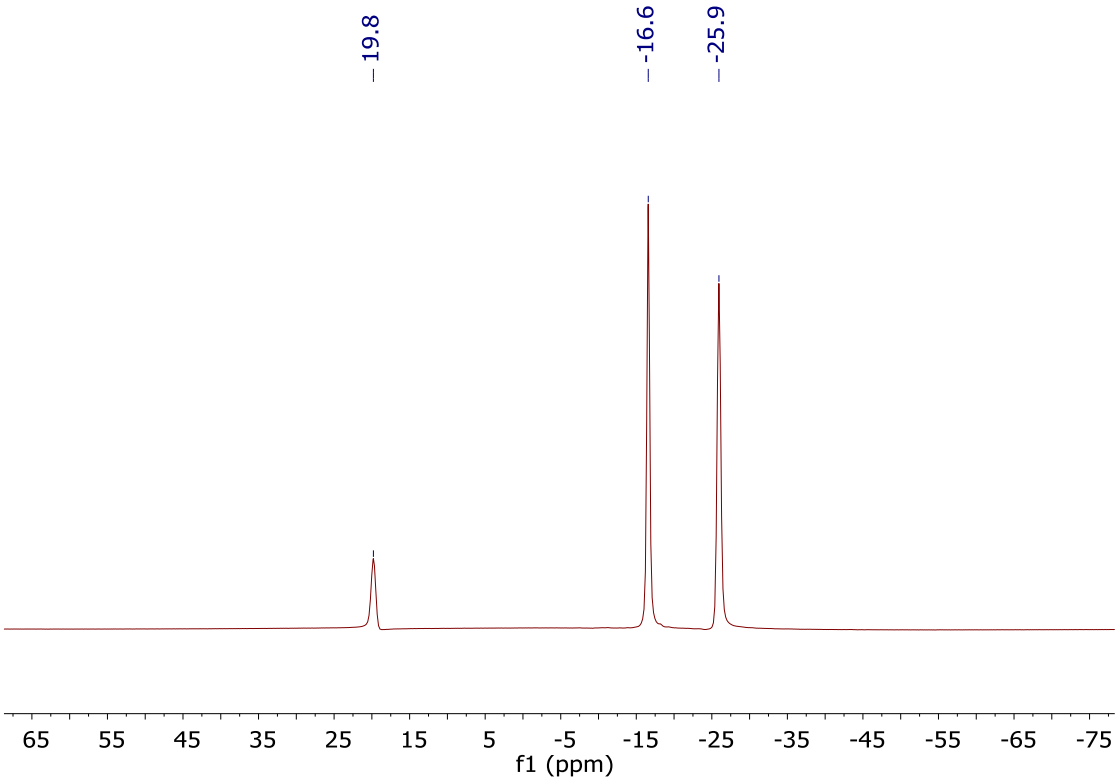

Figure 4-11. ^{11}B (^{1}H-dec) NMR of 1-isomer **17[Cs$^+$]** in acetonitrile-d_3.

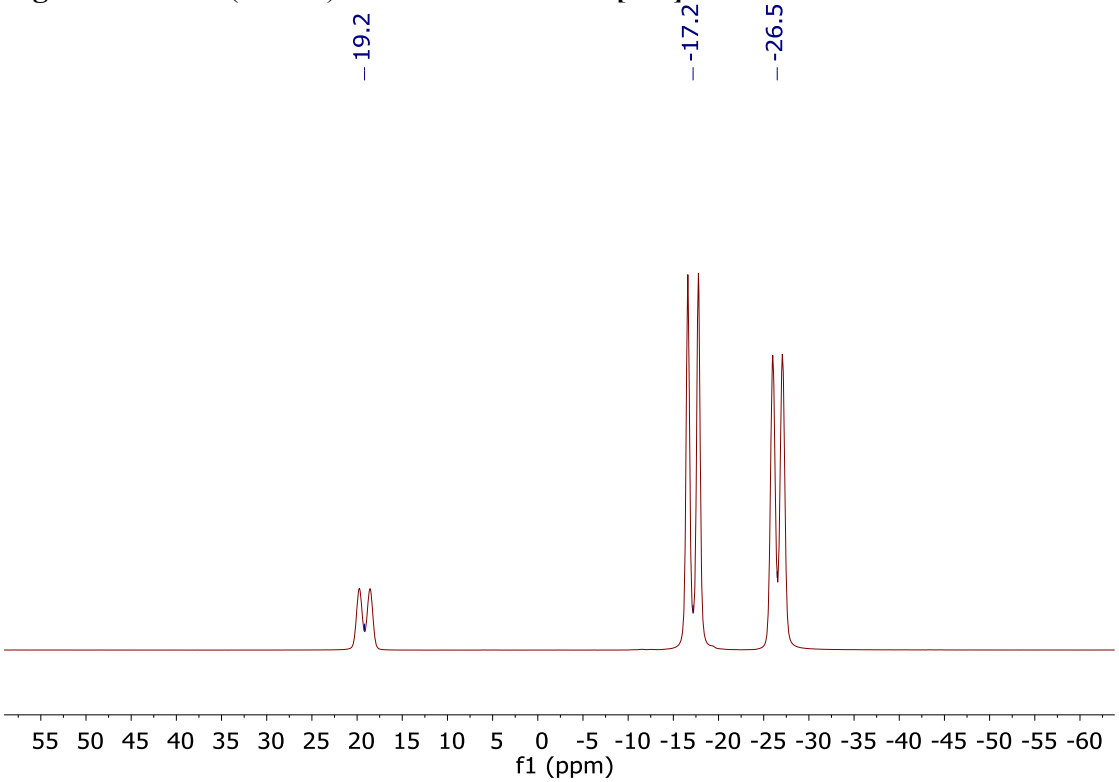

Figure 4-12. ^{11}B NMR of 1-isomer **17[Cs$^+$]** in acetonitrile-d_3.

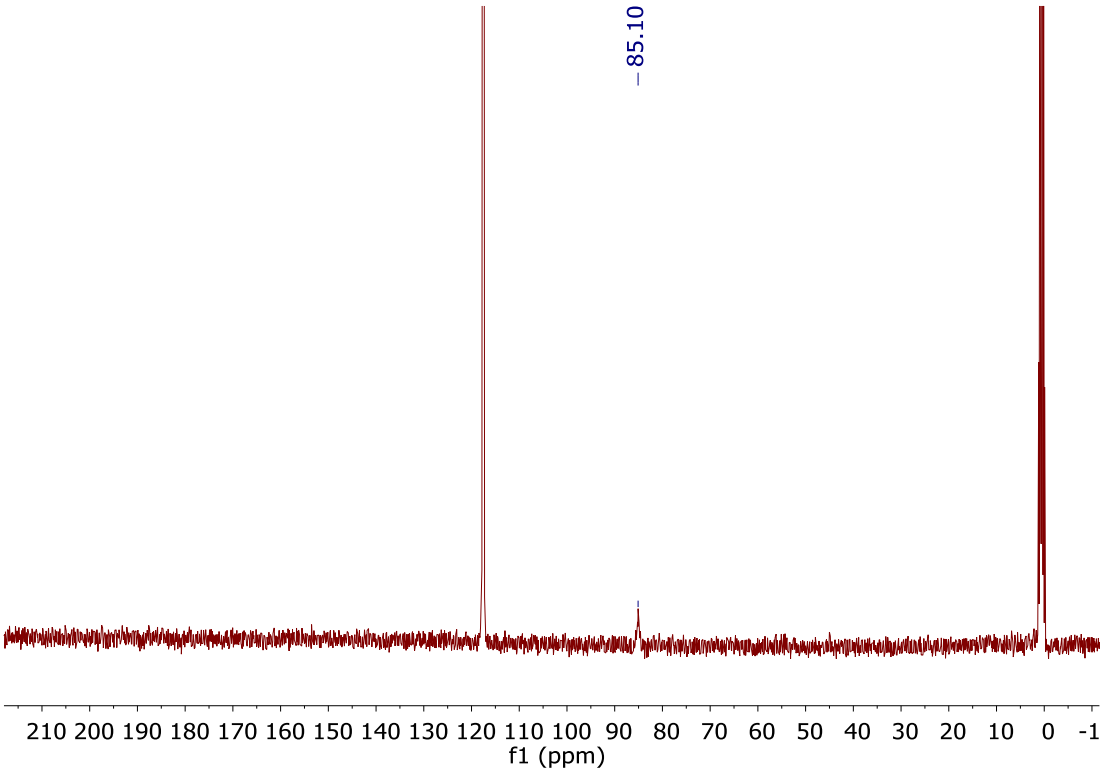

Figure 4-13. ^{13}C-(^{1}H-dec) NMR of 1-isomer **17[Cs^+]** in acetonitrile-d_3.

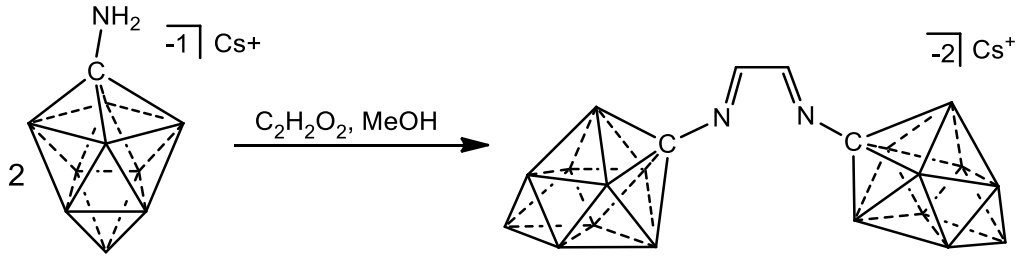

Scheme 4-10. Synthesis of 10-Vertex Dianionic Carboranyl Diimine **18**

Glyoxal ($O_2C_2H_2$) aqueous solution (40 % w/w, 130 mg, 2.2 mmol) was added to a solution of $CsNH_2CB_9H_9$, **17** (1.20 g, 4.4 mmol) dissolved in methanol (15 mL) and the reaction mixture stirred for 24 hours. Volatiles were removed under vacuum to afford the crude diimine as a light brown powder. The resulting yield of the Cs^+ diimine salt **18** was 98% (1.22 g, 2.2 mmol) ^{1}H NMR (400 MHz, acetonitrile-d_3, 25 °C): δ = 8.94 (s, 2H), 2.70-0.0 (bm, 18H, B-H); ^{13}C-(^{1}H-dec) NMR (125 MHz, acetonitrile-d_3, 25 °C): δ = 165.2; ^{11}B-(^{1}H-dec) NMR (96 MHz, acetonitrile-d_3, 25 °C): δ = 26.2, -17.4, -25.2 ppm.

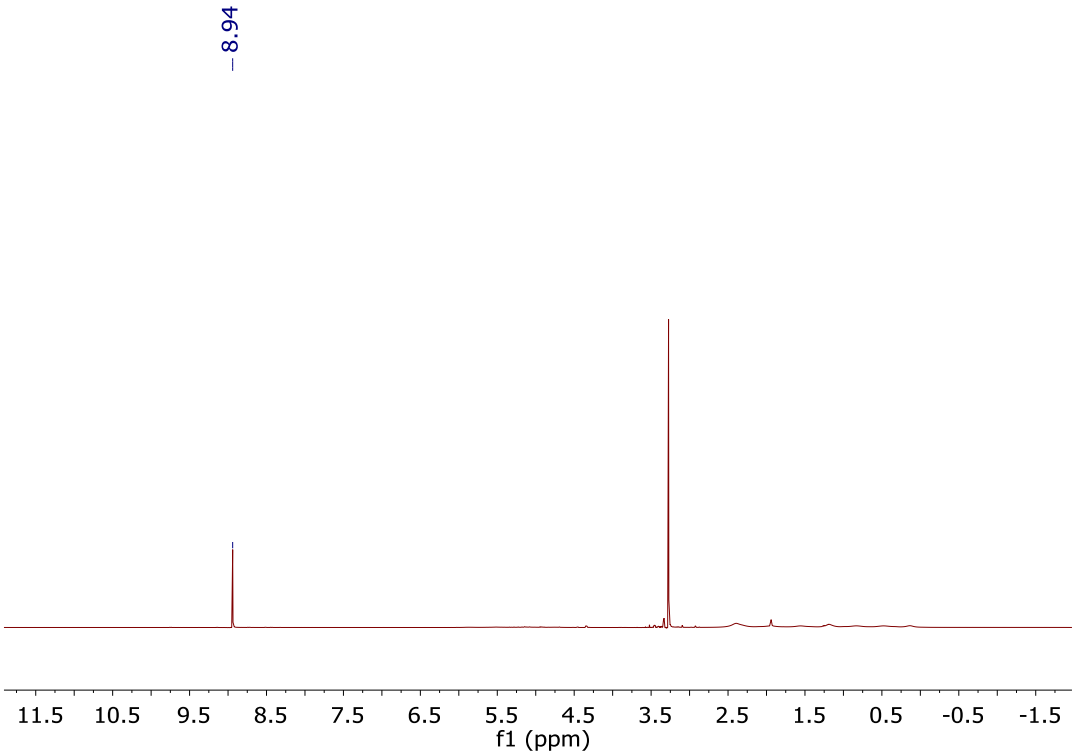

Figure 4-14. ^{1}H-NMR of **18[Cs^{+}]** in acetonitrile-d$_3$. MeOH is seen at 48.9 ppm.

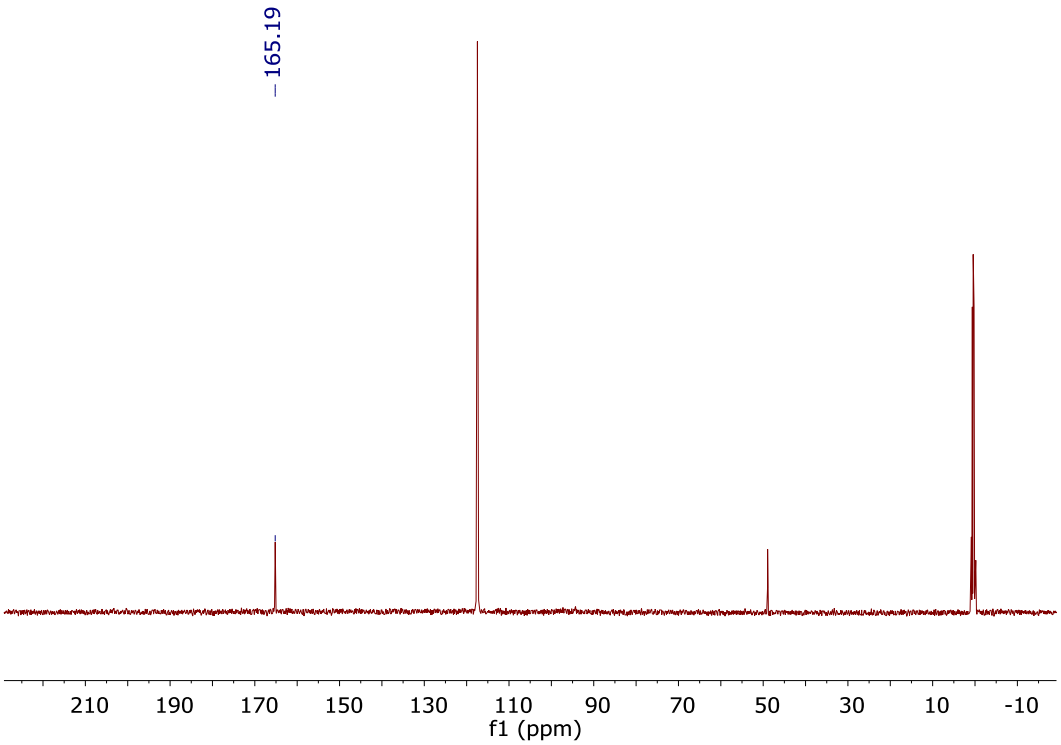

Figure 4-15. ^{13}C-(^{1}H-dec) NMR of **18[Cs^{+}]** in acetonitrile-d$_3$. MeOH is seen at 48.9 ppm.

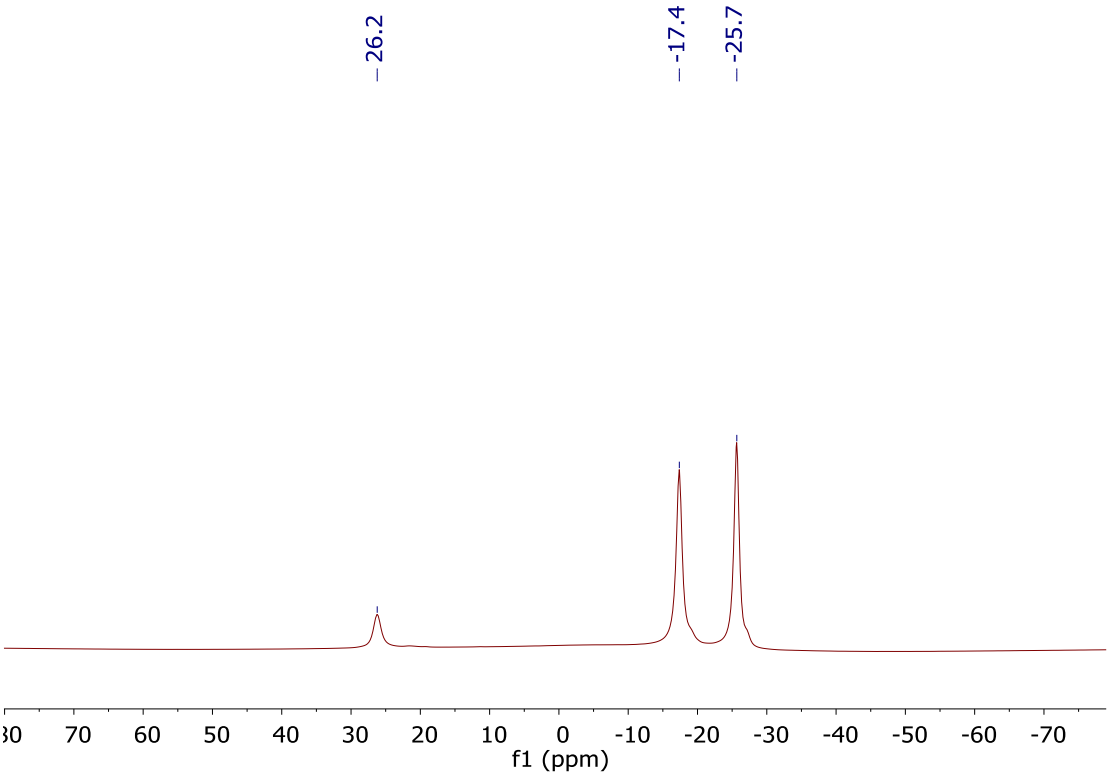

Figure 4-16. ^{11}B-(^{1}H-dec) NMR of **18[Cs^{+}]** in acetonitrile-d_3.

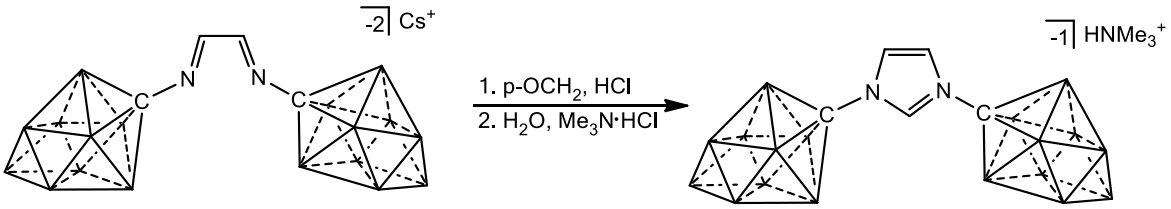

Scheme 4-11. Synthesis of 10-Vertex Imidazolium Salt **19**

Without further purification, the crude diimine **18[Cs$^+$]** (1.22 g, 2.2 mmol) was dissolved in a solution of ethyl acetate (10 mL). A second solution of 2M HCl/diethyl ether (4 mL) was added to paraformaldehyde (79 mg, 2.6 mmol) and stirred for 30 minutes. The mixture of paraformaldehyde and HCl/diethyl ether was then added to the ethyl acetate solution dropwise and stirred for three hours. Subsequent removal of all volatiles under high vacuum afforded **9** as a crude mixture. Impurities were removed by washing the product with boiling water, followed by cation exchange to the corresponding $HNMe_3^+$ salt through the addition of 1.3 equivalents of trimethylammonium hydrochloride in H_2O. The resulting yield of the $HNMe_3^+$ imidazolium salt **19[Me$_3$NH$^+$]** was 76% (473 mg, 1.70 mmol) ^{1}H NMR (300 MHz, acetone-d_6, 25 °C): δ = 10.26 (t, $^4J(H,H)$ = 1.72 Hz, 1H), 8.45 (d, $^4J(H,H)$ = 1.72 Hz, 2H), 3.25-0.0 (bm, 18H, B-H); ^{13}C-(^{1}H-dec) NMR (125 MHz, acetone-d_6, 25 °C): δ = 139.3, 125.9, 73.7; ^{11}B-(^{1}H-dec) NMR (96 MHz, acetone-d_6, 25 °C): δ = 31.0, -15.4, -25.2 ppm. HRMS (negative mode ESI/APCI) [M]- m/z calc'd for $N_2C_5B_{18}H_{21}^-$ = 304.3498; Found = 304.3491.

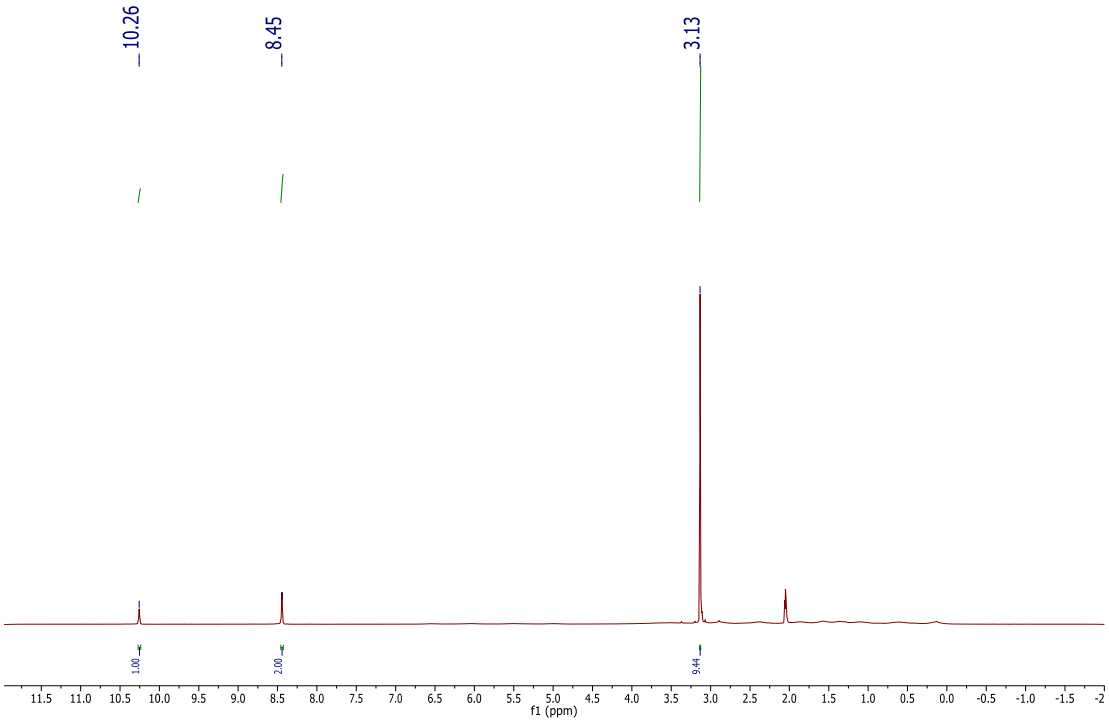

Figure 4-17. ^{1}H-NMR of **19[Me_3NH^+]** in acetone-d_6. The peak at 3.13 ppm is due to Me_3NH^+ countercation.

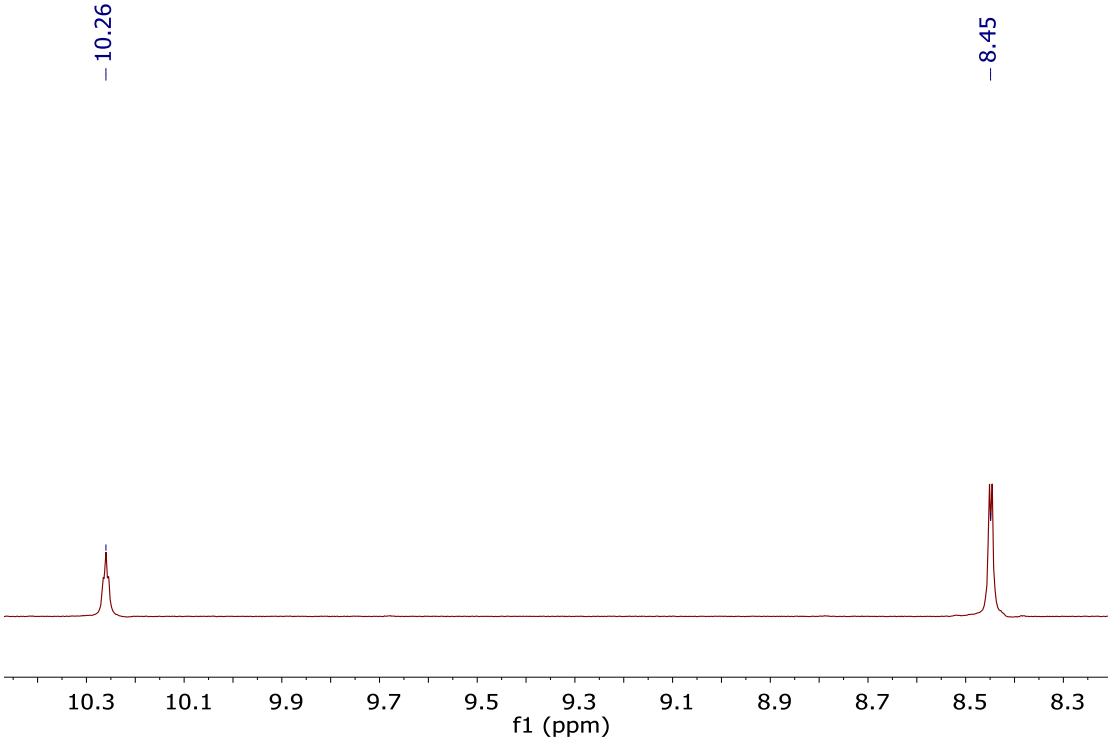

Figure 4-18. An expanded view of the aromatic region of the ^{1}H-NMR of **19[Me_3NH^+]** in acetone-d_6, showing the small $^{4}J(H,H)$ coupling through the imidazolium ring.

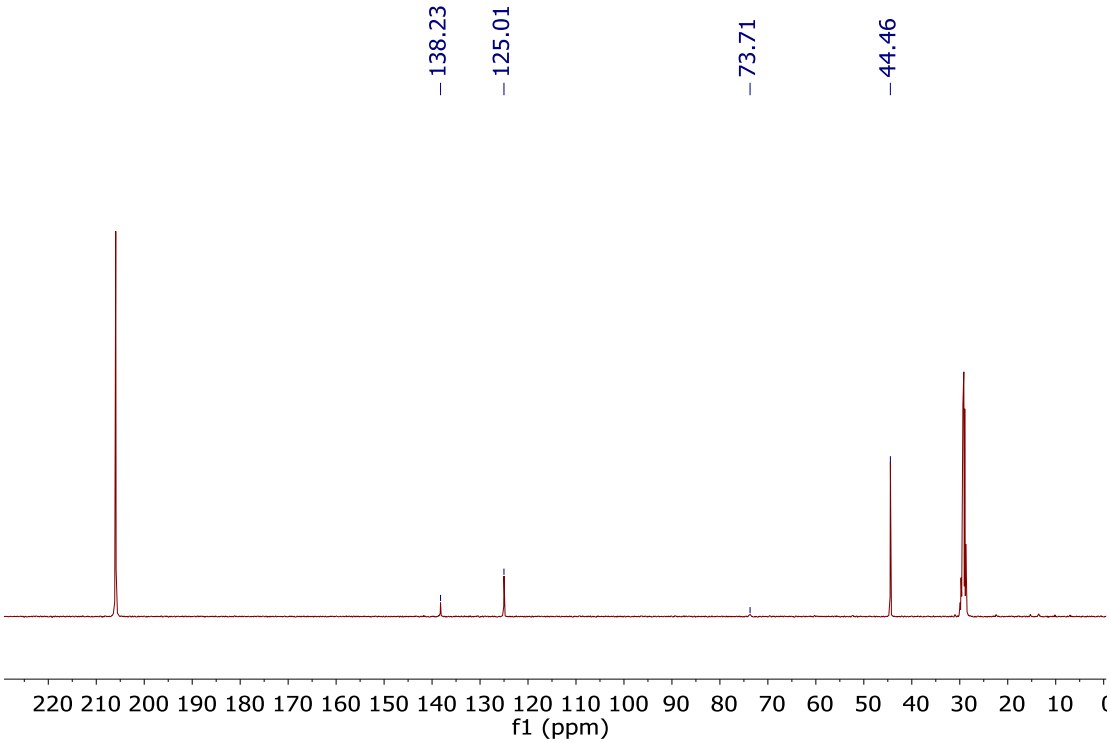

Figure 4-19. ^{13}C-(^{1}H-dec) NMR of **19[Me_3NH^+]** in acetone-d_6. The peak at 44.46 ppm is due to Me_3NH^+ countercation.

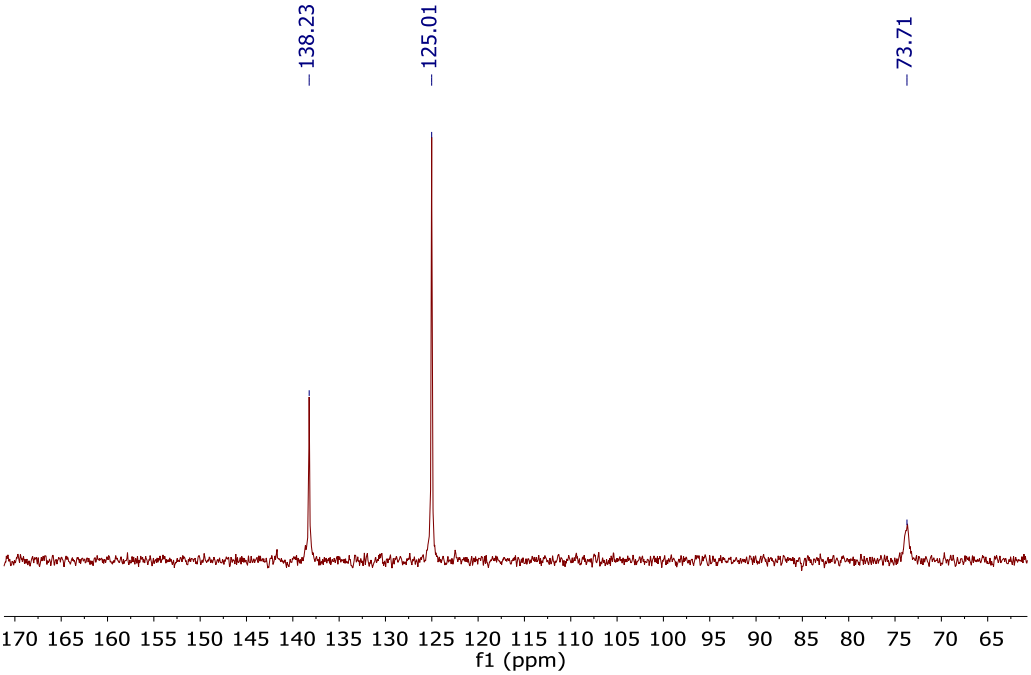

Figure 4-20. An expanded view of the ^{13}C-(^{1}H-dec) NMR of **19[Me_3NH^+]** in acetone-d_6 showing the resonance of the carborane carbon at 73.71, as well as the carbon resonances of the imidazolium ring.

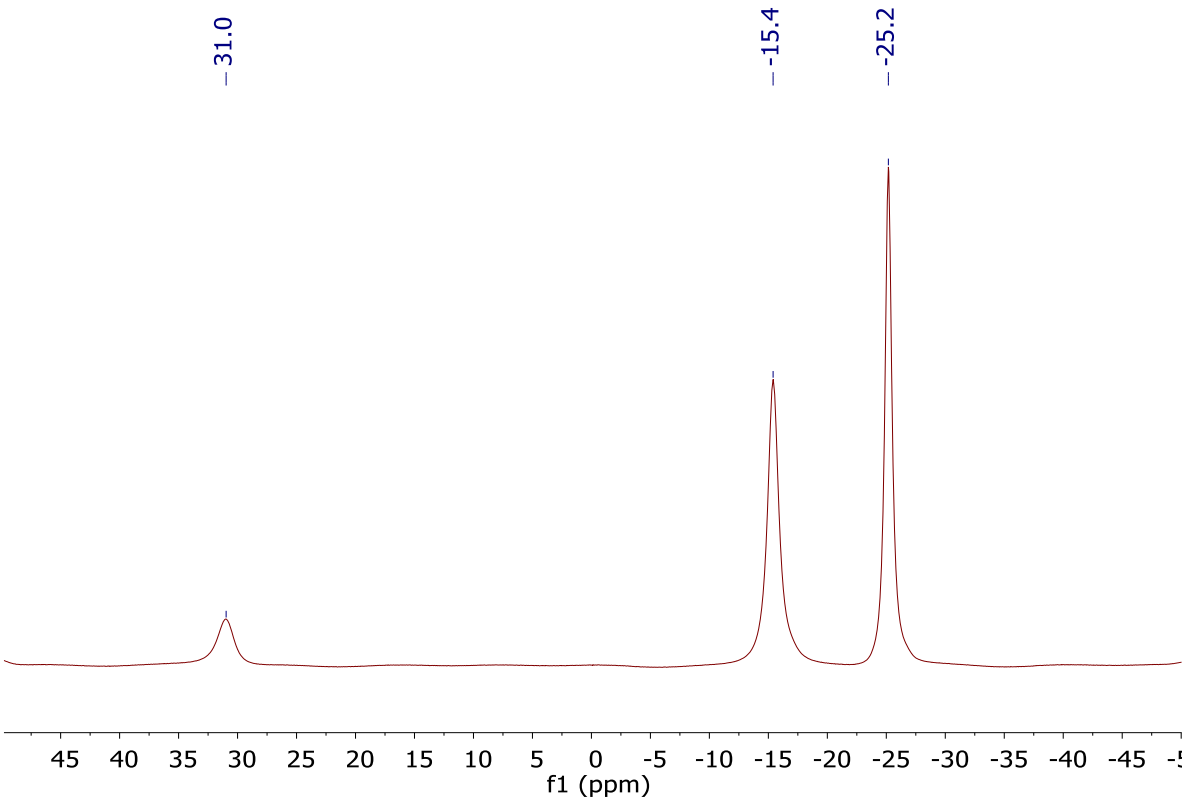

Figure 4-21. ^{11}B-(^{1}H-dec) NMR of **19[Me_3NH^+]** in acetone-d_6.

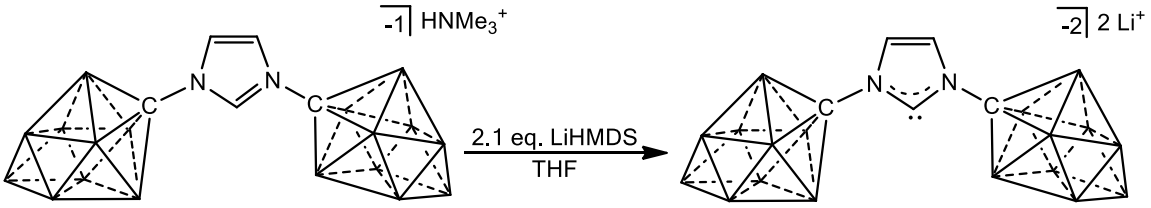

Scheme 4-12. Synthesis of Normal Li^+ NHC, **20[Li^+]**

A vial equipped with a stir bar was loaded with 310 mg (0.82 mmol) of **19[Me_3NH^+]** and 5 mL of THF. In a second vial, 2.1 equivalents (10 mg, 1.72 mmol) of LiHMDS was added and dissolved in THF (5 mL). The two THF solutions were combined, the vial capped, and the mixture stirred for 1 hour. The THF solution was added dropwise to a stirring vial of diethyl ether (20 mL), precipitating a light brown powder. The precipitate was left stirring in diethyl ether for 30 minutes. The solvent was decanted from the precipitate, and the remaining volatiles were removed under vacuum, affording the product **20[Li^+]** in 92% yield (454 mg, 0.75 mmol) (Note: Li^+ countercations contain 4 coordinated THF molecules). ^{1}H NMR (400 MHz, THF-d_8, 25 °C): δ = 7.75 (s, 2H), 0.01-2.75 (bm, 18H, B-H); ^{13}C-(^{1}H-dec) NMR (125 MHz, THF-d_8, 25 °C): δ = 197.72, 121.58, 79.34; ^{11}B-(^{1}H-dec) NMR (96 MHz, THF-d_8, 25 °C): δ = 31.4, -21.8, -22.2 ppm.

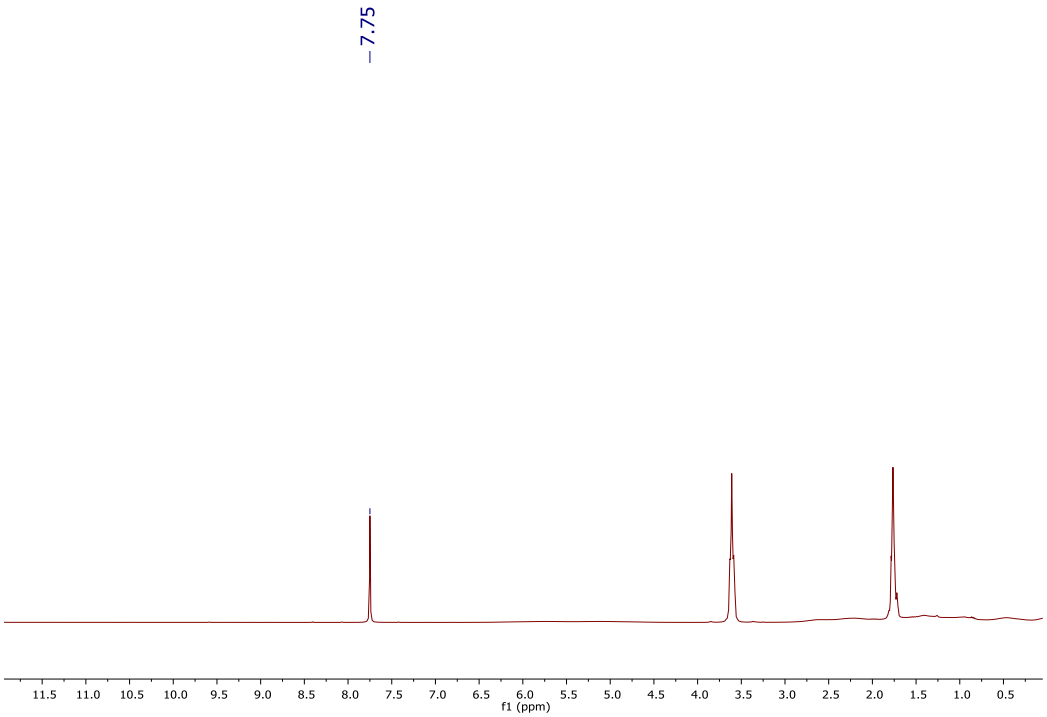

Figure 4-22. ^{1}H-NMR of **20[Li^{+}]** in THF-d$_{8}$.

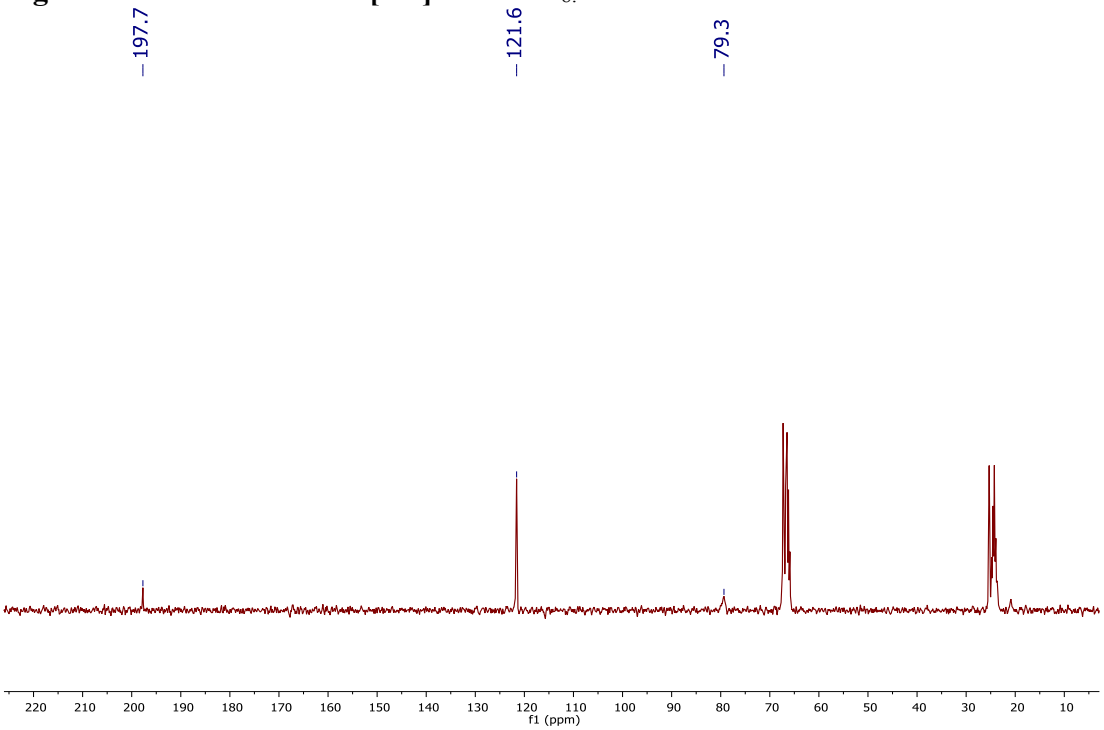

Figure 4-23. ^{13}C-(^{1}H-dec) NMR of **20[Li^{+}]** in THF-d$_{8}$.

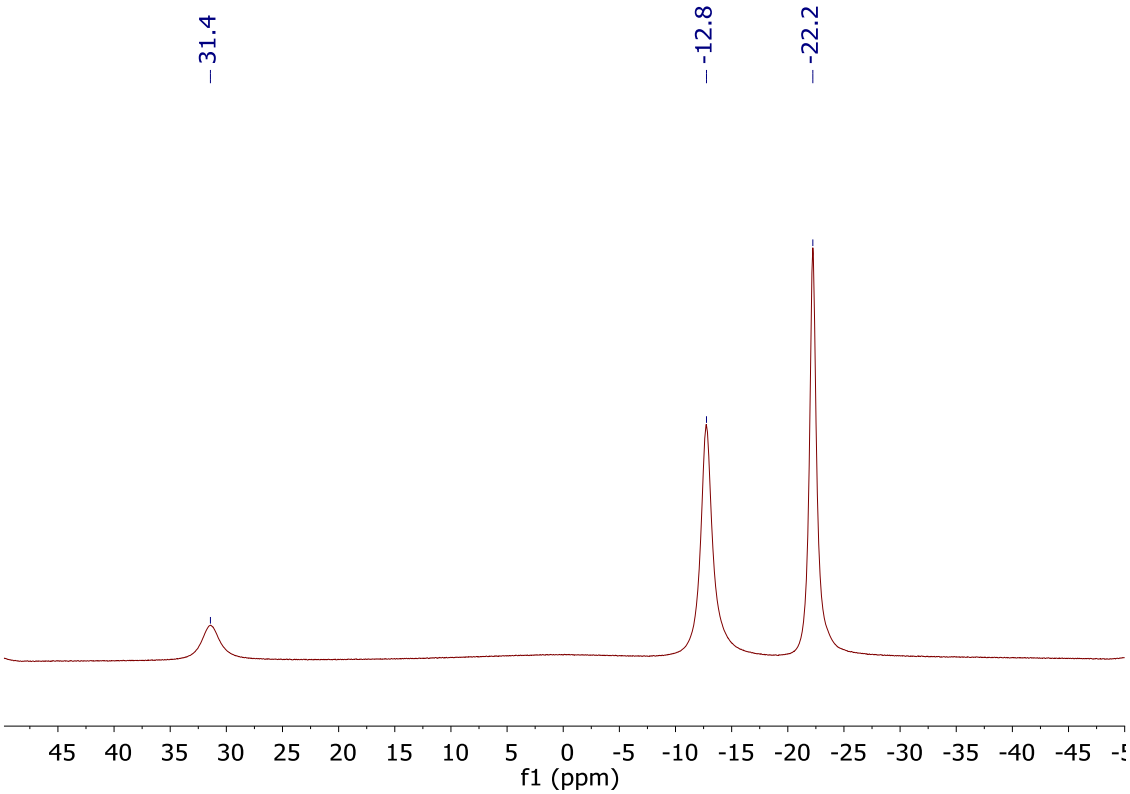

Figure 4-24. ^{11}B-(^{1}H-dec) NMR of **20[Li^{+}]** in THF-d$_8$

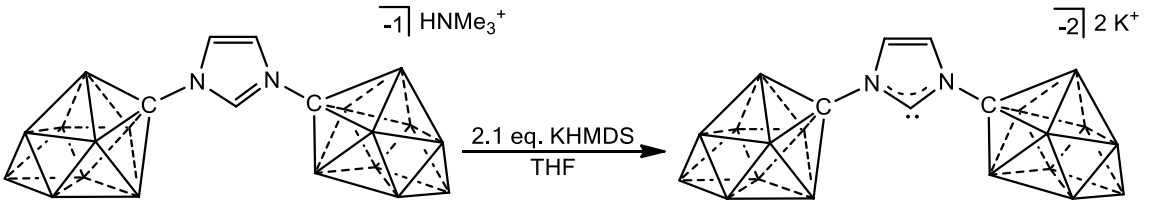

Scheme 4-13. Synthesis of Normal K^+ NHC, **20[K^+]**

A vial equipped with a stir bar was loaded with 260 mg (0.69 mmol) of **19[Me_3NH^+]** dissolved in THF (5 mL). In a second vial, 2.1 equivalents (279 mg, 1.4 mmol) of KHMDS was dissolved in THF (5 mL) and added to the fist vial containing **9**. The vial was capped and the mixture stirred for 1 hour. The THF reaction solution was added dropwise to a stirring vial of diethyl ether, precipitating a brown powder. The precipitate was left stirring in diethyl ether for 30 minutes. The solvent was decanted from the precipitate, and the remaining volatiles were removed under vacuum, affording the product **20[K^+]** in 89% yield (459 mg, 0.61 mmol). (Note: K+ countercations contain 4 coordinated THF molecules). Crystals suitable for a single crystal X-ray diffraction study were grown at -30 °C by layering a THF solution of **20[K^+]** with diethyl ether. ^{1}H NMR (500 MHz, THF-d_8, 25 °C): δ = 7.72 (s, 2H), 2.50-0.0 (bm, 22H, B-H); ^{11}B-(^{1}H-dec) NMR (96 MHz, THF-d8, 25 °C): δ = 30.5, -12.7, -22.1 ppm.

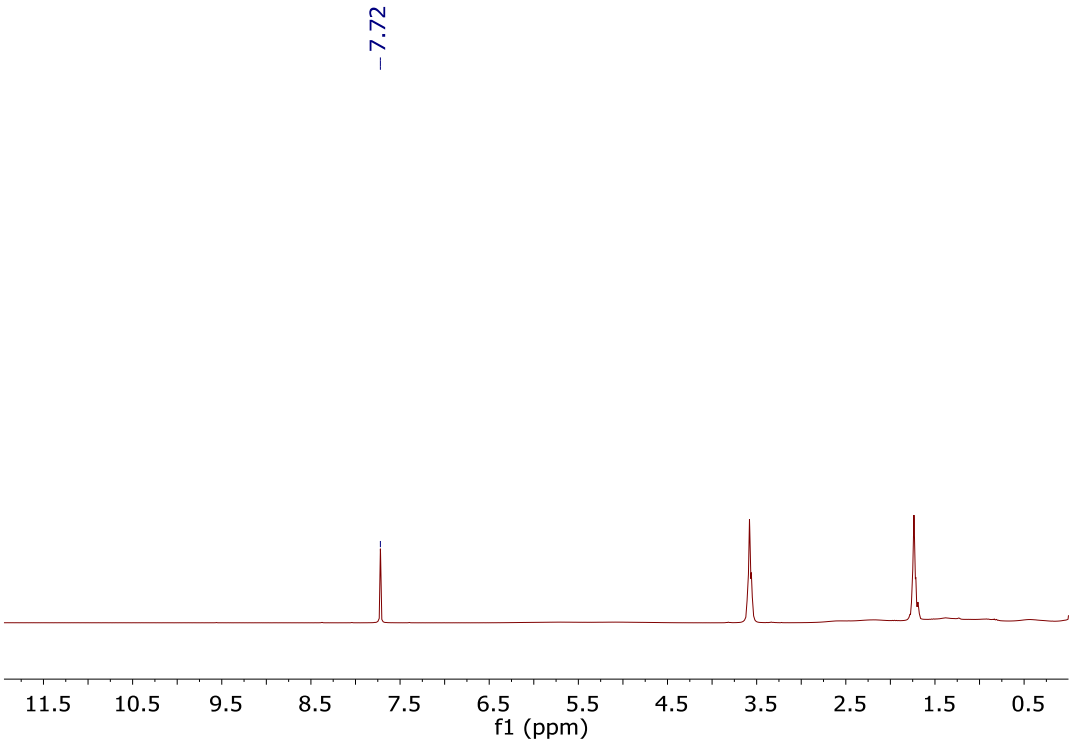

Figure 4-25. ^{1}H-NMR of **20[K^{+}]** in THF-d$_8$

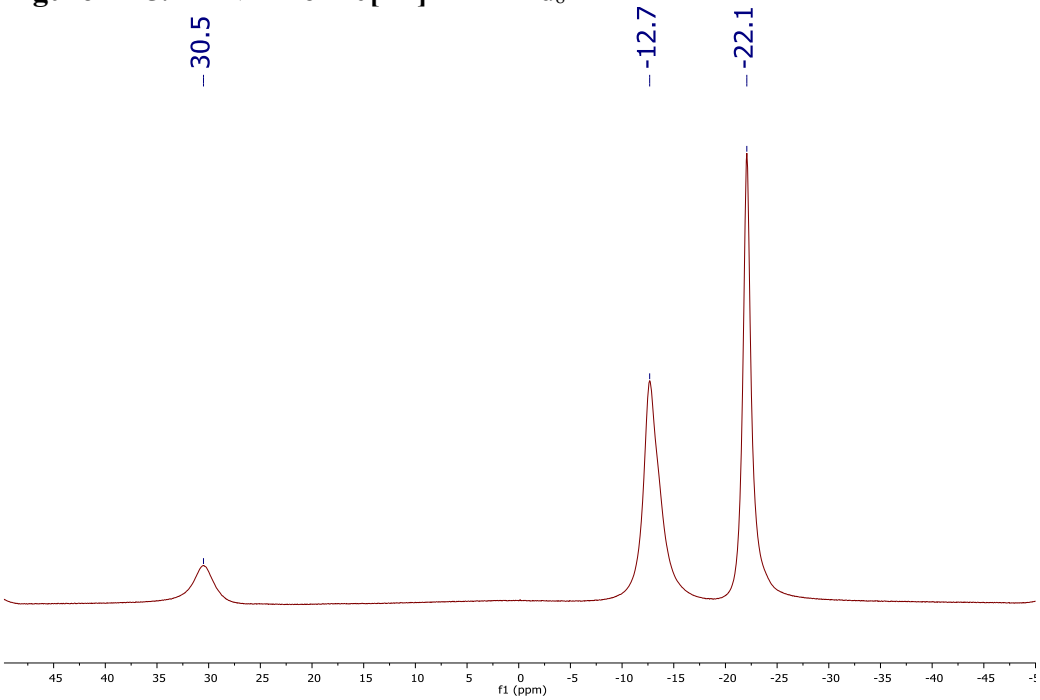

Figure 4-26. ^{11}B-(^{1}H-dec) NMR of **20[K^{+}]** in THF-d$_8$

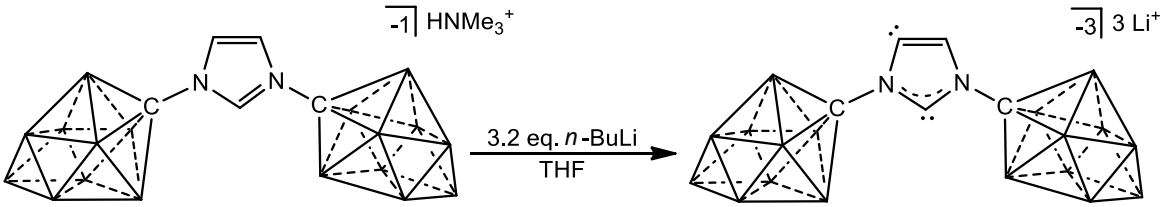

Scheme 4-14. Synthesis of Doubly Deprotonated Li^+ NHC **22[Li^+]**

A vial equipped with a stir bar was loaded with 190 mg (0.50 mmol) of **19[Me_3^+NH]**. In a second vial, 3.2 equivalents (102 mg, 0.15 mL, 1.6 mmol) of neat *n*-butyllithium was dissolved in diethyl ether (7 mL) and added to the vial containing **19**. The vial was capped and the mixture stirred. Upon initial addition of the Et_2O mixture to **19**, an oil formed. After vigorous stirring for 3 hours, the oil developed into a white precipitate. The solvent was decanted from the precipitate, and the remaining volatiles were removed under vacuum, affording the product **22[Li^+]** in 97% yield (370 mg, 0.49 mmol) (Note: 3 Li+ countercations contain 10 total coordinated THF molecules). ^{1}H NMR (700 MHz, THF-d_8, 25 °C): δ = 7.00 (s, 2H), 0.01-2.65 (bm, 18H, B-H); ^{13}C-(^{1}H-dec) NMR (125 MHz, DME, 25 °C): δ = 197.6, 169.3, 128.8, 90.0, 83.3; ^{11}B-(^{1}H-dec) NMR (96 MHz, THF-d_8, 25 °C): δ = 31.4, -21.8, -22.2 ppm.

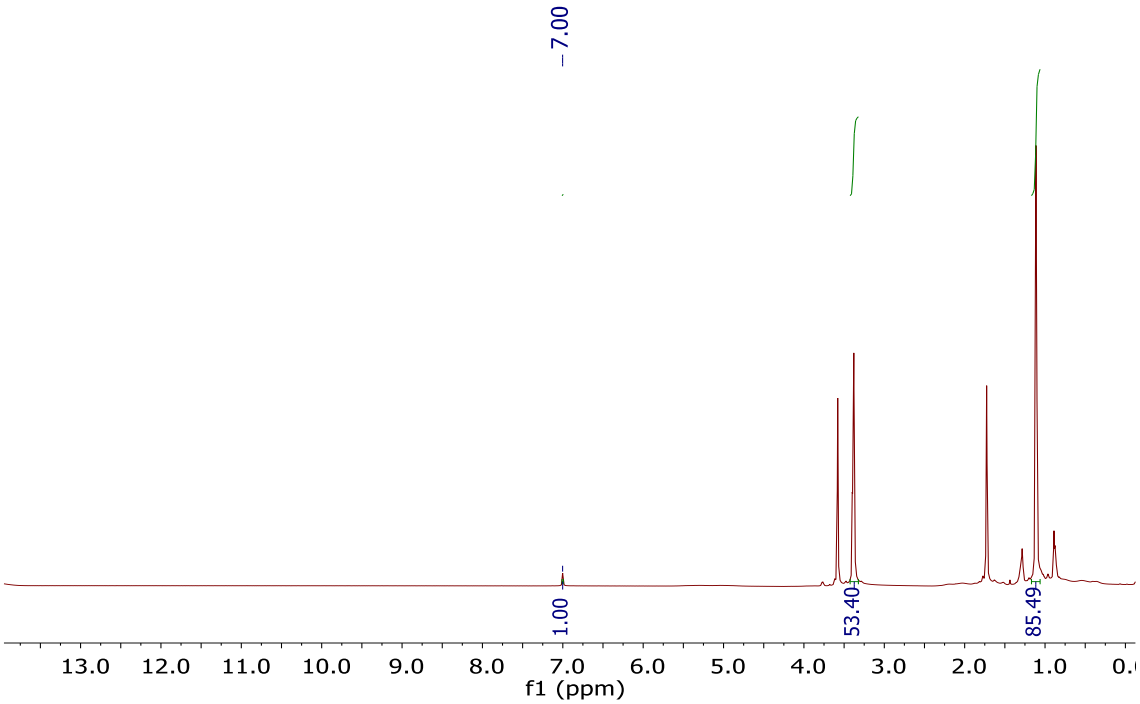

Figure 4-27. ^{1}H-NMR of **22[Li^{+}]** in THF-d$_{8}$. Note the presence of diethyl ether at 3.38 and 1.12 ppm, and H-grease at 0.91 and 1.29 ppm.

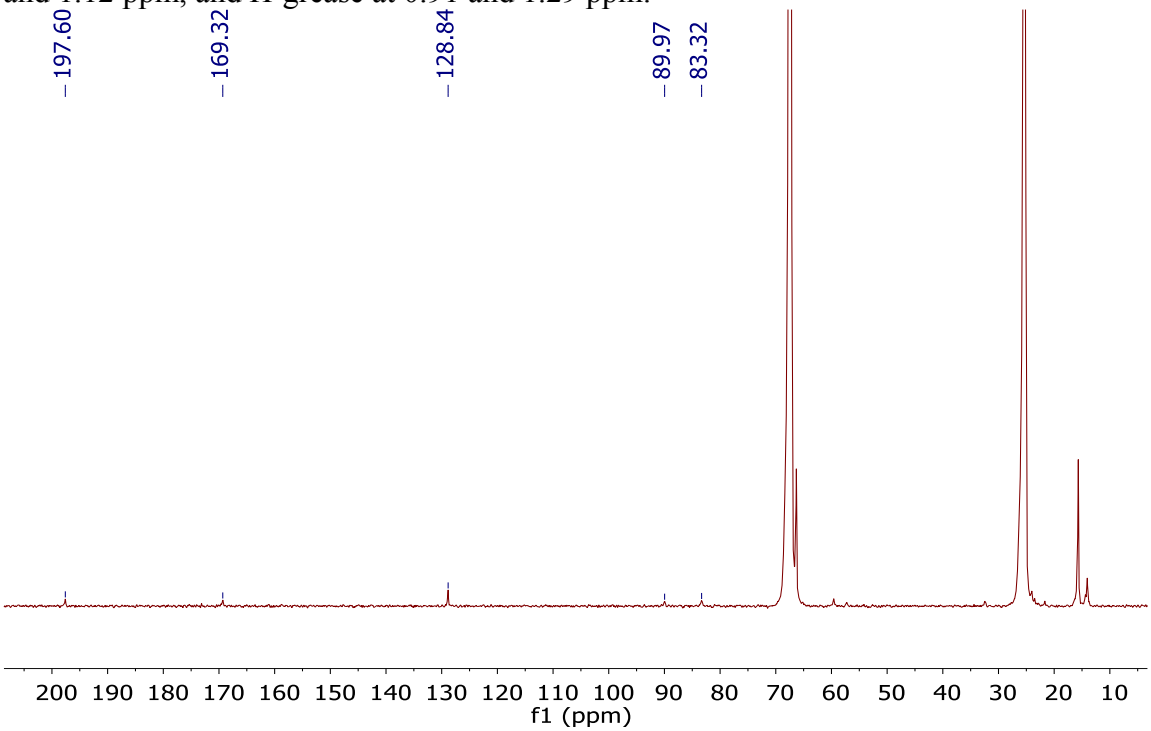

Figure 4-28. ^{13}C-(^{1}H-dec) NMR of **22[Li^{+}]** in THF-d$_{8}$. Coordinated diethyl ether is seen at 15.7 and 66.3 ppm. Trace n-butyllithium is seen at 14.0, 21.7, and 32.5 ppm.

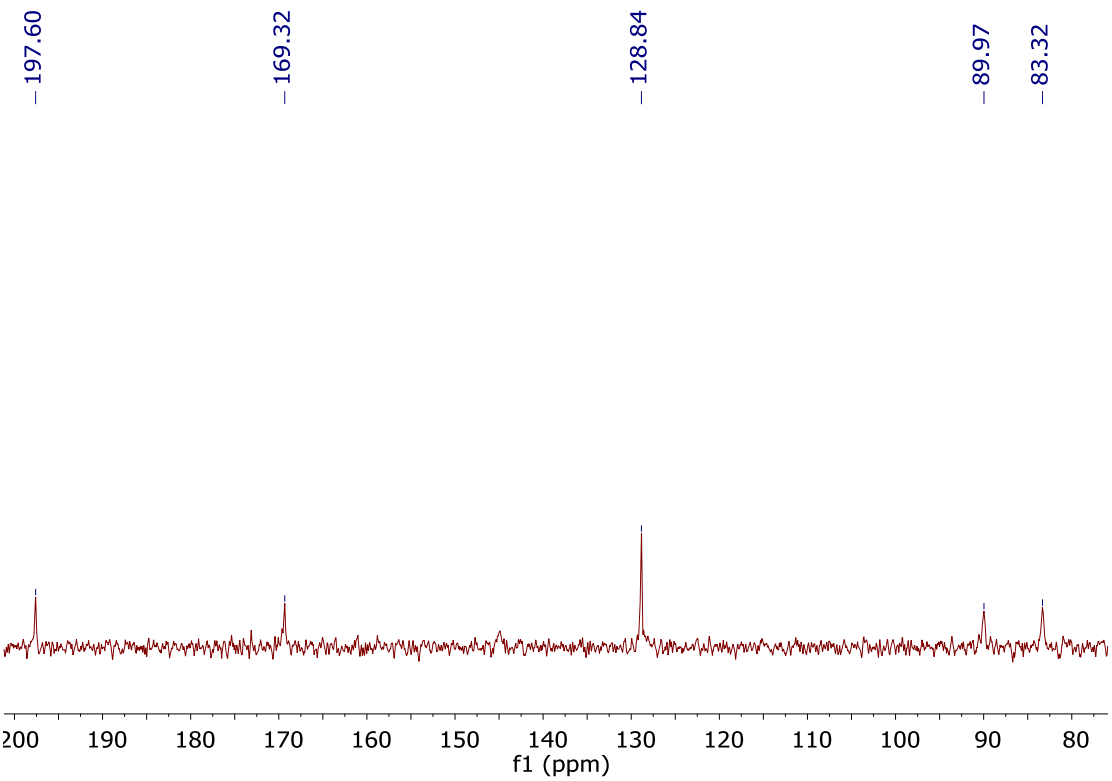

Figure 4-29. An expanded view of the ^{13}C-(^{1}H-dec) NMR spectrum of **22[Li^{+}]** in THF-d_8.

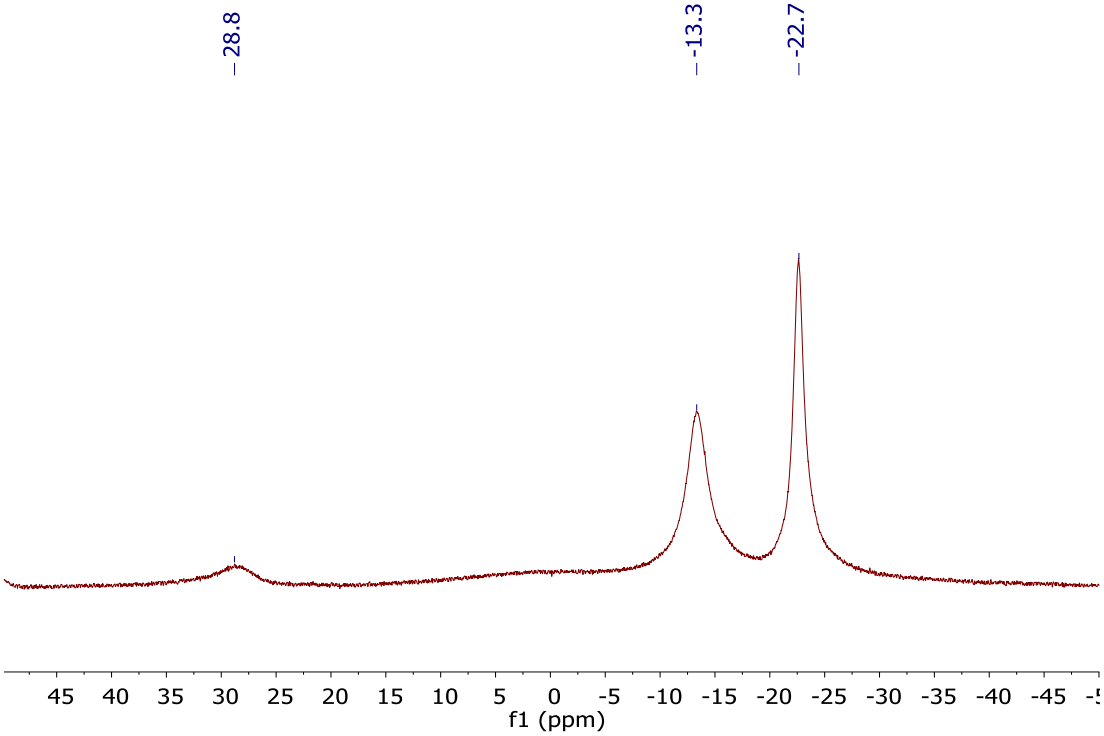

Figure 4-30. ^{11}B-(^{1}H-dec) NMR of **22[Li^{+}]** in THF-d_8.

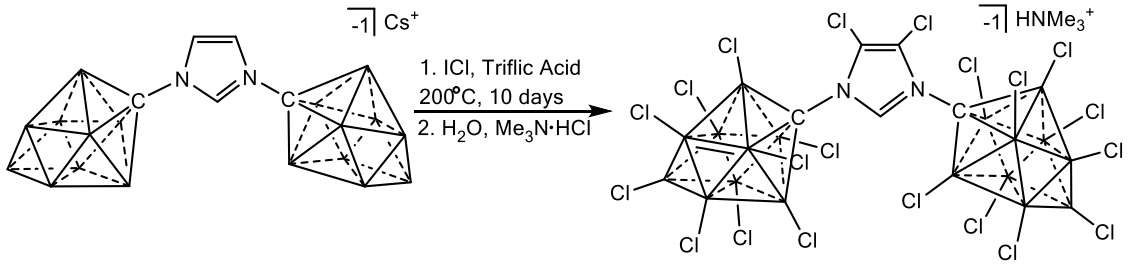

Scheme 4-15. Synthesis of Chlorinated Imidazolium Salt $C_5N_2B_{18}Cl_{20}H$, **23**

A Teflon-lined bomb reactor (Berghof DAB-3) equipped with a stir bar was loaded with 1.12 grams (3.2 mmol) of **19[Cs$^+$]**. Iodine monochloride (68 g, 21mL) and triflic acid (50 mL) were slowly added under a blanket of dry argon. The reactor was sealed (use torque specs from the instruction manual, ca. 30 NM), placed behind a blast shield and heated to 200 °C for 10 days in a copper shot bath. Reaction progress was monitored via mass spec. After ten days, the reactor was allowed to cool to room temperature, opened and the solution was transferred into a round bottom flask. Excess ICl and triflic acid were removed via trap-to-trap distillation at 180°C. The remaining compound was dissolved in 150 mL of EtOAc. The EtOAc solution was then washed with 50 mL of 10% $NaHSO_3$ aqueous solution. The EtOAc was removed on a rotary evaporator and 1.5 equivalents of trimethylammonium hydrochloride in a 100 mL solution of water was added, affording the product **23[Me$_3$NH$^+$]** in 81% yield (2.78 g, 2.6 mmol). ^{1}H NMR (400 MHz, THF-d$_8$, 25 °C): δ = 9.51 (s, 1H); ^{13}C-(^{1}H-dec) NMR (125 MHz, THF-d$_8$, 25 °C): δ = 141.71, 124.83; ^{11}B-(^{1}H-dec) NMR (96 MHz, THF-d$_8$, 25 °C): δ = 27.6, -0.05, -2.78 ppm. HRMS (negative mode ESI/APCI) [M]- m/z calc'd for $N_2C_5B_{18}Cl_{20}H^-$ = 992.5583; Found = 992.5597.

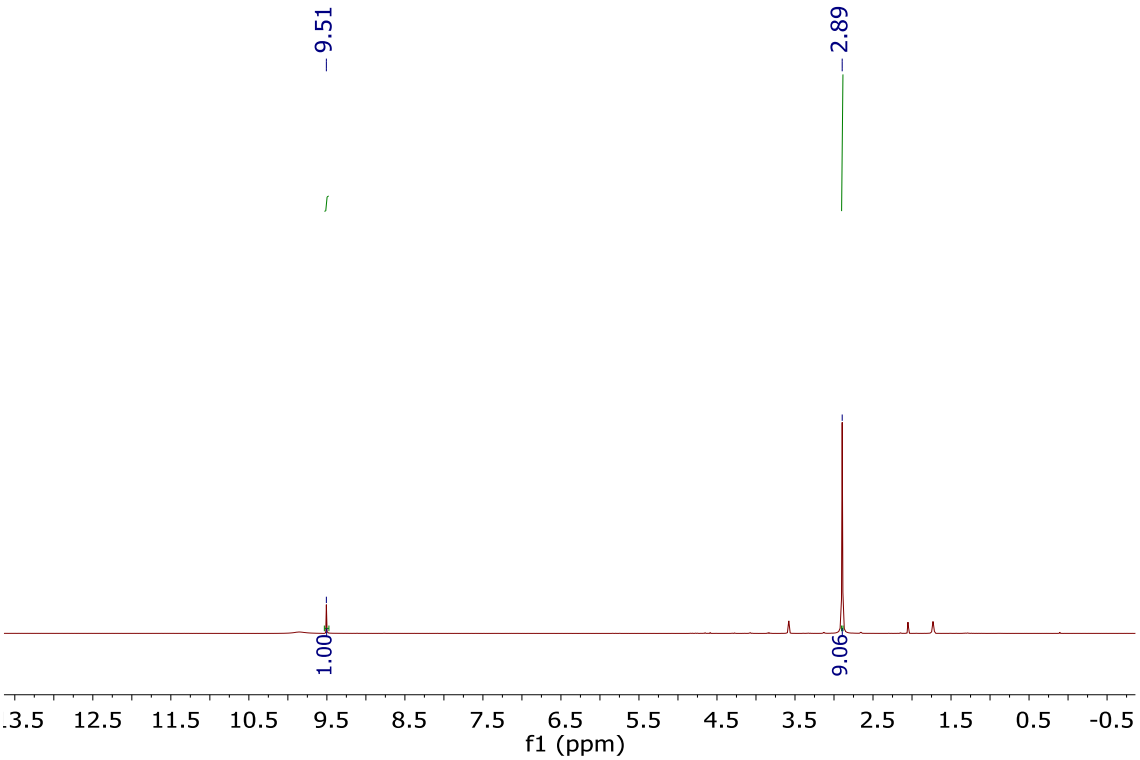

Figure 4-31. ^{1}H-NMR of **23[Me_3NH^+]** in THF-d_8. The peak at 2.89 ppm is due to Me_3NH^+ countercation. Note the presence of acetone at 2.05 ppm.

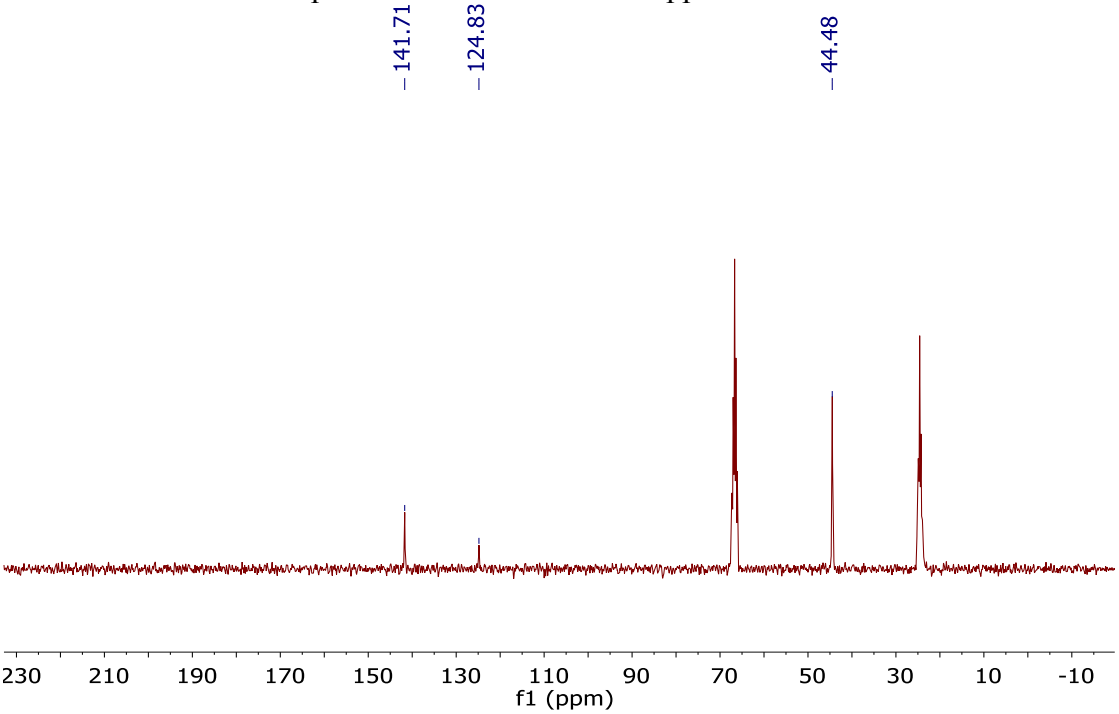

Figure 4-32. ^{13}C-(^{1}H-dec) NMR of **23[Me_3NH^+]** in THF-d_8. The peak at 44.48 ppm is due to Me_3NH^+ countercation.

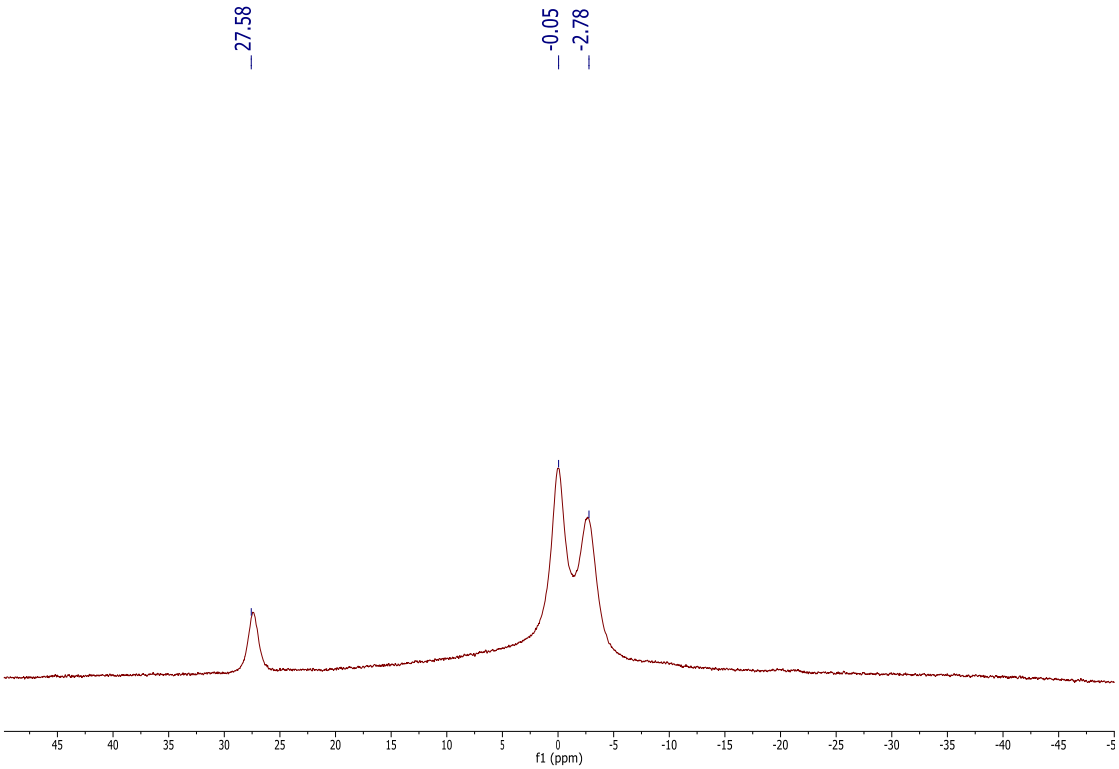

Figure 4-33. ^{11}B NMR of **23[Me_3NH^+]** in THF-d_8.

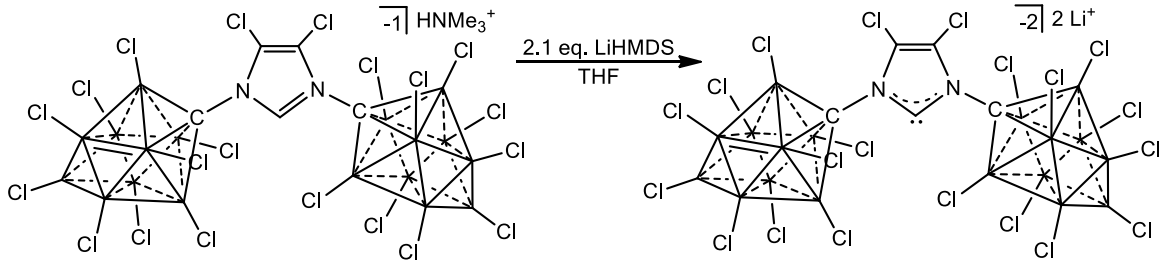

Scheme 4-16. Synthesis of Normal Cl20 Li^+ NHC **24**

A vial equipped with a stir bar was loaded with 200 mg (0.18 mmol) of **23[Me_3NH^+]** and 3 mL of THF. In a second vial, 2.1 equivalents (64 mg, 0.38 mmol) of LiHMDS was added and dissolved in THF (3 mL). The two THF solutions were combined, the vial capped, and the mixture stirred for 1 hour. The THF solution was added dropwise to a stirring vial of diethyl ether (20 mL), precipitating a light brown powder. The precipitate was left stirring in diethyl ether for 30 minutes. The solvent was decanted from the precipitate, and the remaining volatiles were removed under vacuum, affording the product **24[Li^+]** in 92% yield (253 mg, 0.16 mmol) (Note: Li^+ countercations each contain 4 coordinated THF molecules). Crystals suitable for a single crystal X-ray diffraction study were grown at -30 °C by layering a THF solution of **24[Li^+]** with diethyl ether. ^{13}C-(^1H-dec) NMR (125 MHz, THF-d_8, 25 °C): δ = 239.0, 117.9, 51.3; ^{11}B-(^1H-dec) NMR (96 MHz, THF-d_8, 25 °C): δ = 22.6, -1.7, -4.1 ppm.

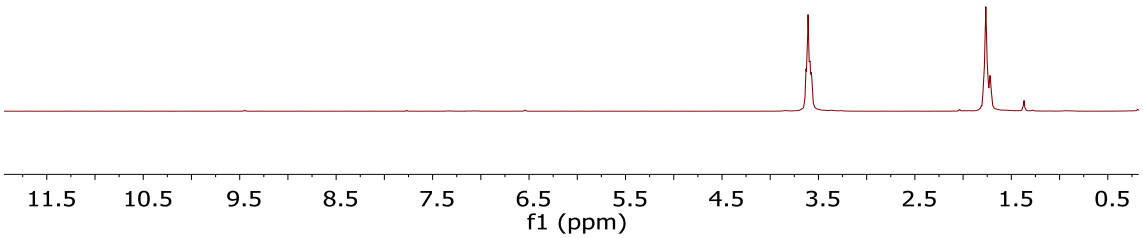

Figure 4-34. ^{1}H NMR of **24[Li^{+}]** in THF-d$_8$. Note: Blank proton NMR showing the disappearance of the C2 proton.

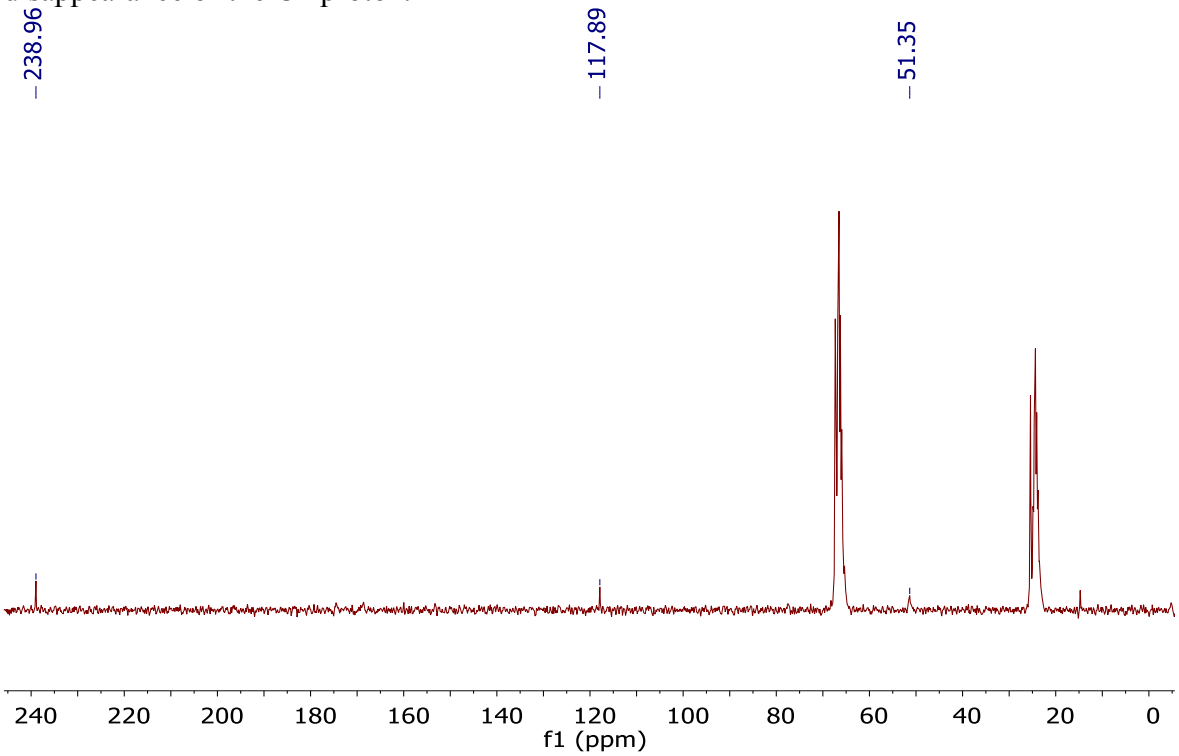

Figure 4-35. ^{13}C-(^{1}H-dec) NMR of **24[Li^{+}]** in THF-d$_8$.

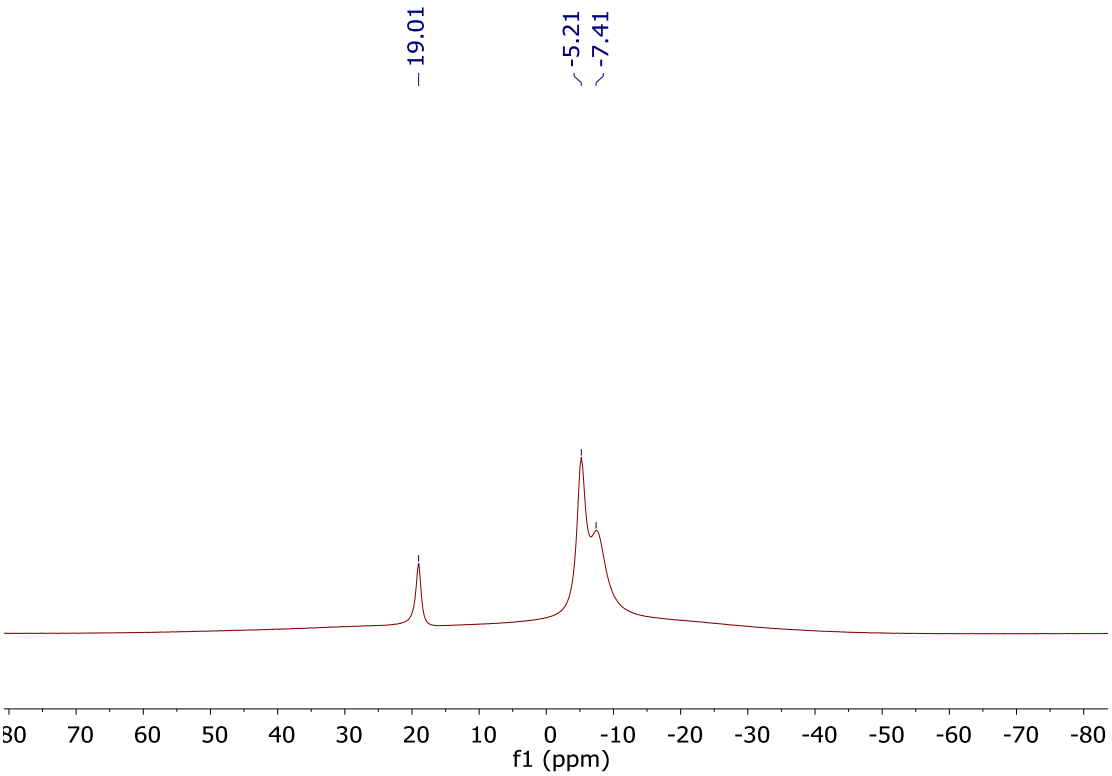

Figure 4-36. ^{11}B NMR of **24[Li$^+$]** in THF-d_8.

Water Stability Experiments of Li^+ NHC 24

A) An NMR sample of **24[Li^+]** in 0.5 mL THF-d_8 was prepared under a nitrogen atmosphere, and then exposed to air for 10 minutes. The sample was checked by ^1H, ^{11}B, and ^{13}C NMR, and upon seeing no protonation, distilled H_2O was added in increments of 0.025 mL, until 0.25 mL of H_2O total was added to the NMR tube. One drop (~0.01 mL) of 10% v/v HCl was added to the sample, protonating **24** and reforming **23.**

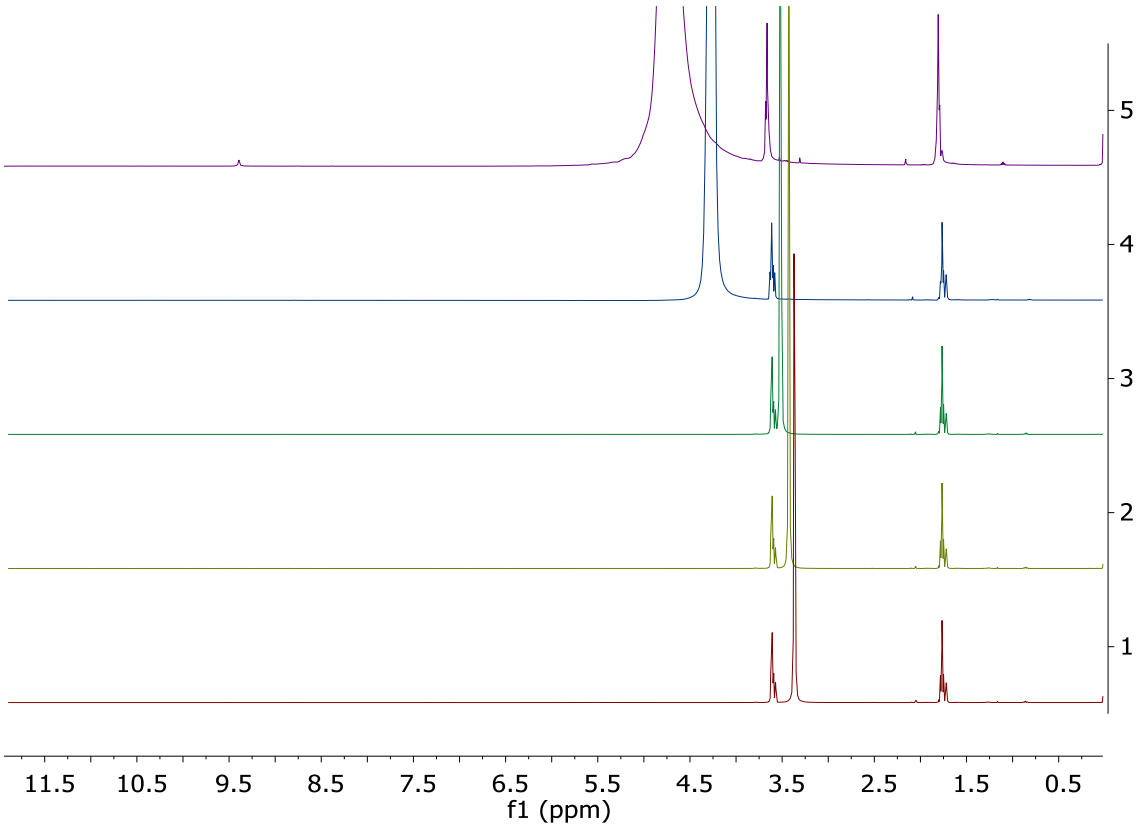

Figure 4-37. ^1H NMR of **24** in THF-d_8. 1.) 0.025 mL H_2O, 2.) 0.050 mL H_2O 3. 0.075 mL H_2O 4.) 0.200 mL H_2O, 5.) 0.250 mL H_2O, 0.01 mL of 10% v/v HCl

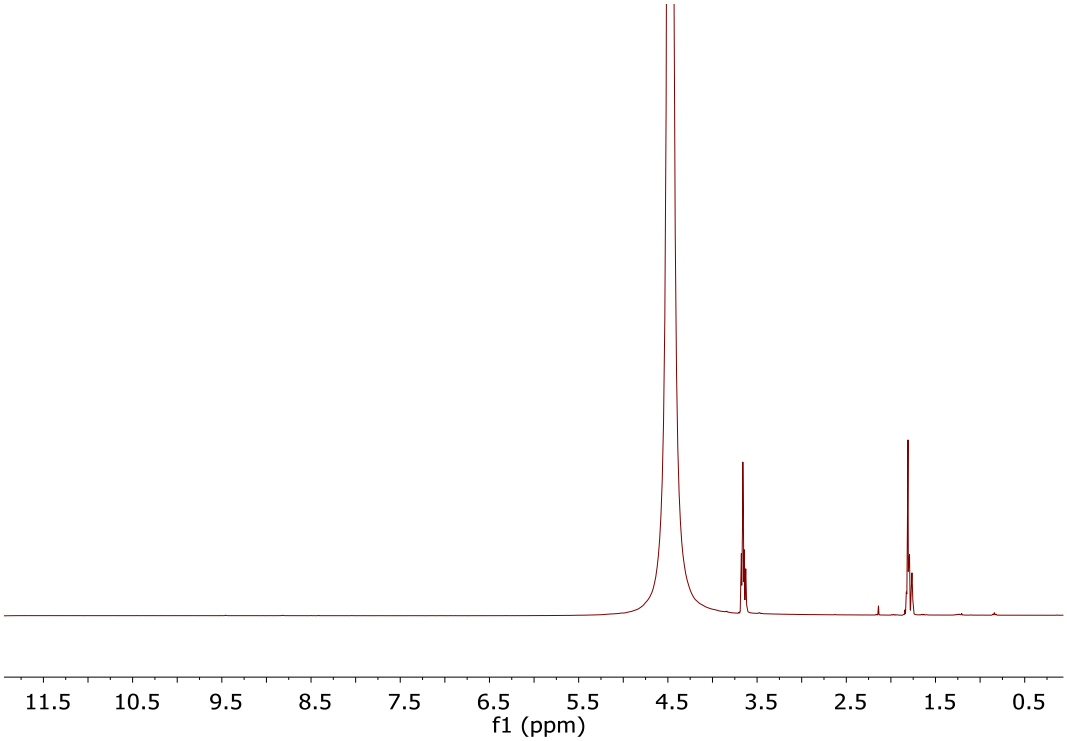

Figure 4-38. ^{1}H NMR of **24** in THF-$d_{8,}$ 0.200 mL H_2O

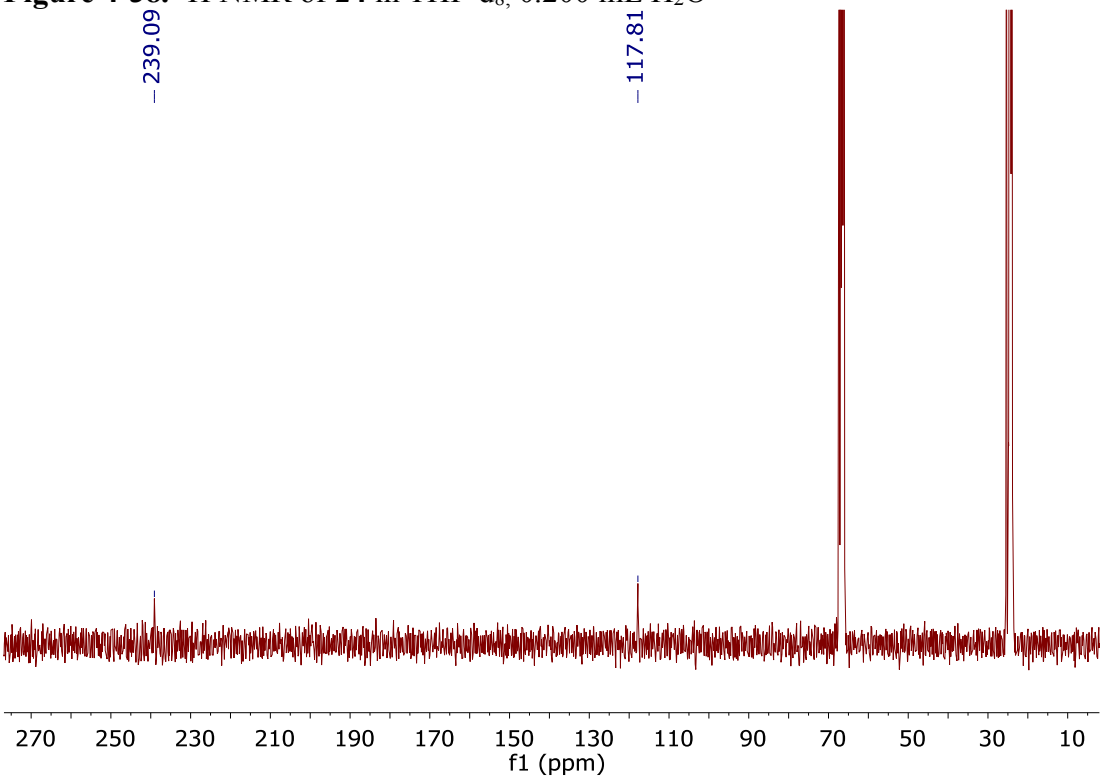

Figure 4-39. ^{13}C NMR of **24** in THF-$d_{8,}$ 0.200 mL H_2O

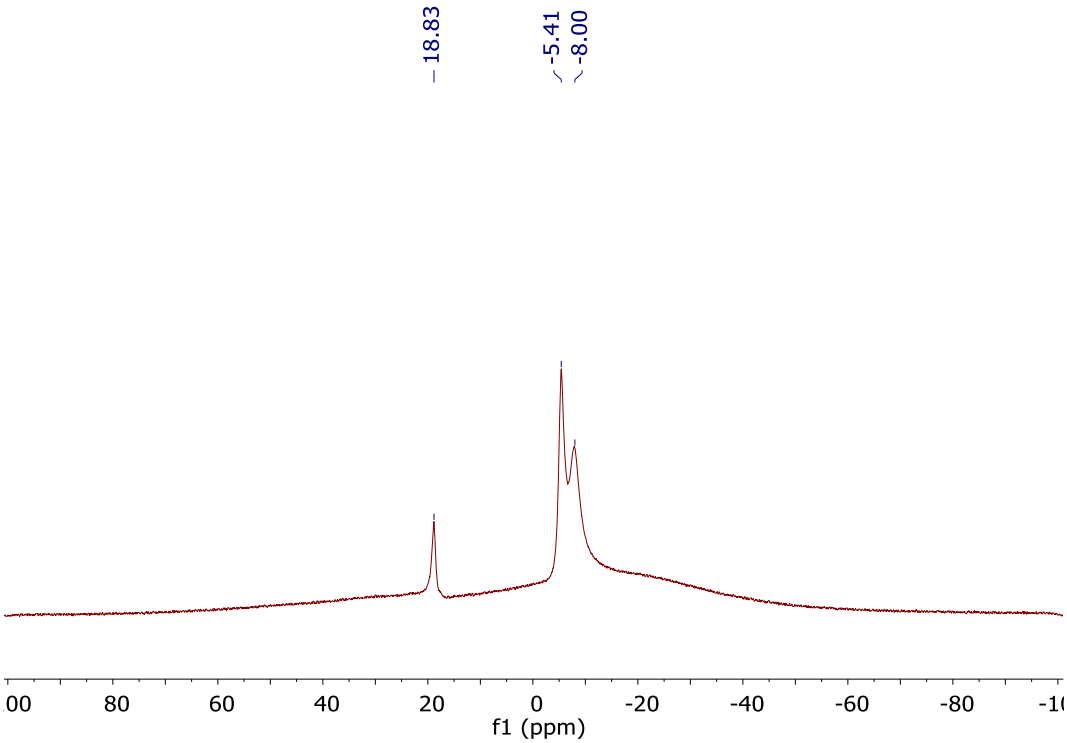

Figure 4-40. ^{11}B NMR of **24** in THF-d_8, 0.200 mL H_2O

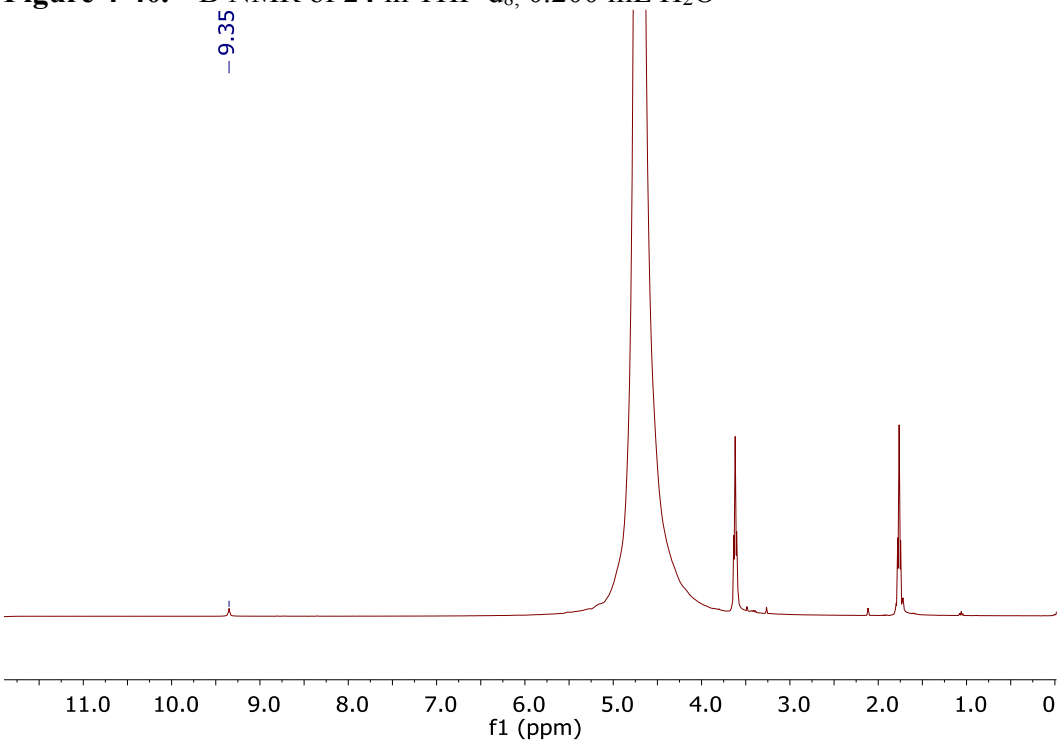

Figure 4-41. ^{1}H NMR of **23** in THF-d_8, 0.250 mL H_2O, 0.01 mL of 10% v/v HCl

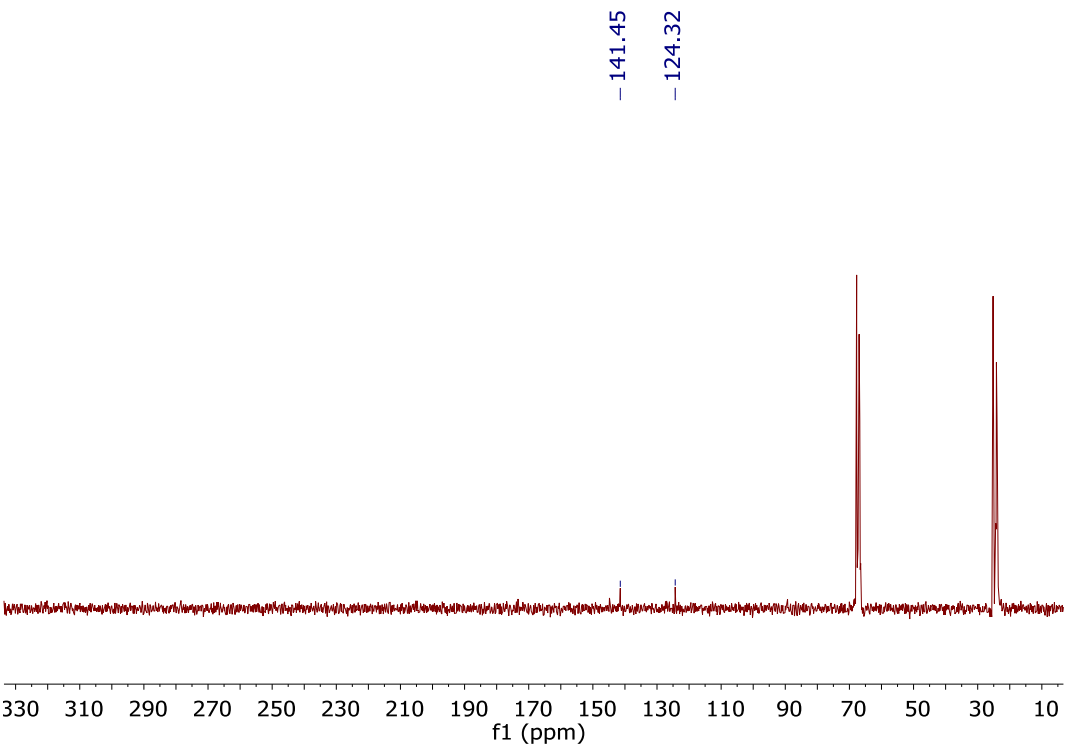

Figure 4-42. ^{13}C NMR of **23** in THF-d_8, 0.250 mL H_2O, 0.01 mL of 10% v/v HCl

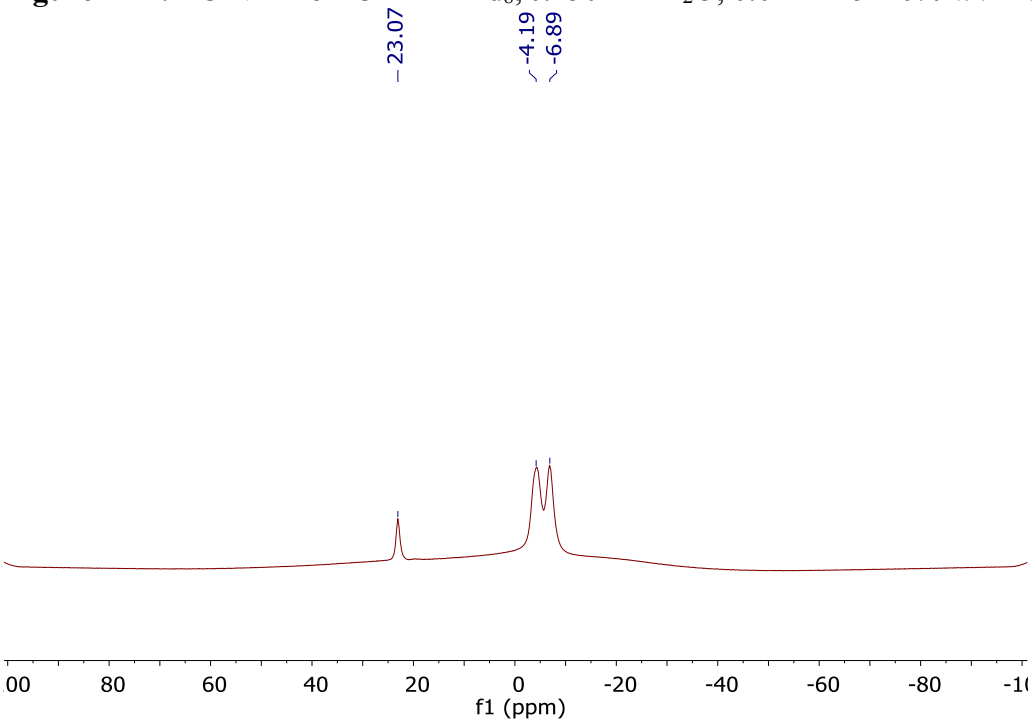

Figure 4-43. ^{11}B NMR of **23** in THF-d_8, 0.250 mL H_2O, 0.01 mL of 10% v/v HCl

B) A suspension of **24** in 0.30 mL was prepared in an NMR tube. Tetrahydrofuran was added dropwise, initially forming two layers. THF was added until **24** was detected in by ^{13}C NMR. The NMR sample containing **24** was protonated with 0.01 mL of 10% v/v HCl added to the sample, reforming **23**.

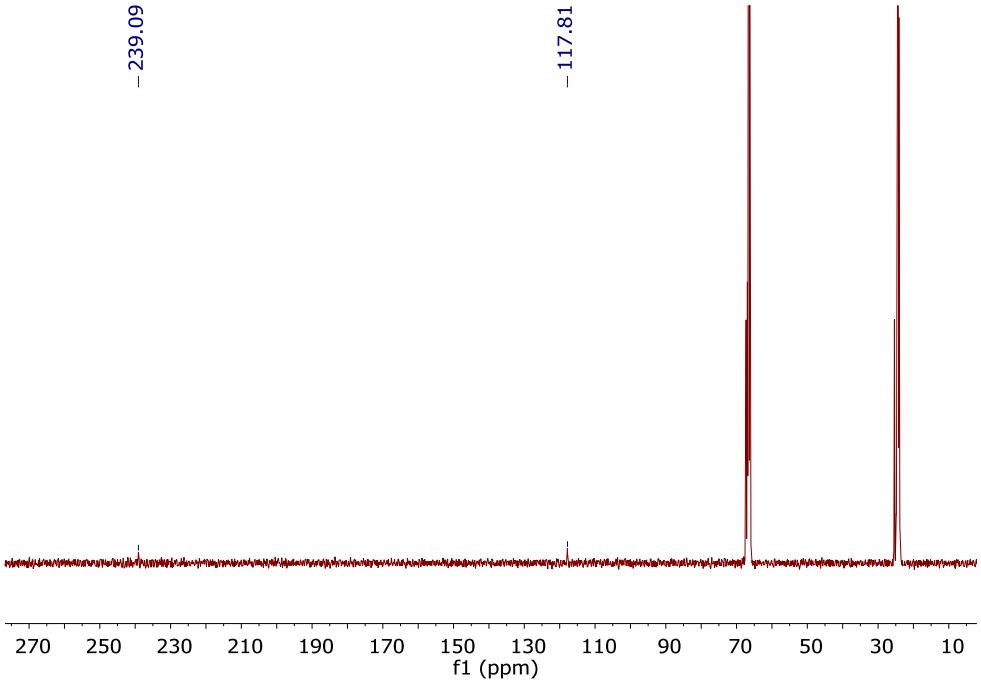

Figure 4-44. ^{13}C NMR of **24** in 0.30 mL H_2O with THF.

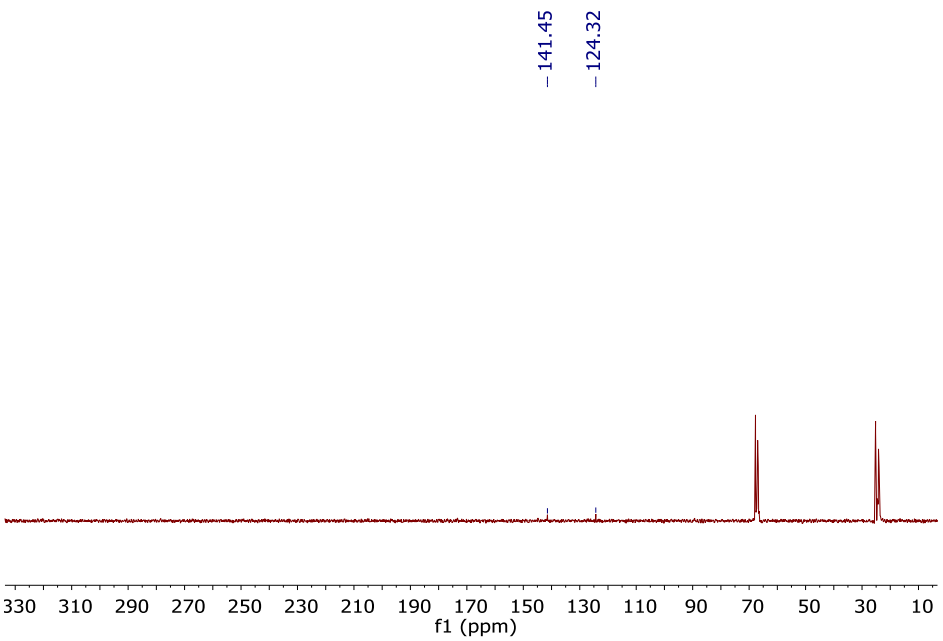

Figure 4-45. ^{13}C NMR of **23** in THF, 0.30 mL H_2O and 0.01 mL of 10% v/v HCl

C) An NMR sample of **24** in 0.5 mL THF-d_8 was prepared under a nitrogen atmosphere, and then exposed to air for 4 hours, allowing the solvent to evaporate. The sample was re-dissolved in acetone-d_6 and checked by ^{1}H, ^{11}B, and ^{13}C NMR. Upon seeing no protonation, distilled H_2O was added in increments of 0.025 mL, until 0.125 mL of H_2O total was added to the NMR tube. After the addition of 0.125 mL H_2O, a small amount of precipitate began to form. The remaining **24** in solution was protonated with 0.01 mL of 10% v/v HCl was added to the sample, reforming **23.** Addition of the acid redissolved the precipitate.

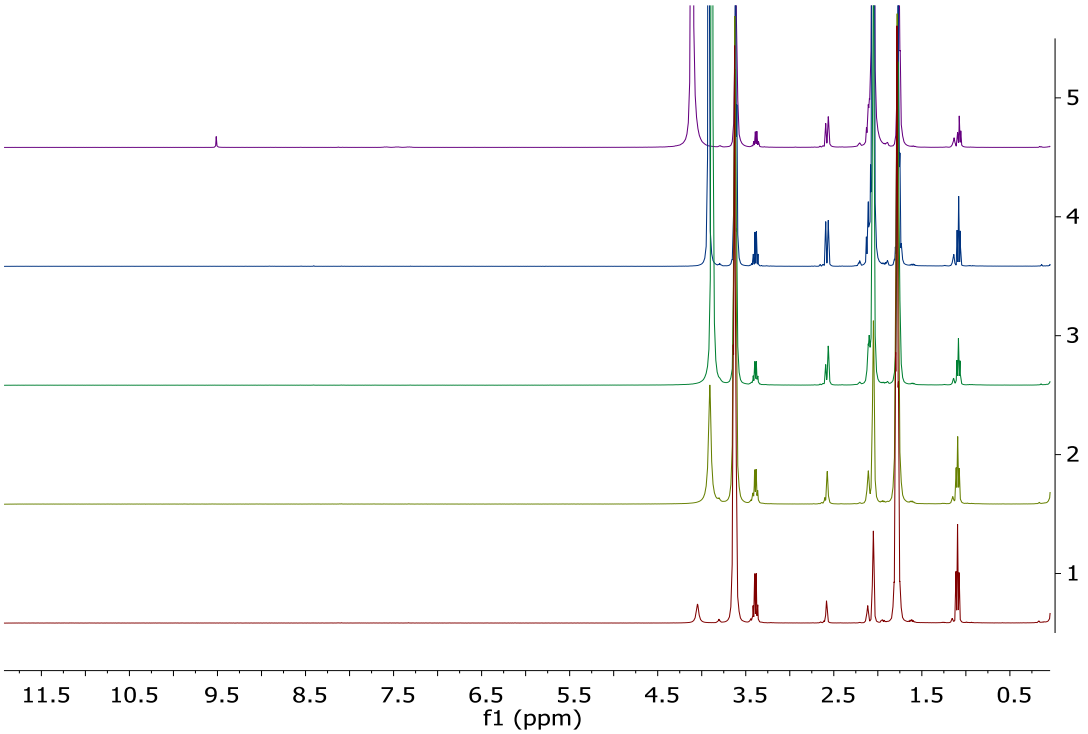

Figure 4-46. ^{1}H NMR of **24** in acetone-d_6. 1.) no additional H_2O, wet acetone-d_6 2.) 0.025 mL H_2O 3.) 0.050 mL H_2O, 4.) 0.075 mL H_2O, 5.) 0.125 mL H_2O, 0.01 mL of 10% v/v HCl (Note: tetrahydrofuran at 1.75 and 3.65, trace diethyl ether at 1.11 and 3.41 ppm)

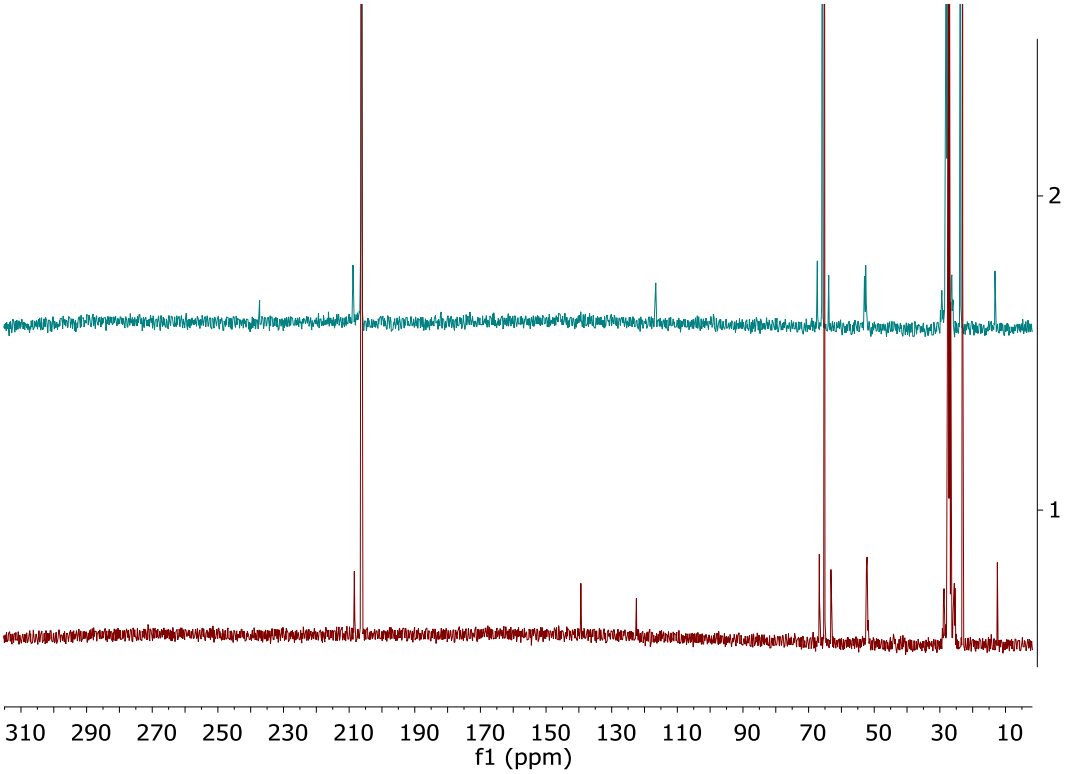

Figure 4-47. ^{13}C NMR: 1.) 0.075 mL H_2O, wet acetone-d_6 2.) 0.125 mL H_2O, 0.01 mL of 10% v/v HCl (Note: THF at 23.8 and 65.8, trace diethyl ether at 13.2 and 63.1 ppm. Peak at 208.8 corresponds to acetone coordinated to Li^+)

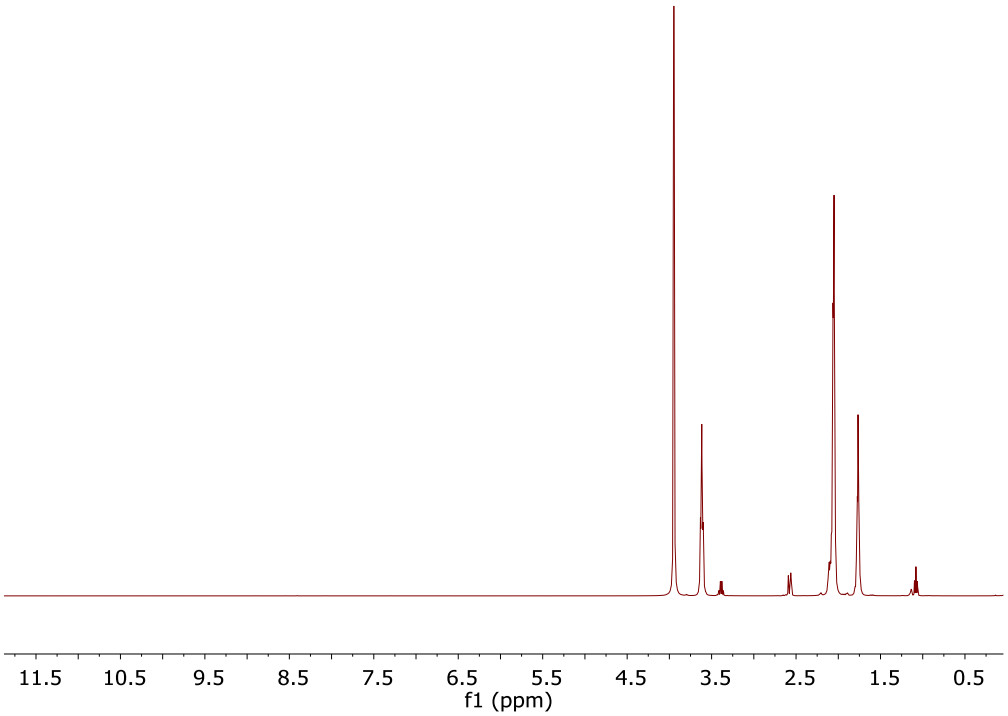

Figure 4-48. ^{1}H NMR of **24** in acetone-d_6, 0.100 mL H_2O (Note: tetrahydrofuran at 1.75 and 3.65, trace diethyl ether at 1.11 and 3.41 ppm)

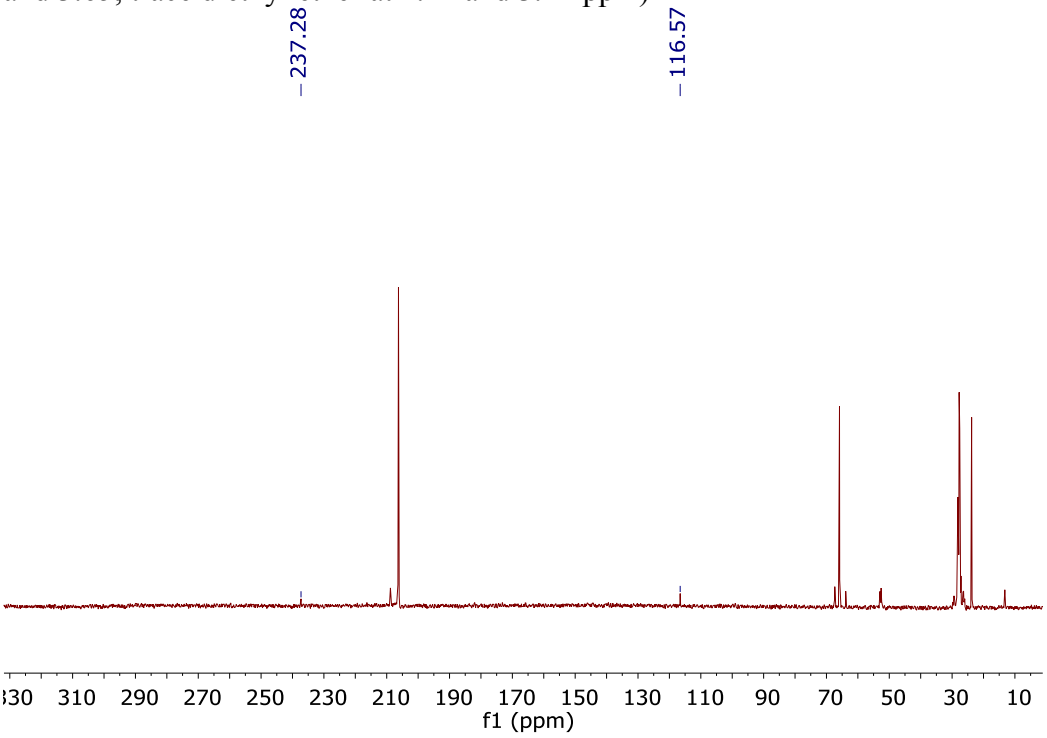

Figure 4-49. ^{13}C NMR of **24** in acetone-d_6, 0.100 mL H_2O (Note: THF at 23.8 and 65.8, trace diethyl ether at 13.2 and 63.1 ppm. Peak at 208.8 corresponds to acetone coordinated to Li^+)

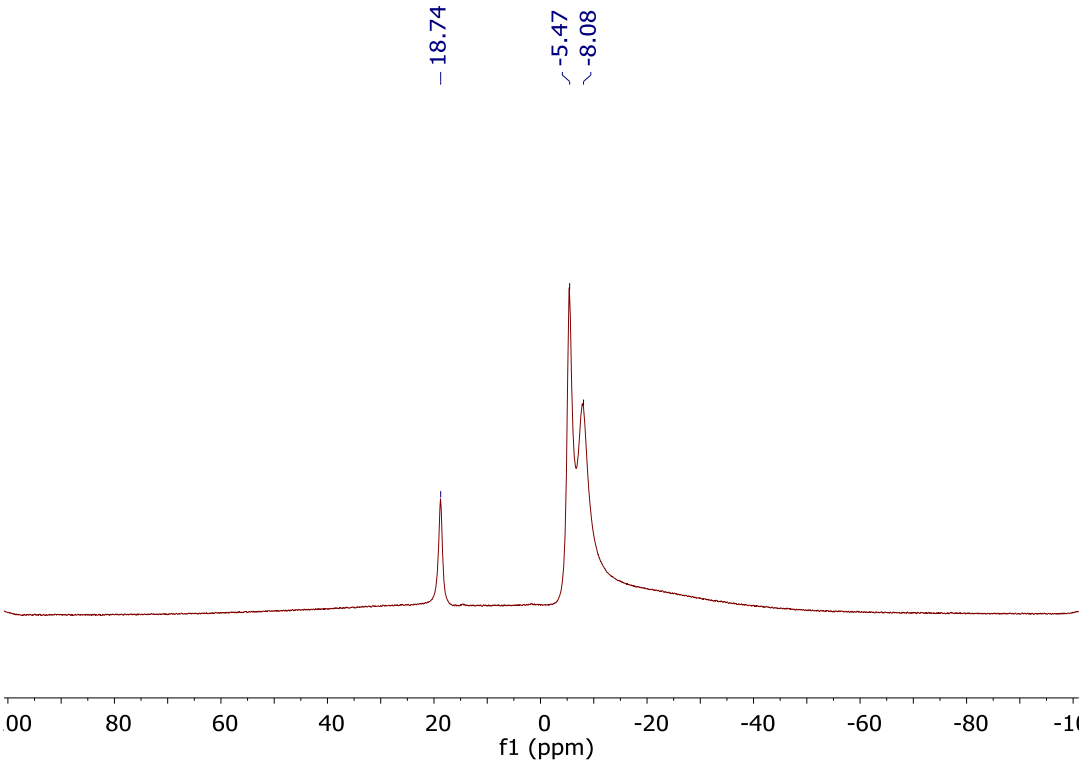

Figure 4-50. ^{11}B NMR of **24** in acetone-d_6, 0.100 mL H_2O

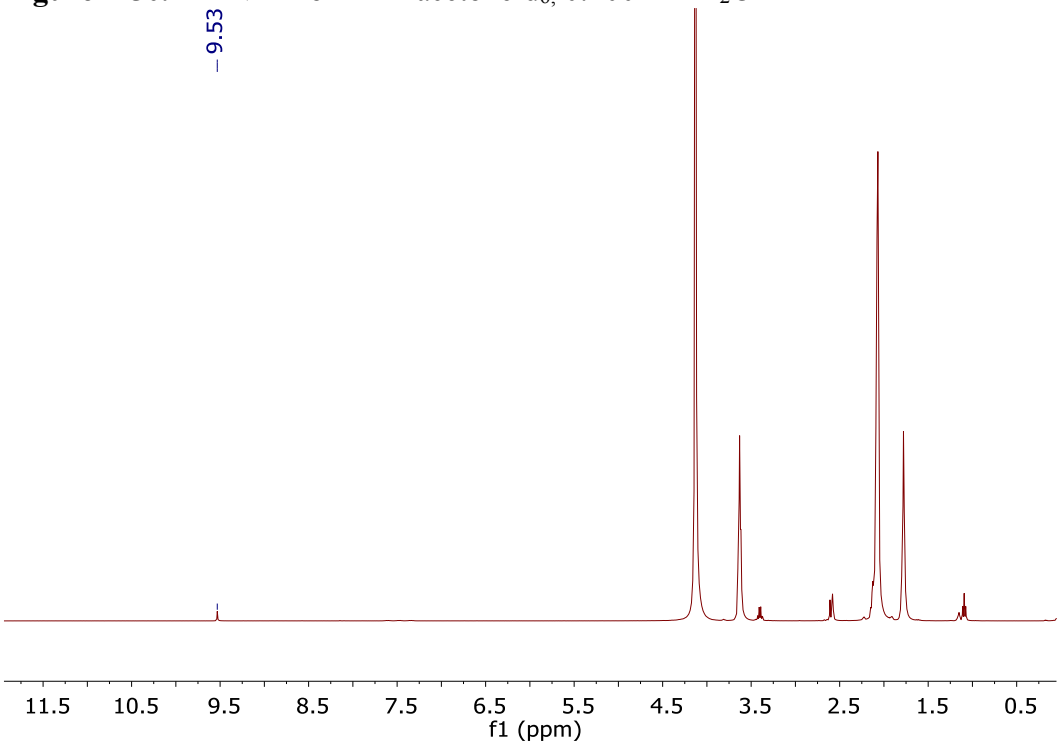

Figure 4-51. ^{1}H NMR of **23** in THF-d_8, 0.125 mL H_2O, 0.01 mL of 10% v/v HCl

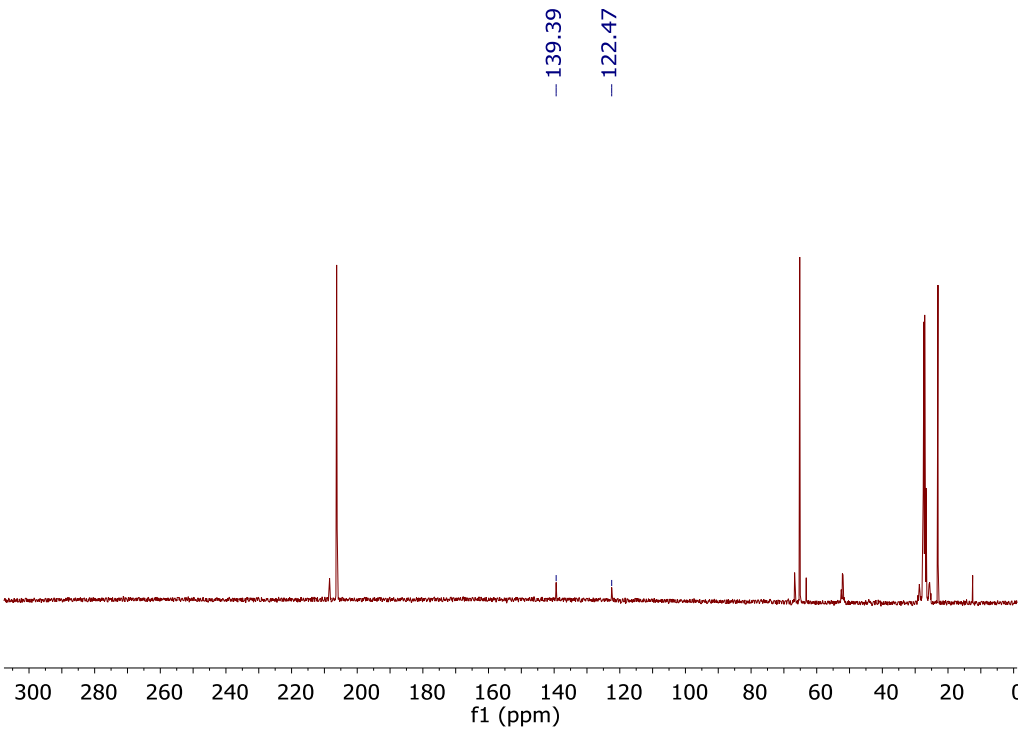

Figure 4-52. ^{13}C NMR of **23** in acetone-d_6, 0.125 mL H_2O, 0.01 mL of 10% v/v HCl (Note: THF at 23.8 and 65.8, trace diethyl ether at 13.2 and 63.1 ppm. Peak at 208.8 corresponds to acetone coordinated to Li^+)

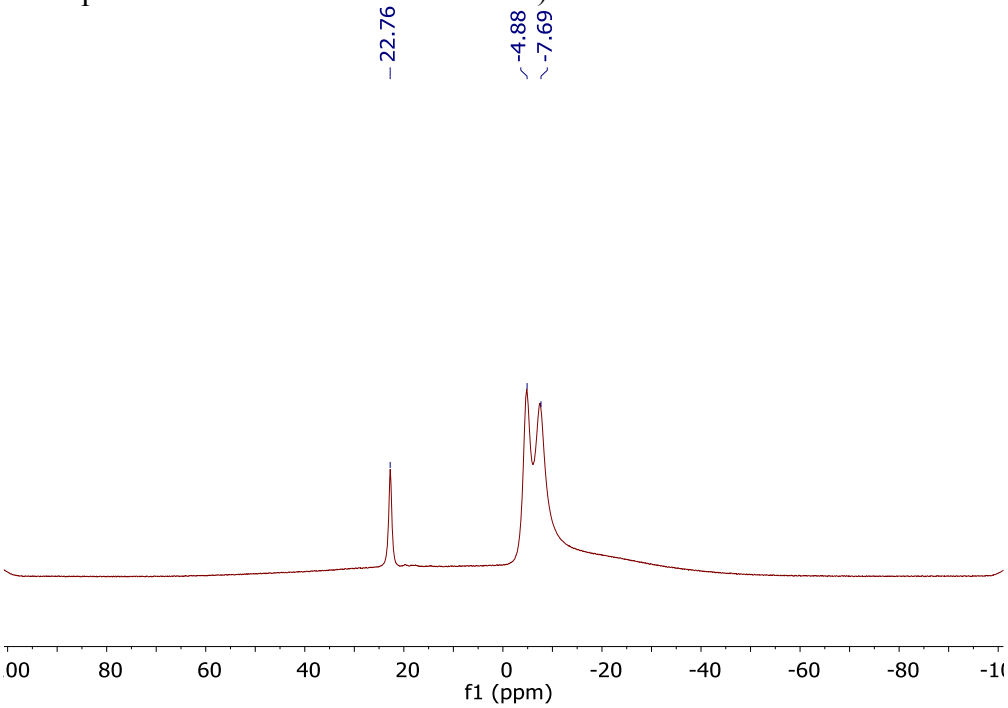

Figure 4-53. ^{11}B NMR of **23** in THF-d_8, 0.125 mL H_2O, 0.01 mL of 10% v/v HCl.

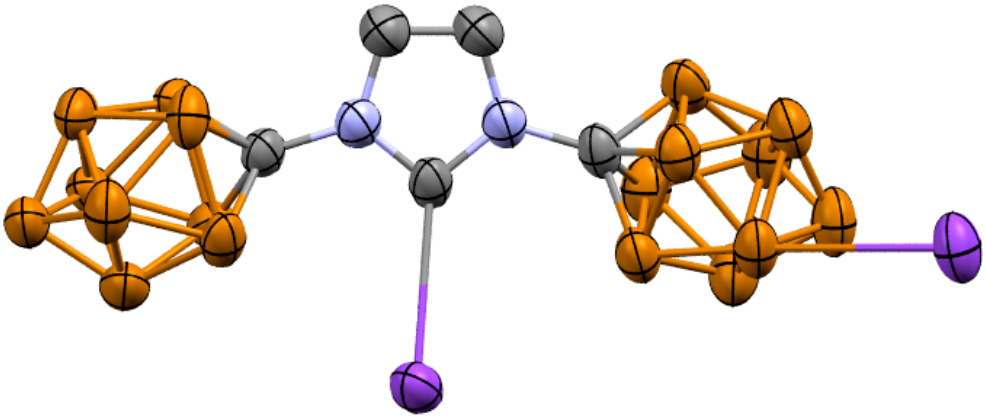

Figure 4-54. Solid-state structure of the 10-Vertex NHC dianion **20[K$^+$]**. For clarity, THF coordinated to the potassium atoms are omitted. Boron = brown, carbon= gray, nitrogen= blue, potassium= purple.

X-Ray Structure Determination for 20[K^+]

Table 4-1. Crystal data and structure refinement for Ama2.

Identification code	vL157SL_70A_0m	
Empirical formula	C33 H76 B18 K2 N2 O7	
Formula weight	885.73	
Temperature	200(2) K	
Wavelength	0.71073 Å	
Crystal system	Orthorhombic	
Space group	A m a 2	
Unit cell dimensions	a = 60.951(6) Å	α= 90°.
	b = 17.6644(17) Å	β= 90°.
	c = 9.8809(10) Å	γ = 90°.
Volume	10638.3(18) $Å^3$	
Z	8	
Density (calculated)	1.106 Mg/m^3	
Absorption coefficient	0.219 mm^{-1}	
F(000)	3776	
Crystal size	0.589 x 0.559 x 0.478 mm^3	
Theta range for data collection	2.005 to 26.022°.	
Index ranges	-75<=h<=75, -21<=k<=21, -12<=l<=12	
Reflections collected	129683	
Independent reflections	10591 [R(int) = 0.0275]	
Completeness to theta = 25.242°	99.9 %	
Absorption correction	Semi-empirical from equivalents	
Refinement method	Full-matrix least-squares on F^2	
Data / restraints / parameters	10591 / 971 / 775	
Goodness-of-fit on F^2	1.100	
Final R indices [I>2sigma(I)]	R1 = 0.0590, wR2 = 0.1698	
R indices (all data)	R1 = 0.0630, wR2 = 0.1747	
Absolute structure parameter	0.038(5)	
Extinction coefficient	n/a	
Largest diff. peak and hole	0.589 and -0.311 e.$Å^{-3}$	

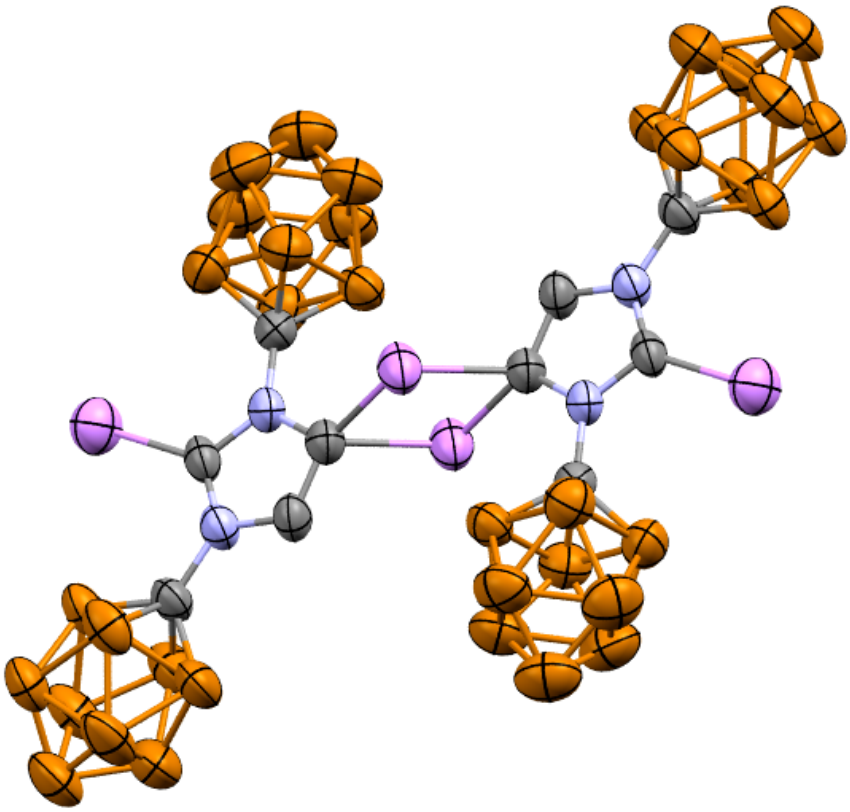

Figure 4-55. Solid-state structure of the dimeric 10-Vertex tri-anionic doubly deprotonated NHC **22[Li^{+}]**. For clarity, THF coordinated to the lithium atoms are omitted, as well as one additional lithium cation. Boron = brown, carbon= gray, nitrogen= blue, lithium= purple.

X-Ray Structure Determination for 22[Li^+]

Table 4-2. Crystal data and structure refinement for vL275SL_0m-5.

Identification code	vL275SL_0m-5	
Empirical formula	C36.83 H82.67 B18 Li3 N2 O7.96	
Formula weight	896.49	
Temperature	190(2) K	
Wavelength	0.71073 Å	
Crystal system	Triclinic	
Space group	P -1	
Unit cell dimensions	a = 9.5622(10) Å	α= 114.0568(16)°.
	b = 18.2827(19) Å	β= 100.8752(17)°.
	c = 18.5319(19) Å	γ = 102.6755(17)°.
Volume	2742.0(5) $Å^3$	
Z	2	
Density (calculated)	1.086 Mg/m^3	
Absorption coefficient	0.066 mm^{-1}	
F(000)	961	
Crystal size	0.531 x 0.211 x 0.066 mm^3	
Theta range for data collection	2.193 to 19.587°.	
Index ranges	-9<=h<=8, -17<=k<=15, 0<=l<=17	
Reflections collected	14348	
Independent reflections	4819 [R(int) = 0.0308]	
Completeness to theta = 25.242°	48.5 %	
Absorption correction	Semi-empirical from equivalents	
Refinement method	Full-matrix least-squares on F^2	
Data / restraints / parameters	4819 / 1104 / 797	
Goodness-of-fit on F^2	1.060	
Final R indices [I>2sigma(I)]	R1 = 0.0703, wR2 = 0.1722	
R indices (all data)	R1 = 0.0949, wR2 = 0.1904	
Extinction coefficient	n/a	
Largest diff. peak and hole	0.228 and -0.217 e.$Å^{-3}$	

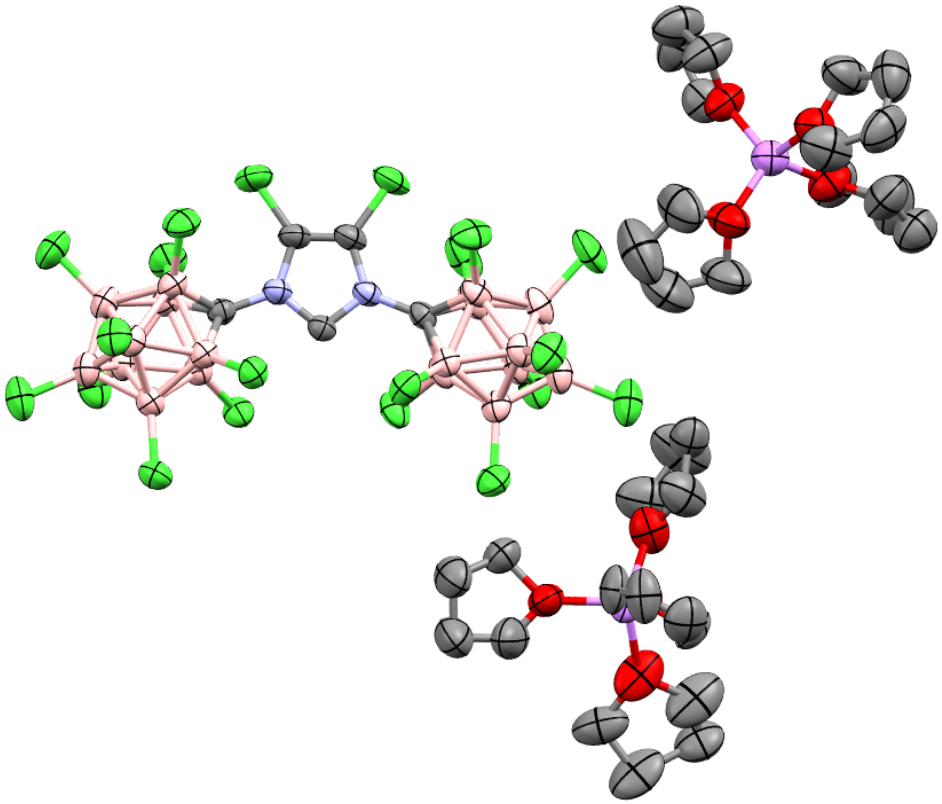

Figure 4-56. Solid state structure of **24[Li$^+$]**. N-heterocycle bond lengths: N1-C1= 1.374(3), C1-N2= 1.376(3), N2-C3= 1.404(3), C3-C2= 1.326(4), C2-N1 = 1.406(3); Nitrogen to carborane carbon bond lengths: C4-N1= 1.428(3), C2-N5= 1.429(3); All atoms of the heterocycle ring are coplanar, sum of internal pentagon angles = 540°; Both N1 and N3 are planar, sum of C-N-C angles = 360°.

X-Ray Structure Determination for 24[Li^+]

Table 4-3. Crystal data and structure refinement for vL180SL_0m.

Identification code	vL180SL_0m	
Empirical formula	C41 H72.96 B18 Cl20 Li2 N2 O9	
Formula weight	1655.43	
Temperature	200(2) K	
Wavelength	0.71073 Å	
Crystal system	Triclinic	
Space group	P -1	
Unit cell dimensions	a = 13.9343(6) Å	α= 105.2353(7)°.
	b = 15.9345(7) Å	β= 91.5694(7)°.
	c = 17.9992(7) Å	γ = 90.0954(8)°.
Volume	3854.4(3) $Å^3$	
Z	2	
Density (calculated)	1.426 Mg/m^3	
Absorption coefficient	0.754 mm^{-1}	
F(000)	1682	
Crystal size	0.327 x 0.172 x 0.135 mm^3	
Theta range for data collection	1.521 to 26.372°.	
Index ranges	-17<=h<=17, -19<=k<=19, -22<=l<=22	
Reflections collected	86693	
Independent reflections	15766 [R(int) = 0.0315]	
Completeness to theta = 25.242°	100.0 %	
Absorption correction	Semi-empirical from equivalents	
Refinement method	Full-matrix least-squares on F^2	
Data / restraints / parameters	15766 / 1413 / 1163	
Goodness-of-fit on F^2	1.032	
Final R indices [I>2sigma(I)]	R1 = 0.0460, wR2 = 0.1222	
R indices (all data)	R1 = 0.0624, wR2 = 0.1340	
Extinction coefficient	n/a	
Largest diff. peak and hole	0.654 and -0.415 e.$Å^{-3}$	

4.8 References

1. Staudinger, H.; Meyer, J. *Helvetica Chimica Acta* **1919**, *2*, 635.

2. Buchner, E.; Curtius, T. *Berichte der deutschen chemischen Gesellschaft* **1885,** *18*, 2377.

3. Moss, R. A.; PLatz, M. S.; Jones, M. *Reactive Intermediate Chemistry* Wiley-Interscience, Hoboken, NJ, 2004.

4. Igau, A.; Grutzmacher, H.; Baceiredo, A.; Bertrand, G. *Journal of the American Chemical Society* **1988**, *110*, 6463.

5. Melaimi, M.; Soleilhavoup, M.; Bertrand, G. *Angewandte Chemie International Edition* **2010**, *49*, 8810.

6. Díez-González, S.; Marion, N.; Nolan, S. P. *Chemical Reviews* **2009**, *109*, 3612.

7. Arnold, P. L.; Casely, I. J. *Chemical Reviews* **2009**, *109*, 3599.

8. Vignolle, J.; Cattoën, X.; Bourissou, D. *Chemical Reviews* **2009**, *109*, 3333.

9. Lin, J. C. Y.; Huang, R. T. W.; Lee, C. S.; Bhattacharyya, A.; Hwang, W. S.; Lin, I. J. B. *Chemical Reviews* **2009**, *109*, 3561.

10. Hahn, F. E.; Jahnke, M. C.; *Angewandte Chemie International Edition* **2008**, *47*, 3122.

11. Arduengo, A. J.; Harlow, R. L.; Kline, M. *Journal of the American Chemical Society* **1991**, *113*, 361.

12. Martin, C. D.; Soleilhavoup, M.; Bertrand, G. *Chemical Science* **2013**, *4*, 3020.

13. Wang, Y.; Robinson, G. H. *Dalton Transactions* **2012**, *41*, 337.

14. Xiong, Y.; Yao, S.; Inoue, S.; Epping, J. D.; Driess, M. *Angewandte Chemie International Edition* **2013**, *52*, 7147.

15. Mondal, K. C.; Roesky, H. W.; Stuckl, A. C.; Ehret, F.; Kaim, W.; Dittrich, B.; Maity, B.; Koley, D. *Angewandte Chemie International Edition* **2013**, *52*, 11804.

16. Schaper, L. A.; Hock, S. J.; Herrmann, W. A.; Kühn, F. E. *Angewandte Chemie International Edition* **2013**, *52*, 270.

17. Dröge, T.; Glorius, F. *Angewandte Chemie International Edition* **2010**, *49*, 6940.

18. Samojłowicz, C.; Bieniek, M.; Grela, K. *Chemical Reviews* **2009**, *109*, 3708.

19. Wanzlick, H. W. *Angewandte Chemie International Edition in English* **1962**, *1*, 75.

20. Wanzlick, H. W.; Schönherr, H. J. *Angewandte Chemie International Edition in English* **1968**, *7*, 141.

21. Grossman, A.; Enders, D. *Angewandte Chemie International Edition* **2012**, *51*, 314.

22. Denmark, S. E.; Beutner, G. L. *Angewandte Chemie International Edition* **2008,** *47*, 1560.

23. Marion, N.; Díez-González, S.; Nolan, S. P. *Angewandte Chemie International Edition* **2007**, *46,* 2988.

24. Enders, D.; Niemeier, O.; Henseler, A. *Chemical Reviews* **2007**,*107,* 5606.

25. Aldeco-Perez, E.; Rosenthal, A. J.; Donnadieu, B.; Parameswaran, P.; Frenking, G.; Bertrand, G. *Science* **2009**, *326*, 556.

26. Crabtree, R. H. *Coordination Chemistry Reviews* **2013**, *257*, 755.

27. Kruger, A.; Albrecht, M. *RSC Catal. Ser.* **2011,** *6,* 134.

28. Kruger, A.; Yang, M.; Raubenheimer, H. G.; Albrecht, M. *Chemical Reviews*, **2009**, *109*, 3445.

29. Kruger, A.; Albrecht, M. *Australian Journal of Chemistry*, **2011**, *64*, 1113.

30. Yang, L.; Kruger, A.; Neels, A.; Albrecht, M. *Organometallics,* **2008,** *27,* 3161.

31. Heckenroth, M.; Kluser, E.; Neels, A.; Albrecht, M. *Angewandte Chemie International Edition* **2007**, *46*, 6293.

32. Wang, Y.; Xie, Y.; Abraham, M. Y.; Wei, P.; Schaefer, H. F.; Schleyer, P. v. R.; Robinson, G. H. *Journal of the American Chemical Society* **2010**, *132*, 14370.

33. Grimes, R. N. In *Carboranes (Second Edition)*; Academic Press: Oxford, 2011, p 1.

34. Douvris, C.; Michl, J. *Chemical Reviews* **2013,** *113*, PR179.

35. Spokoyny, A. M. *Pure Applied Chemistry*, **2013**, *85*, 903.

36. Brusselle, D.; Bauduin, P.; Girard, L.; Zaulet, A.; Vinas, C.; Teixidor, F.; Ly, I.; Diat, O. *Angewandte Chemie International Edition* **2013**, *52*, 12114.

37. Olid, D.; Nunez, R.; Vinas, C.; Teixidor, F. *Chemical Society Reviews* **2012**, *41*, 3445.

38. Scholz, M.; Hey-Hawkins, E. *Chemical Reviews,* **2011***, 111*, 7035.

39. Valliant, J. F.; Guenther, K. J.; King, A. S.; Morel, P.; Schaffer, P.; Sogbein, O. O.; Stephenson, K. A. *Coordination Chemistry Reviews* **2002**, *232*, 173.

40. Reed, C. A. *Accounts of Chemical Research* **2010**, *43*, 121.

41. Boere, R. T.; Bolli, C.; Finze, M.; Himmelspach, A.; Knapp, C.; Roemmele, T. L. *Chemistry, A European Journal* **2013**, *19*, 1784.

42. Bolli, C.; Kochner, T.; Knapp, C. *Zeitschrift für anorganische und allgemeine Chemie* **2012**, *638,* 559.

43. Ramirez-Contreras, R.; Bhuvanesh, N.; Zhou, J.; Ozerov, O. V. *Angewandte Chemie International Edition* **2013**, *52,* 10313.

44. Himmelspach, A.; Finze, M.; Raub, S. *Angewandte Chemie International Edition* **2011,** *50*, 2628.

45. Douvris, C.; Nagaraja, C. M.; Chen, C.-H.; Foxman, B. M.; Ozerov, O. V. *Science*, **2008**, *321*, 1188.

46. Shao, B.; Bagdasarian, A. L.; Popov, S.; Nelson, H. M. *Science* **2017**, *355,* 1403.

47. Lavallo, V.; Wright, J. H.; Tham, F. S.; Quinlivan, S. *Angewandte Chemie International Edition* **2013**, *52*, 3172.

48. El-Hellani, A.; Lavallo, V. *Angewandte Chemie International Edition*, **2014**, *53*, 4489.

49. Kolychev, E. L.; Kronig, S.; Brandhorst, K.; Freytag, M.; Jones, P. G.; Tamm, M. *Journal of the American Chemical Society* **2013**, *135,* 12448.

50. Kronig, S.; Theuergarten, E.; Daniliuc, C. G.; Jones, P. G.; Tamm, M. *Angewandte Chemie International Edition*, **2012,** *51,* 3240.

51. Knoth, W. H. *Inorganic Chemistry* **1971**, *10*, 598.

52. Ringstrand, B.; Bateman, D.; Schoemaker, R. K.; Janousek, Z. *Collection of Czechoslovak Chemical Communications* **2009**, *74*, 419.

53. McArthur, S. G.; Jay, R.; Geng, L.; Guo, J.; Lavallo, V. *Chemical Communications* **2017**, *53*, 4453.

54. Tsang, C.-W.; Yang, Q.; Sze, E. T.-P.; Mak, T. C. W.; Chan, D. T. W.; Xie, Z. *Inorganic Chemistry* **2000**, *39*, 3582.

55. Estrada, J.; Lugo, C. A.; McArthur, S. G.; Lavallo, V. *Chemical Communications* **2016**, *52,* 1824.

56. Jelinek, T.; Stibr, B.; Plesek, J.; Thornton-Pett, M.; D. Kennedy, J. *Journal of the Chemical Society, Dalton Transactions* **1997**, 4231.

57. Asay, M. J.; Fisher, S. P.; Lee, S. E.; Borchardt, D.; Tham, F. S.; Lavallo, V. *Chemcial Communications* **2015**, *51*, 5359.

58. Fisher, S. P.; El-Hellani, A.; Tham, F.; Lavallo, V. *Dalton Transactions* **2016**, *45*, 9762.

59. Knoth, W. H. *Journal of the American Chemical Society* **1967**, *89*, 1274.

60. Franken, A.; Kilner, C. A.; Kennedy, J. D. *Chemical Communications* **2004**, 328.

61. Brellochs, B.; Backovsky, J.; Stibr, B.; Jelinek, T.; Holub, J.; Bakardjiev, M.; Hnyk, D.; Hofmann, M.; Cisarova, I.; Wrackmeyer, B. *European Journal of Inorganic Chemistry* **2004**, *18*, 3605.

62. Ringstrand, B.; Balinski, A.; Franken, A.; Kaszynski, P. *Inorganic Chemistry* **2005**, *44*, 9561.

63. Base, K. S., B.; Dolansky, J.; Duben, J. *Collection of Czechoslovak Chemical Communications* **1981**, *46*, 2345.

64. Jelinek, T.; Plešek, B.; Heřmánek, S. *Journal of Organometallic Chemistry* **1986**, *307*, C13.

Chapter 5: Synthesis of Unsymmetrical 10-Vertex N-Heterocyclic Carbenes

5.1 Introduction

In 2013, the Lavallo research group disclosed the synthesis of polyanionic N-heterocyclic carbenes (NHCs)[1] featuring two N-bound 12-vertex carborane anions.[2-6] Through judicious choice of bases, the selective deprotonation of the anionic imidazolium salt **6** was achieved to afford normal (C-2) NHC **12** (*via* LiHMDS), abnormal[7-11] (C-5) NHC **15** (*via* LDA, −78 °C), or the doubly deprotonated[12-15] (C-2/C-5) NHC **16** (*via* *n*-butyllithium) from a single precursor (Chapter 4, Scheme 4-1). Such selectivity of NHC formation had not been previously achieved in deprotonation reactions with imidazolium salts that contained *N*-hydrocarbon groups. We became curious to see if it was possible to prepare unsymmetrical NHCs featuring both carborane and hydrocarbon substituents and investigate if the same selectivity for NHC formation could be achieved.

The following year, we disclosed the synthesis of unsymmetrical N-heterocyclic carbenes (NHCs) that contained a single N-bound icosahedral carborane anion substituent (Scheme 5-1).[16] One of the most elegant and versatile methods to synthesize unsymmetrically substituted imidazolium salts was reported by Fürstner and co-workers.[17] This method involves the heterocyclic interconversion of oxazolinium salts via reaction with amines. These oxazolinium salts are readily tunable at N and is synthesized in three steps from commercially available starting materials. The mesityl substituted oxazolinium cation was reacted with anionic carboranyl amine **4**, followed by treatment with acid, and produced the zwitterionic imidazolium species **25**. Deprotonation of this zwitterion with alkali hexamethyldisilazide bases cleanly afforded the normal C-2 NHC complexes **26[Li$^+$]** or **26[K$^+$].** However, the attempted

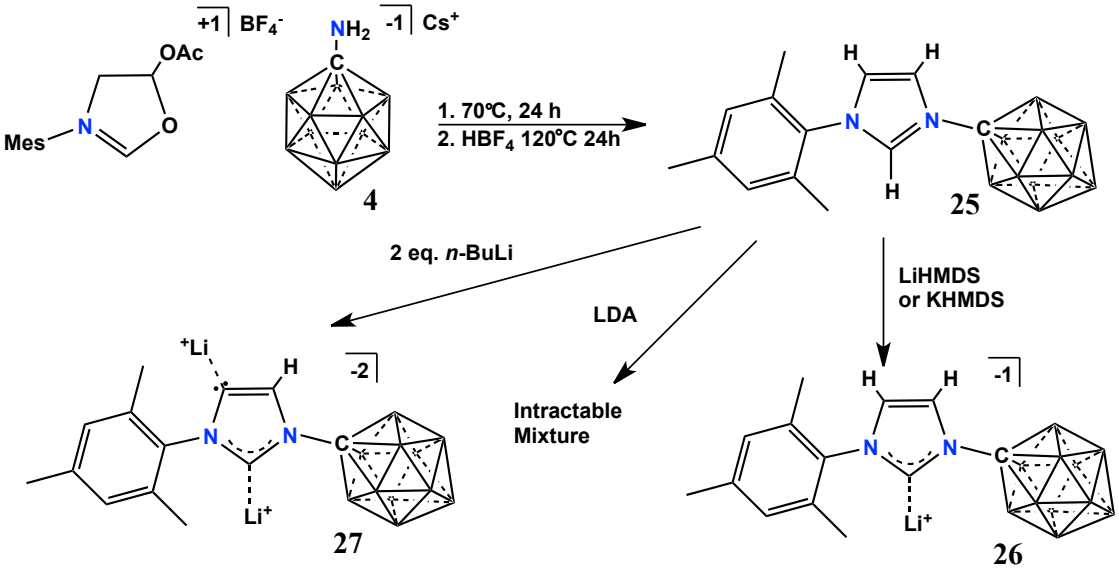

Scheme 5-1. Synthesis of unsymmetrical imidazolium zwitterion featuring a mesityl and 12-vertex carboranyl substituents, **25**. Subsequent deprotonation to form the unsymmetrical normal NHC anion **26**, and the doubly deprotonated dianion **27**.

deprotonation of the zwitterion with LDA to selectively form an abnormal NHC led to an intractable mixture. This result indicated that in order to achieve selective imidazolium backbone deprotonation, two anionic icosahedral *N*-carboranyl groups are required. Deprotonation of the imidazolium with three equivalents of *n*-butyllithium resulted in the selective formation of C-2/C-5 deprotonation species **27[Li$^+$]**, revealing an unprecedented directing effect of the anionic icosahedral carborane substituent. Following this work, my labmate Steven Fisher successfully demonstrated that these carboranyl N-heterocyclic carbenes are suitable ligands for transition metal complexes.[18] Both the unsymmetrical mono-anionic and symmetrical dianionic carboranyl NHCs (**12** and **26**) readily reacted with $ClAuSMe_2$ to afford the zwitterionic and anionic Au(I) dimethyl sulfide adducts.

Both the unsymmetrical mono-anionic and symmetrical dianionic carboranyl NHCs were constructed using the 12-vertex icosahedral carborane anion **2**. Due to availability, the

most common carboranes used in ligand design are not the anionic species **2**, but instead are derived from the neutral icosahedral dicarbaborane cluster **1** (C_2B_{10}).[19-21] While the neutral cluster offers many distinct characteristics,[19] it exhibits reactivity that is potentially undesirable for catalysis, such as facile B–H cyclometallation[22] and B-vertex extrusion reactions[23] to afford *nido*-carboranes. The latter reaction has been developed by Teixidor and Viñas to produce novel anionic phosphines and other ligands, featuring *nido*-cluster substituents.[19,24-28] More recently, my labmate Jess Estrada utilized the susceptibility of *o*-carborane **1** to undergo B-vertex extrusion for the formation of an unsymmetrical imidazolium zwitterion bearing a nido-carborane.[29] This was also accomplished via reaction with Fürstner's N-mesityl oxazolinium salt.[17] He was able to selectively deprotonate the bridging hydride of the open cluster nido-carborane, producing the monoanionic dicarbollide ion. Subsequent deprotonation resulted in the formation of the N-dicarbollide dianion.

5.2 Results and Discussion

Due to my recent work with the symmetrical N-carboranyl imidazolium featuring the 10-vertex carborane **19**, I became curious to see if I could also synthesize the 10-vertex analog of the unsymmetrical imidazolium **25**. Reacting the mesityl substituted oxazolium cation with the 10-vertex carborane amine **17**, followed by treatment with acid, did indeed produce the analogous zwitterionic species **28** (Scheme 5-2). In the ^{1}H NMR, three distinct doublets of doublets are present from the imidazolium ring protons (9.34 ppm, $^4J_{H\text{-}H}$ = 2.0, 1.8 Hz (C-2); 8.29 ppm, $^3J_{H\text{-}H}$ = 2.0 Hz, $^4J_{H\text{-}H}$ = 1.8 Hz (C-4); 7.62 ppm, $^4J_{H\text{-}H}$ = 2.0 Hz, $^3J_{H\text{-}H}$ = 2.0 Hz (C-5)). The ^{13}C NMR spectrum displays three resonances (142.3 (C-2), 126.4 (C-4), 124.8 (C-5) ppm) for the imidazolium carbons.

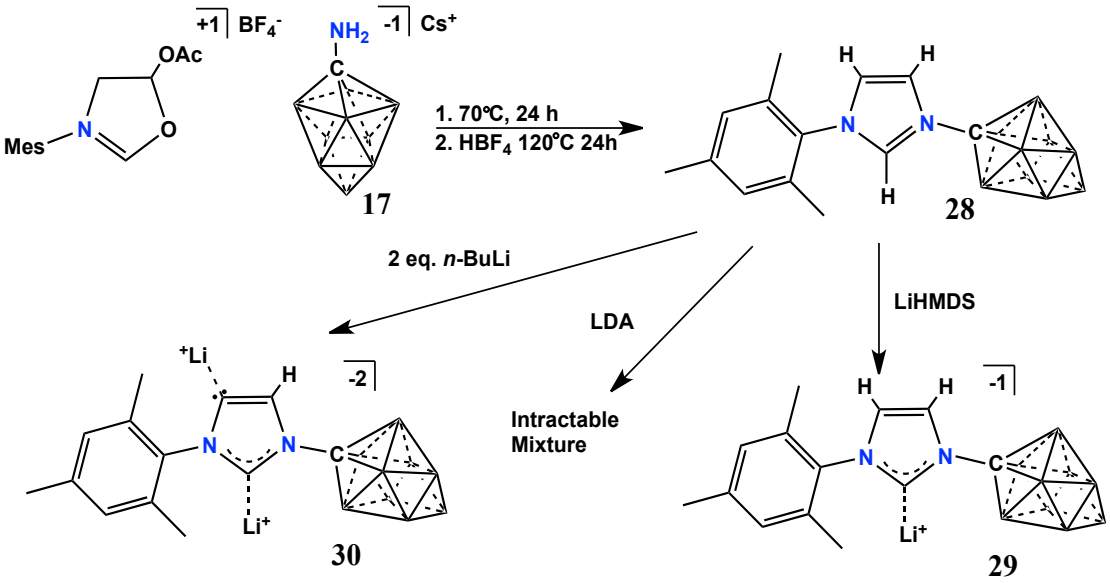

Scheme 5-2. Synthesis of unsymmetrical imidazolium zwitterion featuring a mesityl and 10-vertex carboranyl substituents, **28**. Subsequent deprotonation to form the unsymmetrical normal NHC anion **29**, and the doubly deprotonated dianion **30**.

Deprotonation of the zwitterionic imidazolium species **28** with LiHMDS affords the unsymmetrical N-heterocyclic carbene **29** according to NMR analysis (Scheme 5-2). The ^{1}H NMR shows the disappearance of the low field C-2 proton at 9.34 ppm and the appearance of two doublets (8.01 ppm and 7.04 ppm, $^{4}J_{H\text{-}H} = 1.5$ Hz), which is consistent with the formation of the normal C-2 NHC. The ^{13}C NMR spectrum of **29[Li^{+}]** displays a resonance at 199.4 ppm for the carbene center, which is in the expected range for aryl substituted imidazolylidenes.

We next explored the possibility of forming the abnormal NHC, analogous to **15**, by reaction of **28** with LDA. All of our attempts to selectively deprotonate the backbone of the imidazolium **28** with LDA led to intractable mixtures of **29** and multiple unidentified compounds. These results agree with the selectivity previously seen with deprotonation of the unsymmetrical 12-vertex carborane imidazolium **25**.[16] Subsequently, we turned our attention to the double deprotonation of **28** with *n*-butyllithium. Previously with the unsymmetrical 12-

vertex carborane imidazolium **25**, deprotonation with two equivalents of *n*-butyllithium resulted in the clean formation of a single isomer of the doubly deprotonated dianionic species **27** (Scheme 5-1). For the 12-vertex species, ^{1}H NMR indicated clear selectivity of deprotonation of the C-5 position of the backbone adjacent to the N-mesityl substituent, and a single crystal X-ray diffraction study confirmed the structure of **27**. It was speculated that this directing effect results from the combination of steric and electrostatic effects induced by the 12-vertex carborane susbstituent. I was curious to see if the same selectivity was observed with the 10-vertex carborane anion. Following treatment of **28** with two equivalents of *n*-butyllithium, the ^{1}H NMR displays one singlet for the remaining proton of the doubly deprotonated ring at 7.20 ppm of the dianion **30**. The ^{13}C NMR of **30** shows an unsymmetrical ring with two low field quaternary resonances at 194.2 and 167.3 ppm that correspond to the C-2 and C-5 deprotonated carbon centers, respectively.

5.3 Conclusion

This chapter describes the synthesis of the zwitterionic imidazolium species **28** featuring N-hydrocarbon and N-carbonyl groups. Deprotonation of the zwitterion species with LiHMDS cleanly affords the normal C-2 NHC complex **29**. Attempted deprotonation of **28** with LDA to selectively form an abnormal NHC led to an intractable mixture. Double deprotonation of **28** with *n*-butyllithium resulted in the selective formation of the C-2/C-5 dianionic species **30**. These results are synonymous with the previously reported deprotonation of the 12-vertex unsymmetrical imidazolium **25**, which exhibited the same incapacity to from an abnormal species and possesses an identical directing effect in the formation of a doubly deprotonated species.

5.4 Experimental

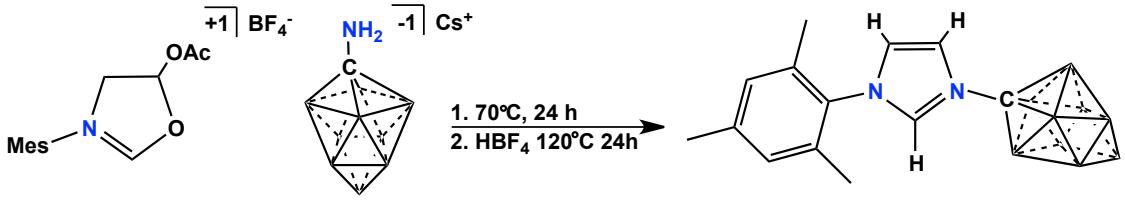

Scheme 5-3. Synthesis of 10-vertex carborane unsymmetrical imidazolium zwitterion **28**

A Teflon stoppered Schlenk was equipped with a stir bar and loaded with 1-mesityl-3-acetoxyoxazolinium tetrafluoroborate (prepared via the Fürstner synthetic route)[17] (1.5 g, 4.5 mmol) and cesium 1-amino-1-carba-*closo*-decaborate **17** (1.28 g, 4.8 mmol). Dry acetonitrile (4 mL) was added to the Schlenk, which was tightly sealed and heated to 70 °C for 24 hours. To the crude reaction mixture, tetrafluoroboric acid diethyl ether complex (1.35 mL, 1.61 mmol) was added. The Schlenk was sealed again and heated to 110 °C for 24 hours. The solution was cooled then poured into a beaker containing sodium bicarbonate (200 mL). Methylene chloride (200 mL) was added and the aqueous phase was further washed with methylene chloride (2 × 100 ml). All volatiles were subsequently removed under vacuum to give a dark brown solid. This solid was crystallized from a concentrated solution of 75% toluene, 25% methanol at 5 °C to give **28** as light colorless blocks. Further concentration of the supernate led to two further crops of crystals (1.10 grams, 74%). ^{1}H NMR (400 MHz, acetonitrile-d_3, 25 °C): δ = 9.34 (dd, $^{4}J(H,H)$ = 2.0, 1.8 Hz, 1H), 8.29 (dd, $^{3}J(H,H)$ = 2.0 Hz, $^{4}J(H,H)$ = 1.8 Hz, 1H), 7.92 (dd, $^{4}J(H,H)$ = 2.0 Hz, $^{3}J(H,H)$ = 2.0 Hz , 1H), 7.16 (s, 2H), 2.37 (s, 3H), 2.16 (s, 6H), 2.72-0.20 (bm, 9H, B-H); ^{13}C (^{1}H-dec) NMR (125 MHz, acetonitrile-d_3, 25 °C): δ = 142.3, 138.7, 135.7, 132.0, 130.5, 126.4, 124.8, 74.9,

21.1, 17.6; ^{11}B (^{1}H-dec) NMR (96 MHz, acetonitrile-d_3, 25°C): δ = 31.3, -15.5, -25.4; ^{11}B NMR (96 MHz, acetonitrile-d_3, 25 °C): δ = 30.9, -15.5, -25.4 ppm.

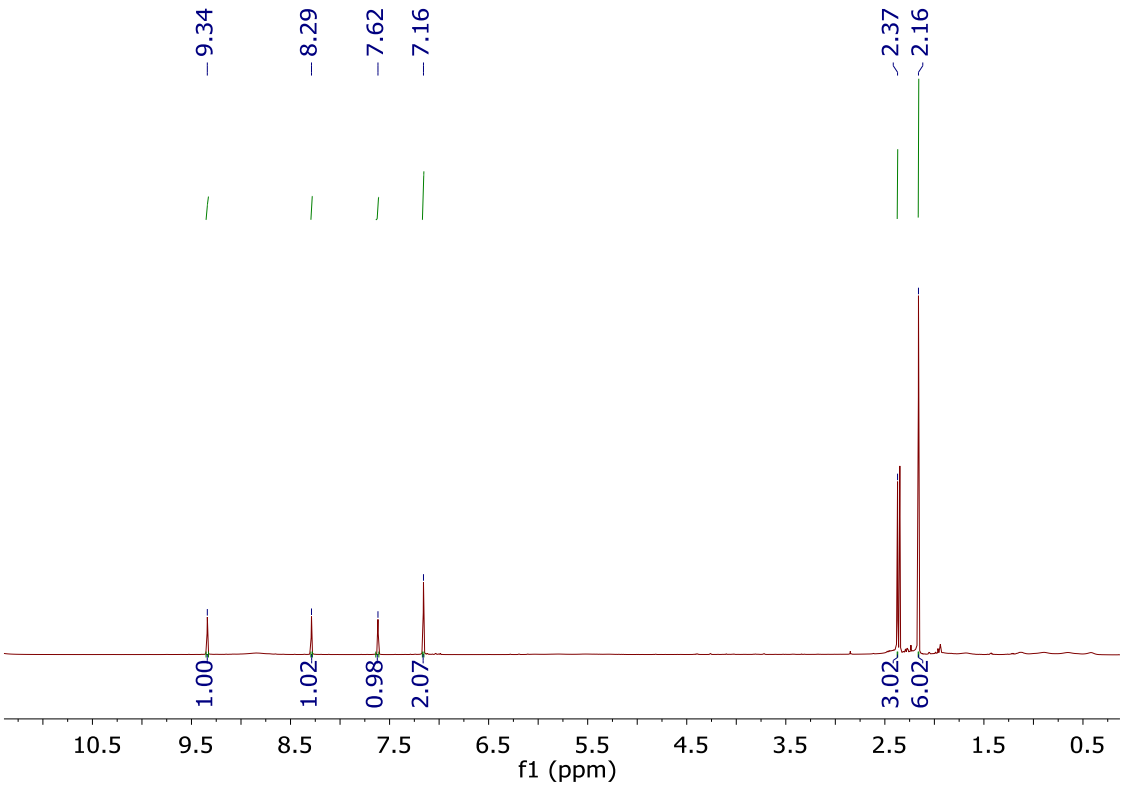

Figure 5-1. ^{1}H NMR of **28** in acetonitrile-d_3.

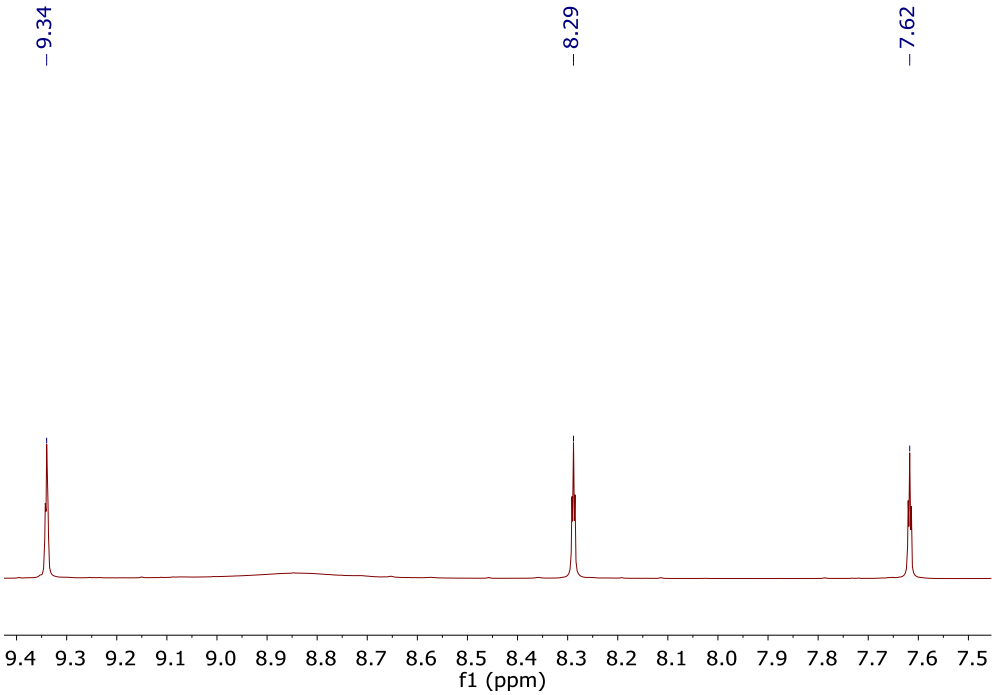

Figure 5-2. ^{1}H NMR of **28** in acetonitrile-d_3; An expanded view of the aromatic region showing the J-coupling of the imidazolium protons.

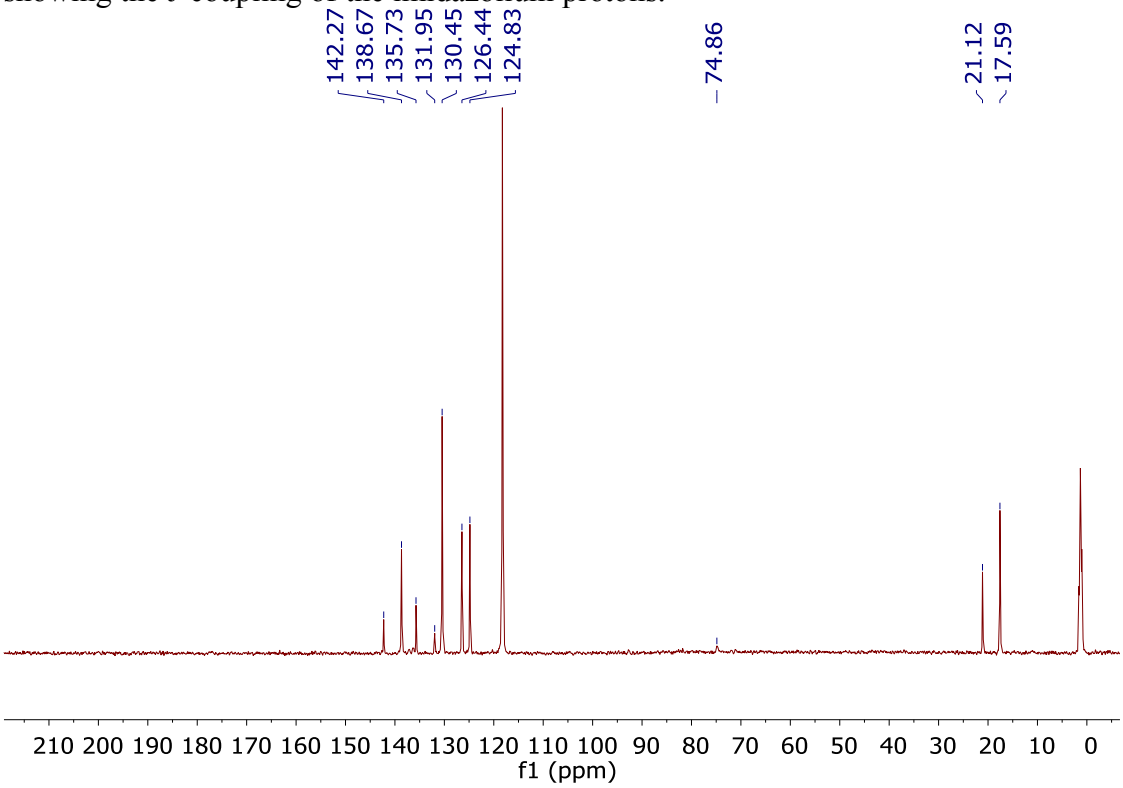

Figure 5-3. ^{13}C (^{1}H-dec) NMR of **28** in acetonitrile-d_3.

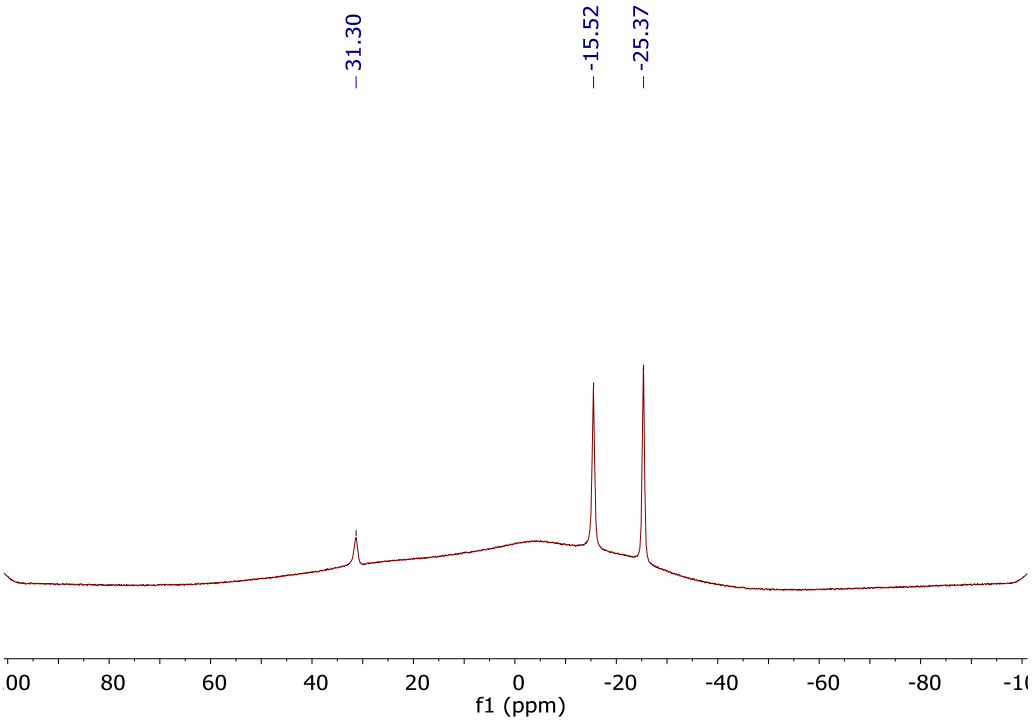

Figure 5-4. ^{11}B (^{1}H-dec) NMR of **28** in acetonitrile-d_3.

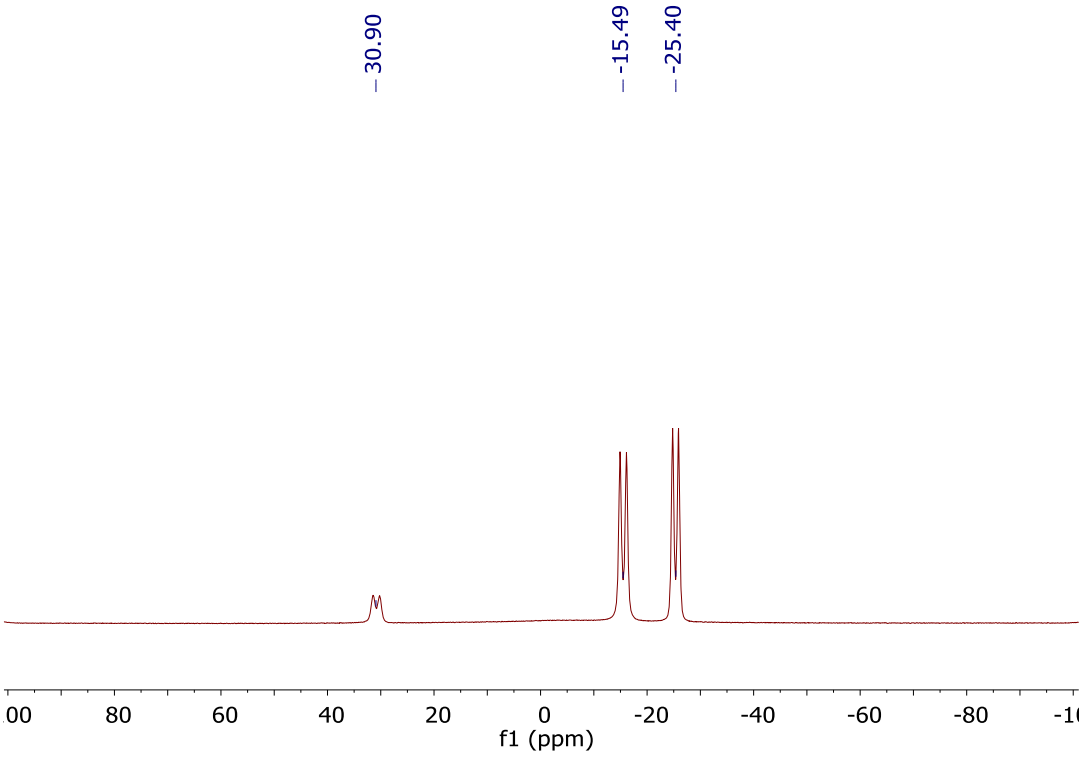

Figure 5-5. ^{11}B NMR of **28** in acetonitrile-d_3.

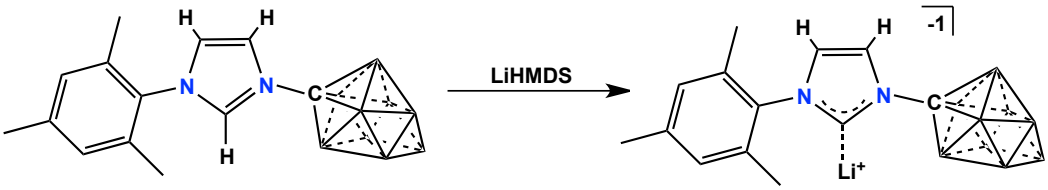

Scheme 5-4. Deprotonation of **28** to form **29[Li$^+$]**

A glass scintillation vial equipped with a stir bar was loaded with **28** (100 mg, 0.33 mmol) and lithium hexamethyldisilazide (60 mg, 0.35 mmol). Tetrahydrofuran (4 mL) was added to the stirring mixture and allowed to react for one hour. The solution was added dropwise to a stirring solution of ether (15 mL) and dried in vacuo to furnish the desired compound, **29[Li$^+$]** (140 mg, 82%). ^{1}H NMR (400 MHz, tetrahydrofuran-d$_8$, 25 °C): δ = 8.01 (d, $^3J(H,H)$ = 1.5 Hz, 1H), 7.04 (d, $^3J(H,H)$ = 1.5 Hz, 1H), 7.03 (s, 2H), 2.34 (s, 3H), 2.13 (s, 6H), 2.50 – 0.50 (bm, 9H, B-H); ^{1}H (^{11}B-dec) NMR (300 MHz, tetrahydrofuran-d$_8$, 25 °C): δ = 8.01 (d, 1H), 7.03 (m, 3H), 5.53 (s, 1H, B-H), 2.34 (s, 3H), 2.13 (s, 6H), 1.93 (s, 4H, B-H), 0.71 (s, 4H, B-H); ^{13}C (^{1}H-dec) NMR (200 MHz, tetrahydrofuran-d$_8$, 25 °C): δ = 199.4, 138.0, 137.8, 135.3, 128.6, 124.1, 120.34, 78.7, 20.0, 16.9 ppm. ^{11}B (^{1}H-dec) NMR (96 MHz, tetrahydrofuran-d$_8$, 25 °C): δ = 27.6, -16.9, -26.3 ppm.

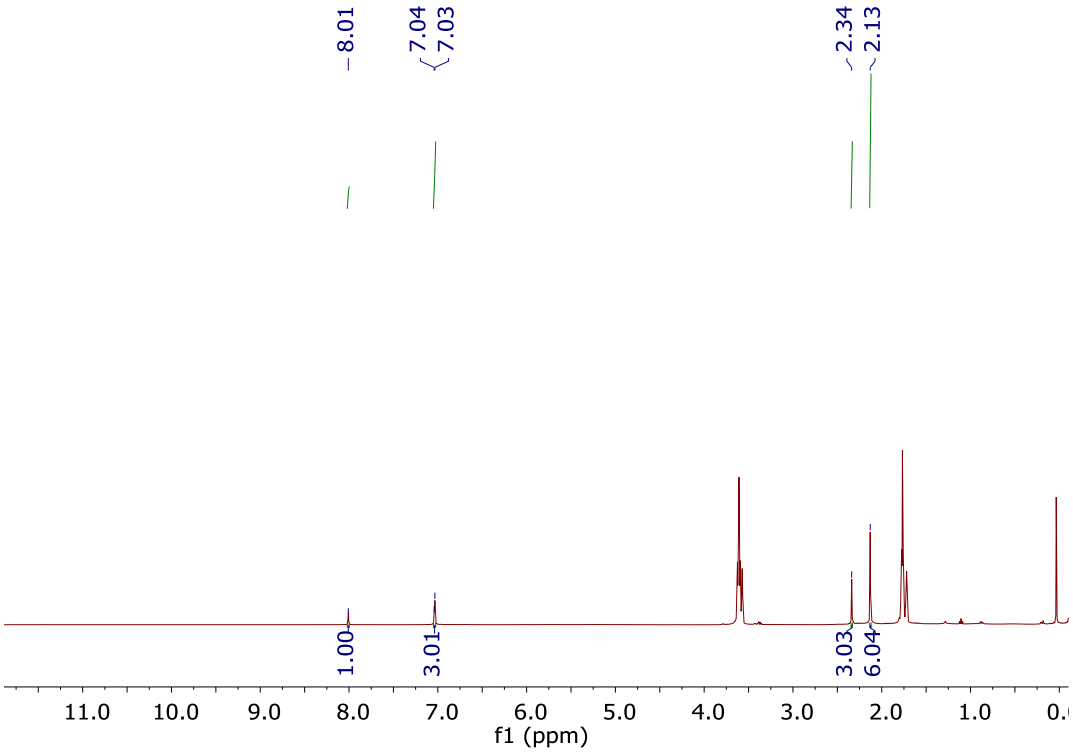

Figure 5-6. ^{1}H NMR of **29** in tetrahydrofuran-$d_{8.}$

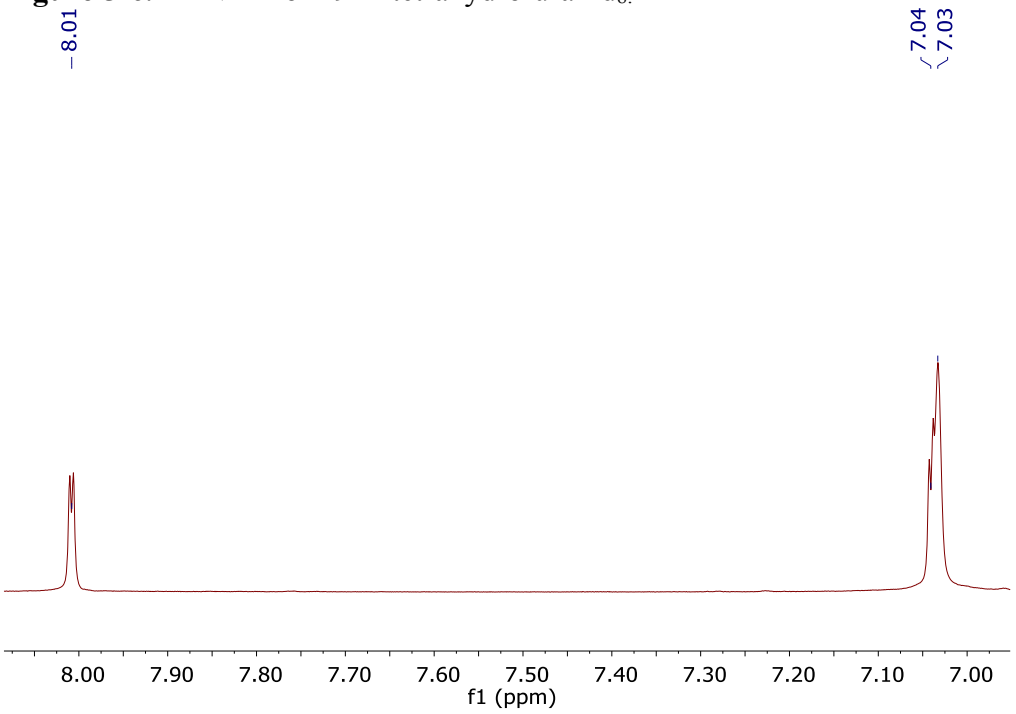

Figure 5-7. An expanded view of the aromatic region of the ^{1}H NMR of **29** in tetrahydrofuran-$d_{8.}$, showing the J-coupling of the imidazolylidene protons.

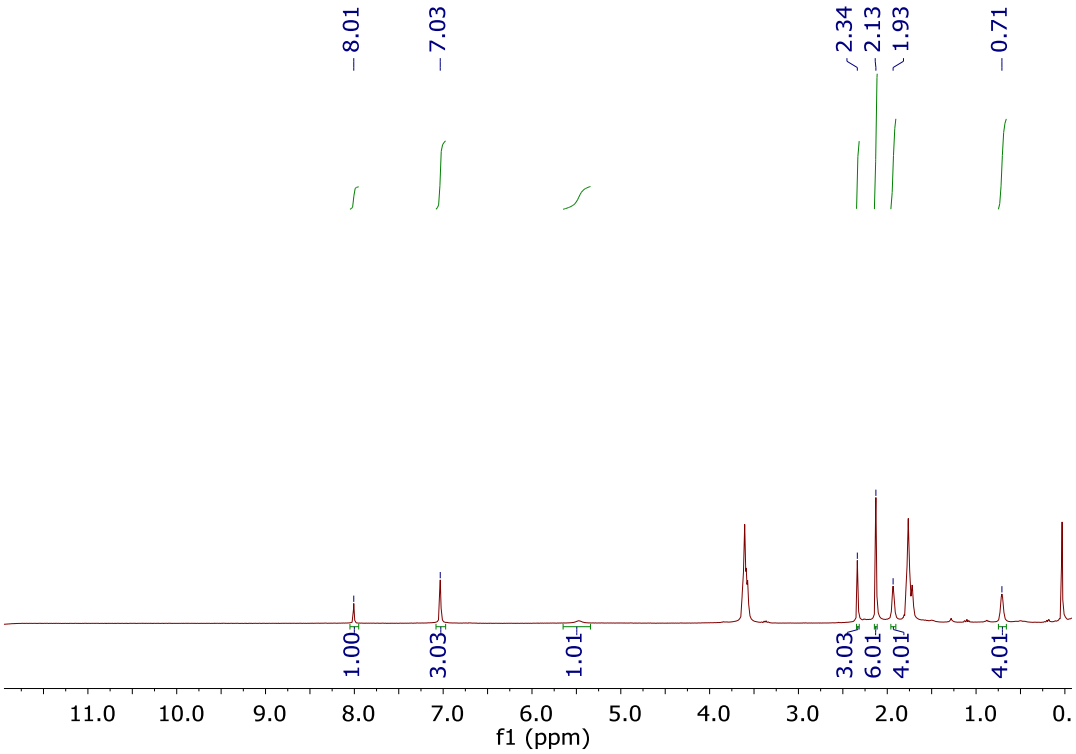

Figure 5-8. ^{1}H (^{11}B-dec) NMR of **29** in tetrahydrofuran-d_8.

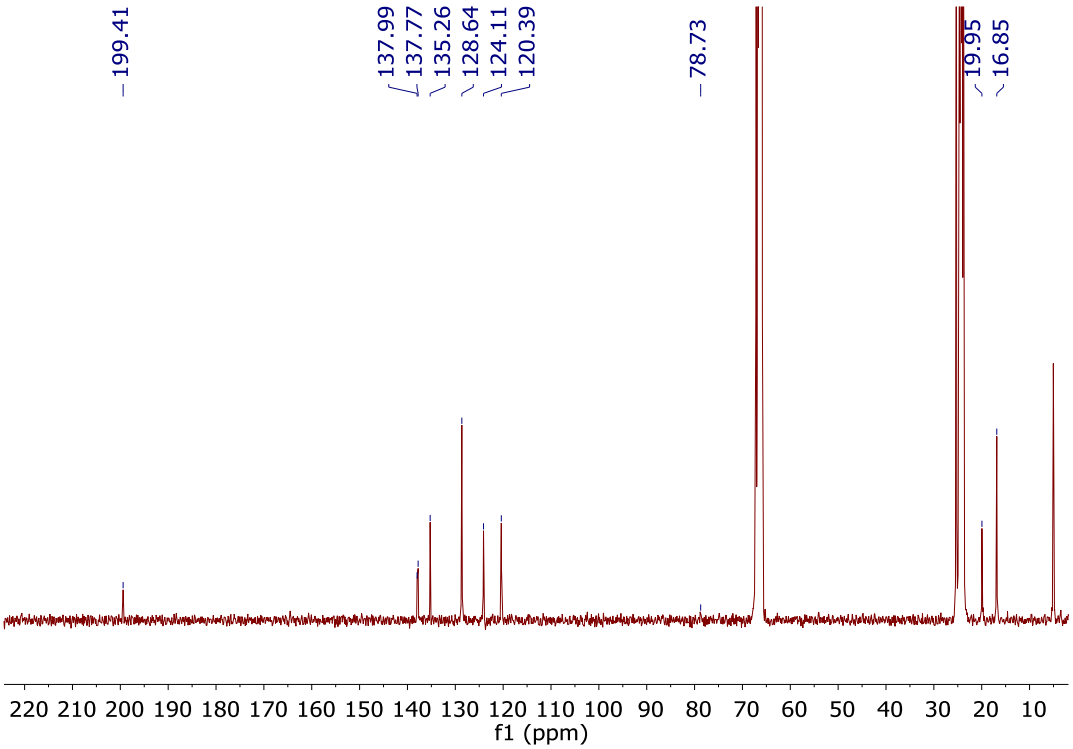

Figure 5-9. ^{13}C (^{1}H-dec) NMR of **29** in tetrahydrofuran-d_8.

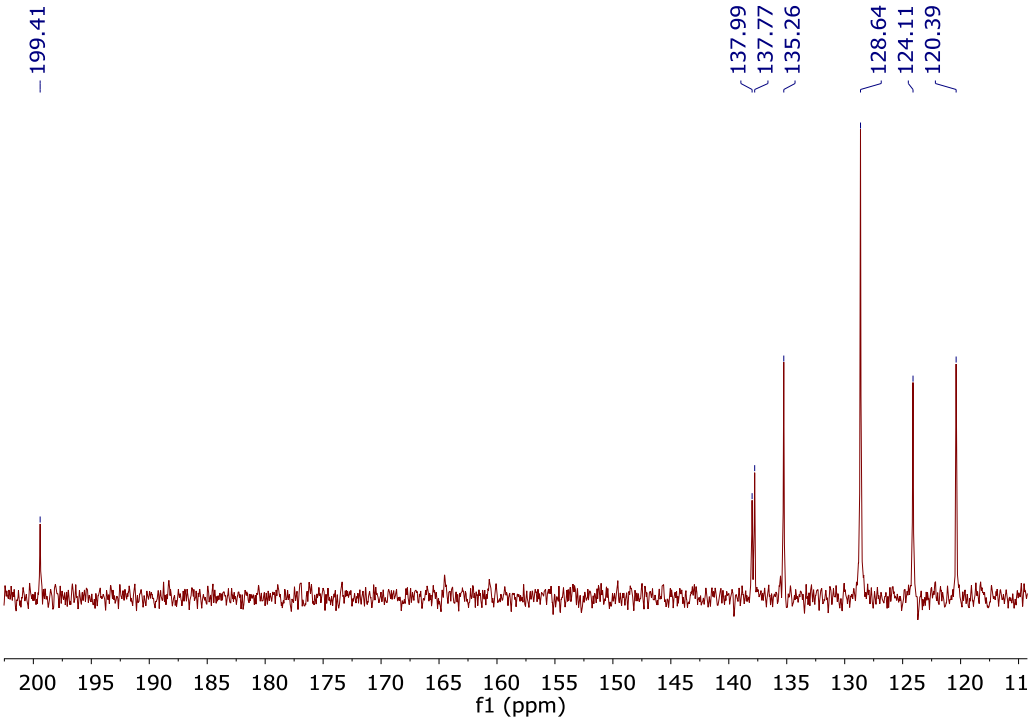

Figure 5-10. An expanded view of the downfield region of the ^{13}C (^{1}H-dec) NMR of **29** in tetrahydrofuran-d_8.

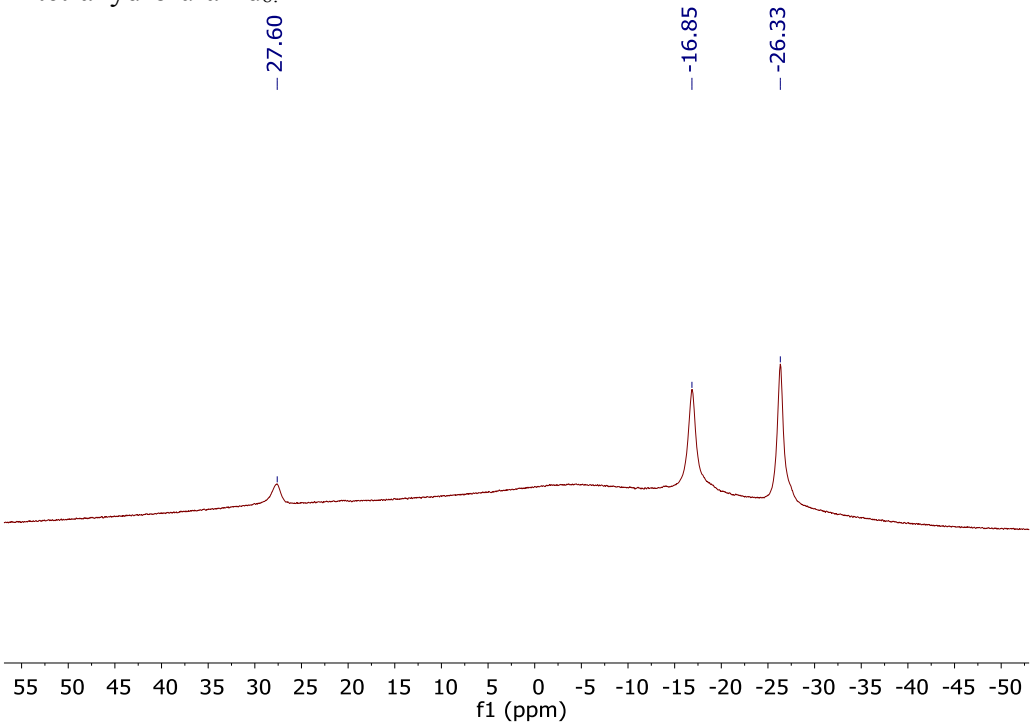

Figure 5-11. ^{11}B (^{1}H-dec) NMR of **29** in tetrahydrofuran-d_8.

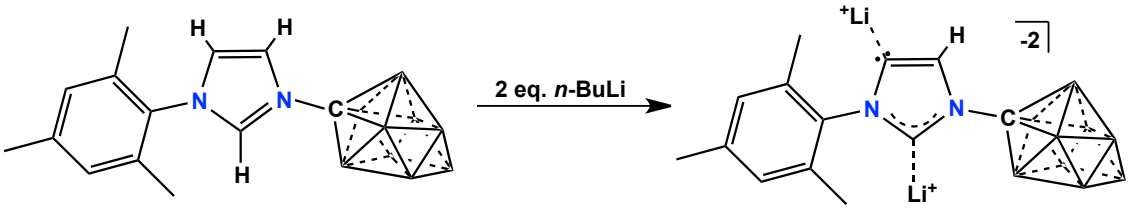

Scheme 5-5. Deprotonation of **28** to form **30[Li$^+$]**

A glass scintillation vial equipped with a stir bar was loaded with **28** (350 mg, 1.15 mmol) and diethyl ether (17 mL). Next, *n*-butyllithium (1.80 mmol) in ether (2 ml) was added to the stirring suspension of **28**. Following the addition of the n-butyllithium, an oil began to form along the walls of the vial. The reaction mixture was vigorously stirred and scraped with a spatula periodically over an hour until a white solid precipitated from the beige solution. The reaction was stirred for another hour and then filtered and washed with diethyl ether. The product **30** was collected as a white solid (767 mg, 89%). (Note: each Li^+ countercation has three THF molecules coordinated) ^{1}H NMR (400 MHz, tetrahydrofuran-d_8, 25 °C): δ = 7.20 (s, 1H), 6.87 (s, 2H), 2.28 (s, 3H), 2.10 (s, 6H), 3.25-0.15 (bm, 9H, BH). ^{1}H (^{11}B-dec) NMR (192.5 MHz, tetrahydrofuran-d_8, 25 °C): δ = 7.20 (s, 1H), 6.87 (s, 2H), 2.28 (s, 3H), 2.10 (s, 6H), 1.85 (s, 4H, B-H), 0.88 (s, 1H, B-H), 0.65 (s, 4H, B-H); ^{13}C (^{1}H-dec) NMR (100 MHz, tetrahydrofuran-d_8, 25 °C): δ = 194.2, 167.3, 146.4, 135.6, 134.1, 129.9, 127.6, 81.4, 20.1, 17.6, 14.4; ^{11}B (^{1}H-dec) NMR (96 MHz, tetrahydrofuran-d_8, 25 °C): δ = 26.3, -15.9, -25.1; ^{11}B NMR (96 MHz, tetrahydrofuran-d_8, 25 °C): δ = 26.2, -15.9, -25.2 ppm.

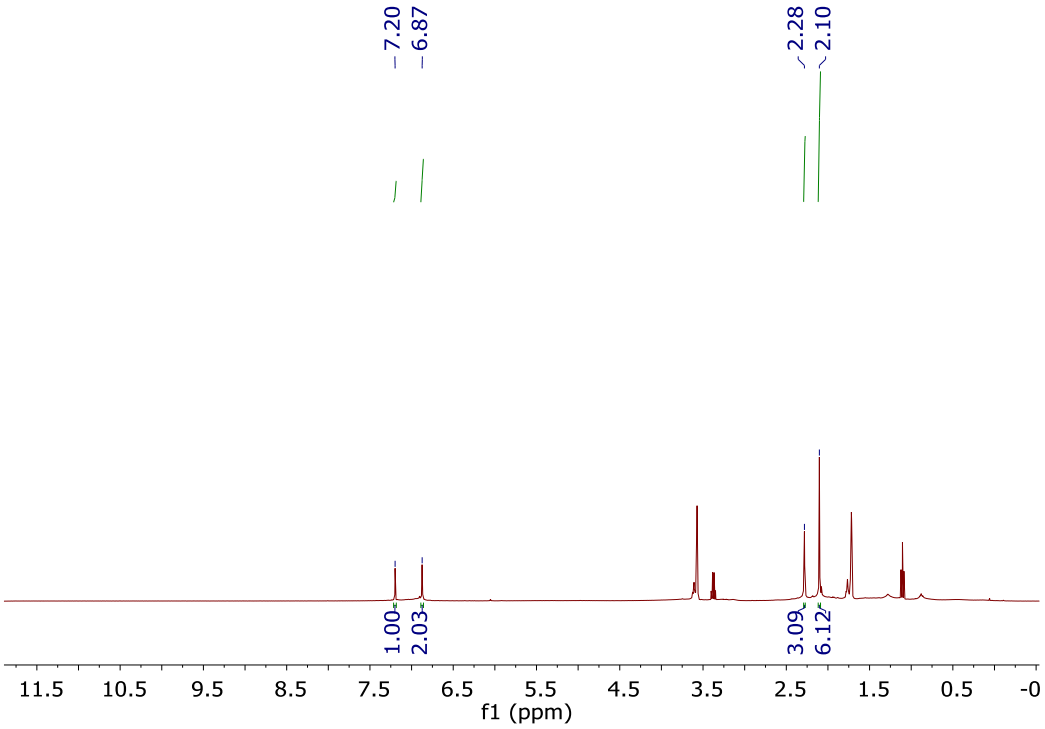

Figure 5-12. ^{1}H NMR of **30** in tetrahydrofuran-d_8. Note the presence of trace diethyl ether at 1.14 and 3.42 ppm.

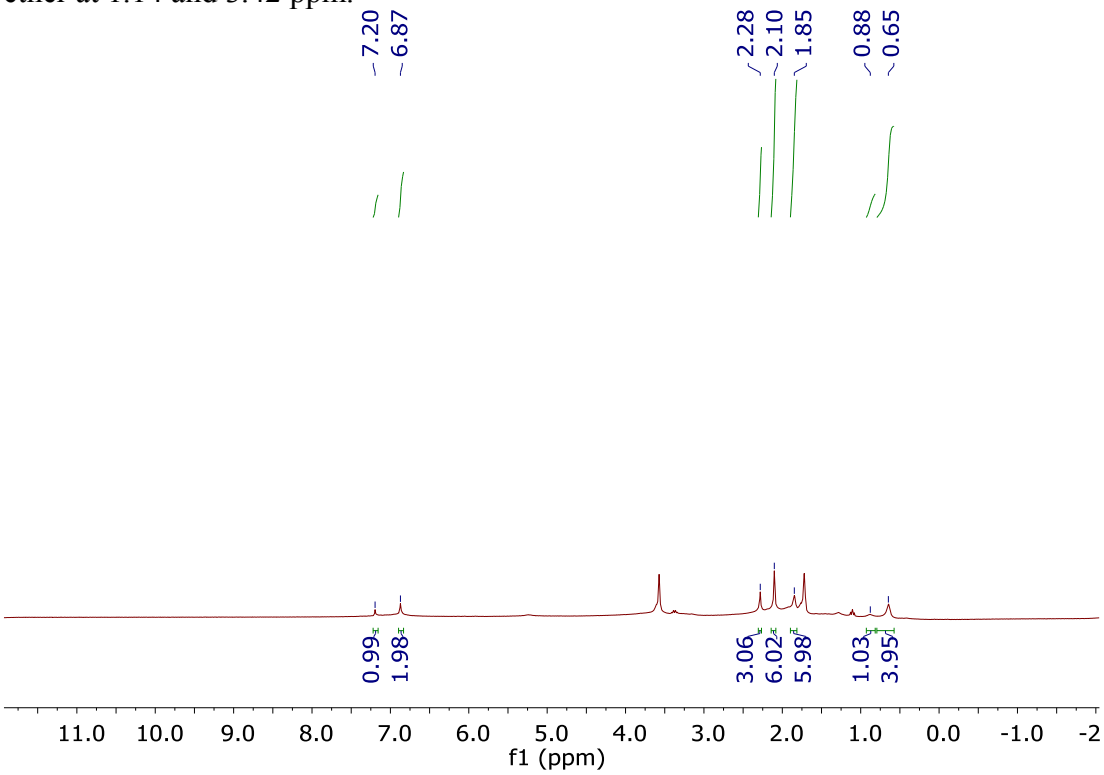

Figure 5-13. ^{1}H (^{11}B-dec) NMR of **30** in tetrahydrofuran-d_8.

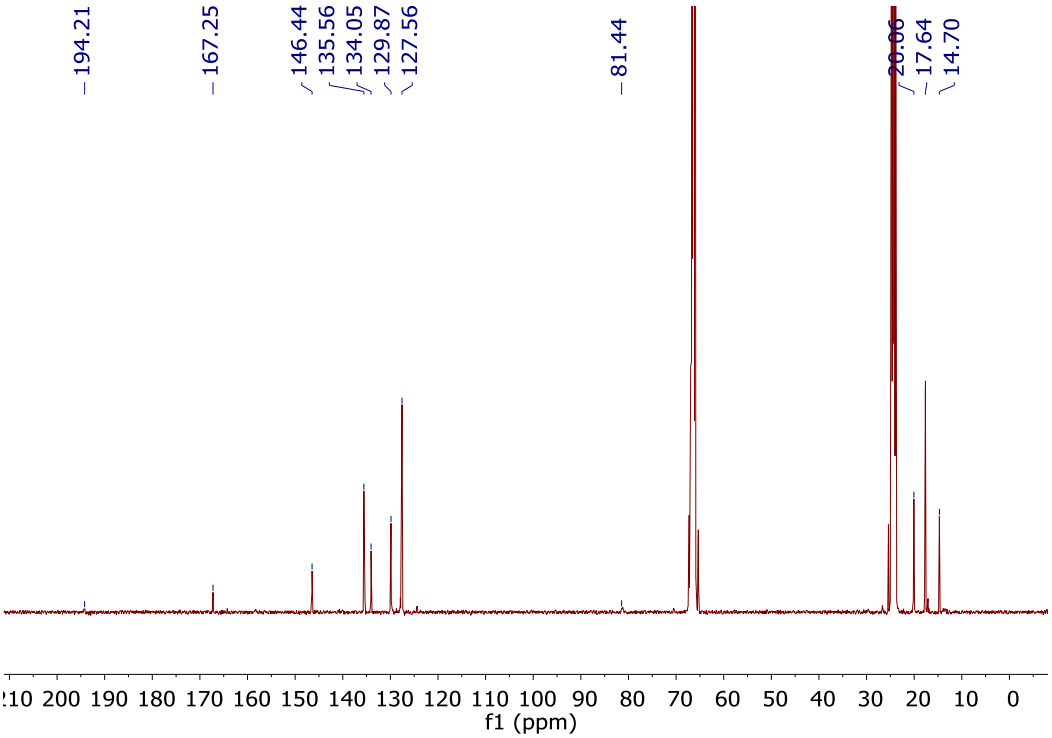

Figure 5-14. ^{13}C (^{1}H-dec) NMR of **30** in tetrahydrofuran-d_8.

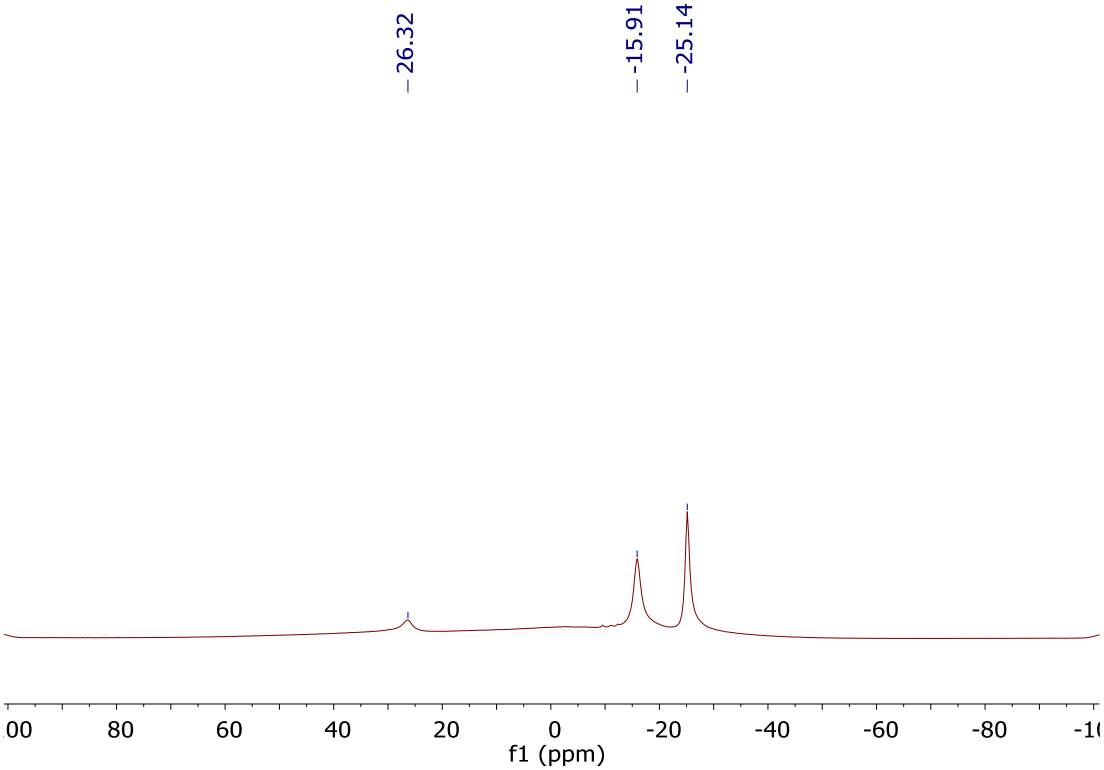

Figure 5-15. ^{11}B (^{1}H-dec) NMR of **30** in tetrahydrofuran-d_8.

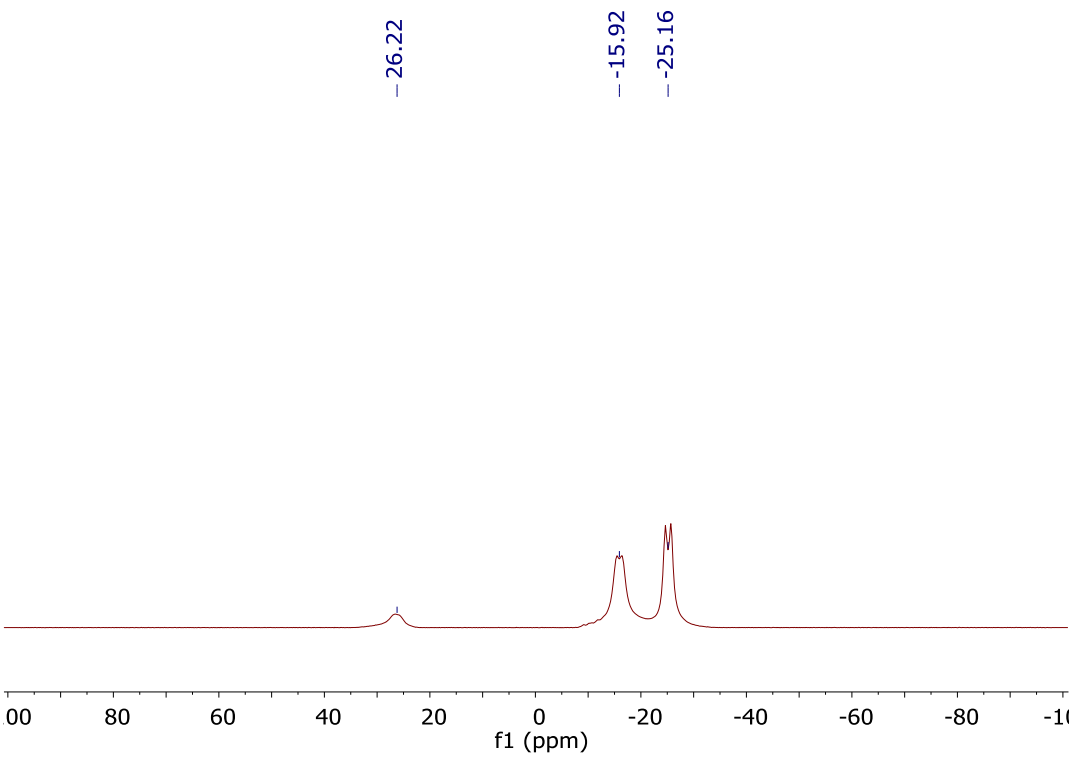

Figure 5-16. ^{11}B NMR of **30** in tetrahydrofuran-d_8.

5.5 References

1. El-Hellani, A.; Lavallo, V. *Angewandte Chemie International Edition* **2014**, *53*, 4489.

2. Izquierdo, F.; Manzini S.; Nolan, S. P. *Chemical Communications* **2014**, *50,* 14926.

3. Hopkinson, M. N.; Richter, C.; Schedler, M.; Glorius, F. *Nature*, **2014**, *510*, 485.

4. Martin, D.; Melaimi, M.; Soleilhavoup M.; Bertrand, G. *Organometallics*, **2011**, *30,* 5304.

5. Diez-Gonzalez, S.; Marion N.; Nolan, S. P. *Chemical Reviews* **2009**, *109*, 3612.

6. Hahn, F. E.; Jahnke, M. C. *Angewandte Chemie International Edition* **2008**, *47*, 3122

7. Crabtree, R. H. *Coordination Chemistry Reviews* **2013**, *257*, 755.

8. Schuster, O.; Yang, L. R.; Raubenheimer H. G.; Albrecht, M. *Chemical Reviews* **2009**, *109*, 3445.

9. Krüger, A.; Albrecht, M. *Australian Journal of Chemistry*, **2011**, *64*, 1113.

10. Grundemann, S.; Kovacevic, A.; Albrecht, M.; Faller J. W.; Crabtree, R. H. *Chemical Communications* **2001**, *21,* 2274.

11. Aldeco-Perez, E.; Rosenthal, A. J.; Donnadieu, B.; Parameswaran, P.; Frenking G.; Bertrand, G. *Science*, **2009**, *326*, 556.

12. Wang, Y.; Xie, Y.; Abraham, M. Y.; Wei, P.; Schaefer, H. F.; Schleyer P. v. R.; Robinson, G. H. *Journal of the American Chemical Society* **2010,** *132*, 14370.

13. Kolychev, E. L.; Kronig, S.; Brandhorst, K.; Freytag, M.; Jones, P. G.; Tamm, M. *Journal of the American Chemical Society* **2013**, *135*, 12448.

14. Kronig, S.; Theuergarten, E.; Daniliuc, C. G.; Jones P. G. Tamm, M. *Angewandte Chemie International Edition* **2012,** *51*, 3240.

15. Wang, Y.; Xie, Y.; Abraham, M. Y.; Gilliard, R. J.; Wei, P.; Campana, C. F.; Schaefer, H. F.; Schleyer P. v. R.; Robinson, G. H.; *Angewandte Chemie International Edition* **2012**, *51,* 10173.

16. Asay, M. J.; Fisher, S. P.; Lee, S. E.; Tham, F. S.; Borchardt, D.; Lavallo, V. *Chemical Communications* **2015**, *51*, 5359.

17. Fürstner, A.; Alcarazo, M.; Cesar V.; Lehmann, C. W. *Chemical Communications*, **2006**, *20,* 217.

18. Fisher, S. P.; El-Hellani, A.; Tham, F. S.; Lavallo, V.; *Dalton Transactions* **2016**, *45*, 9762.

19. Scholz, M.; Hey-Hawkins, E. *Chemical Reviews* **2011**, *111*, 7035.

20. Li, Y.; Carroll, P. J.; Sneddon, L. G. *Inorganic Chemistry* **2008**, *47,* 9193.

21. Kusari, U.; Li, Y.; Bradley M. G.; Sneddon, L. G. *Journal of the American Chemical Society* **2004**, *126*, 8662.

22. Hoel E. L.; Hawthorne, M. F. *Journal of the American Chemical Society* **1975**, *97*, 6388.

23. Wiesboeck, R. A.; Hawthorne, M. F. *Journal of the American Chemical Society* **1964**, *86*, 1642.

24. Teixidor, F.; Flores, M. A.; Viñas, C.; Kivekäs R.; Sillanpää, R. *Organometallics*, **1998**, *17*, 4675.

25. Viñas, C.; Nuñez, R.; Teixidor, F.; Kivekäs R.; Sillanpää, R. *Organometallics*, **1996,** *15*, 3850.

26. Teixidor, F.; Ayllon, J. A.; Viñas, C.; Kivekas, R.; Sillanpää, R.; Casabo, J. *Inorganic Chemistry* **1994**, *33*, 1756.

27. Teixidor, F.; Ayllon, J. A.; Viñas, C.; Kivekas, R.; Sillanpää, R.; Casabo, J. *Journal of Organometallic Chemistry* **1994**, *483*, 153.

28. Teixidor, F.; Ayllon, J. A.; Viñas, C.; Kivekas, R.; Sillanpää, R.; Casabo, J. *Journal of the Chemical Society, Chemical Communications* **1992**, *18*, 1281.

29. Estrada, J.; Lavallo, V. *Angewandte Chemie Internation Edition* **2017**, *56*, 9906.

Chapter 6: Reversible Silver Electrodeposition from Boron Cluster Ionic Liquid (BCIL) Electrolytes

6.1 Introduction

Electrodeposited metallic structures are ubiquitous in modern technologies (e.g., batteries, protective coatings, displays, and microchips) and emerging technologies such as resistive memory and reconfigurable electronics.[1,2] The broad utility of electrochemically deposited structures grows as new electrolytes enable electrodeposition in increasingly challenging environments. Controlled reversible electrodeposition of metallic structures offers tunable optical properties and electrical conductivity along with the ability to adapt the electrochemical system to changing application needs. This adaptability is appealing in the context of reconfigurable electronic components which could extend a device's lifetime through in situ restructuring.

Early electrodeposition methods used aqueous electrolytes because of the solubility of common metal ions.[1] The development of non-aqueous electrolytes has enabled safe electrodeposition of water sensitive metals for new electro-chemical applications such as high-density energy storage.[3] Additionally, electrodeposition from ionic liquids has emerged as a potential alternative to organic solvent electrolytes, presenting new opportunities for electrodeposition in high vacuum and hostile environments such as electron microscopes and plasma chambers.[4]

Ionic liquids (ILs) are salts with low melting points (typically <100 °C) that combine the high ion solubility of aqueous media, the chemical flexibility of organic solvents, and low volatility.[7] With molten salts, wide electrochemical windows are achievable.[7] The versatility of ILs is increased by tailoring the cation−anion pairs for

individual applications.[5] Yet, despite the numerous cation−anion pairs that can form ionic liquids, much of ionic liquid tunability is achieved by modifying the cationic component.[5,6] This disparity is largely due to the synthetic availability of cationic molecular scaffolds such as ammonium, phosphonium, and heterocyclic motifs. Conversely, ionic liquids in which the anionic component engenders the IL properties are scarce and the anions are seldom amenable to additional functionalization.[7-10] Furthermore, the relative instability of commonly used IL anions limits the longevity of IL-based electrochemical devices. This becomes especially problematic when designing systems which require prolonged operation time. Therefore, we sought to develop an ionic liquid that contains a highly stable and easily tunable anionic component. Such "anion-based" ILs could use the metal of interest as the cation and enable high metal loadings suitable for rapid electrodeposition. Anionic polyhedral boranes represent a class of modular molecular building blocks suitable for designing "anion-based" boron cluster ionic liquids (BCILs).[11,12] Their robust boron-cluster framework provides an anionic scaffold amenable to tuning of melting point, solubility, and redox potential.[13,14] In collaboration with the Spokoyny research group from University of California, Los Angeles, we set out to develop an all-ionic electrolyte suitable for reversible deposition of silver films. Specifically, we describe an all-ionic electrolyte to reversibly

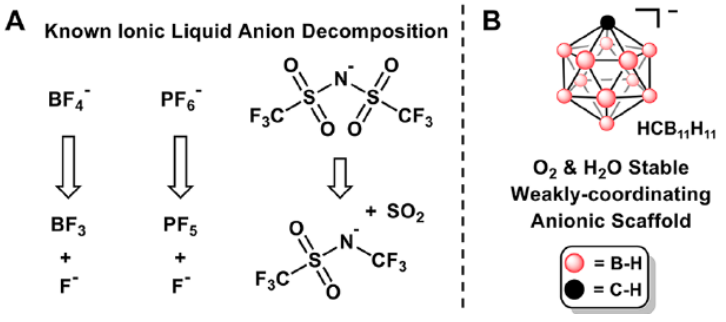

Figure 6-1. A: Examples of decomposition products of commonly used ionic liquid anions. **B**: Illustrative representation of monocarborane anion used in this chapter.

deposit silver films for the purpose of controlling infrared (IR) emission from an electrochemical cell as a means of actively regulating thermal emission. This technology complements existing approaches to controlling thermal emission from spacecraft surfaces.[15-18] Importantly, BCILs represent a critical component allowing these devices to perform reliably without having to exclude air and moisture, common contaminants that are introduced during electrochemical device assembly that are difficult to remove.

Silver films play an important technological role as electrical conductors and optical coatings. Silver offers unique advantages over other transition metals because of its high spectral reflectivity, high electrical conductivity, and corrosion resistance.[19] These qualities make silver an attractive metal for tuning the properties of spacecraft surfaces. Additionally, the low volatility of IL electrolytes offers a means of performing electrodeposition in high vacuum environments. Because of its positive reduction potential, only small voltages are required to electrodeposit silver from ionic salt precursors.[1] Electrodeposition of silver was historically performed using cyanide-based electrolytes due to the formation of stable $Ag(CN)_x^{1-x}$ complexes.[1] However, the toxicity of aqueous cyanide baths lead to the development of silver electrodeposition from ILs and organic solvents.[5,20] These non-aqueous electrolytes were suitable for reversible silver electrodeposition and served as proof-of-concept works for electrochemically modulated optical films.[21-23] The reversibility in these systems is attained from the halide-trihalide redox couples (X^-/X_3^- X = Cl, Br, or I)[24,25] and stable $[AgX_2]^-$ complexes.[26] Despite these advances, reversibility in all-ionic electrolytes was limited only to a handful of ILs. The majority of these, however, still generate unstable, volatile, or corrosive decomposition

products (Figure 6-1).[27,28] In this report, we describe our work with the Spokoyny group on creating an electrolyte for silver deposition containing a stable anion amenable to additional functionalization.

6.2 Results and Discussion

The Spokoyny group at UCLA developed a salt metathesis reaction between 1-butyl-3-methyl-imidazolium bromide, [BMIM]Br, and silver mono-carborane, $Ag^{+}[HCB_{11}H_{11}^{-}]$, to generate a boron cluster ionic liquid, **BCIL-1**, with high silver content

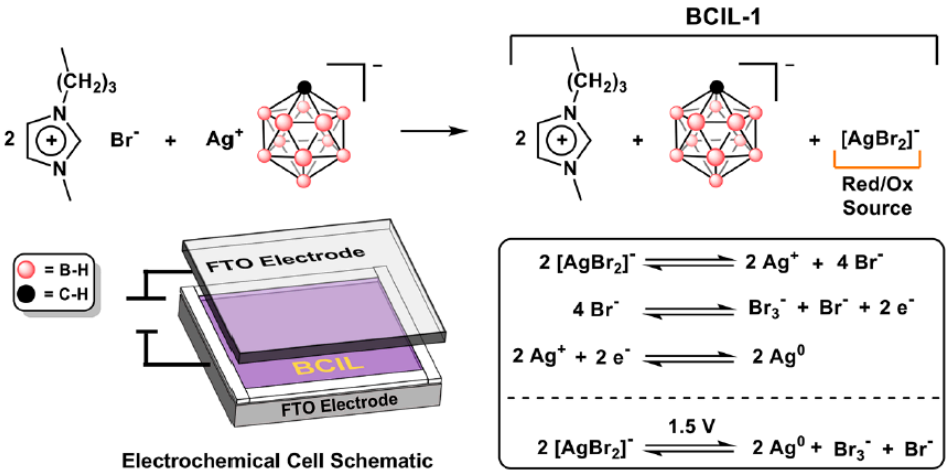

Figure 6-2. Formation of **BCIL-1** by mixing [BMIM]Br with $Ag[HCB_{11}H_{11}]$. Inset shows elementary steps associated with silver electrodeposition in **BCIL-1**.

(Figure 6-2). The Lavallo group synthesized the silver mono-carborane via a salt metathesis reaction between $Cs^{+}[HCB_{11}H_{11}^{-}]$ **1** and $AgNO_3$ with an 82% yield. This ionic liquid features an inert ionic matrix of $[BMIM]^{+}$ and $[HCB_{11}H_{11}^{-}]$ ions with $[AgBr_2]^{-}$ ions acting as the primary redox species (Figure 6-2). Dialkylimidazolium cations and monocarborane anions were selected due to their electro-chemical stability and weakly coordinating characteristics suitable for designing an inert ionic matrix.[29]

The Spokoyny research group prepared **BCIL-1** between two FTO electrodes to form a transparent, two-electrode electrodeposition cell (Figure 6-2). Cyclic voltammograms (CVs) show a reduction peak corresponding to reduction of silver complexes to form silver deposits at the working electrode. Electrodeposition begins at −1.5 V vs FTO with a distinct current loop occurring in the cathodic region which indicates a nucleation-limited deposition.[20] Reversing the polarity of the electrochemical cell toward +0.3 V vs FTO leads to dissolution of the silver deposits at the working electrode back into

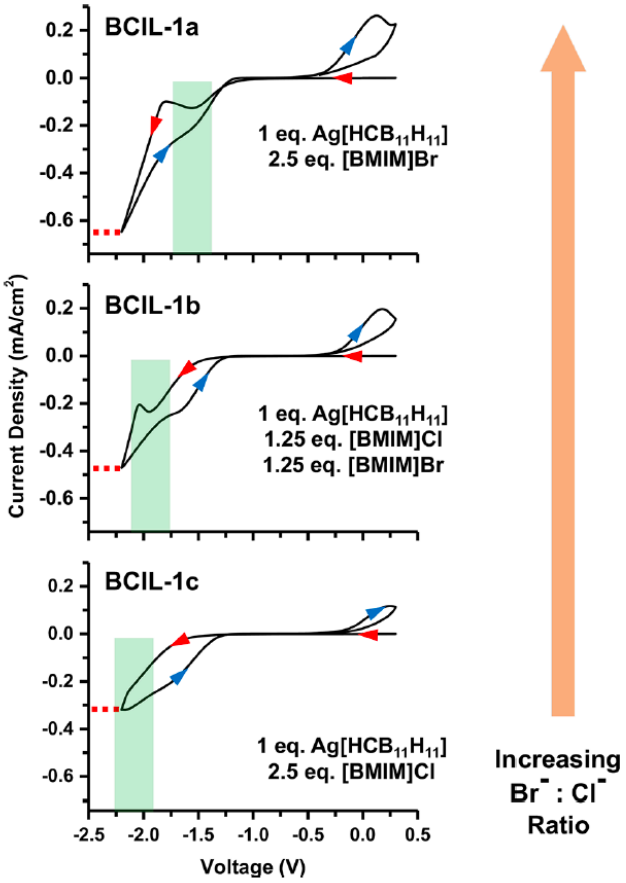

Figure 6-3. Two-electrode cyclic voltammograms (100 mV/s) of **BCIL-1** without $CuBr_2$ additive. Increasing the Br^-:Cl^- ratio increases the electrodeposition current. Red and Blue arrows indicate cathodic and anodic sweep direction, respectively. Green areas indicate the composition dependent FTO, $[AgX_2]^-$ X_3^-, Ag^0, FTO process, red dashed lines indicate the maximum electrodeposition current density at -2.3 V vs. FTO counter electrode.

the electrolyte. They observed that halide and metal ion additives can affect the rate of the silver deposition and etching . A general feature of these IL based electrolytes is an excess of halide, X^- (X = Br or Cl), to Ag^+. Typically, X^-:Ag^+ ion ratios of 2.5:1 were sufficient to fully dissolve the silver salts at room temperature. The excess halide promotes the formation of $AgBr_x^{1-x}$ species and provides additional halide ions to access the halide-trihalide (X^-/X^{3-}) redox couple.

As the composition of the electrolyte is varied from chloride-rich to bromide-rich the potential for silver electrodeposition shifts to less cathodic potentials (Figure 6-3). This dependence on halide identity in the BCIL provides a simple method for tuning the onset of silver reduction and the current density of silver electrodeposition. Similar irreversible behavior in previously reported optical modulation devices were resolved by adding Cu(II) salts.[20,22] Related studies on the effects of $CuBr_2$ in [BMIM]Br ionic liquids found that $CuBr_2$ complexes were effective at etching copper films.[30] Likewise, addition of 10 mol % $CuBr_2$ (relative to Ag^+) to **BCIL-1** dramatically improved the reversibility of the ionic liquid formulation, generating **BCIL-2** (Figure 6-4). Noteworthy was the change in film dissolution dynamics, wherein silver films deposited in the presence of Cu(II) were readily removed and exhibited larger oxidative currents.

Previously, it has been shown that water content present in ILs during their ambient handling can alter the reversibility of silver deposition.[31] Importantly, **BCIL-2** containing devices placed into a 98% humidity chamber did not experience alterations in device performance. CV experiments showed identical operating currents even after 4 days at

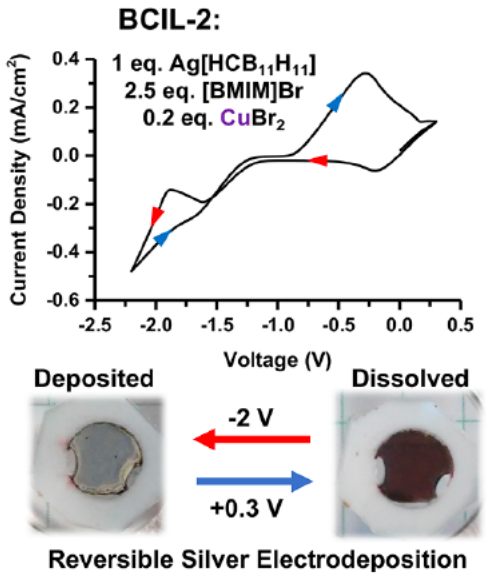

Figure 6-4. Representative cyclic voltammogram (100 mV/s) of **BCIL-2**, red and blue arrows indicate forward (deposition) and reverse (dissolution) potential sweep direction, respectively.

these conditions. Such water tolerance enabled an easy benchtop assembly. Despite the electrochemical and moisture stability of **BCIL-2**, a gradual decrease in electrodeposition current was observed during electrochemical cycling of **BCIL-2** cells. After leaving the electrochemical cell overnight at room temperature, the electrodeposition current through the cell decayed and redox features became indistinguishable. Visual inspection of the electrolyte showed partial crystallization of the BCIL. Heating the cell to 60 °C for 1 hour dissolved the visible crystallites thereby restoring the cell to the original performance. This ultimately suggests that formation of small crystallites leads to reduced ion mobility and electrodeposition current.

Contrary to prevailing approaches of changing the physical properties of ILs by altering the cation, we sought to inhibit crystallite formation by functionalizing the monocarborane anion **2**. I prepared several monocarboranes functionalized with alkyl groups (Scheme 6-1). After deprotonating the carbon vertex with *n*-butyllithium, the carborane dianion is washed with hexanes to remove excess base. The carborane dianion is prepared in a solution of tetrahydrofuran and the alkyl halide is added directly to the reaction mixture, forming the corresponding functionalized carborane. Three different

alkyl functionalized carboranes (**31**, **32**, **33**, Figure 6-5) were prepared, and all of the crude reaction solutions revealed 70-90% conversion to the desired products by ^{11}B NMR analysis. The functionalized carborane anions **31** and **32** are less soluble as cesium salts

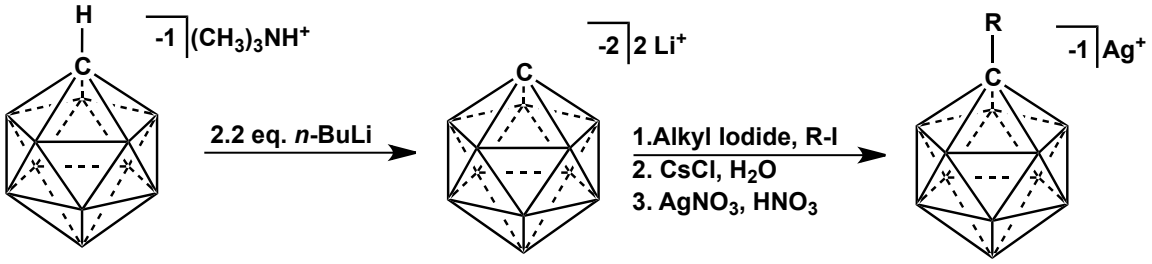

Scheme 6-1. Synthesis of alkyl-functionalized carborane silver salts

than the unfunctionalized carborane **2[Cs$^+$]** and were separated via recrystallization from an aqueous solution of CsCl. When attempting to purify **33** via cation exchange, the crude product formed a layer of viscous oil that was immiscible with water at the recrystallization step. Further purification of **33** was not addressed, and the functionalized anions **31** and **32** were prepared as the corresponding silver mono-carboranes via a salt metathesis reaction with $AgNO_3$, resulting in 80% and 72% yields, respectively.

A third electrolytic mixture, **BCIL-3**, was prepared by the Spokoyny research group using the monocarborane functionalized with a sec-butyl group appended on the carbon vertex of the boron-rich cluster, **31[Ag$^+$]**. Both alkyl carborane silver salts **31[Ag$^+$]** and **32[Ag$^+$]** were initially used generate the

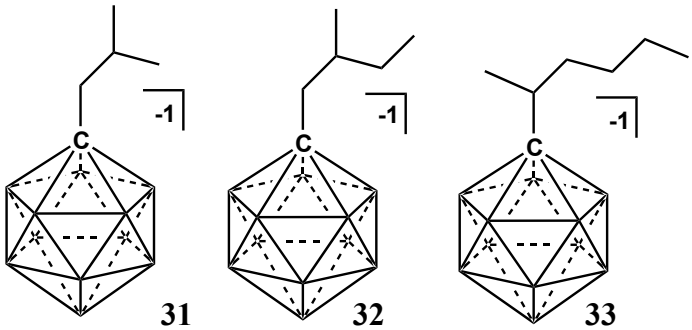

Figure 6-5. Functionalized carborane anions **31**, **32**, and **33,** from left to right. The crude product of **33** was a viscous oil and not isolated.

corresponding a boron cluster ionic liquid via a salt metathesis reaction with 1-butyl-3-methyl-imidazolium bromide, [BMIM]Br, however **BCIL-3** (synthesized from **31[Ag^+]**) exhibited superior properties as an ionic liquid electrolyte and is only presented in this work. An electrochemical cell containing **BCIL-3** was kept at room temperature for 24 hours and the deposition currrents were comparable to those obtained from freshly prepared **BCIL-3** suggesting that, at this time scale, no observable crystallization occurs and hence the device performance remains unaffected. This is in contrast to the previous results with **BCIL-2**, where partial crystallization of the liquid occurred overnight. (Figure 6-6, A). Heating of the **BCIL-3** cell to 60 °C for 1 hour further increased the electrodeposition current (Figure 6-6, B).

The Spokoyny group monitored the quality of the electrodeposited films using a 633 nm laser to correlate the film growth to the electrochemical behavior of the cells. Extended electrochemical cycling of a **BCIL-3** cell revealed a decay in reflectance change likely due to partial crystallization of **BCIL-3**. These effects were mitigated by heating the cell every 40 cycles (Figure 6-6, C) to restore reflectance changes of up to 80%. The silver film electrodeposition from **BCIL-3** can reach maximum reflectance within ∼3 s when applying a −2.5 V cathodic potential, and it can be quickly removed by reversing the polarity of the electrochemical cell to +2.5 V (Figure 6-6, C). Oxidative etching of the electrodeposited silver film is likely accelerated by electro-migration of halides toward the working electrode and subsequent removal of electrodeposited silver as solvated silver halide anions.[20-23] Applying a voltage (−1.8 V) for 450s produced a thick film which could be analyzed by scanning electron microscopy (SEM).[32] Consistent with nucleation-limited

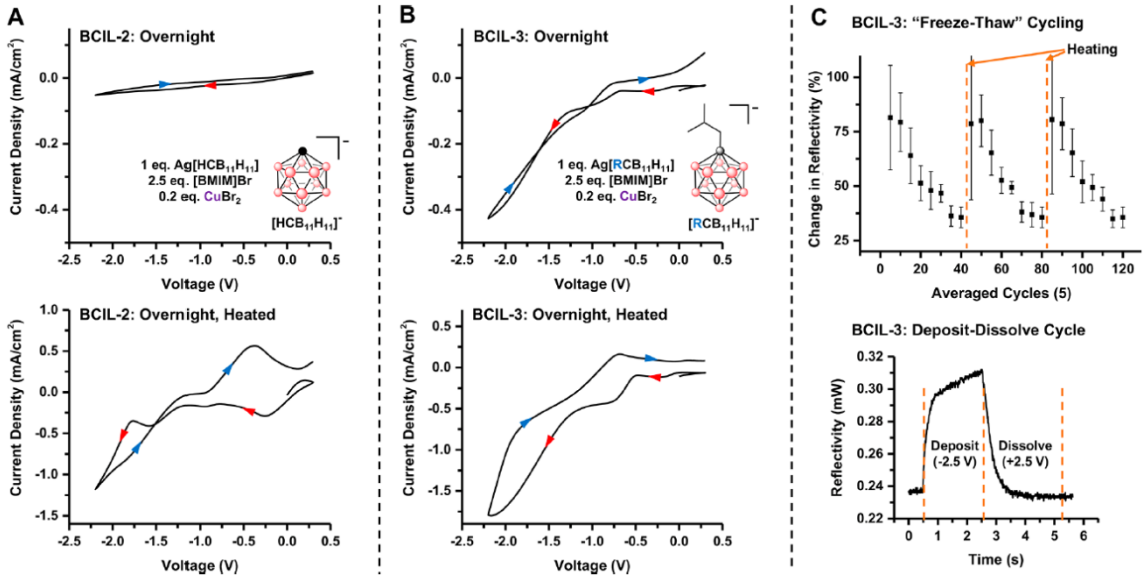

Figure 6-6. A and B: Two-electrode cyclic voltammograms (100mV/s) of **BCIL-2** and **BCIL-3** after equilibrating at ambient conditions overnight and after heating the cell to 60 °C, top and bottom, respectively. Red and blue arrows indicate cathodic and anodic sweep direction. C: Change in reflectivity at 633 nm of **BCIL-3** during extended "freeze-thaw" cycling and during a single deposition-dissolution cycle (top and bottom, respectively). The cell was regenerated every 40 cycles by heating to 60 °C.

deposition, the silver deposits grow as a film of silver crystallites approximately 500 nm in diameter. EDX elemental mapping shows two types of silver-containing deposits, an underlying Ag film with AgBr crystals on top of the film. The AgBr deposits likely formed during the washing of the working electrode, as described previously.[21]

6.3 Conclusion

In collaboration with the Spokoyny group, we prepared a stable, all-ionic electrolyte designed around the weakly coordinating carborane framework for reversible electrodeposition of silver films. The metal-rich boron cluster ionic liquid (BCIL) electrolytes enable rapid, reversible silver electrodeposition. This air and moisture stable electrolyte was used to deposit metallic films in an electrochemical cell to tune the

emissivity of the cell in situ, demonstrating a proof-of-concept design for spacecraft thermal control.[33,34] The ionic composition presents opportunities for electrodeposition in extreme environments (such as high temperature and low pressure). The development of ionic liquids enables electrodeposition in high vacuum environments and presents opportunities for creating electrochemically adaptive and regenerative spacecraft components.

6.4 Experimental

The previous experimental data has been published and may be obtained online at DOI: 10.1021/acsami.7b19302.

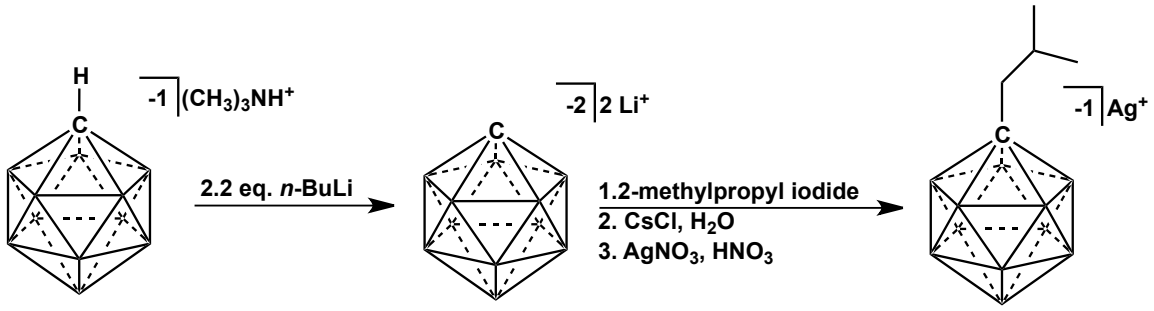

Scheme 6-2. Synthesis of *S*-Butyl Silver Monocarborane (Ag[*s*-butyl$CB_{11}H_{11}$]) **31**

Li[*closo*-1-LiCB11H11] was prepared according to literature[35]: under an inert atmosphere, 2.0 grams (9.8 mmol) of **2[Me_3NH^+]** was dissolved in 10 mL THF in a 20 mL scintillation vial equipped with a stir bar. 2.2 equivalents of 2.5 M *n*-butyllithium in hexanes was added and the mixture was allowed to stir for 3 hours. The resulting solution was added dropwise to a 250 mL round bottom flask containing 70 mL hexanes while stirring, resulting in a white precipitate. The solvent was decanted and the remaining white precipitate dried under vacuum. The isolated white precipitate was dissolved in 10 mL THF. Two equivalents of 1-iodo-2-methylpropane were added to the reaction solution and stirred for 90 minutes. The solution was removed from inert conditions, organic solvents were removed *in vacuo*, and the crude product was added to 50 mL H2O. The alkylated carborane product **31** was purified using the following salt exchange procedure: Trimethylammonium hydrochloride was added in excess to the aqueous solution, precipitating the $(CH_3)_3NH$ alkyl carborane salt. The solution was filtered and the precipitate was redissolved in approximately 80 mL

slightly basic H2O with an excess of CsCl. The solution was concentrated down to 30-40 mL, and upon cooling to room temperature the Cs^+ salt of the alkylated carborane product precipitated as a white crystalline solid. A concentrated solution of 1.3 grams of Cs^+ 2-methylpropyl-1-carborane, $Cs[(C_4H_9)CB_{11}H_{11}]$ was prepared by heating in 50 mL of slightly acidic DI water (3-5 drops of concentrated HNO3). 1.1 equivalents of AgNO3 was dissolved in 5 mL or less and added to the aqueous solution. An off-white precipitate formed immediately, and the solution was cooled to room temperature and then filtered from the aqueous solution. The collected solid was stirred in acetone and subsequently gravity filtered, extracting $Ag[(C_4H_9)CB_{11}H_{11}]$ **31[Ag^+]** from precipitated salts. $Ag[(C_4H_9)CB_{11}H_{11}]$ final yield of 0.96 g, 79.7%. ^{1}H NMR (300 MHz, acetone-d_6, 25°C): δ = 2.83 – 0.45 (bm, 11H, B-H), 1.72 (d, 2H, ^{3}*J(H,H)* = 2.0 Hz) 1.64 (m, 1H), 0.82 (d, 6H, ^{3}*J(H,H)* = 2.0 Hz); ^{1}H (^{11}B-dec) NMR (300 MHz, acetone-d_6, 25°C): δ = 1.88 (s, 6H, B-H), 1.75 (s, 5H, B-H), 1.72 (d, 2H, ^{3}*J(H,H)* = 2.0 Hz) 1.64 (m, 1H), 0.82 (d, 6H, ^{3}*J(H,H)* = 2.0 Hz); ^{11}B (^{1}H-dec) NMR (96 MHz, acetone-d_6, 25°C): δ = -8.3, -9.7; ^{11}B NMR (96 MHz, acetone-d_6, 25°C): δ = -7.5, -9.0, -10.4 ppm.

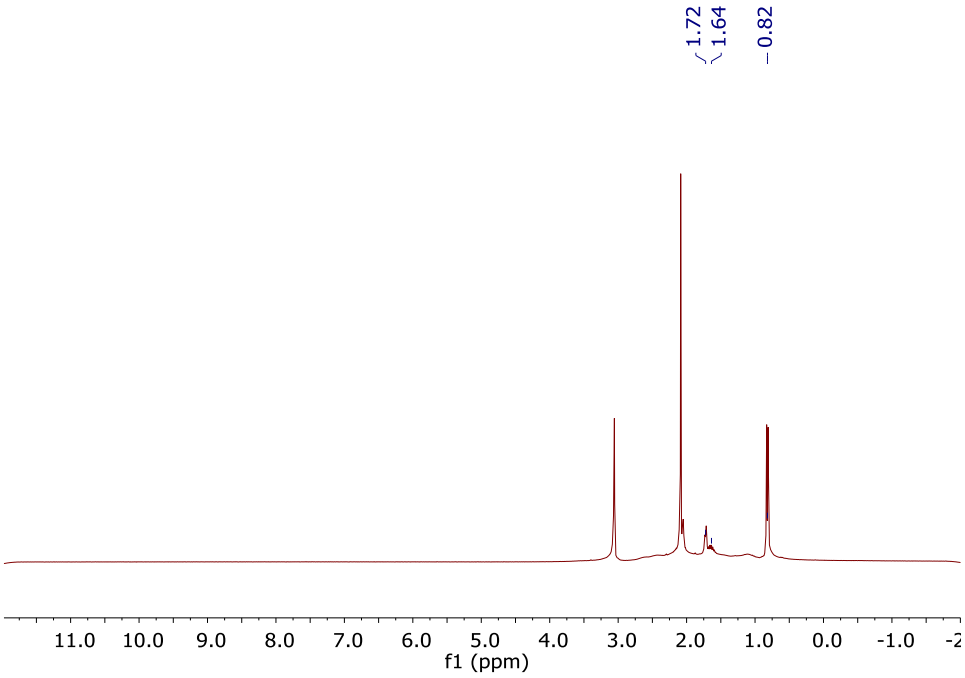

Figure 6-7. ^{1}H NMR spectrum of **31[Ag^{+}]** in acetone-d$_6$. Note: the peaks at 3.05 and 2.09 ppm are from H$_2$O and acetone, respectively.

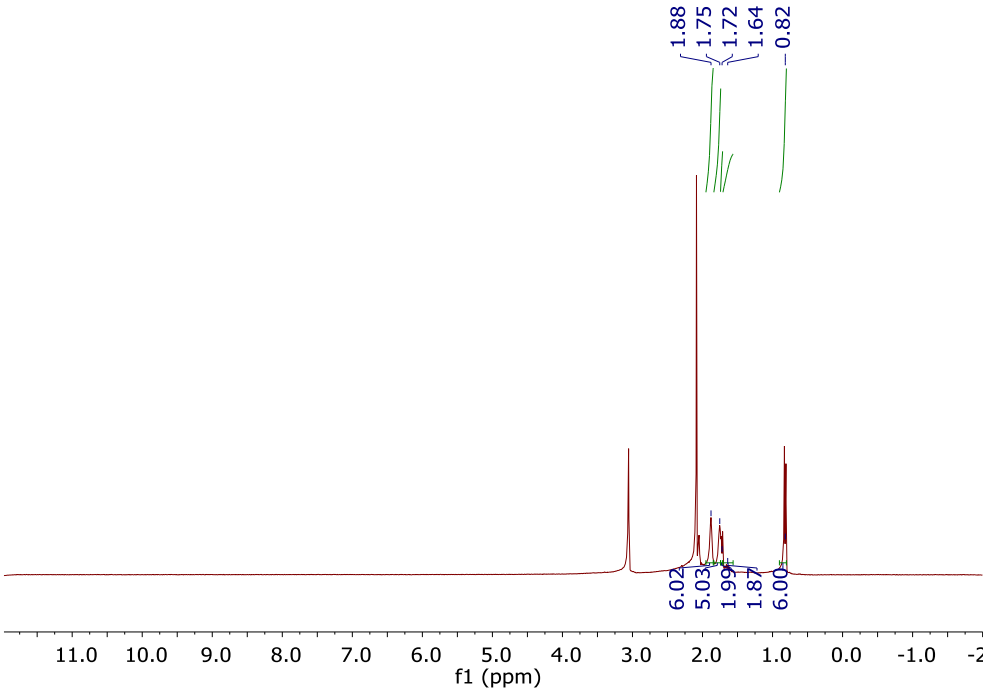

Figure 6-8. ^{1}H (^{11}B-dec) NMR spectrum of **31[Ag^{+}]** in acetone-d$_6$. Note: the peaks at 3.05 and 2.09 ppm are from H$_2$O and acetone, respectively.

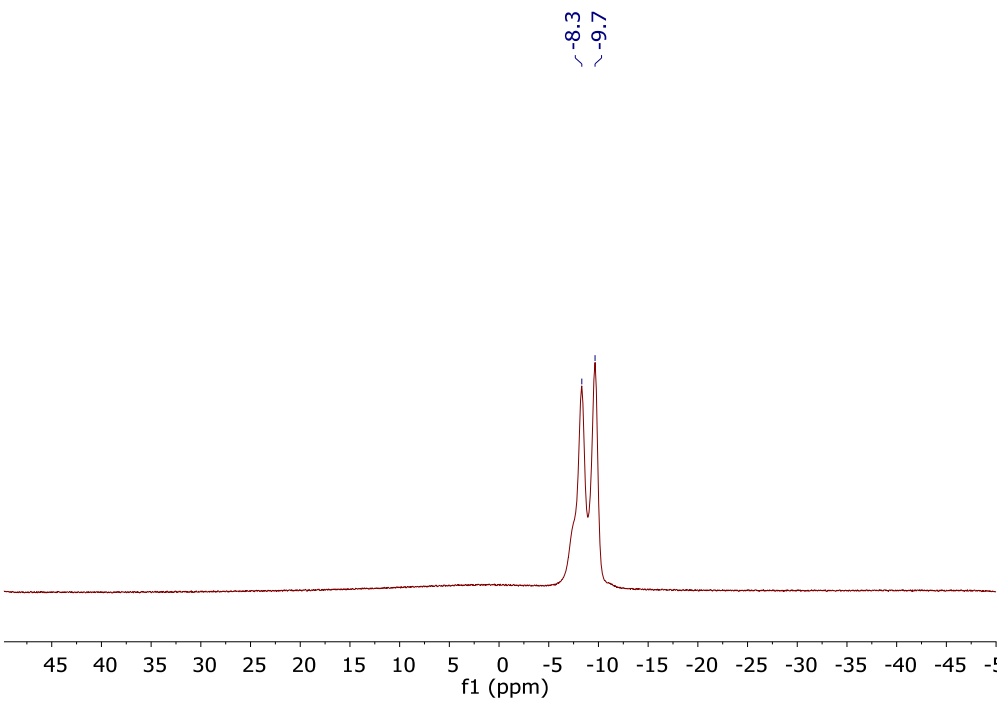

Figure 6-9. ^{11}B (^{1}H-dec) NMR spectrum of **31[Ag^+]** in acetone-d_6.

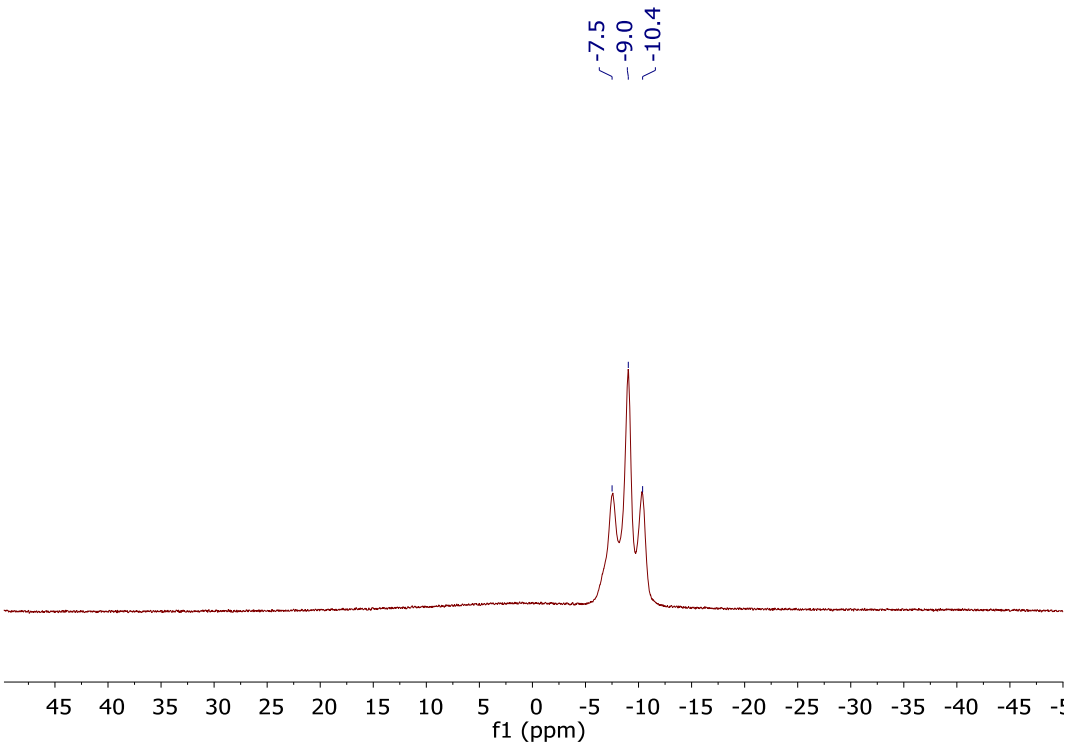

Figure 6-10. ^{11}B NMR spectrum of **31[Ag^+]** in acetone-d_6.

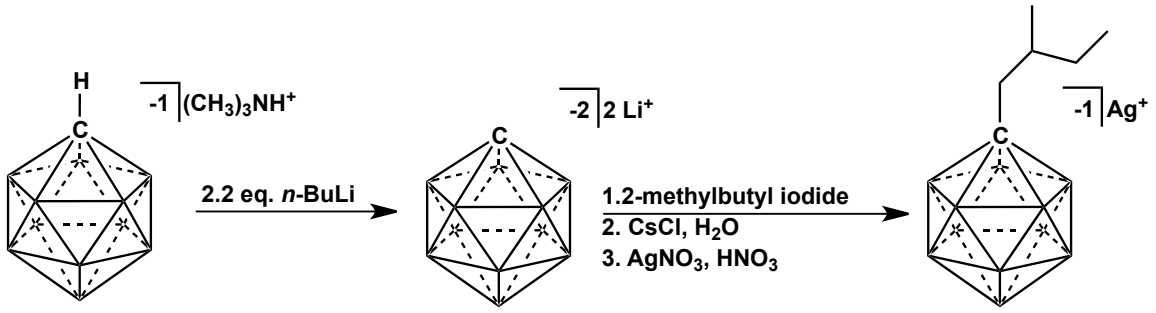

Scheme 6-3. Synthesis of *S*-Pentyl Siver Monocarborane (Ag[*s*-pentyl$CB_{11}H_{11}$]) **32**

Li[*closo*-1-Li$CB_{11}H_{11}$] was prepared according to literature[35]: under an inert atmosphere, 3 grams (14.7 mmol) of **2[Me_3NH^+]** was dissolved in 10 mL THF in a 20 mL scintillation vial equipped with a stir bar. 2.2 equivalents of 2.5 M *n*-butyllithium in hexanes was added and the mixture was allowed to stir for 3 hours. The resulting solution was added dropwise to a 250 mL round bottom flask containing 70 mL hexanes while stirring, resulting in a white precipitate. The solvent was decanted and the remaining white precipitate dried under vacuum. The isolated white precipitate was dissolved in 10 mL THF. Two equivalents of 1-iodo-2-methylbutane were added to the reaction solution and stirred for 90 minutes. The solution was removed from inert conditions, organic solvents were removed *in vacuo*, and the crude product was added to 50 mL H_2O. The alkylated carborane product **32** was purified using the following salt exchange procedure: Trimethylammonium hydrochloride was added in excess to the aqueous solution, precipitating the $(CH_3)_3NH$ alkyl carborane salt. The solution was filtered and the precipitate was redissolved in approximately 80 mL slightly basic H_2O with an excess of CsCl. The solution was concentrated down to 30-40 mL, and upon cooling to room temperature the Cs^+ salt of the alkylated carborane product precipitated as a white crystalline solid. A concentrated solution of 1.3 grams of Cs^+ 2-

methylbutyl-1-carborane, $Cs[(C_5H_{11})CB_{11}H_{11}]$ **32** was prepared by heating in 50 mL of slightly acidic DI water (3-5 drops of concentrated HNO_3). 1.1 equivalents of $AgNO_3$ was dissolved in 5 mL or less and added to the aqueous solution. An off-white precipitate formed immediately, and the solution was cooled to room temperature and then filtered from the aquenous solution. The collected solid was stirred in acetone and subsequently gravity filtered, extracting $Ag[s\text{-pentyl}CB_{11}H_{11}]$ **32[Ag^+]** from precipitated salts. $Ag[(C_5H_{11})CB_{11}H_{11}]$) final yield of 860 mg, 72%. ^{1}H NMR (300 MHz, acetone-d_6, 25 °C): δ = 2.83 – 0.45 (bm, 11H, B-H), 1.80 (m, 2H), 1.35 (m, 1H), 1.20 (m, 2H), 0.81 (t, 3H, $^3J(H,H)$ = 2.0 Hz) 0.79 (d, 3H, $^3J(H,H)$ = 2.0 Hz); ^{1}H (^{11}B-dec) NMR (300 MHz, acetone-d_6, 25 °C): δ = 1.85 (s, 6H, B-H), 1.80 (m, 2H), 1.75 (s, 5H, B-H), 1.35 (m, 1H), 1.20 (m, 2H), 0.81 (t, 3H, $^3J(H,H)$ = 2.0 Hz) 0.79 (d, 3H, $^3J(H,H)$ = 2.0 Hz); ^{11}B (^{1}H-dec) NMR (96 MHz, acetone-d_6, 25 °C): δ = -9.5, -10.6; ^{11}B NMR (96 MHz, acetone-d_6, 25 °C): δ = -8.7, -10.1, -11.4 ppm.

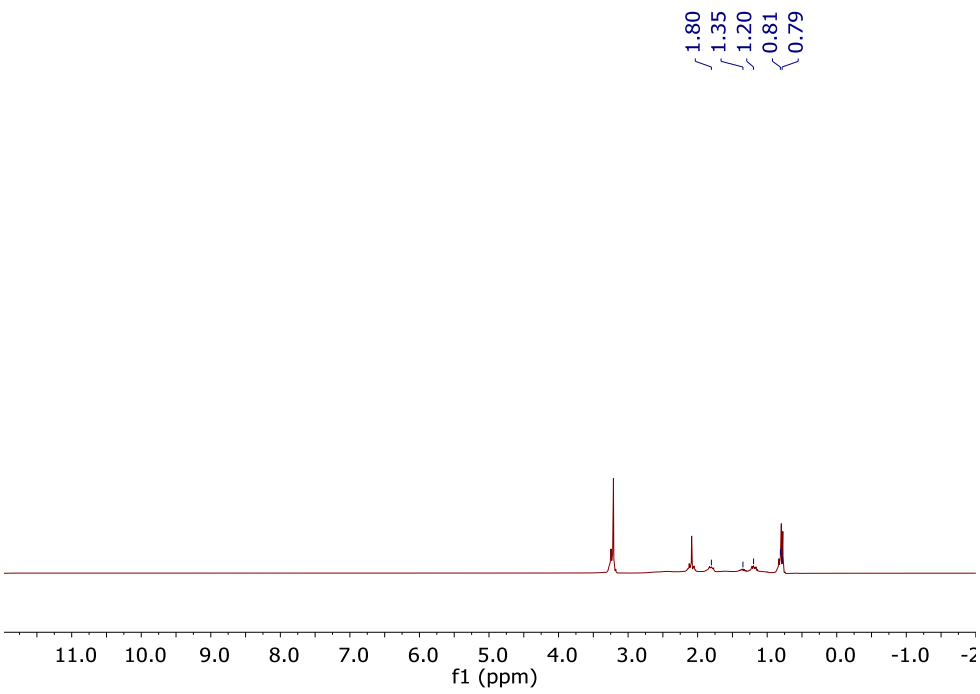

Figure 6-11. ^{1}H NMR spectrum of **32[Ag^{+}]** in acetone-d$_6$. Note: the peaks at 3.11 and 2.09 ppm are from H_2O and acetone, respectively.

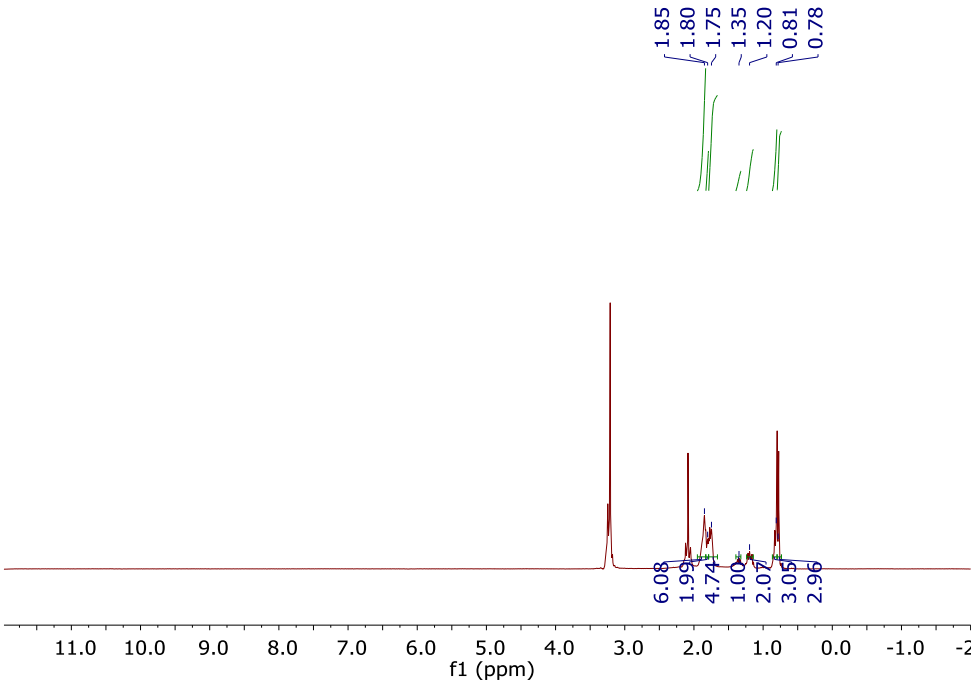

Figure 6-12. ^{1}H (^{11}B-dec) NMR spectrum of **32[Ag^{+}]** in acetone-d$_6$. Note: the peaks at 3.05 and 2.09 ppm are from H_2O and acetone, respectively.

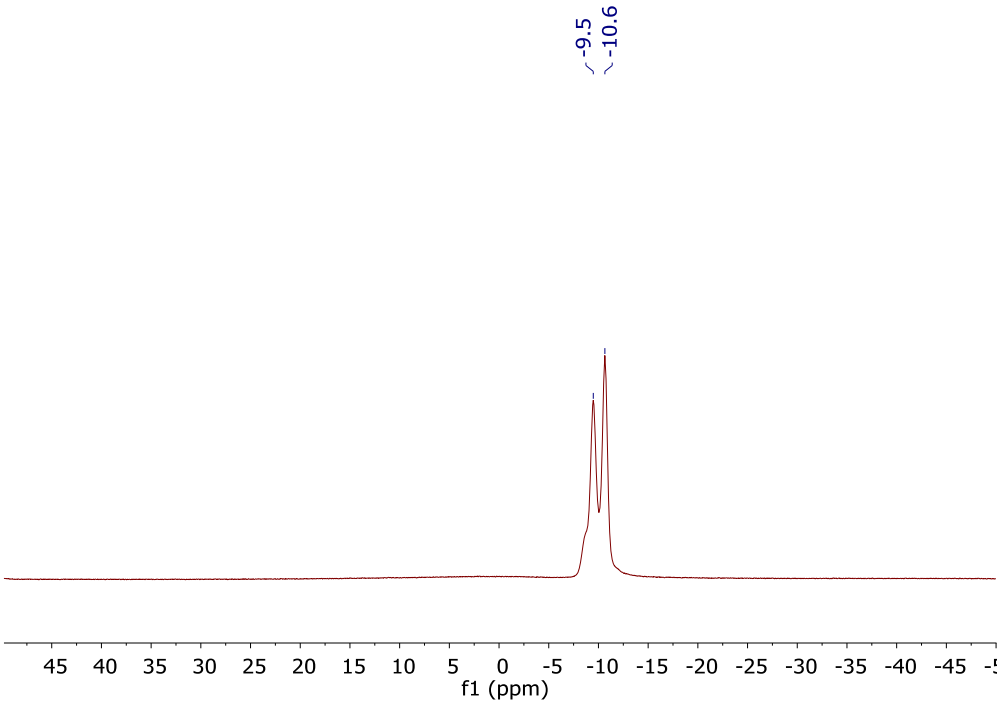

Figure 6-13. ^{11}B (^{1}H-dec) NMR spectrum of **32[Ag^{+}]** in acetone-d$_6$.

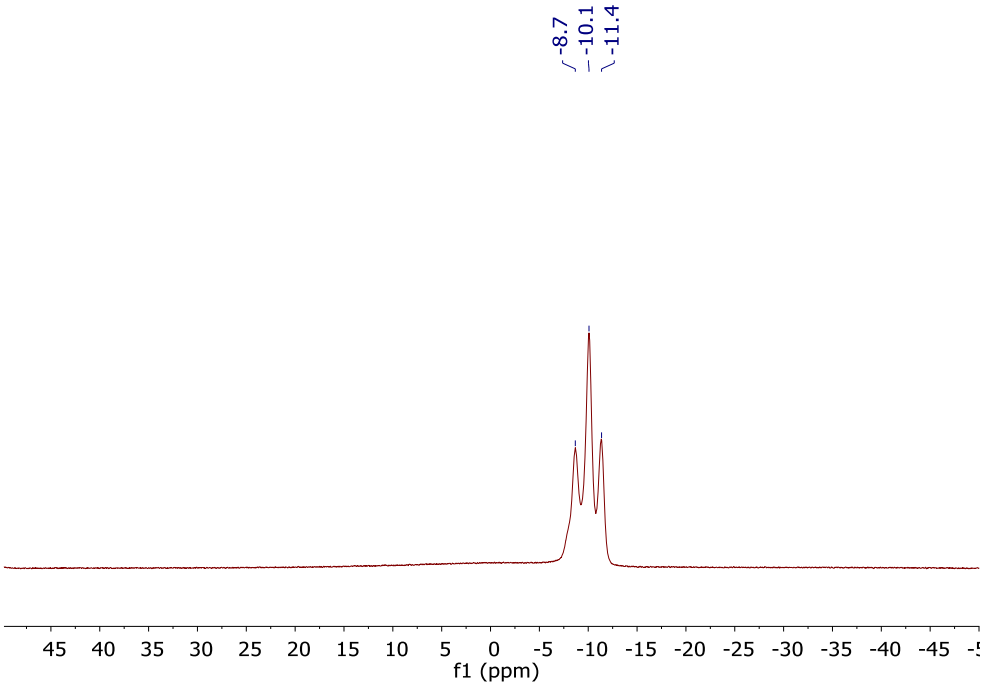

Figure 6-14. ^{11}B NMR spectrum of **32[Ag^{+}]** in acetone-d$_6$.

6.5 References

1. Schlesinger, M., Paunovic, M., Eds.; *Modern Electroplating*; John Wiley & Sons: Hoboken, NJ, **2014**.

2. Harada, A.; Yamaoka, H.; Watanabe, K.; Kinoshita, K.; Kishida, S.; Fukaya, Y.; Nokami, T.; Itoh, T. *Chemical Letters* **2015**, *44,* 1578.

3. Watanabe, M.; Thomas, M. L.; Zhang, S.; Ueno, K.; Yasuda, T.; Dokko, K. *Chemical Reviews* **2017**, *117*, 7190.

4. Kuwabata, S.; Tsuda, T.; Torimoto, T. *Journal of Physical Chemistry Letters* **2010***, 1*, 3177.

5. Simka, W.; Puszczyk, D.; Nawrat, G. *Electrochimica Acta* **2009***, 54*, 5307.

6. Baker, G. A.; Baker, S. N.; Pandey, S.; Bright, F. V. *Analyst* **2005***, 130*, 800.

7. Zeng, Z.; Twamley, B.; Shreeve, J. *Organometallics* **2007**, *26*, 1782.

8. Türp, D.; Wagner, M.; Enkelmann, V.; Müllen, K. *Angewandte Chemie, International Edition* **2011***, 50,* 4962.

9. Shkrob, I. A.; Marin, T. W.; Wishart, J. F. *Journal of Physical Chemistry B* **2013***, 117*, 7084.

10. Gelinas, B.; Das, D.; Rochefort, D. *ACS Applied Materials and Interfaces* **2017***, 9,* 28726.

11. Vöge, A.; Gabel, D. *In Boron Science: New Technologies and Applications*; Hosmane, N. S., Ed.; CRC Press, Boca Raton, FL, **2012**; pp 807−826.

12. Reed, C. A. *Chemical Communications* **2005***, 0*, 1669.

13. Zhu, Y.; Hosmane, N. S. *European Journal of Inorganic Chemistry* **2017***, 2017*, 4369.

14. Sivaev, I. B. *Chemistry of Heterocyclic Compounds* **2017***, 53*, 638.

15. Shannon, K. C., III; Sheets, J.; Groger, H.; Williams, A. *Proceedings of SPIE* **2009**, *7330*, 73300F.

16. Chandrasekhar, P.; Zay, B. J.; Lawrence, D.; Caldwell, E.; Sheth, R.; Stephan, R.; Cornwell, J. *Journal of Applied Polymer Science* **2014***, 131*, 40850.

17. Farrar, D.; Douglas, D. M.; Swanson, T.; Collins, C.; Darrin, A.; Osiander, R. *AIP Conference Proceedings* **2007***, 880*, 73.

18. Bergeron, B. V.; White, K. C.; Boehme, J. L.; Gelb, A. H.; Joshi, P. B. *Journal of Physical Chemistry C* **2008***, 112,* 832.

19. Rumble, J. R., Ed.; *CRC Handbook of Chemistry and Physics, 98th ed*.; CRC Press/Taylor & Francis: Boca Raton, FL, **2018**.

20. Reyna-Gonzaĺez, J.M.; Reyes-Lopẹz, J.C.; Aguilar-Martínez,M. *Electrochimica Acta* **2013***, 94,* 344.

21. Stocker, H. J.; Van Uitert, L. G.; Loomis, T. C.; Koch, F. B. *Journal of the Electrochemical Society* **1981***, 128*, 746.

22. Mascaro, L. H.; Kaibara, E. K.; Bulhões, L. O. *Journal of the Electrochemical Society* **1997**, *144*, L273.

23. Lu, W.; Fadeev, A. G.; Qi, B.; Mattes, B. R. *Journal of the Electrochemical Society* **2004**, *151*, H33.

24. Popov, A. I.; Geske, D. H. *Journal of the American Chemical Society* **1958**, *80*, 5346.

25. Allen, G. D.; Buzzeo, M. C.; Villagrań, C.; Hardacre, C.; Compton, R. G. *Journal of Electroanalytical Chemistry* **2005***, 575*, 311.

26. Luehrs, D. C.; Iwamoto, R. T.; Kleinberg, J. *Inorganic Chemistry* **1966***, 5,* 201.

27. Freire, M. G.; Neves, C. M. S. S.; Marrucho, I. M.; Coutinho, J. A. P.; Fernandes, A. M. *Journal of Physical Chemistry A* **2010***, 114,* 3744.

28. Wang, B.; Qin, L.; Mu, T.; Xue, Z.; Gao, G. *Chemical Reviews* **2017***, 117*, 7113.

29. Douvris, C.; Michl, J. *Chemical Reviews* **2013***, 113*, PR179.

30. Grishina, E. P.; Kudryakova, N. O.; Pimenova, A. M. *Protection of Metals and Physical Chemistry of Surfaces* **2017***, 53*, 663.

31. Basile, A.; Bhatt, A. I.; O'Mullane, A. P.; Bhargava, S. K. *Electrochimica Acta* **2011***, 56,* 2895.

32. SEM studies required thicker Ag films because of etching of the films by solvent used to remove excess BCIL and expose the underlying Ag deposits.

33. Rybicki, G. B.; Lightman, A. P., *Fundamentals of Radiative Transfer, Radiative Processes in Astrophysics*; Wiley−VCH: Weinheim, Germany, **2004**.

34. Clawson, J. F.; Tsuyuki, G. T.; Anderson, B. J.; Justus, C. G.; Batts, W.; Ferguson, D.; Gilmore, D. G. *Spacecraft Thermal Environments. In Spacecraft Thermal Control Handbook, 2nd ed.*; The Aerospace Press: Reston, VA, **2002**; Vol. 1: Fundamental Technologies, pp 21−69.

35. Jelinek, T.; Baldwin, P.; Scheidt, R.; Reed, C.A. *Inorganic Chemistry* **1993**, *32*, 1982.

Conclusion

Since the 1960's, carboranes have evolved from an item of molecular curiosity to utility in various fields ranging from energy storage to cancer treatment. Despite the variety of applications investigated with carborane clusters, incorporation in catalyst design by covalently tethering the anion as a ligand substituent has been explored only very recently. The use of the 12-vertex carborane anion as a ligand group was a novel method first published by the Lavallo group for the development of transition metal catalysts. The cluster is inherently more stable and resistant to reactivity than *o*-carborane and has been demonstrated as a successful phosphine ligand substituent for transition metal complexes.

The major focus of my research was to further explore the application of the anionic carborane as a ligand R-group. Initially, I investigated potential metal complexes and catalytic activity of the diimine and N-heterocyclic carbenes functionalized with the 12-vertex carborane anion. These ligands did not readily bind to a wide range of metals in the same fashion as the carborane functionalized phosphine ligands. This lack of reactivity was attributed to the steric bulk of the 12-vertex carborane and possibly the anionic charge of the ligands. To remedy this, I implemented the 10-vertex carborane anion. This cluster is smaller in size with a less delocalized charge, making this cluster a stronger donor. Additionally, the smaller steric profile would not interfere with coordination a metal center.

A large component of my thesis work consisted of developing a synthetic route for the imidazolium functionalized with the 10-vertex carborane anion and the corresponding N-heterocyclic carbenes. After successfully synthesizing these materials, I sought to expand this new class of NHCs by functionalizing the imidazolium cluster. In contrast to

the 12-vertex imidazolium, not only can the clusters be substituted with chlorine atoms, but the backbone is substituted as well. The chlorination of an imidazolium backbone has been reported once previously in literature, with unexpected air stability. The NHC with fully chlorinated carborane clusters and backbone was not only air stable but also remained unprotonated in the presence of water. The conclusion of my work with NHC ligand structures was the development of the unsymmetrical imidazolium bearing the 10-vertex carborane on one nitrogen and a mesityl R-group on the other.

The work presented in this thesis paves the way for the development of unique transition metal complexes. The next step of this project, the development of transition metal complexes, will demonstrate if utilizing a smaller, stronger donor cluster does indeed enhance the ability of this ligand motif to bind to a metal. Due to the charged nature of the carborane ligand structure, future metal complexes will be advantageous for an array of catalytic systems. The 10-vertex carborane imidazolium has many unexplored routes of cluster modification that will be advantageous for fine tuning the electronic and steric profile of this ligand.

Although the 12-vertex carborane anion is more prolific in contemporary chemistry, there are still unexplored avenues for applications. In collaboration with the Spokoyny group from UC Los Angeles, we were able to modify the carborane to target desired material properties. The unfunctionalized carborane anion had previously been used to synthesize an ionic liquid electrolyte for silver deposition, however this solution crystallized over time. Functionalizing the carborane at the carbon vertex with an alkyl chain prevented the formation of crystalline particles in solution. This ionic liquid was then

utilized for reversible silver deposition demonstrating a proof-of-concept design for spacecraft thermal control.

The versatile nature of carboranes and their prospective applications in numerous fields of chemistry is demonstrated in this work. Although some of the presented projects have reached conclusion, the vast majority of this work involves the synthesis of novel ligands and the ability of functionalize these ligands. This class of ligands has yet to be explored and presents the opportunity for countless further investigations and hopefully opens the door to new and exciting chemistry.